Technische Universität München

TUM School of Life Sciences

Control of deposit layer formation for optimized milk protein fractionation by microfiltration hollow fiber membranes

Roland Patrick Matthias Schopf

Vollständiger Abdruck der von der TUM School of Life Sciences der Technischen Universität München zur Erlangung des akademischen Grades eines

Doktor der Ingenieurwissenschaften (Dr.-Ing.)

genehmigten Dissertation.

Vorsitzender:		Prof. Dr. Wilfried Schwab
Prüfer der Dissertation:	1.	Prof. Dr.-Ing. Ulrich Kulozik
	2.	Prof. Dr.-Ing. Harald Klein
	3.	Prof. Dr.-Ing. Jörg Hinrichs

Die Dissertation wurde am 12.11.2021 bei der Technischen Universität eingereicht und durch die TUM School of Life Sciences am 27.04.2022 angenommen.

Meiner Familie

„Dass ich erkenne, was die Welt
Im Innersten zusammenhält.“

— Johann Wolfgang von Goethe, 1808
Buch Faust I. Eine Tragödie, Vers 382 f.

Danksagung

Die vorliegende Arbeit entstand im Rahmen meiner Tätigkeit am Lehrstuhl für Lebensmittel- und Bioverfahrenstechnik der Technischen Universität München im Zeitraum von Juni 2017 bis September 2021.

Mein besonderer Dank gilt meinem Doktorvater Herrn Univ. Prof. Dr.-Ing. habil. Ulrich Kulozik, der dieses Projekt initiierte und mich betreute. Er gewährte mir ein Höchstmaß an wissenschaftlicher Freiheit und stellte mir hervorragende Einrichtungen und Mitarbeiter für die Durchführung meiner Experimente zur Verfügung. Darüber hinaus hat er meine persönliche und pädagogische Entwicklung voll unterstützt.

Herrn Dr.-Ing. Hans-Jürgen Heidebrecht danke ich für seinen Beitrag zum Projekt, seine kontinuierliche Unterstützung bei der Lösung wissenschaftlicher Probleme und seine hervorragende fachliche und persönliche Betreuung meiner Masterarbeit, die mich mit dem wissenschaftlichen Umfeld vertraut machte. Meiner Mentorin Frau Dr.-Ing. Jannika Dombrowski danke ich für ihren Beitrag zu meinem Promotionsvorhaben.

Ich danke allen Mitarbeitern des Instituts, die mein Vorhaben unterstützt haben: Hervorheben möchte ich in diesem Zusammenhang den Beitrag des Teams der Institutswerkstatt: Christian Ederer, Franz Fraunhofer und Erich Schneider; des technischen Personals: Andreas Matyssek, Michael Reitmaier und Günther Unterbuchberger; des Laborteams: Heidi Wohlschläger, Claudia Hengst, Hermine Roßgoderer, Annette Brümmer-Rolf und Christine Haas; und des Sekretariats: Friederike Schöpflin, Sabine Becker und Sabine Grabbe. Meinen Studenten Dilara Arar, Johanna Linner, Ramona Schmitz, Hatice Cetin, Florian Schmidt, Jonathan Spitzer und Felix Desch, die mit ihrer theoretischen und praktischen Arbeit maßgeblich zum Gelingen dieser Arbeit beigetragen haben. Meinen Bürokollegen Malou Warncke und Dr.-Ing. Mine Özcelik Kocak danke ich für ihre ständige Unterstützung und die angenehme Atmosphäre.

Darüber hinaus möchte ich mich bei allen anderen Kollegen und Freunden bedanken, insbesondere bei Malou Warncke, Regina Haindl, Dr.-Ing. Ingrun Kieferle, Maria Weinberger, Franziska Kurz, Dr.-Ing. Martin Hartinger, Andreas Matyssek, Christian Kürzl und Simon Schiffer für die wissenschaftlichen Diskussionen, tolle Urlaube und sportliche Herausforderungen. Nur mit euch ist es eine unvergessliche Zeit meines Lebens geworden.

Last but not least gilt mein größter Dank meiner Familie für ihre unermüdliche Unterstützung und den persönlichen Ausgleich.

Contents

Abbreviations

Latin symbols

A_{cross}	Free cross-section	m^2
$a_{integral}$	Integral fit parameter a	-
a_{local}	Local fit parameter a	-
A_M	Active membrane surface	m^2
ATR-FTIR	Attenuated total reflection - Fourier-transform infrared spectroscopy	
$b_{integral}$	Integral fit parameter b	-
b_{local}	Local fit parameter b	-
BSA	Bovine serum albumin	
$c_{cas,conc}$	Concentration of casein in the concentrate	$g\ L^{-1}$
$c_{cas,milk}$	Concentration of casein in the native skim milk	$g\ L^{-1}$
$C_{DF,n}/C_{DF,0}$	Absolute level of protein decrease	-
CF	Concentration factor	-
CFD	Computational fluid factor	
$c_{i,per}$	Concentration of a component i in the permeate	$g\ L^{-1}$
$c_{i,ret}$	Concentration of a component i in the retentate	$g\ L^{-1}$
$c_{Protein}$	Concentraion of proteins	$g\ L^{-1}$
CTM	Ceramic tubular membranes	
D	Diffusion coefficient	$m^2\ s^{-1}$
d_{equiv}	Equivalent channel diameter	m
DF	Diafiltration	
d_h	Inner hydraulic diameter	m
d_i	Inner diameter	m
d_p	Particle diameter	m
F_A	Adhesion force	N
F_F	Friction force	N
F_L	Lift force	N
F_y	Drag force	N
F_y	Drag force of the filtration flow	N
h_d	Deposit thickness	m
HFM	Hollow fiber membranes	
IgA	Immunoglobulin A	

IgG	Immunoglobulin G	
IgM	Immunoglobulin M	
J	Flux	L m^{-2} h^{-1}
J_{CF}	Flux at specific CF	L m^{-2} h^{-1}
J_0	Pure water permeability	m^{-2} h^{-1} bar^{-1}
k_B	Boltzmann constant	J K^{-1}
L	Membrane length	m
LPO	Lactoperoxidase	
$\dot{m}_{back}$	Back diffusion	g m^{-2} h^{-1}
$\dot{m}_i$	Mass flow of a component i	g m^{-2} h^{-1}
MF	Microfiltration	
MRI	Magnetic resonance imaging	
NF	Nanofiltration	
NMR	Nuclear magnetic resonance	
P	Pressure	bar
PES	Polyether sulfone	
p_{in}	Pressure at the membrane inlet	bar
p_{out}	Pressure at the membrane outlet	bar
p_{per}	Pressure on permeate side	bar
p_{ret}	Pressure on retentate side	bar
PVDF	Polyvinylidene fluoride	
RARE	Rapid Acquisition with Relaxation Enhancement	
RC_i	Retention or sieving of a component i	%
R_D	Deposit layer resistance	m^{-1}
Re	Reynolds number	-
R_F	Total filtration resistance	m^{-1}
RF	RARE factor	-
R_M	Membrane resistance	m^{-1}
RO	Reverse osmosis	
RP-HPLC	Reversed-phase high pressure liquid chromatography	
SWM	Spiral-wound membranes	
T	Absolute temperature	K
t	Time	h

T_R	Repetition time	h
Tr_i	Transmission of a component i through the membrane	%
TRIS	Tris(hydroxymethyl)aminomethane	
UF	Ultrafiltration	
UTP	Uniform transmembrane pressure	
$\dot{V}_{feed}$	Feed volume flow	L h^{-1}
$\dot{V}_{Per}$	Permeate volume flow	L h^{-1}
$V_{DF,0}$	Initial hold-up volume for DF	L
$V_{DF,n}$	Total volume of the added DF medium	L
v_m	Mean crossflow velocity	m s^{-1}
V_{Mod}	Membrane module volume	m^3
v_y	Velocity in y direction	m s^{-1}

Greek symbols

α-la	α-lactalbumin	
β-lg	β-lactoglobulin	
γ_T	Wall shear rate	s^{-1}
Δp_L	Axial pressure drop along membrane length L	bar m^{-1}
$\Delta p_{TM,mean}$	Mean transmembrane pressure	bar
Δp_{TM}	Transmembrane pressure	bar
δ_{lam}	Height of the laminar sublayer	m
η	Dynamic viscosity	Pa s
Θ	Packing density	m^2 m^{-3}
ϑ	Temperature	°C
λ	Friction factor	-
Π	Osmotic pressure	bar
τ_W	Wall shear stress	Pa
φ	Density	kg m^{-3}
ϕ	Correction factor to the Stokes drag force	-

1 General introduction

Membrane filtration is an important process unit operation with high economical impact in many industrial areas, such as in pharmaceutical production, medical devices functionality, and food production. The operational field is wide, ranging from gas separation and blood dialysis up to water treatment, biotechnological downstream processing, or wine and beer clarification for purification, concentration, or fractionation of components. The main limitation of membrane processes is that the substance to be retained tends to be deposited on the membrane surface (so-called fouling), which can block the membrane pores and form a deposit layer producing an additional filtration resistance, reducing flux and transmission.

When processing complex bio-suspensions in fermenters or colloidal solutions like milk, wine or beer, macromolecules such as proteins, polysaccharides, and particles, e.g., microorganisms, are primarily involved in the formation of the deposit layer. To investigate the phenomenon of deposit layer formation and to optimize microfiltration (MF), in this thesis skim milk was used as a filtration medium targeting the fractionation of the main protein fractions, casein and whey protein, by crossflow microfiltration in a diafiltration (DF) mode.

This study is particularly about the investigation of fouling by the retained larger protein fraction, the caseins, during milk protein fractionation under varying process conditions. The structure of the deposit layer along the flow path over the membrane surface depending on the composition and amount of the deposited proteins was characterized. Hollow fiber membranes (HFM) were assessed regarding their filtration performance compared to industrially established module types, spiral-wound membranes (SWM), and ceramic tubular membranes (CTM).

In brief, filtration performance and deposit layer formation on HFM along the flow path was investigated by a non-invasive and non-destructive measurement combined with the characterization of the deposit layer in terms of protein amount and protein composition. Combining the obtained results, the optimal filtration parameters for pre-concentration before starting DF were assessed. Further to that, deposit layer formation was investigated in a multi-channel CTM to assess the intensity of deposit formation in the outer channels compared to the ones located in the center of the tubular bundle.

To establish a deeper understanding, the mechanisms of flux decline in relation to the physicochemical properties of milk proteins and the deposit layer formation, various aspects in this context were investigated and separately reported in five peer-reviewed publications, forming the main results chapters of this thesis. The following introduction provides the basic technological and methodological background and a wider state of knowledge compared to the more concise introductory chapters of the publications.

1.1 Pressure-driven membrane filtration processes

1.1.1 Basic principles of the membrane-based transport mechanism

The application of the pressure-driven membrane filtration processes range from MF and ultrafiltration (UF) to nanofiltration (NF) and reverse osmosis (RO) according to the pore size of the membrane and the required pressure (Figure 1.1).

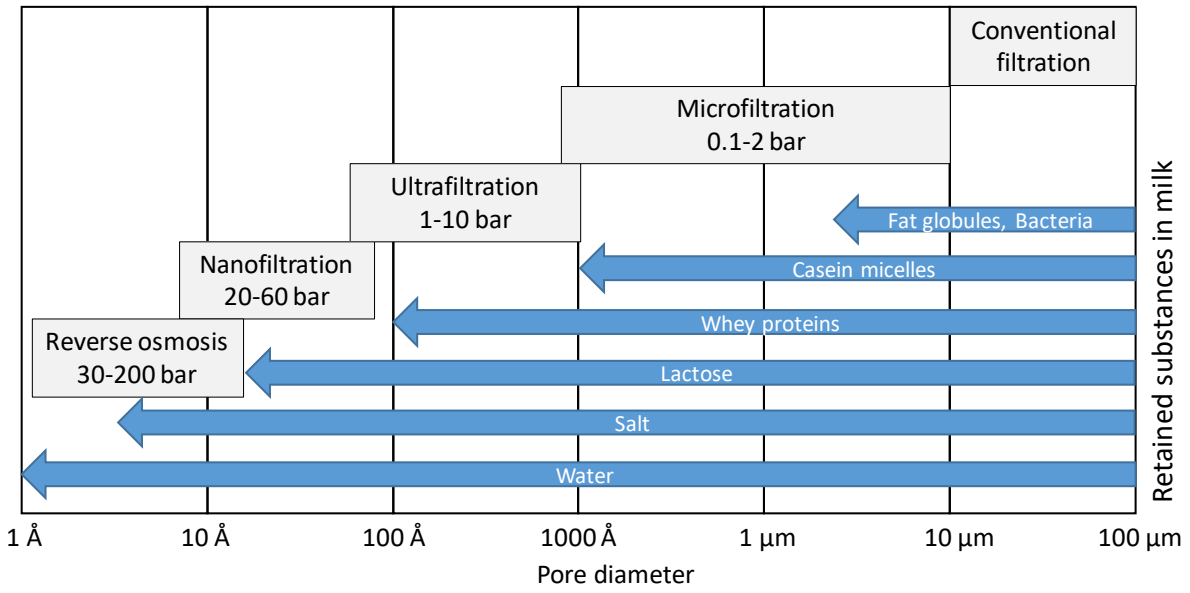

Figure 1.1. Applications of membrane process according to their pore diameter and the retained substances in milk (adapted from Baker (2008)(Page 7; Figure 1.2)).

The basic separation mechanism for MF, UF, and partially also for NF, is molecular sieving through increasingly fine pores. MF membranes with a pore size of 0.1-10 µm are widely used to separate fat globules, bacteria, and colloidal particles. Casein micelles can be separated as well using a MF nominal pore size of 0.1 µm.

UF is commonly used to concentrate macromolecules, e.g., whey proteins, or in a diafiltration mode to fractionate biological macromolecules, while low molecular constituents are transported through the membrane convectively by the aqueous phase.

During NF, polysaccharides such as lactose can be rejected and these membranes allow the separation of monovalent from polyvalent ions due to the electrostatic interaction of ions with the polymeric membrane material.

The most important application of RO is desalination of sea or brackish water, because it is capable of almost complete retention of all dissolved substances from water, producing desalted water as permeate. RO membranes are considered free of discrete pores.

Milk protein fractionation is possible with an MF nominal pore size of 0.1-0.2 µm to separate the larger caseins (mainly retained in the retentate) from the smaller whey proteins (mainly in the permeate) by applying pressure as the driving force producing

the flow of aqueous phase. Smaller particles than the membrane pore size can pass the membrane into the permeate by convective transport. Particles larger than the membrane pores are selectively retained at the membrane surface. The transmembrane pressure (Δp_{TM}) is defined as the pressure difference between the retentate side (p_{ret}) and the permeate side (p_{per}) according to Equation (1.1).

$$\Delta p_{TM} = p_{ret} - p_{per} \tag{1.1}$$

According to Darcy's law (Equation (1.2)), the specific permeate volume flow or flux (J) can be determined as:

$$J = \frac{\dot{V}_{per}}{A_M} = \frac{\Delta p_{TM}}{\eta \cdot R_F} \tag{1.2}$$

where $\dot{V}_{per}$ is the permeate volume flow, A_M the active membrane surface, η the permeate viscosity, and R_F the total filtration resistance, respectively.

The transmission of the proteins through the membrane (Tr_i), is calculated as the ratio of their concentration in the permeate ($c_{i,per}$) and the concentration in the retentate ($c_{i,ret}$) for each protein component i (Equation (1.3)):

$$Tr_i = \frac{c_{i,per}}{c_{i,ret}} \cdot 100\% \tag{1.3}$$

The sieving or retention (RC_i) of the particles is defined in Equation (1.4) as:

$$RC_i = 100\% - Tr_i \tag{1.4}$$

Based on J and $c_{i,per}$, the whey protein mass flow ($\dot{m}_i$) was calculated as the most decisive criteria for milk protein fractionation:

$$\dot{m}_i = J \cdot c_{i,per} \tag{1.5}$$

Tr_i and $\dot{m}_i$ can be used to determine the fractionation rate and efficiency.

1.1.2 Dead-end, crossflow and direct flow filtration

Three main operational modes of filtration processes can be distinguished according to the flow of the feed towards are along the membrane surface (Figure 1.2). In the static filtration mode, e.g., dead-end filtration, the feed flows directly towards the membrane surface. The feed flow has to permeate through the membrane pores as the only way open for exiting the module. Particles larger than the membrane pores are rejected as they cannot pass the membrane and stay in the retentate accumulating at the membrane surface, over time building a growing filter cake. With increasing time, the filter cake height at the membrane surface increases and the flux therefore steadily decreases. Below a certain flux, which can subjectively be defined as a critical value, the

membrane has to be cleaned. Thus, dead-end filtration is a discontinuous process with short intervals of filtration and cleaning.

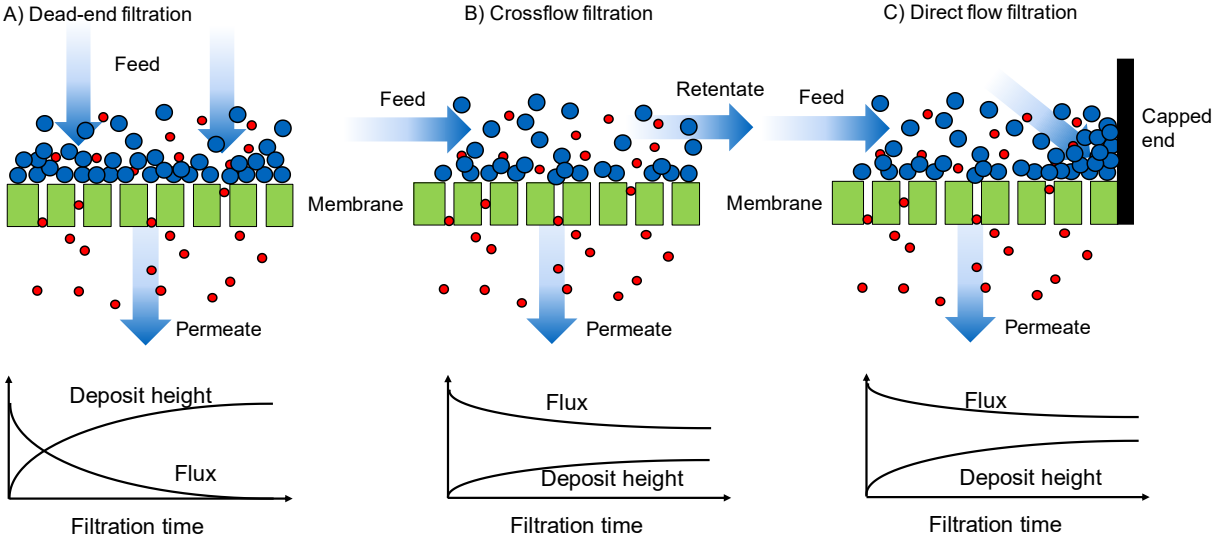

Figure 1.2. A) Dead-end, B) Crossflow filtration (adapted from Ripperger and Altmann (2002) (Page 20, Figure 1)) and C) Direct flow filtration (adapted from Xu et al. (2017) (Page 324, Figure 1).

In contrast to that, crossflow filtration is an option to counteract deposit layer formation by deposit removing forces. The feed flows tangentially along the membrane surface. Due to frictional effects, shear forces, and lift forces, the deposition of particles on the membrane surface can be mitigated. This keeps flux up as well as filtration time before cleaning of the membrane is required. After an initial phase of unavoidable material deposition, steady-state filtration conditions could be reached. Flux, transmission, and deposit layer height are then relatively stable over time. Friction at the membrane surface causes a reduction of static pressure on the retentate side. In crossflow filtration, the mean $\Delta p_{TM,mean}$, can be calculated from the pressure at the membrane inlet (p_{in}) at the membrane outlet (p_{out}) and at p_{per} as follows (Equation (1.6)):

$$\Delta p_{TM,mean} = \frac{p_{in} + p_{out}}{2} - p_{per} \tag{1.6}$$

In crossflow filtration, the shear forces and the wall shear stress (τ_W) depend on the pressure drop (Δp_L) along the membrane. Δp_L can be calculated as the difference between p_{in} and p_{out} as follows (Equation (1.7)):

$$\Delta p_L = p_{in} - p_{out} \tag{1.7}$$

τ_W is determined for the flow through a tubular channel as a function of the friction factor (λ), the density (φ), and the mean crossflow velocity (v_m) according to Equation (1.8):

$$\tau_W = \frac{\lambda \cdot \varphi \cdot v_m^2}{8} \tag{1.8}$$

where λ is a function of the Reynolds number (Re). Δp_L is determined by the length of the membrane (L) and the inner hydraulic diameter (d_h) according to Equation (1.9):

$$\Delta p_L = \frac{1}{2} \cdot \lambda \cdot \frac{L}{d_h} \cdot \varphi \cdot v_m^2 \tag{1.9}$$

Equation (1.8) and Equation (1.9) lead to Equation (1.10):

$$\Delta p_L = \frac{\tau_W \cdot d_h}{4 \cdot L} \tag{1.10}$$

v_m can be calculated with $\dot{V}_{feed}$ as the feed volume flow and A_{cross} as the free cross-section according to Equation (1.11):

$$v_m = \frac{\dot{V}_{feed}}{A_{cross}} \tag{1.11}$$

The state of flow can be characterized by Re (Equation (1.12)):

$$Re = \frac{\varphi \cdot v_m \cdot d_h}{\eta} \tag{1.12}$$

The feed velocity will be reduced at the membrane surface due to friction effects, thus a laminar sublayer will occur. The height of the laminar sublayer (δ_{lam}) could be calculated according to Equation (1.13):

$$\delta_{lam} = \frac{5 \cdot \eta}{\sqrt{\tau_w \cdot \varphi}} \tag{1.13}$$

At the membrane surface, there is no crossflow velocity, but the velocity (v_y) linearly increases in the laminar sublayer within the range of the distance to the membrane surface (y) (Equation (1.14)):

$$v_y = \frac{\tau_w}{\eta} \cdot y \tag{1.14}$$

Another processing mode is the so-called direct flow mode (Figure 1.2 C). In this processing mode, HFM with closed ends are used for the treatment of water with lower fouling potential, which combines a filtration cycle operated in dead-end filtration with a regular intermittent backwash (Xu et al., 2017). The end of the hollow fiber is closed so that the filtration runs in dead-end mode. Fouling will occur during filtration and flux will decrease. To counteract this, frequent backwashes are performed. The advantage of the direct flow mode is that due to very low crossflow velocity, energy use is quite

moderate and the Δp_L is reduced. Therefore, this should reduce length-dependent filtration, but filtration characteristics are closer to dead-end filtration.

1.1.3 Model for the deposit layer removal during crossflow filtration

The mechanistic model for deposit layer removal during crossflow filtration has been established in the literature so far. In crossflow filtration, the tangential flow towards the membrane induces a wall shear stress. Therefore, molecular back diffusion, as well as shear-induced diffusion, can occur. Zydney and Colton (1986) described a crossflow filtration model with shear-induced diffusion for particle sizes ranging from 0.1 to 20 µm. By increasing the crossflow velocity, the shear rate increases and thus, the shear-induced diffusion will also increase along the particles that are small enough. With increased diffusion, fewer particles can deposit on the membrane surface, and flux and transmission increase. Song and Elimelech (1995) extended the model by taking van-der-Waals forces and electrostatic particle interactions into account. Fritz (1995) described the particle deposition as a superposition of the mass transport forced by the flow with a dispersive mass transport that counteracts convection. However, there are also mechanistic models for deposit layer removal that focus on the forces acting on a single particle during crossflow filtration. The most important model, the lift force model takes the hydrodynamic forces and the frictional forces acting on a particle into account. A short summary of some numeric simulations is given by Makabe et al. (2021). The balance of forces between the lift force (F_L) into the bulk solution and the drag force (F_y) of the filtrate flow towards the membrane determines the deposition or removal of a particle on the membrane surface (Figure 1.3).

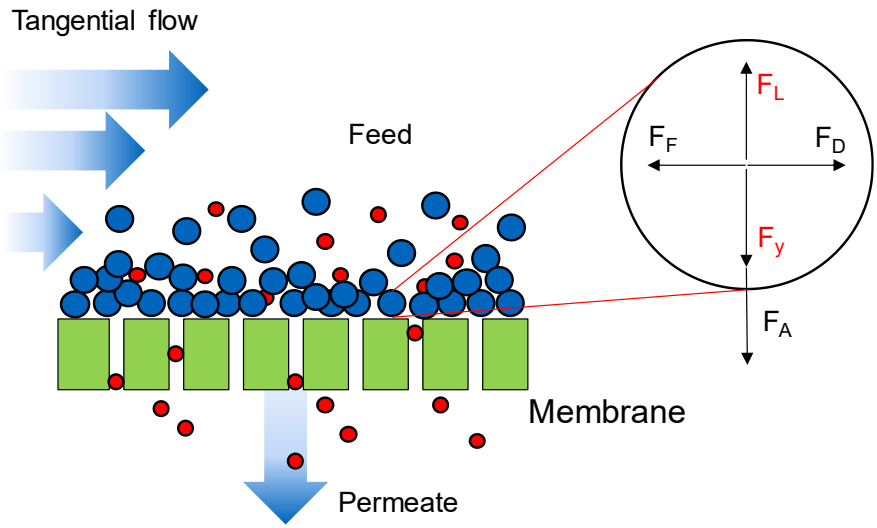

Figure 1.3. Microscopic model for hydrodynamic forces and the frictional forces during particle deposition (adapted from Ripperger and Altmann (2002) (Page 21, Figure 6)). F_L as lift force, F_D as drag force of the crossflow, F_F as friction forces, F_y as drag force of the filtration flow, and F_A as adhesion force.

The F_L can be calculated according to McLaughlin (1993) (Equation (1.15)):

$$F_L = 0.358 \cdot \frac{\tau_w^{1.5} \cdot d_p^3 \cdot \varphi^{0.5}}{\eta} \cdot f\left(d_p, \eta, \tau_w, \varphi\right) \tag{1.15}$$

with d_p as particle diameter and a correction function $f(d_p, \eta, \tau_w, \varphi)$ that can be solved numerically. F_y can be calculated on the Stokes' law (Equation (1.16)):

$$F_y = F_{Stokes} = 3 \cdot \pi \cdot \eta \cdot d_p \cdot J \cdot \Phi \tag{1.16}$$

with ϕ as a correction factor to the Stokes drag force. Comparing Equation (1.15) with Equation (1.16), it is obvious that changing d_p has a higher impact on F_L than on F_y. Increasing particle diameter would lead to a higher lift force by the power of three. It should be noted that the lift force model itself could not completely explain particle removal or deposition, since only larger particles are affected by the hydrodynamic lift force.

1.2 The skim milk system for protein fractionation

Bovine milk is a natural product containing water, fat, milk proteins, lipids, lactose, and salt (Table 1.1).

Table 1.1. The composition of bovine skim milk averaged over feeding-related seasonal variations (Töpel, 2016) (Page 4-6, Table 2.1).

Organic constituents	**Concentration, g kg^{-1}**	**Inorganic constituents**	**Concentration, g kg^{-1}**
Lipids	30-45	Water	860-880
Protein	32-36	Ions	6.0-7.5
Caseins	26-30	*Cations*	2.8-3.7
α_{S1}	10.3-11.9	Calcium	1.00-1.40
α_{S2}	2.6-3.1	Magnesium	0.10-0.15
β	9.9-11.9	Sodium	0.35-0.60
κ	3.3-3.5	Potassium	1.35-1.55
Whey proteins	6.0-6.2	Anions	3.2-3.8
α-lactalbumin	1.2-1.3	Carbonate	0.2
β-lactoglobulin	3.1-3.5	Chloride	0.8-1.4
Serum albumin	0.4	Sulfate	0.1
others	1.9-2.3	Phosphate	2.1
Carbohydrates	46-48		
α-lactose-hydrate	17.7-18.0		
β-lactose	29-30		
others	0.07		

The main component of the carbohydrates in bovine milk is lactose, which could interact with the milk proteins to reduce denaturation during heating (Andrews and Varley, 1994). Increasing the lactose content also increases the permeate viscosity and thus the flux during MF decrease, but the whey protein transmission stays constant (Adams et al., 2015b). Gernedel (1980) and Taddei et al. (1988) reported an effect of lactose on the flux to the integration of lactose in the deposit layer and thus to the increased adsorption properties.

Salts are present in bovine milk in different forms: monovalent ions like sodium, potassium, and chloride, divalent calcium, and trivalent phosphate. A distinction is made between genuinely dissolved ions and colloidal salts, which also include salts bound to macromolecules. The ionic strength is decisive for the electrostatic interaction between milk proteins. The salts bound to proteins as well as the non-dissociated and therefore neutral salts do not contribute to the shielding of the surface charge in the diffuse bilayer. Le Berre and Daufin (1998) showed that an increase of NaCl leads to an increase of the reversible deposit layer resistance. Increasing the calcium concentration leads to more connected and bound casein micelles (Jimenez-Lopez et al., 2008) reducing effective membrane pore size. This could be also shown in UF (Gernedel, 1980; Kessler, 2002). Due to a more intense deposit layer formation with an increased concentration of soluble calcium, the flux was reduced (Adams et al., 2015b).

1.2.1 Caseins

The major fraction of the milk proteins are the caseins which could be divided into κ-, α_{S1}-, α_{S2}-, and β-casein according to their decreasing electrophoretic mobility at pH 6.6 (Schmidt, 1980). The caseins have an amphiphilic molecular structure. They are structured in the form of micelles having a complex structure (Figure 1.4).

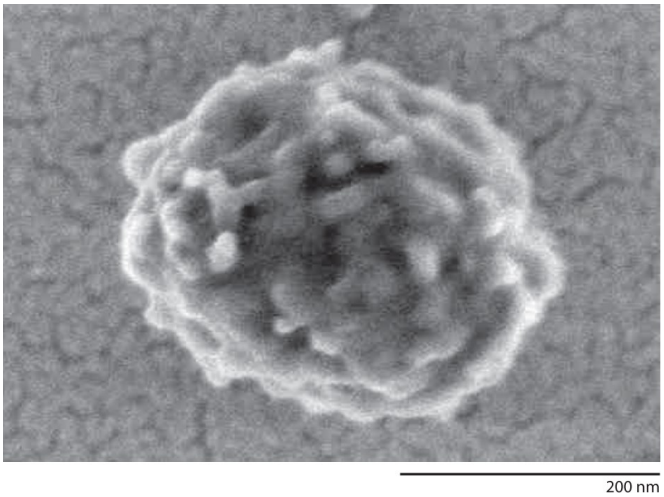

Figure 1.4. Field-emission scanning electron microscopy image of a casein micelle (Dalgleish and Corredig, 2012) (Page 453, Figure 2).

Thus, casein micelles have a particle size distribution ranging from 50 to 400 nm. If caseins are microfiltered in the pore size range of 0.05 to 0.2 µm, it can be expected that most caseins will be rejected (Kersten, 2001). According to Le Berre and Daufin (1996), a casein rejection of up to 99% could be reached. However, filtration at a temperature below 20 °C, β-casein can diffuse out of the micelle due to the reduced hydrophobic interactions at low temperatures and permeate (Samuelsson et al., 1997). The casein micelles are comparably stable under normal technical pressure conditions (Gebhardt et al., 2012), shear stress, or heating (Dumpler, 2017).

The exact casein micelle structure has not been finally determined so far. Dalgleish and Corredig (2012), Holt et al. (2013), and Horne (2020) provide an overview of the various model paradigms. The most widely agreed model and current state of knowledge is the so-called nanocluster model.

As shown in Figure 1.5, the micelles consist of aggregates of α_{S1}-, α_{S2}-, and β-casein plus calcium phosphate accumulated in nanoclusters (Holt et al., 2013). Due to hydrophobic interactions between this casein monomers (Horne, 2003) as well as calcium-bridging, hydrogen bonding, and van der Waals interactions (Dalgleish, 2011), the micelles are stabilized.

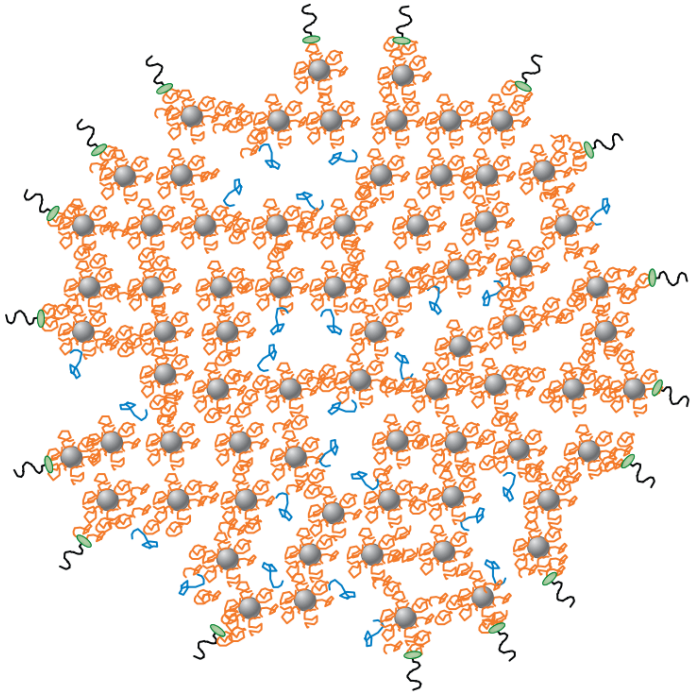

Figure 1.5. Schematic diagram of a casein micelle with α_s-and β-caseins (orange), calcium phosphate nanoclusters (gray spheres), β-casein (blue), para-κ-casein (green) and the caseinomacropeptide chains (black) (Dalgleish and Corredig, 2012) (Page 455, Figure 3).

The casein micelle does not have a homogeneous κ-casein layer at the surface (Figure 1.5), but a relatively open surface structure with gradually decreasing density, which makes the micelle interior easily accessible so that up to 3.7 g hydrate water (McMahon and Oommen, 2008), can be absorbed into the structure. This renders the casein micelle compressible, which is an important aspect with regard to the structural behavior of the deposited layer comprised of casein micelles. Dalgleish and Corredig (2012) mentioned water channels or permeable regions in the structure of the micelles so that water and small molecules like β-casein can diffuse out and into the micelle, e.g., during cooling and heating. Therefore, the casein micelle has to be considered more as a soft, compressible, and permeable sponge-like sphere with a higher amount of water than an inert round particle.

This view is also supported by the research results of Bouchoux et al. (2009a). These authors could show that at a casein concentration above 178 g L^{-1}, the micelles are packed closer, become dehydrated, and start to aggregate. A gel-like structure was formed due to high osmotic stress (Bouchoux et al., 2010). At lower casein concentrations, the hairy layer prevents the casein micelles to aggregate due to their steric repulsion. Commonly, such high casein concentration would not be expected during skim milk MF, but due to the accumulation directly at the membrane surface, casein concentration higher than 178 g L^{-1} could be reached in the deposit layer, thus reducing water permeation and whey protein transmission, which will be discussed later.

1.2.2 Whey proteins

Besides the casein fraction, the other main protein fraction in bovine milk is the so-called whey protein consisting of β-lactoglobulin (β-lg), α-lactalbumin (α-la), bovine serum albumin (BSA), immunoglobulins (IgG, IgA, and IgM), lactoperoxidase (LPO) and minor amounts of other proteins. In contrast to the caseins, the whey proteins are much smaller with a particle size ranging from 2 to 8 nm (Fig. 1.3). In milk MF, it would theoretically be expected that whey proteins could pass the membrane to 100% due to their low particle size relative to the membrane pore size. However, the layer of retained casein micelles produces a dense structure with its own retentive effect in addition to the membrane.

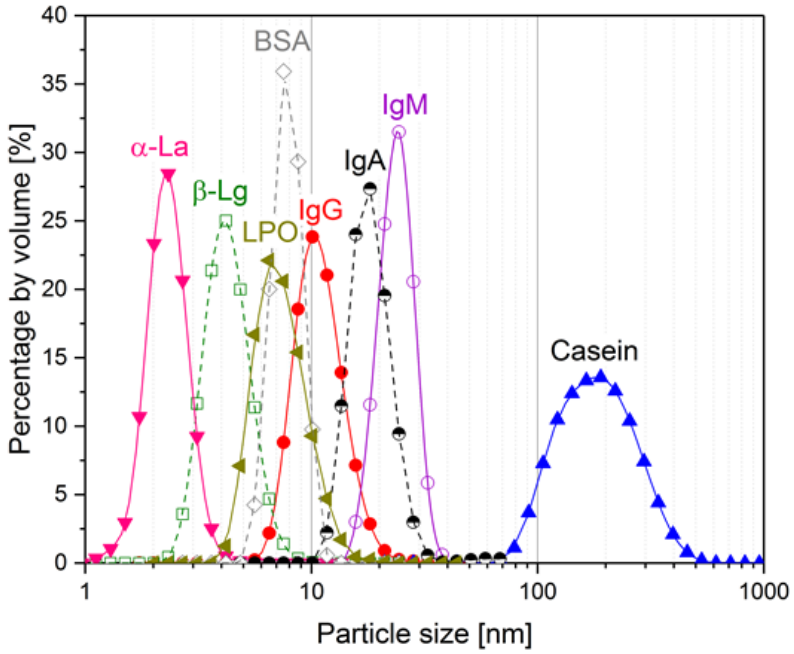

Figure 1.6. Particle size distribution of native whey proteins and casein micelles (Heidebrecht and Kulozik, 2019) (Page 5, Figure 2).

The separation results between caseins and whey protein, however, also depend on the ionic and pH environment, which are influencing the whey protein structures and size as well as their interaction potential with other proteins of the same of different protein species. β-lg (Figure 1.7 A) is the major protein fraction of the whey proteins (50%) made up of 162 amino acids, a molecular weight of 18.3 kDa, an isoelectric point of pH 5.2, two internal disulfide bridges stabilizing the globular structure and a free reactive SH-group able to create disulfide bonds with other proteins (Töpel, 2016). β-lg provides some genetic variants, e.g., β-lg A and B (Kontopidis et al., 2004), and different quaternary structures dependent on temperature and pH (Belitz et al., 2008). At pH 5.5-7.5, β-lg is a dimer, at pH 3.5-5.5 an octamer, and at pH<3.5 or pH>7.5 a monomer, which can affect the separation by size. At temperatures above 40 °C, β-lg has only a monomeric form (Belitz et al., 2008). These conformational changes could

increase the reactivity of β-lg with other proteins, mainly the κ-casein binding on the micelle surface, due to the exposure of the reactive free sulfhydryl group (Tolkach and Kulozik, 2007). If β-lg is bound to the casein micelle surface, the interaction between casein micelles would be reduced, leading to a less compact deposit layer.

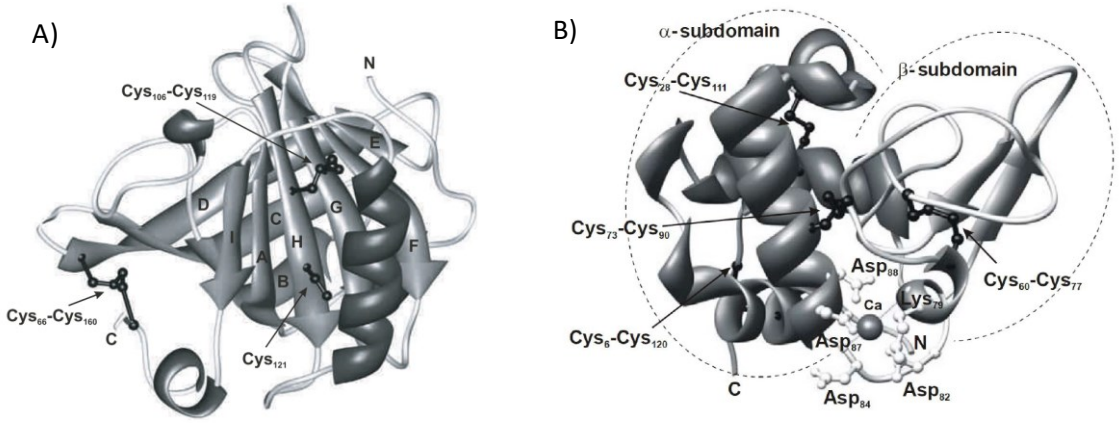

Figure 1.7. A) Molecular structure of β-lg (Tolkach and Kulozik, 2007) (Page 303, Figure 1). B) Molecular structure of α-la (Tolkach, 2007) (Page 10, Figure 2.2).

α-la (Figure 1.7 B) is the second largest protein fraction of the whey proteins (12%) made up of 123 amino acids, a molecular weight of 14.2 kDa, an isoelectric point of pH 4.8, four stabilizing disulfide bridges, and a bound calcium ion (holo form) for stabilization of the globular structure between two domains of the molecule (Töpel, 2016).

1.3 Fouling phenomena and deposit layer formation

1.3.1 Concentration polarization

During filtration, the flux convectively transports particles towards the membrane. Particles smaller than the pore size could theoretically permeate through the membrane into the permeate. Lager particles are rejected by the membrane and concentrated at the membrane surface despite the removing hydrodynamic forces. This effect is called concentration polarization (Zydney and Colton, 1986). Figure 1.8 shows a model of concentration polarization in crossflow mode filtration and the related potential fouling at the membrane surface.

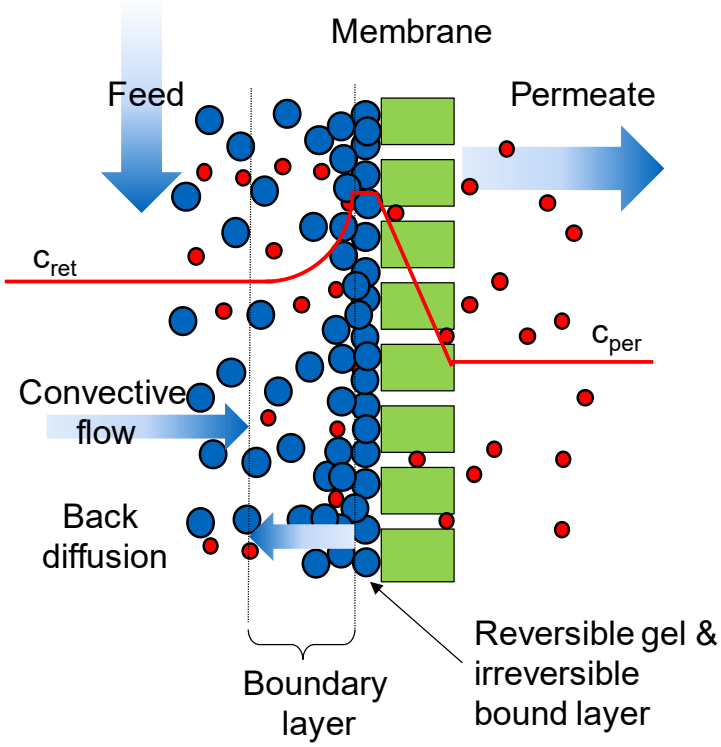

Figure 1.8. Model of the concentration polarization and the fouling at the membrane surface (adapted from Goosen et al. (2005) (Page 39, Figure 1)).

Due to the convective flow towards the membrane, the particles will to some extent be deposited on the membrane surface and fouling as well as deposit layer formation will occur. Since laminar flow conditions occur near the membrane, the back diffusion ($\dot{m}_{back}$) from the membrane takes place as Brownian motion in correlation to the concentration gradient in the boundary layer (Equation (1.17)):

$$\dot{m}_{back} = -D \cdot \frac{d\, c_{i,ret}}{d\, \delta_{lam}} \tag{1.17}$$

The diffusion coefficient (D) is determined as the ratio of the thermal energy $k_B \cdot T$ with the friction of the particle and can be calculated according to the Stokes-Einstein-equation (Equation (1.18)):

$$D = \frac{k_B \cdot T}{6 \cdot \pi \cdot \eta \cdot d_p} \tag{1.18}$$

with the Boltzmann constant (k_B) and the absolute temperature (T). The diffusion will decrease by increasing d_p and it mainly affects only particles with a size below 100 nm (Baruah and Belfort, 2003). Regarding milk filtration, casein micelles with a size of $d_{50,3}$ = 182 nm (Heidebrecht and Kulozik, 2019) would not be much affected by the back diffusion. According to Ripperger and Altmann (2002), larger particles influenced by the hydrodynamic interactions during crossflow filtration are deposited less on the membrane surface. However, casein micelles would consequently not be significantly influenced by both effects, back diffusion or the hydrodynamic interactions, due to the particle size (Figure 1.9).

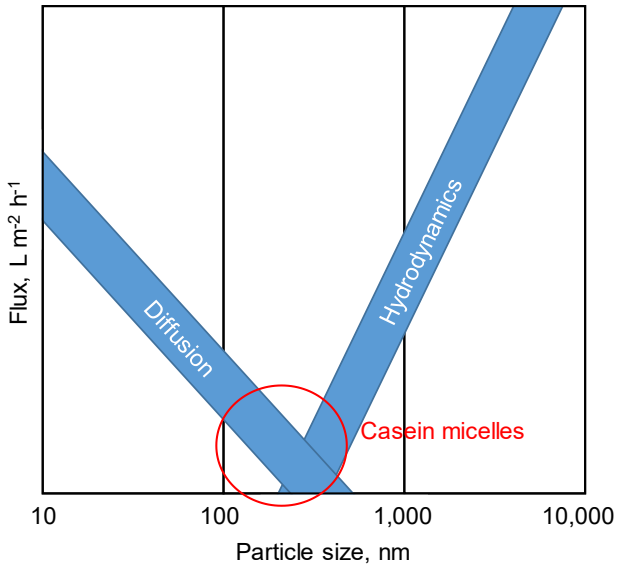

Figure 1.9. Flux as a function of the particle size, the influence of the diffusion and hydrodynamic interactions on the particle deposition during filtration, and the marked area of the range of the casein micelles particle sizes (adapted from Ripperger and Altmann (2002) (Page 22, Figure 9)).

Thus, the deposition of the micelles on the membrane surface will take place and fouling will be the main issue. When steady-state conditions are reached, the back diffusion and the permeation through the membrane will be in dynamic equilibrium. The mass transfer can be calculated according to Equation (1.19):

$$J \cdot c_{i,ret} - D \cdot \frac{d\, c_{i,ret}}{d\, \delta_{lam}} + J \cdot c_{i,per} = 0 \tag{1.19}$$

The concentration of the particles increases from the feed solution ($c_{i,ret}$) towards the membrane in the boundary layer reaching its maximum directly at the membrane surface, where a reversible gel layer and an irreversible bound layer are formed (Figure

1.8). The slope of the concentration increase depends on the filtration process conditions and thus on the intensity of fouling.

1.3.2 Effect of membrane fouling on flux and retention

Next to the membrane, fouling layers have a second filtration resistance with an additional retention effect, which reduces whey protein transmission in the case of milk microfiltration. The R_F is the sum of the membrane resistance (R_M) and deposit layer resistance (R_D) according to Equation (1.20):

$$R_F = R_M + R_D \tag{1.20}$$

R_D leads to a flux decline according to Equation (1.2). If fouling occurs, there will be a change in the filtration characteristics of the membrane (Figure 1.10).

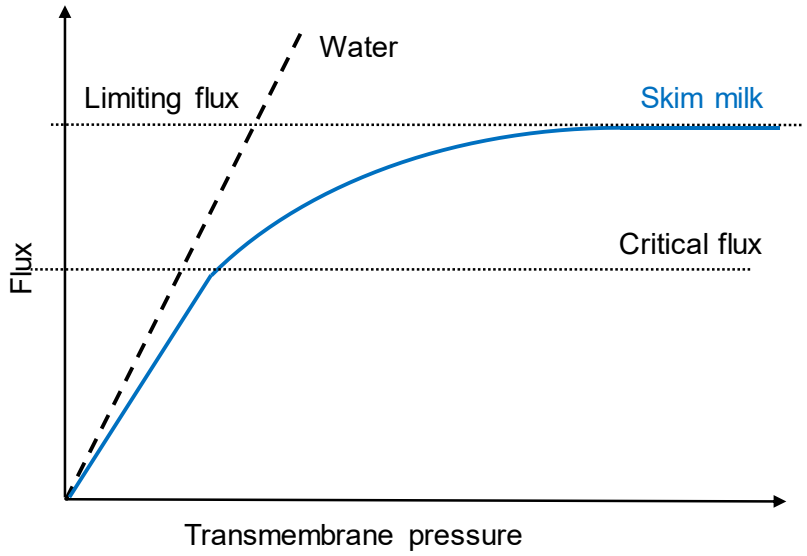

Figure 1.10. Flux as a function of the Δp_{TM} for pure water and skim milk (adapted from Bacchin et al. (2006) (Page 45, Figure 3)).

The flux of skim milk at first increases linearly by increasing Δp_{TM} until the so-called critical flux (or better: the critical transmembrane pressure) is reached (Bacchin, 2004). Up to this point, membrane-based filtration conditions prevail. Then, the fouling increases and the deposit layer resistance influences the filtration behavior more and more. Increasing Δp_{TM} leads to an increase in flux and thus to an increase in the drag forces towards the membrane. Thus, more deposition and fouling occurs. The flux levels off and reaches a limiting value, the so-called limiting flux (Field et al., 1995). The flux is independent of the Δp_{TM}. The filtration behavior mainly depends on the fouling intensity. A further increase of Δp_{TM} will be compensated by the fouling layer (which is compressible in the case of hydrated casein micelles forming the deposit) and the flux stays constant.

Astudillo-Castro (2015) described an exponential model to predict the critical and limiting flux during skim milk MF. However, this model is limited because the flux does not start directly at the origin, but at a higher, minimal Δp_{TM} value (Astudillo-Castro et al., 2020). The authors attributed this to the fact that in skim milk MF, some Δp_{TM} needs to be applied to achieve permeate flux. This is not surprising, since the membrane resistance and the concentration polarization must be overcome to achieve permeate flux according to Equation (1.2).

1.3.3 Fouling mechanisms

The mechanism and the degree of fouling are mainly influenced by the particle size and charge, the membrane properties, e.g., material or pore size distribution, the hydrodynamic conditions, and the geometry of the membrane module (Cui et al., 2010). The literature describes several fouling mechanisms. Four main different blocking mechanisms for particle filtration, better known as the blocking filtration law of Hermia (1982), can be distinguished (Figure 1.11).

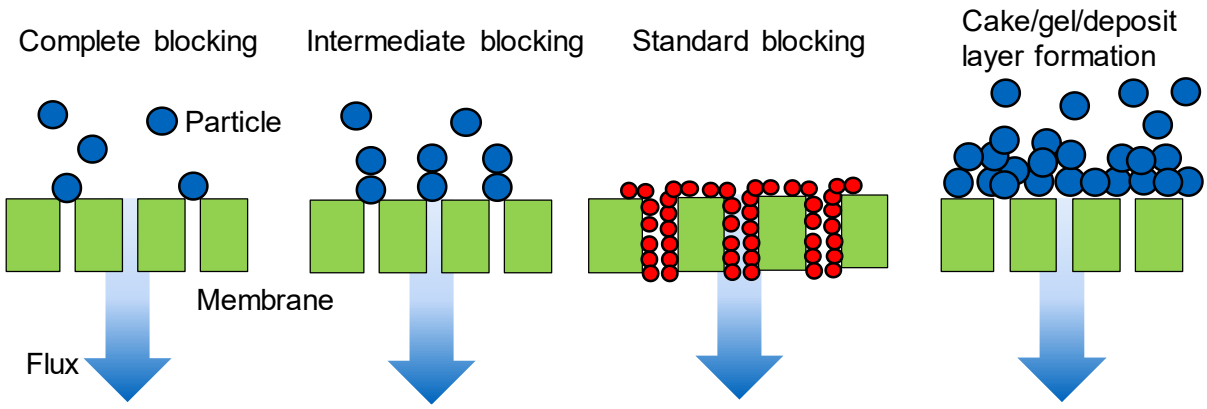

Figure 1.11. Fouling mechanism for pore blocking (adapted from Iritani (2013) (Page 147, Figure 1).

For fouling effects at the surface, there are different models (Kimura and Sourirajan, 1967; Vilker et al., 1981; Zydney and Colton, 1986) than for pore blocking and/or pore constriction (Hermans and Bredée, 1935; Hermans et al., 1936; Grace, 1956; Hermia, 1982), deposit layer formation (Shirato et al., 1979; Reihanian et al., 1983; Chudacek, 1984), and solute adsorption (Iritani et al., 1991). The complete blocking and the intermediate blocking describe the pore plugging due to particles reaching the top surfaces of pores. During complete blocking, the probability of blockage during filtration is constant. The number of blocked pores is directly proportional to the filtrate volume. The particles are not superimposed on each other. Pore blockage occurs especially at the start of the filtration when the membrane is clean and no particles are deposited on the membrane surface. In intermediate blocking, the particles settle on other particles. The pore blockage rate is proportional to the number of open pores. After an initial phase,

complete and intermediate blocking would not play a major role anymore compared to the deposit layer formation (Iritani et al., 2015) since skim milk is a particle-rich solution. The particles in skim milk, mainly casein micelles, will block the pores in a few minutes and deposit on the whole membrane surface.

The standard blocking deals with the pore constriction caused by the deposition of particles onto the pore wall. The particle diameter is smaller than the pore size. Solid-liquid separation occurs owing to the deposition of particles on the pore wall. The pore narrows as filtration progresses and the pore volume decreases in proportion to the filtrate volume per membrane area. The filtration rate decreases as the pore size decreases. Regarding milk filtration, the small whey protein could mainly interact on the pore wall. However, Zulewska and Barbano (2013) could show that pore narrowing by whey proteins is not the main driver of fouling in skim milk MF.

A fouling layer is composed of the particles or molecules accumulating on the membrane. Particles are deposited on the membrane surface. Concerning skim milk filtration, the main fouling mechanism is deposit layer formation by casein micelles on the membrane surface. Nevertheless, the other mechanisms will also occur during filtration.

1.3.4 Gel and deposit layer formation

Regarding deposit layer formation during skim milk filtration, the deposit layer mainly consists of casein micelles. Therefore, the deposit layer is more or less porous and compressible. However, the structure of the deposit layer could be influenced by several factors, e.g., feed protein concentration, resistance and charge of the membrane, and flow properties like crossflow velocity, wall shear stress, and transmembrane pressure. In the following, some of the recent key results regarding the structure of the deposit layer are discussed.

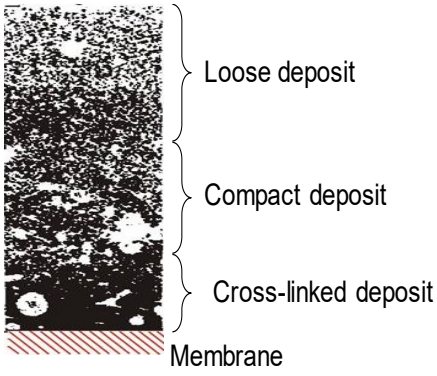

Figure 1.12. Electron micrographs of a deposit layer during dead-end RO (adapted from Glover and Brooker (1974) Page 94, Plate 1).

Glover and Brooker (1974) investigated the deposit layer structure during dead-end RO by electron microscopy showing an 11 nm thick, continuously dense, cross-linked deposit directly adjacent to the membrane following an electron-lucent zone with a compact deposit of 10–15 nm to a main bulk of loose deposit, which is 30 µm (Figure 1.12). The density of the packing of the granules increases with proximity to the membrane. France et al. (2021b; 2021a) summarized the effect of the filtration temperature on flux, transmission, and thus, deposit layer formation where they could show that

at high processing temperatures like 55 °C, a more intensive deposit layer formation takes place compared to low processing temperatures around 10 °C. Piry et al. (2012) could show that the flux decreases with increasing membrane resistance, but whey protein transmission increases. They think this is caused by a less intensive and less compact deposit layer formation when filtrating with membranes with increased membrane resistance. In the initial phase, the drag forces are reduced and thus, fewer proteins will be deposited on the membrane surface and they will be less compacted due to the lower flux values (Kühnl et al., 2008).

Moreover, Kühnl et al. (2010) reported that acidification of the skim milk from pH 6.8 to 5.9 and the associated reduction in repulsion between the micelles result in a significantly more compact deposit layer with lower porosity. This results in flux reduction. Also, Beckman et al. (2010; 2013) could show that flux is reduced with increasing interactions of the casein micelles. They concentrated the feed to higher protein concentrations and thus the concentration at the membrane surface was also higher, which led to significant flux reduction. But Hartinger and Kulozik (2020) explained the effect of increased protein concentration on the deposit layer formation with an increase in deposit layer height instead of increased compaction since the flux is decreased but the whey protein transmission stays constant. This conforms to the results of Bouchoux et al. (2009b), who reported that casein micelles become more densely packed before they are compressed due to their dewatering. This micelle dewatering will lead to the collapse of the micellar structure and the deposited caseins form a gel-like layer (Bouchoux et al., 2010).

Qu et al. (2012; 2015) reported that the compressed, dewatered casein micelles forming a gel layer are responsible for flux reduction and that the gel layer has a retention effect on whey protein transmission due to increased fouling resistance. The formation of a gel layer is stabilized by hydrophobic and electrostatic interactions. Therefore, the critical osmotic pressure was calculated at 0.35 bar, which is responsible for the formation of the irreversible gel layer (Qu et al., 2012). Bouchoux et al. (2014) described that the osmotic pressure (Π) increases in the deposit layer towards the membrane surface. In contrast, the feed pressure (P) is reduced during the flow through the deposit layer due to frictional losses, in the same range as the increase of Π (Figure 1.13).

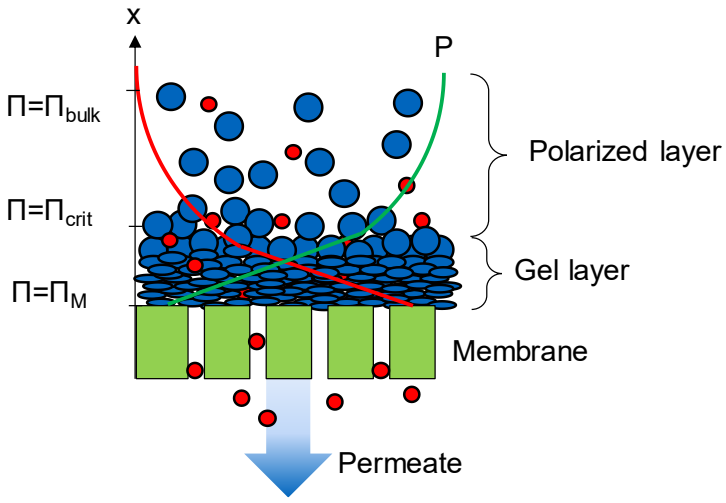

Figure 1.13. Model for gel layer formation. The increase of osmotic pressure (Π) from the bulk solution through the deposited casein micelles to the membrane and the corresponding decrease of the feed pressure (P) (adapted from Bouchoux et al. (2014) (Page 23, Figure 1).

It can be seen in Figure 1.13 that the effect of gel layer formation will increase too, when Δp_{TM} increases, and this will have a negative effect on whey protein transmission. Schiffer et al. (2020) could show that the intrinsic structure of the deposit layer is changed at high Δp_{TM} and that these changes are irreversible. Thus, the highest applied transmembrane pressure defines the structure of the deposit layer and thus the filtration efficiency (Schiffer et al., 2020).

Hartinger et al. (2020c) reported an increase in flux and whey protein transmission by increasing crossflow velocity. They explained their findings with a less intensive deposit layer and higher wall shear stress leading to less intensive concentration polarization. However, this effect is limited. Schiffer et al. (2020) could identify a critical τ_w where the flux is maximized and a limiting τ_w where no further changes in flux and thus no structural changes in the deposit layer occur.

1.4 Membrane modules and flow properties

There are many different types of membrane modules. Many requirements must be considered in module development: mechanical, chemical, and thermal stability, high packing density, uniform distribution of flow across the module, high solids loading capability, low-cost manufacturing, good cleaning capability, and low pressure drops (Melin and Rautenbach, 2007). However, not all membrane modules exhibit these requirements and compromises are made. The milk processing industry mainly uses two different types of membranes: CTM and SWM.

1.4.1 Ceramic multichannel tubular membranes

The filtration direction is inside-out so that the feed flows through the channels and the permeate flows in the radial direction through the membrane to the outside (Figure 1.14). CTM consist of a support and a selective layer. The selective layer with a maximum thickness of 2 µm (Baker, 2008) has the required pore size distribution for separation and is located on the inside of the channels. The supporting layer has larger pores and stabilizes the membrane module.

The selective layer material can be made of different materials like Al_2O_3, TiO_2, and ZrO_2. The manufacturing processes are described by Mulder (1996) and Cheryan (1998). Schiffer et al. (2021) investigated the effect of different selective layers on the flux and whey protein transmission during skim milk MF. They reported a flux decrease by increasing Δp_{TM} for Al_2O_3 and TiO_2 after reaching the limiting flux due to an increased fouling resistance. Moreover, when comparing CTM with different pore sizes from 0.05 to 0.2 µm, Jørgensen et al. (2016) reported that the pore size distribution is the main point of filtration performance in terms of whey protein transmission.

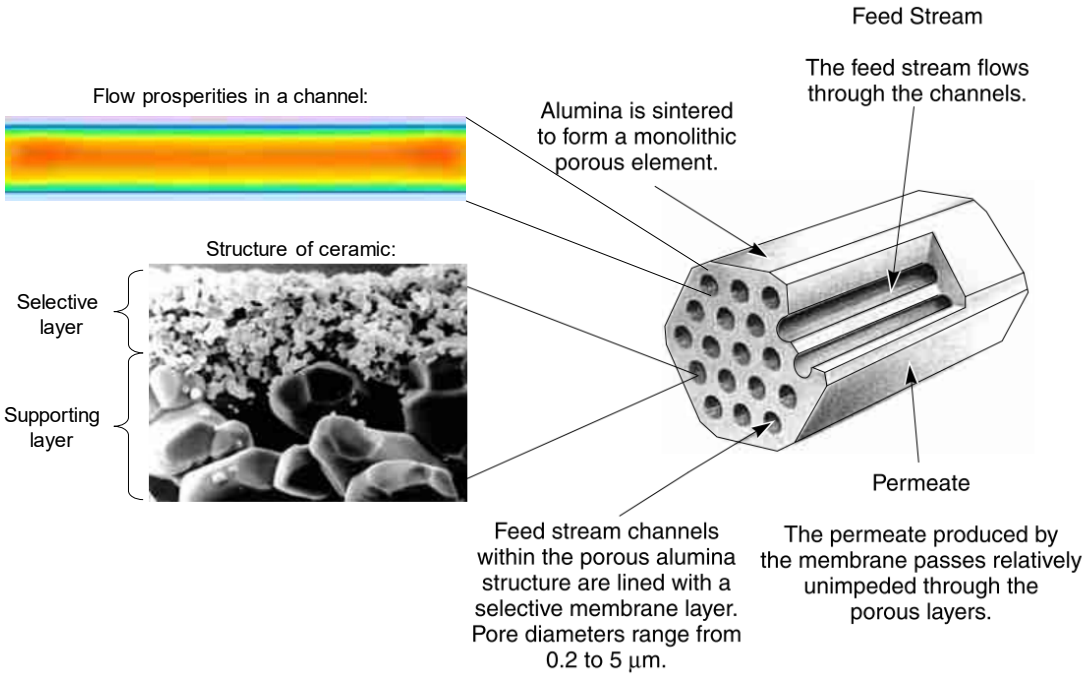

Figure 1.14. Schematic illustration of a CTM element (Baker, 2008) (Page 130, Figure 3.30) with the flow properties in a channel via computer fluid dynamics (Kavianipour et al., 2017) (Page 25, Figure 13) and a scanning electron micrograph of the selective and the supporting layer (adapted from Baker (2008) (Page 130, Figure 3.30)).

There are several pro- and counter-arguments for CTM. Due to the ceramic material, CTM have high resistance against harsh operation and cleaning conditions like sterilization or low pH acidic cleaning. However, due to the high-temperature sintering process (up to approx. 1400 °C) of the ceramic, manufacturing costs are energy extensive. CTM have a clearly defined flow geometry, but the flow conditions are not equally distributed (Figure 1.15).

Due to their simple geometry, CTM have no dead flow spots and thus are easy to clean. Moreover, according to Bottino et al. (1994), CTM can be considered to be hydraulically smooth. Thus, Equation (1.8) for τ_w and Equation (1.9) for Δp_L can be applied. Due to the large free cross-sections, the Δp_L in CTM is low and a high feed volume flow per membrane area has to be attained to reach high crossflow velocity. However, the low packing density leads to the necessity of connecting several CTM modules in series. The deflections and the cross-sectional jumps from the inlet and outlet of the modules contribute more to the Δp_L than the individual membrane tubes themselves and therefore mean a significant increase in energy demand (Melin and Rautenbach, 2007).

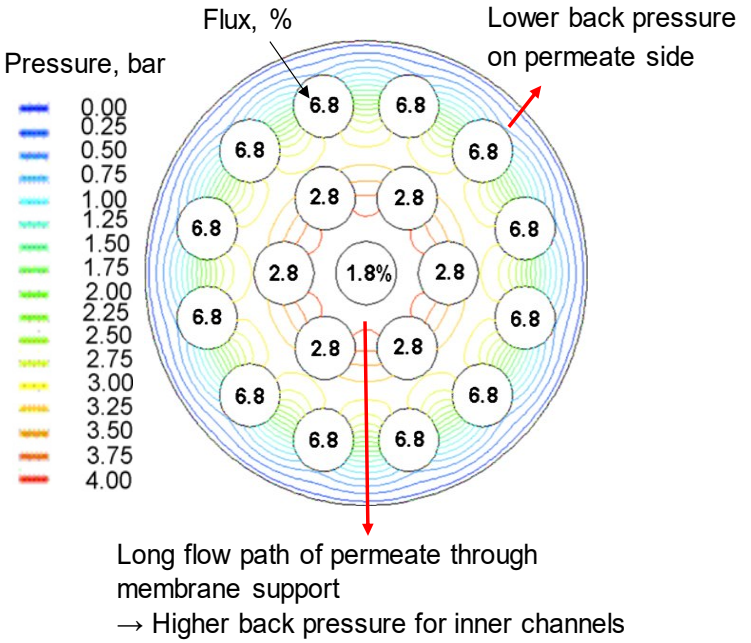

Figure 1.15. Illustration of the permeate pressure and flux distribution of a 19-channel membrane (adapted from Ghidossi et al. (2010) (Page 489, Figure 13)).

The filtration performance of CTM can be influenced by varying the membrane geometry. Different channel cross-sectional shapes (Springer et al., 2010) can be used or the number of channels (Hurt et al., 2015b) can be varied to improve flux and transmission. Adams et al. (2015a) reported a better control of deposit formation and an increase in flux due to increased shear forces when comparing diamond-shaped with round-shaped channels. Astudillo-Castro (2015) showed an increase in the limiting flux by decreasing the channel diameter of CTM. If the channel diameter is reduced while the outer module diameter stays the same, the membrane surface will increase. Ghidossi et al. (2006) could show that an increase in membrane area will lead to more permeate volume flow for water filtration. Adams and Barbano (2016) compared a 6 mm with a 4 mm channel membrane and showed that the module can be operated at a different pressure drop and crossflow velocity. However, not only the flow properties on the feed side are quite important, but the permeate side also has to be considered. The effect of backpressure on the permeate side on flux and protein transmission varies depending on the number of channels and their position with the tubular bundle (Figure 1.15), which was assessed for water filtration by computational fluid dynamics by Ghidossi et al. (2010). There is an uneven water flux distribution between the individual channels in a CTM. This distribution depends on the distance between the channels and the outer rim of the module. Owing to the longer permeate flow path from the inner channels to the edge of the module element, the contribution of the inner channels to the total flux was lower than that of the outer channels. Thus, the backpressure was higher and, therefore, Δp_{TM} and the flux of the inner channels decreased (Ebrahimi et al., 2018).

1.4.2 Spiral wound membranes

An alternative to CTM are polymeric SWM. The module architecture of SWM is more complex. One or more membrane pockets with spacer nets in between are fixed and wound around a perforated central permeate collection tube (Figure 1.16).

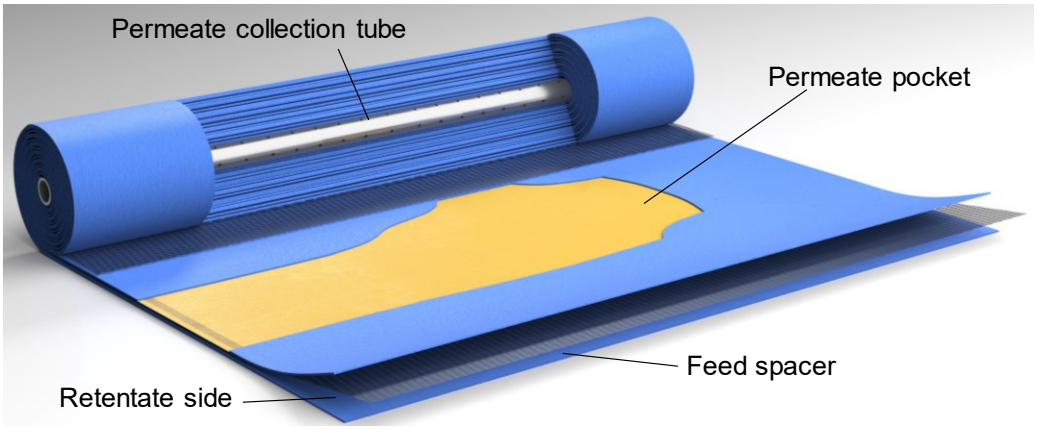

Figure 1.16. Illustration of a SWM (adapted from Hartinger et al. (2019b) (Page 8, Figure 5)).

Feed spacers cause turbulence even under nominally laminar flow conditions. Geraldes et al. (2002) investigated the flow properties in SWM caused by the spacers and showed a critical Reynolds number in the range of 100-150, dependent on spacer geometry. Permeate spacers keep a flow path open for the permeate towards the central collection tube. At the front and rear part of the module, the SWM is stabilized by anti-telescoping devices, which prevent the membrane sheets to shift under the influence of friction exerted by feed flow through the module (Baker, 2008).

However, SWM provide a high membrane area per module volume, the so-called packing density (Θ), which can be calculated as a ratio of A_M and the module volume (V_{Mod}) (Equation (1.21)):

$$\Theta = \frac{A_M}{V_{Mod}} \tag{1.21}$$

SWM are made of polymeric membranes, which are less energy extensive during production and have fewer acquisition costs compared to ceramic membranes (Melin and Rautenbach, 2007). Nevertheless, owing to the complex geometry there are no free cross-sections and the flow conditions within the module between the membrane sheet layers are inhomogeneous. This leads to an increased Δp_L and an enhanced deposit layer formation behind the spacer net filaments, which are difficult to clean. Furthermore, SWM are limited in applying higher levels of crossflow velocity and the Δp_L due to axial friction forces, which would displace the membrane sheets from each other, the so-called telescoping. Due to the mechanical stability, SWM should be used up to an Δp_L of 1.3 bar m^{-1} (Hartinger et al., 2020c).

Moreover, SWM are difficult to clean and provide flow dead spots. Fouling is the main issue in SWM (Hartinger et al., 2019a). There are areas opposite the spacer filaments that have high crossflow velocities, but also areas with lower overflow velocities (Kavianipour et al., 2017). These areas are caused by the spacer geometry (Figure 1.17). In some cases, higher crossflow velocities and turbulence occur directly at the membrane, leading to different wall shear stresses (Koutsou et al., 2013) and to increased deposit layer removal. However, there is an inhomogeneous deposit layer formation on the membrane surface (Hartinger et al., 2020a).

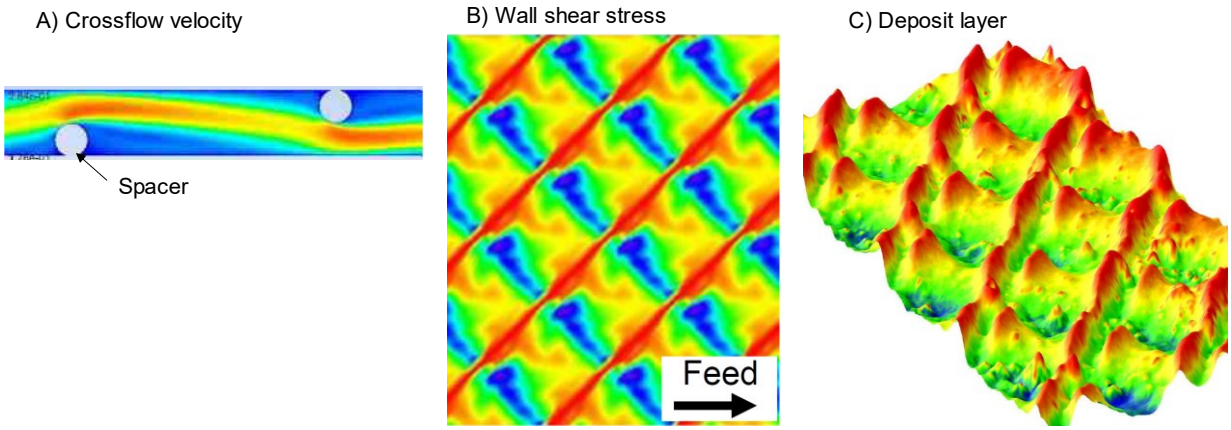

Figure 1.17. A) Crossflow velocity on the feed side via computational fluid dynamics (Kavianipour et al., 2017) (Page 25, Figure 13). B) Wall share stress distribution at the diamond spacer filaments via computational fluid dynamics (Koutsou et al., 2009) (Page 243, Figure 11). C) Deposit layer formation with diamond spacer filaments via topographic imaging (Hartinger et al., 2020a) (Page 10, Figure 7).

1.4.3 Hollow fiber membranes

A possible alternative to the commonly used CTM and SWM are HFM, as they combine the advantages of both membrane systems, including a large membrane area per module, good cleanability, free crossflow sections, low manufacturing cost, small energy expenditure during operation, and high separation efficiency (Baker, 2008). Therefore, HFM are in many applications the membrane system of choice and widely used in the industry for different purposes, e.g., as bioreactors in the cell culture process (Careri, 2005; Lehmkuhl et al., 2018), as medical devices in blood dialysis (Yamamoto et al., 2005), or as contactors in gas stripping (Luhr, 2016). Moreover, HFM are used for liquid-liquid or solid-phase micro-extraction (Zhu et al., 2002; Basheer and Lee, 2004).

In the food industry, HFM are also commonly used in MF, UF, NF, or RO applications, e.g., for drinking water production (Cano et al., 2012; Panglisch et al., 2019), waste water filtration (Ebrahimi et al., 2015), juice clarification (Kirk et al., 1983), and beer and wine filtration (Cimini and Moresi, 2016). However, HFM have not gained

acceptance in the dairy industry. Thompson and deMan (1975) and Garoutte et al. (1982) reported the use of UF HFM for skim milk concentration showing an increase in protein content. Cheryan and Kuo (1984) reported on the UF of cheese whey using HFM and showed a higher energy input compared to SWM. Patel and Reuter (1985) showed during skim milk UF that caseins are primary foulants. Pouliot et al. (1993) reported on the fractionation of casein hydrolysate via UF HFM. However, MF HFM has not been investigated yet with the purpose of milk protein fractionation.

Compared to CTM, ceramic HFM have the advantage that their packing density/module volume is higher and more membrane area can be installed per module. In addition, the sintering process (temperatures up to 2000 °C) used to manufacture HFM takes only about one day due to the smaller wall thickness, whereas it takes about 4-7 days for the manufacture of CTM (Melin and Rautenbach, 2007). This results in 3-4 times lower energy costs for the production of HFM. The bundling of the HFM requires only one additional work step so that the costs are approx. 20-30% lower compared to CTM multi-channel elements (Baker, 2008). In addition to these lower investment costs, the reduced membrane resistance due to the smaller wall thickness is important, i.e., a lower flow rate is required to achieve a certain Δp_{TM}. Service life extensions can be achieved by backflushing for a short time and thus periodically removing the deposit layer. More effective cleaning from the outside to the inside (backflushing) is possible, which allows shortening of cleaning cycles and enables longer production cycles (Wiese et al., 2019).

For polymeric HFM, the production methods have been improved in recent years, so that it is now possible to produce a defined and narrow pore size distribution of the membrane within the range of 0.1-1 µm, which is essential for targeted protein separation by size using MF. Another reason for the dominance of CTM and SWM in the field of MF in the dairy sector is that HFM were originally used for lower viscosity substrates, e.g., water, and therefore only small inner diameters < 1 mm were available, which are less suitable for more viscous fluids such as milk. In terms of membrane area per module, e.g., 30 m²/0.047 m³, and area-specific costs, HFMs are superior to ceramic membranes.

HFM were first developed by Mahon (1966). Reviews about the development of HFM are given by Baum et al. (1976), Moch (1995), and McKelvey et al. (1997). The single fibers with a diameter of 50-3,000 µm are put together to form a bundle and glued at both ends into a pressure tube, the so-called potting, forming a membrane module (Figure 1.18).

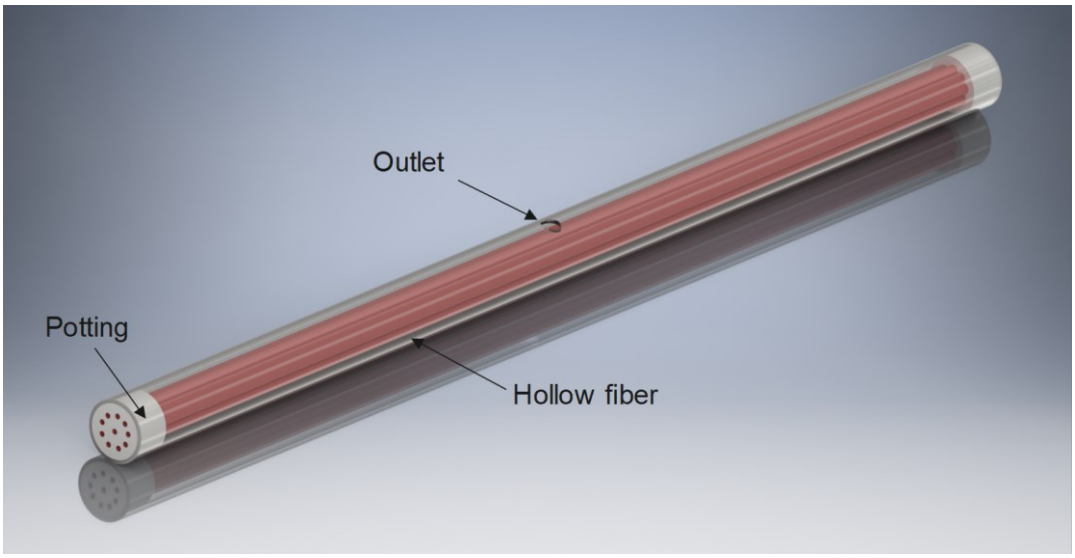

Figure 1.18. Schematic illustration of a lab-scale hollow fiber membrane module with ten hollow fibers.

Quality control has to ensure that the module contains no broken or defective fibers. Ceramic HFM were produced like CTMs (Baker, 2008). Typically, only two processes are used to produce polymeric HFM: solution spinning and melt spinning (Luelf et al., 2016). Solvents and other additives can be added to the spinning so that the polymerization can be better controlled and flux will be increased. The typical polymeric materials are polyether sulfone (PES) and polyvinylidene fluoride (PVDF).

Depending on the inside-out or the outside-in direction of the filtration, the selective layer is either on the inside or the outside of the fiber (Figure 1.19). A good overview of outside-in filtration with submerged HFM is given by Akhondi et al. (2017).

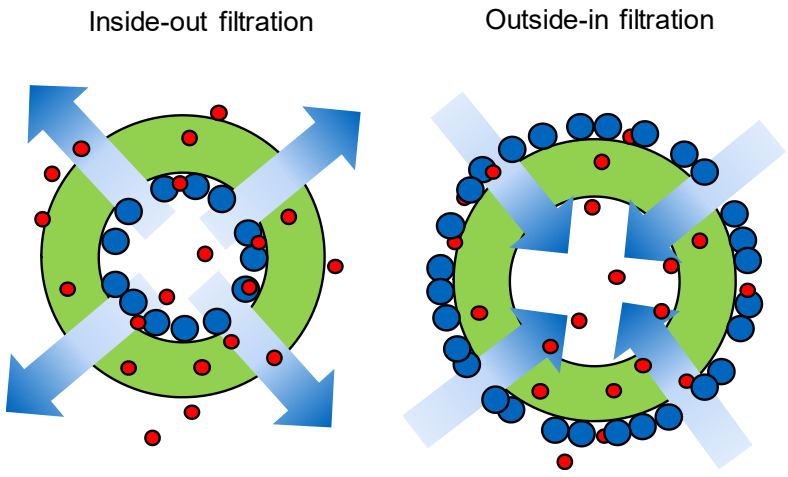

Figure 1.19. Filtration direction seen in cross-section with deposit layer formation.

The advantages of inside-out filtration are the better-controlled fouling due to the open cross-section and the controlled hydrodynamic conditions. However, the downside is that the active membrane area based on the inner diameter is much smaller than the one based on the outer diameter (Xu et al., 2017). The advantages of outside-

in filtration are that the feed can contain a high amount of solid particles and the filtration area per module is higher compared to inside-out filtration. However, due to the hydrodynamic conditions for outside-in filtration, the hollow fiber bundle is more affected by fouling and thus, more difficult to clean compared to inside-out filtration.

Deposit layer formation is also an issue in HFM for all feed systems (Laksono et al., 2020). Several aspects can be optimized for better filtration performance. Yeo and Fane (2005) reported that due to the hydrodynamics, the arrangement of a single fiber within a module has a high impact on flux and transmission. Chang and Fane (2001) showed that the effect of the fiber diameter on the flux with submerged hollow fibers increased with the increase in turbulence around the fibers. These effects are taken up and a model for the prediction of flux is given by Yoon et al. (2004) for outside-in water filtration. Based on this, Kuhn and Briesen (2021) determined the length-dependent filtration in submerged HFM and optimized fiber diameter and length. Xu et al. (2017) proved a model for optimization of the HFM wall thickness during direct flow mode for water filtration.

However, not only fiber diameter, length, and wall thickness are important factors influencing filtration performance, but flow behavior in the inner side of a HFM can be influenced, too. Laukemper-Ostendorf et al. (1998) investigated the flow behavior by NMR showing the spatial flow-velocity distribution, but the experiments were only carried out at velocities of up to 5 cm s^{-1}. Some examples to influence the feed flow behavior are concentric rods bearing various geometries (Yeh, 2000), helical rod structure (Broussous et al., 2000), and helical baffle (Horie et al., 2018). Luelf et al. (2017) suggested sinusoidal shaped HFM, which would increase mass transfer by gas-liquid contacting experiments. In contrast to this, Armbruster et al. (2018) increased HFM wall thickness by inserting 3D-printed mixer geometries which affect fouling and improve the flux during filtration with humic acid. Wiese et al. (2019) reported that they have polymerized a helix in the inner side of a HFM. This should serve as a flow breaker and lead to an increased turbulence inside the fibers. Thus, fouling could be counteracted. Schork et al. (2021) could visualize the deposit layer formation of a helical ridge HFM by compressed sensing magnetic resonance imaging (MRI) during crossflow filtration. However, the effect of an increased shear rate on the deposit layer and its abrasive effects along the helical ridge could not be assessed.

1.5 Concepts of the membrane process and analytical methods

1.5.1 Industrial membrane processes: feed-and-bleed and diafiltration process

In industrial-scale applications, milk protein separation requires the use of several modules, operated in stages with several modules per stage to achieve required throughputs, product qualities, and yields. Several membrane modules are put into series and parallel connections. A part of the feed flow is recirculated in a loop system to achieve the required crossflow conditions before the next loop system is reached, the so-called feed-and-bleed process (Figure 1.20). The number of loops, as well as the number of membranes per loop, can be varied according to the required product qualities and yields. Membrane modules can vary in membrane length and module diameter.

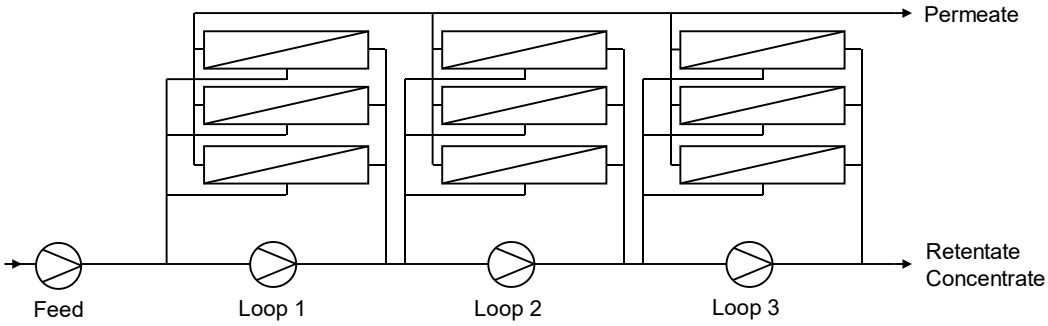

Figure 1.20. Membrane module arrangement for industrial milk protein fractionation in the feed-and-bleed process.

Due to the recirculation of a partial flow, the circuit feed volume flow and the module feed volume flow are not identical. The hydraulic conditions in the module can be adjusted with the recirculation rate, independently of the feed. The task of the feed pump is to pump the feed solution into the system and to provide the required pressure level for the whole system. In contrast to this, the loop pumps are required for maintaining the flow rate or the turbulent flow regime. Due to the friction effects, the Δp_{TM} in the front part is higher than in the rear part. Thus, several membranes operate outside of their Δp_{TM} optimum, leading to reduced filtration performance in terms of flux and whey protein transmission due to increased deposit layer formation. Usually, the first and the last loops are used for concentrating the skim milk and the middle loops are used for the DF process. The feed concentration is reached during the removal of permeate. The concentration factor (CF) is calculated as the ratio of the concentration of casein in the concentrate ($c_{cas,conc}$) against that in the native skim milk ($c_{cas,milk}$) (Equation (1.22)):

$$CF = \frac{c_{cas,conc}}{c_{cas,milk}} \tag{1.22}$$

However, during concentration, not enough whey proteins could be reduced to reach purities above 80% of the casein fraction. Therefore, filtration has to be carried out in the DF process. In Figure 1.21, the DF process is shown for a single filtration loop and the connection of an MF with an UF plant to use UF permeate as DF medium.

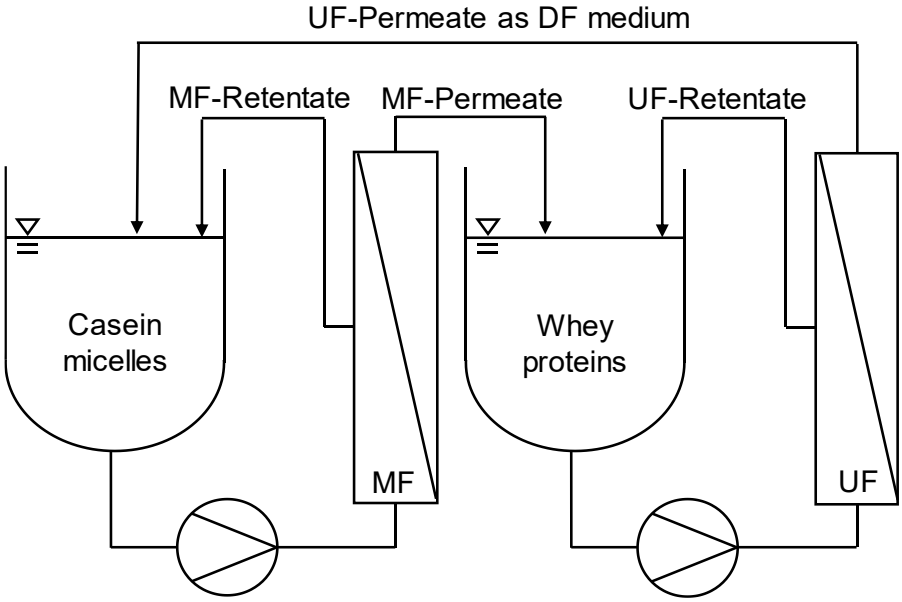

Figure 1.21. Filtration in diafiltration mode with a combination of MF and UF plants (adapted from Heidebrecht and Kulozik (2019) (Page 3, Figure 1)).

In the MF, caseins were retained and collected in the MF tank whereby whey proteins were washed out, permeated into the MF permeate, and collected in the UF tank. In order to gain UF permeate as DF medium, an UF is carried out whereby the whey proteins are retained in the UF retentate. The DF medium does not contain these components. In this particular case, the whey proteins are meant to be removed from the feed. However, not only UF permeate, but also water or milk serum can be used as DF medium to dilute the MF retentate and continuously wash out the whey proteins from the MF tank. This process is run until the target purity of the casein fraction is reached. One DF step corresponds to the addition of DF medium in the amount of the initial feed volume. The absolute level of protein decrease ($C_{DF,n}/C_{DF,0}$), is defined as a function of the transmission and the number of DF steps as the ratio of the total volume of the added DF medium ($V_{DF,n}$) against the initial hold-up volume ($V_{DF,0}$) according to Reitmaier et al. (2021) (Equation (1.23)).

$$\frac{C_{DF,n}}{C_{DF,0}} = e^{Tr_i \cdot \frac{V_{DF,n}}{V_{DF,0}}} \tag{1.23}$$

During the DF process, the filtration time (t) required to obtain one DF step at a target concentration level is defined according to Heidebrecht and Kulozik (2019) (Equation (1.24)).

$$t = \frac{V_{DF,0}}{Tr_i \cdot J_{CF}} \cdot ln\left(\frac{C_{DF,n}}{C_{DF,0}}\right) \tag{1.24}$$

1.5.2 Analysis of deposit layer formation

To investigate the accumulated deposits and their distribution on the membrane surface with regard to their chemical or structural properties, indirect or destructive techniques for qualitative and quantitative analysis are widely used (Chen et al., 2004a; Li et al., 2012; Suwal et al., 2015). However, if indirect or destructive techniques are applied, the filtration has to be stopped and the Δp_{TM} is reduced to zero. Changes in the height and the internal structure of the deposit layer are then expected, but the deposited layer is dissolved as a result of the relaxation for the ambient pressure. The open question is how pressure affects the behavior of the deposit's chemical composition and height. Moreover, *ex situ* measurements require the removal and destruction of the membrane in order to gain access to the deposited material.

In addition, some studies have been performed with the aim of qualitatively and quantitatively explaining the structure of the deposit (Delaunay et al., 2008; Ng et al., 2018; Hartinger et al., 2020a; Hartinger et al., 2020b; Weinberger et al., 2021). The correlation between the chemical analysis of the deposit layer and its height has not been well established yet. There are also a few studies about real-time *in situ* measurements summarized in Han et al. (2021). Delaunay et al. (2008) showed that the deposit layer height on UF membranes are around 100 µm via ATR-FTIR (attenuated total reflection - Fourier-transform infrared spectroscopy). Hartinger et al. (2020b; 2020a) reported an average of 5.6 g m^{-2} deposited caseins on flat sheet membranes analyzed by reversed-phase high pressure liquid chromatography (RP-HPLC). They dissolved the proteins, which were deposited and bound on the membrane by an insertion of the membranes into protein dissolving buffers. Moreover, they visualized the inhomogeneous deposit layer formation dependent on the structure of the spacer via false color and topographic images. However, this method is limited to a total protein concentration up to 10 g m^{-2}, which was already exceeded in the areas behind the spacer filaments. Weinberger et al. (2021) investigated the type of stabilizing bonds in casein micelle-based deposit layers by dissolving the deposit layer in different buffers. In contrast to Hartinger et al. (2020a), Weinberger et al. (2021) scraped the deposited proteins mechanically off from the membrane surface. However, it remains questionable whether all deposited proteins, as well as the irreversibly bound proteins on the membrane, could be analyzed when the deposited proteins are manually removed

from the membrane surface. Certainly, the proteins bound to or in the membrane pores could not be reached with this method. However, the proteins deposited closest to the membrane surface are precisely those that contribute most to the gel-structure change of the surface layer (Qu et al., 2012) and are mainly responsible for the reduction in flux and transmission (Steinhauer et al., 2015b).

There is some literature dealing with the deposit layer formation *in situ* visualization to assess the growth of a deposit layer during filtration of diverse materials as a function of filtration time. These works studied model systems consisting of inorganic particles or defined hydrocolloids such as alginate in an aqueous solution. A good overview of *in situ* techniques is given in the review by Li et al. (2017). Using nuclear magnetic resonance (NMR), Yao et al. (1995) could visualize the deposit layer formation caused by concentration polarization in oil-water emulsions. Based on this, Xu et al. (2009a) monitored the fouling of oily wastewater in HFM via ultrasonic reflectometry. They showed that the flux decline was caused mainly by deposit layer formation and the compaction of the oil droplets to a dense structure (Xu et al., 2009b). However, deposited casein micelles would not react like oil droplets.

Also, investigations using NMR with fixed particles were performed to investigate the permeate flux distribution and the non-uniform deposit layer growth occurring along the membrane (Buetehorn et al., 2011). Buetehorn et al. (2011) showed with submerged HFM that the flux increases linearly by decreasing the vertical distance from the point of permeate extraction resulting in thicker deposit layers. Airey et al. (1998) investigated deposit layer formation of colloidal silica suspensions with an average particle size of 12 nm by NMR micro-imaging. The authors could show the deposit layer formation in tubular membranes which was much thicker around the bottom of the lumen than around the top. They argued with the result of the gravity-induced flow of the polarization layer around the membrane wall. Based on these findings, Bannwarth et al. (2016) reported on the deposit layer formation with silica particles in inside-out filtration with HFM by *in situ* electrical impedance analysis. These authors showed a decrease in the deposit layer porosity during filtration. Thus, the lower deposition area for the particles in inside-out filtration results in a higher packing density of the silica particles and thus lower deposit layer porosity (Bannwarth et al., 2016).

To conclude, there are some new approaches regarding to the qualitative and quantitative analysis of the deposit layer. However, they all have their limitations regarding the model system oil droplets or silica particles, or they are destructive and *ex situ* measurements. Therefore, the deposit layer should ideally be investigated with an *in situ* and non-destructive method concerning composition, density, and height, which, with its capabilities and limitations, was investigated, here represented as chapter 3.

1.5.3 Length dependency of milk and other complex media filtration

All module systems dependent on their structure will have different flow properties and therefore, differences in spatial effects as a function of membrane length, which will influence filtration performance in terms of flux, deposit layer formation, and transmission. However, there are different points of view on the formation of deposit layers as a function of membrane length.

Gernedel (1980) observed a decreasing filtrate flux over the membrane length during skim milk UF. He attributed this to an axial transport of the already deposited material and thus to an increase in the deposit layer height in the longitudinal direction of the membrane, ignoring the pressure loss along the membrane. Contrary to the statements of Gernedel (1980), Riesmeier et al. (1989) found a decrease in the deposit layer height along the membrane during crossflow filtration of microbial suspensions of *E. coli* and *S. cerevisiae* using tubular and plate membranes (0.2 µm) made of polypropylene using scanning electron microscope images, which they justified by the Δp_L. The tubular membrane was divided into four identically sized sections, each 15 cm long, and Δp_L was determined separately for each one. Thus, a linear behavior of the length-dependent Δp_L could be demonstrated. As a direct consequence of this observation and based on scanning electron micrographs, Riesmeier et al. (1989) proved the decrease of the deposit layer height in the flow direction.

Klein and Kottke (1996) assessed a length dependence of the deposit layer by an optical laser measurement of quartz flour suspensions during MF, which was dependent on the crossflow velocity. At low velocities with a Reynolds number in the range of $4{,}000 < Re < 100{,}000$, a change of the smooth surface layer into a layer characterized by regular longitudinal grooves along the membrane could be observed; this resulted in a decrease of the deposit layer in the flow direction. At high flow velocities, a uniform deposit layer was observed. In addition, a change in particle deposition was observed depending on the crossflow velocity. At high wall shear stresses and decreasing filtrate flow, small particles formed the main component of the surface layer, while at the same time larger particles were increasingly removed from the structure.

Moreover, Cho and Fane (2002) examined the deposit layer along the entire membrane length. After the concentration of anaerobic bacteria by MF, the membrane was dissected and analyzed to obtain a detailed overview of the fouling behavior. An intensely formed deposit layer at the end of the membrane was determined, with the porous membrane surface still visible at the inlet. These results explain the decreasing flux along the length and support the claim of a deposit layer growing in the longitudinal direction. A possible explanation for this phenomenon was described as the formation of vortices near the flow inlet that remove the deposit layer.

Further studies considered the length dependence when different filtration fluids were used but at low permeate volume flow rates and low shear rates or crossflow velocities (Romero and Davis, 1990, 1991; Song and Elimelech, 1995, 1995; Bacchin et al., 2002; Bacchin, 2004). Under these conditions, the Δp_L has little effect on the filtration result, so that the derived model equations predict the greatest deposit layer height in the region of the membrane exit (Figure 1.23).

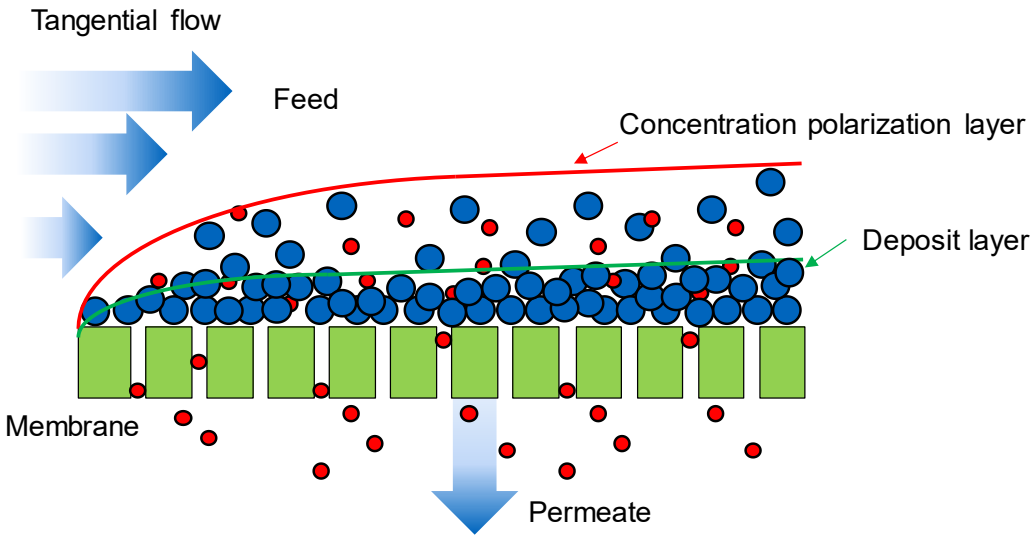

Figure 1.22. Illustration of a deposit layer formation model. Highest deposit layer height at the rear part of the membrane (adapted from Song and Elimelech (1995) (Page 3393, Figure 1)).

In contrast, Gésan et al. (1993) found the strongest protein fouling at the membrane inlet in MF of whey protein using CTM (0.14 µm), which can be partly explained by the model of Mondor and Moresoli (2000). Taking into account the Δp_{TM}, the maximum deposit layer height is predicted after a certain distance from the membrane inlet, after which it decreases towards the membrane outlet. However, the model was set up using monodisperse thinned latex suspensions of 0.53 µm without considering intermolecular adhesive forces.

Piry et al. (2008; 2012) studied casein/whey protein fractionation using a sectioned CTM. They interpreted the observed decrease in flux with a concomitant increase in permeation along the membrane to mean that the deposit layer was more intense at the membrane entrance due to the higher Δp_{TM} and less intense toward the membrane exit (Figure 1.23 B).

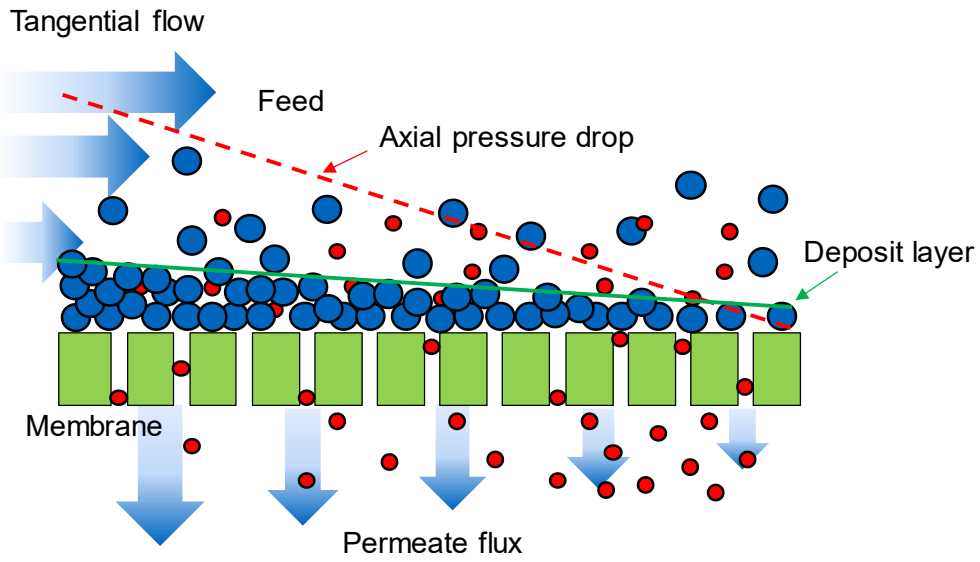

Figure 1.23. Model of deposit layer formation. Highest deposit layer height at the front part of the membrane (adapted from Piry (2011) (Page 80, Figure 5.19)).

Based on this, Hartinger et al. (2019b) investigated the spatial effects in SWM by sectioning the membrane pockets of a SWM. However, it is unknown whether the deposit layer is thicker or more compact at the membrane inlet and how it changes in time and space.

To conclude, spatial effects will occur in all membrane modules. Methods to study the effect of membrane length of HFM were developed in this work.

2 Motivation and objectives

In the separation and concentration processes for biopolymers filtration, fouling is a key issue reducing the membrane performance in terms of flux, protein transmission, and mass transport over the membrane. Taking the theoretical background presented in Chapter 1 into consideration it can be concluded that there are several knowledge gaps regarding structure, composition, and formation of fouling during the filtration of complex biogenic media like milk. Therefore, the objective was to investigate the phenomenon of fouling by retained proteins during milk protein fractionation regarding the formation of the deposit layer under varying process conditions as well as the characterization of the structure of the length-dependent deposit layer in correlation to the composition and amount of the deposited proteins.

Chapter 1.4.1 and 1.4.2 show that alternative membrane systems could be beneficial to address both the improvement of separation efficiency and the effective deposit layer control. Further, this work aimed at qualifying HFM as an alternative membrane system to be used for milk protein separation to optimize the fractionation process. Based on the insights in fouling, the same effects on deposit layer formation can be expected on HFM as well as on the commonly used membrane systems like CTM and SWM. However, HFM take advantages of a better deposit layer control due to free cross-sections, lower Δp_L (like CTM), and high packing density at low manufacturing costs (like SWM). The hypothesis is that the variation of local pressure and flow conditions has a higher impact on flux and transmission of HFM, resulting in a higher fractionation efficiency when compared to CTM and SWM.

The focus of this work was to investigate the formation and structure of the deposit layer under different process conditions to optimize milk protein fractionation by the effective control of deposit layer formation which is then applied to all membrane systems.

A method has to be developed to correlate the structural information with the amount and composition of protein in the deposit layer. A first step was taken towards assessing the suitability and capability of an *in situ*, non-invasive, and non-destructive measurement method based on magnetic resonance imaging (MRI) to visualize deposit layer formation during dead-end filtration in correlation to the filtration pressure and temperature. The gained deposit layer height information was correlated with the amount and composition of the deposited proteins by RP-HPLC (Schopf et al., 2020).

In addition, the length-dependent effects on the deposit layer formation in HFM were investigated. Although the basic expectation of spatial effects in HFM are similar to CTM and SWM, they cannot be transferred directly due to the different pressure and flow conditions in hollow fibers. A method was developed to measure and access the

length-depended effects in HFM. The spatial distribution of flux and whey protein transmission along the flow path as a function of the Δp_{TM} and feed volume flow rate was investigated with HFM modules with different lengths to identify the optimal process conditions in terms of Δp_{TM}, Δp_L, crossflow velocity, flux, whey protein transmission, and module length (Schopf et al., 2021a).

Based on this, a comparison with similarly sized commercial modules was performed. Milk protein fractionation was carried out with HFM, SWM, and CTM as membrane systems at their whey protein mass flow optimum to compare flux, transmission, and whey protein mass flow concerning the module footprints, and to use the module performance as the assessment criteria (Schopf et al., 2021b).

As the results showed that HFM could provide higher protein mass flow per module compared to SWM and CTM due to higher feed volume flow owing free cross-sections, optimal process conditions were determined for the degree of pre-concentration and the DF process conditions. The efficiency of fractionation was investigated according to the pre-concentration before starting DF when using UF permeate as DF medium for transferring the whey proteins into the permeate (Schopf and Kulozik, 2021).

CTM could also be manufactured with a smaller channel diameter to converge hollow fibers diameter which will increase the packing density of CTM modules as it does in HFM modules. However, the permeate flow will have different resistance to the outer rim of the element dependent on the channel position. This is expected to affect flux, the convective transport of proteins towards the membrane area, and thus the deposit layer formation. Due to different pressure and flow condition between the inner and outer channels, we investigated the deposit layer formation as a function of the number of channels in a multi-channel CTM (Schopf et al., 2022).

3 Structural Characterization of Deposit Layer during Milk Protein Microfiltration by Means of *In situ* MRI and Compositional Analysis [1]

Roland Schopf [a),*,#], Nicolas Schork [b),#] , Estelle Amling [b)], Hermann Nirschl [b)], Gisela Guthausen [b),c)], and Ulrich Kulozik [a)]

a) Chair of Food and Bioprocess Engineering, Technical University of Munich, Weihenstephaner Berg 1, 85354 Freising, Germany
b) Institute of Mechanical Process Engineering and Mechanics, Karlsruhe Institute of Technology, 76131 Karlsruhe, Germany
c) Chair of Water Chemistry and Water Technology, Karlsruhe Institute of Technology, 76131 Karlsruhe, Germany

* Corresponding author

\# First and second author contributed equally

Summary and contribution of the doctoral candidate

Fouling is the main issue in microfiltration. Owing to the deposition of large particles on the membrane surface and the increased filtration resistance the flux, the transmission, and the mass flow of smaller particles as the pore size is significantly reduced. Mainly casein micelles will be retained, deposit on the membrane surface and form a deposit layer. However, knowledge about the formation and the structure of the deposit layer under different process conditions is lacking. The main topic here is that the most analytical techniques are *ex situ* measurements stopping filtration and destroying the deposit layer to analyze the composition of the fouling. But, it is not taken into account that pressure has a decisive influence on the formation and the structure of the deposit layer.

Therefore, the focus of this work was to investigate the formation and structure of deposit layer under different process conditions to optimize milk protein fractionation

[1] Original publication: Schopf et al. (2020): Schopf, Roland; Schork, Nicolas; Amling, Estelle; Nirschl, Hermann; Guthausen, Gisela; Kulozik, Ulrich. 2020. Structural Characterization of Deposit Layer during Milk Protein Microfiltration by Means of *In Situ* MRI and Compositional Analysis. Membranes 10 (4). DOI: 10.3390/membranes10040059. Adapted original manuscript. Adaptions of the manuscript refer to enumeration type, citation style, spelling, notation of units, format, and merging all lists of references into one at the end of the dissertation. No special permission is required to reuse all or part of article published by MDPI.

which is then applied to all membrane systems. For this purpose, MRI is used as a novel method for deposit layer observation to visualize for the first time the deposit layer height and density on HFM formed during the filtration of milk *in situ*, non-invasively, and non-destructively as well as spatially resolved. This ongoing method was applied to correlate the structural information with the protein amount and composition of the deposit layer.

An *in situ*, non-invasive, and non-destructive measurement method based on MRI was used to visualize deposit layer formation during dead-end filtration in correlation to the filtration pressure and temperature. We characterized fouling in ceramic HFM during milk protein fractionation with time-dependent visualization and calculation of the deposit height. Thus, a correlation between the time-dependent fouling and integral filtration parameters in terms of the pressure and the filtration temperature was performed to gain a better scientific understanding of the local filtration, the deposit layer formation, and the fouling mechanism. The gained deposit layer height was then correlated with the amount and composition of the deposited proteins by RP-HPLC.

This paper is the result of a close collaboration between two research teams from the Technical University of Munich and the Karlsruhe Institute of Technology. The first and the second author contributed equally. The substantial contributions of the doctoral candidate to this study were to develop the experimental concept and the design of the study after critically reviewing the literature. The doctoral candidate performed the filtration experiments and the analytical part via RP-HPLC including data processing, interpretation, and discussion. The part with the MRI experiments was independently performed from the other institute including imaging, data processing, interpretation, and discussion. Upon peer-review, the doctoral candidate mainly wrote and revised the manuscript together with the second author. The co-authors initiated the study, contributed to the project outline, the execution of experiments, the discussion of results prior to submission, editing the manuscript, and the revision of the manuscript.

Abstract

Milk protein fractionation by microfiltration membranes is an established but still growing field in dairy technology. Even under crossflow conditions, this filtration process is impaired by the formation of a deposit by the retained protein fraction, mainly casein micelles. Due to deposition formation and consequently increased overall filtration resistance, the mass flow of the smaller whey protein fraction declines within the first few minutes of filtration. Currently, there are only a handful of analytical techniques available for the direct observation of deposit formation with opaque feed media and membranes. Here, we report on the ongoing development of a non-invasive and non-

destructive method based on magnetic resonance imaging (MRI), and its application to characterize deposit layer formation during milk protein fractionation in ceramic hollow fiber membranes as a function of filtration pressure and temperature, temporally and spatially resolved. In addition, the chemical composition of the deposit was analyzed by reversed-phase high pressure liquid chromatography (RP-HPLC). We correlate the structural information gained by *in situ* MRI with the protein amount and composition of the deposit layer obtained by RP-HPLC. We show that the combination of *in situ* MRI and chemical analysis by RP-HPLC has the potential to allow for a better scientific understanding of the pressure and temperature dependence of deposit layer formation.

Keywords: fouling; fractionation; casein; whey protein; filtration resistance

Graphical abstract:

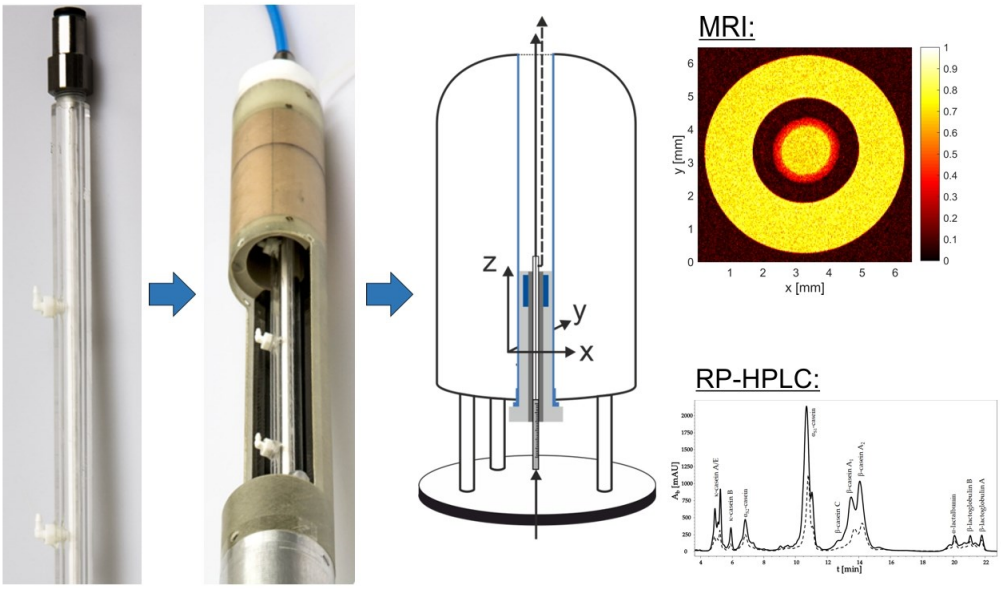

3.1 Introduction

Milk protein fractionation by microfiltration (MF) membranes is a still growing field in dairy technology and a lead technology for the valorization of complex food materials such as milk by making single fractions available with their unique individual functional properties. It is generally known that, in membrane filtration, a considerable accumulation of retained material on the membrane surface occurs, in particular during milk protein fractionation by MF.

During MF of food systems, material accumulations at the membrane surface mainly consist of biopolymers such as proteins or polysaccharides (Kersten, 2001; Kulozik and Kersten, 2002; Panglisch, 2003; Schiffer et al., 2018). This applies even under

crossflow conditions, where the wall shear stress only reduces the amount of deposited material, but a complete prevention of material accumulation cannot be achieved (Le Berre and Daufin, 1996; Hartinger et al., 2019a; Hartinger et al., 2019c). This is referred to deposit formation (Gésan et al., 1993). In applications in dairy technology, the deposit primarily consists of casein micelles, the main protein component in milk (Jimenez-Lopez et al., 2008; Jimenez-Lopez et al., 2011; Heidebrecht et al., 2018; Heidebrecht and Kulozik, 2019). Previous studies showed that the total filtration resistance considerably increases as a function of time and processing conditions owing to the deposit layer formation and cross-linking of proteins in the deposit, which leads to a steep decline in flux with filtration time in the very first minutes after filtration started (Bacchin, 2004; Kühnl et al., 2010; Field and Pearce, 2011; Kühnl, 2011; Steinhauer et al., 2011). In protein fractionation by MF, deposit formation by the fraction of the larger proteins (casein micelles) has a decisive negative effect since it hinders the desired permeation of the smaller whey proteins (Hartinger and Kulozik, 2020). Therefore, the deposit layer formation correlates with a loss in separation efficiency and throughput (Kulozik and Kersten, 2002). This is not only of relevance for the overall fractionation result of the whole module. Since in crossflow membrane filtration the transmembrane pressure decreases along the flow path from module inlet to outlet, the extent of deposit formation varies accordingly, while the shear stress almost stays the same as at the inlet. As found by Hartinger et al. (2019a), Piry et al. (2012), and Kulozik & Kersten (2002) using custom-made module systems able to measure flux and permeate composition in segregated modules separately, the targeted maximum of whey protein permeation is achieved only at or towards the end of the module. At this point, the ratio of transmembrane pressure and shear stress shifts to the benefit of shear forces imposed on already deposited or depositing material. Deposit formation is thus reduced where the transmembrane pressure is gradually reaching lower levels, while shear forces transporting deposited material away from the membrane surface stay the same (if one neglects the minimal amount of permeate reducing the volume flow from module inlet to outlet). Kühnl et al. (2010) and Steinhauer et al. (2015a) have further extended these insights by indirectly studying the effect of colloidal interactions between particles in the deposited layer at the membrane. There is room for optimizing the efficiency of, e.g., milk protein fractionation by creating more or less open porous deposits as a result of varying attractive or repulsive forces between particles as a function of pH and ionic strength. It would be of interest to be able to assess these structural details *in situ*, but a capable method does not yet exist.

To investigate the accumulated material with regard to their chemical or structural properties, indirect or destructive techniques are widely used. Because the deposit layer changes its appearance, composition, and density upon pressure release, the

deposit layer should ideally be investigated *in situ* and non-destructively. Furthermore, changes in height and inner structure are expected because the deposited layer expands due to relaxation under ambient pressure conditions. In addition, *ex situ* measurements require the removal and destruction of the membrane in order to get access to the deposited material.

In comparison to previously investigated clear model fluids, multiple complications arise: (1) milk is an in-transparent fluid and (2) membrane systems, such as tubular ceramic or polymeric hollow fibers that are operated in inside-out filtration mode, are difficult to be analyzed by direct observation methods, e.g., by optical means.

In previous studies (Çulfaz et al., 2011; Arndt et al., 2016a; Arndt et al., 2017; Schuhmann et al., 2018; Schork et al., 2019; Schuhmann et al., 2019), nuclear magnetic resonance imaging (MRI) was used as a non-invasive and non-destructive technique to assess the growth of a deposit layer during filtration of diverse materials as a function of filtration time. These works mostly studied model systems consisting of inorganic particles or defined hydrocolloids such as alginate in an aqueous solution. Skim milk as an in-transparent feed medium and especially the deposit layer formation in ceramic hollow fiber membranes were also studied (Arndt et al., 2016b; Schork et al., 2018) to prepare the methodology of the MRI measurements. MRI was applied on skim milk as a complex medium and to establish the required sample preparation to achieve the necessary contrast difference for MRI analysis and to develop the mathematical data processing protocol. When using MRI, spatially and time-resolved information about density and height of the deposit layer can therefore be obtained for skim milk filtration in inaccessible, optically in-transparent module housings to directly and *in situ* assess deposit formation.

Beyond this, membrane filtration performance depends on the processing conditions such as pressure, temperature, and filtration time. However, it is unclear whether the time-dependent filtration performance depends on the effect of the change in deposit height because of protein accumulation or the change in porosity due to deposit compaction. When trying to better understand these effects and changes of the deposit layer it is obvious that this gap in knowledge needs to be filled to explain the impact of deposit layer formation on flux reduction. Furthermore, an answer to questions regarding the impairment of permeation of solutes through the combined layers of membrane and deposit material is of interest because the deposit layer acts as an additional filtration resistance in the form of a secondary membrane.

Regarding processing conditions, it is known that a loss in static pressure not only occurs along the flow path (Δp_L), i.e., along a membrane but also inside the deposited material when the permeate flows towards the membrane surface because of frictional pressure losses, thus reducing the transmembrane pressure (Δp_{TM}) (Tiller et al., 1999).

For a layer of compressible and deformable casein micelles, the pressure loss results in an increase in compaction and, thus, in higher deposits´ densities or reduced porosities (Steinhauer et al., 2015a). A reduction of flux with filtration time during MF of whey proteins has been attributed to an increase of the deposit layer height alone (Steinhauer et al., 2015b), Apart from that, some studies were performed to qualitatively and quantitatively elucidate the structure of the deposit (Chen et al., 2004b; Delaunay et al., 2008; Suwal et al., 2015; Li et al., 2016; Li et al., 2017; Ng et al., 2018). However, a correlation between the chemical analysis of the deposit layer and *in situ* measured layer has not been shown so far. The methods developed in (Çulfaz et al., 2011; Arndt et al., 2016b; Schork et al., 2018) are applied to get more insight into the details of the deposit´s composition regarding the ratio of casein and whey protein. Additionally, there is still a lack of understanding of how pressure affects the behavior of the deposit's chemical composition and height.

Apart from Δp_L and $\Delta p_{TM,}$ temperature (ϑ) is a variable in membrane filtration that results in increasing flux and, therefore, a higher convective transport of protein towards the membrane surface at higher temperatures. Its influence on deposit formation and filtration efficiency is still the subject of current research (Piry, 2011). In industrial applications, the MF process of skim milk is operated either at a rather low temperature (10–15 °C) (Hartinger et al., 2019b) or rather high temperatures of about 45–55 °C (Hurt, 2015). Higher temperatures yield higher fluxes mainly due to the lower product viscosity but may promote denaturation and also microbial growth to some extent, especially in long-term operations between cleaning cycles (Kersten, 2001). Meanwhile, lower temperatures keep microbial growth better under control, but yield low fluxes and induce migration of β-casein into the permeate, thus reducing the purity of the whey protein fraction (van Hekken and Holsinger, 2000; Crowley et al., 2015). Despite the fact that cold filtration is by now more frequently applied in industrial applications, little is known about the effect of low temperature in milk MF on the deposition of casein micelle layers.

Many models exist that try to determine the filtration phenomena by evaluating the macroscopic data such as the permeate flux or pressure drop (Bolton and Apostolidis, 2017). The deposit formation is affected by more than only one of these effects: pore blocking, pore constriction, cake formation, solute adsorption, and concentration polarization (Iritani and Katagiri, 2016). In the case of the *in situ* measurement by MRI, the deposit formation during skim milk filtration is observed on a microscale where it was already shown that parts of the deposit layer behave differently as the pressure is released as a part of it diffuses back into the membrane lumen (Schork et al., 2019).

In summary, the purpose of this study is to apply MRI *in situ* to assess milk protein deposits on MF membranes applied for milk protein fractionation under processing

conditions relevant for practical situations. MRI is currently in ongoing development to be applied in various filtration processes. MF was at first operated in dead-end mode to measure the impact of Δp_{TM}, filtration time, and filtration temperature. To correlate MRI results with chemical composition and the permeation of proteins, reversed-phase high-performance liquid chromatography (RP-HPLC) analysis of the deposit layer was performed. These data allow a compositional characterization of the deposit layer and could thus lead to a deeper understanding of mechanisms responsible for the reduction of flux and protein permeation caused by deposited materials on membrane surfaces.

3.2 Materials and Methods

3.2.1 Reconstituted Skim Milk Solution

The skim milk solution was produced by re-dispersion of 'low heat skim milk powder' from 'milk and whey ingredients', Sachsenmilch Leppersdorf GmbH, Germany. The composition of the reconstituted skim milk is listed in Table 3.1. 103.2 g of the skim milk powder was dissolved in V_{water} = 1 L of demineralized water, which resulted in 2.8 %w/w of casein, a total protein content of 3.5 %w/w, and pH 6.6, as is typical for bovine milk (Walstra and Jenness, 1984; Jenness, 2012). All experiments were performed at room temperature (ϑ = 22 °C). Viscosities of water and permeate were measured with an Anton Paar MCR 302 rheometer (Anton Paar, Graz, Austria) using the double-gap geometry. The rehydrated skim milk powder is referred to as skim milk hereafter (Schuhmann et al., 2019).

Table 3.1. Composition of the skim milk.

Content or Property of the Re-dispersed Skim Milk	Value Determined by Manufacturer (%w/w)	Measured Value
Casein protein	2.8	
Whey protein	0.7	
Fat	0.06	
Lactose	5.61	
Ash	0.8	
pH		6.6
ϑ		22 °C
η_{Water}		0.992 mPa s
η_{Milk}		1,477 mPa s
$\eta_{Permeate}$		1.106 mPa s
φ_{Milk}		0,9977 kg dm^{-3}

3.2.2 Ceramic Hollow Fiber Membranes

The ceramic hollow fiber membranes, provided by MANN + HUMMEL GmbH, Ludwigsburg, Germany, were operated in inside-out filtration mode. The selective layer of α-Al_2O_3 was on the inner surface of the channel. The hollow fiber has an inner diameter

of d_i = 1.9 mm and an outer diameter of d_o = 3.2 mm. The nominal average pore diameter, as stated by the manufacturer, is approximately 100 nm. The hollow fiber membranes have an average pure water permeability of J_0 = 438.5 L m^{-2} h^{-1} bar^{-1} and a membrane resistance R_M of 8.28 · 10^{11} m^{-1}. One single hollow fiber membrane was used in the MRI measurements for each filtration pressure and temperature.

3.2.3 MRI Contrast Agent

A contrast agent in the form of magnetic iron oxide nanoparticles (MIONs) with a concentration of c_{Fe} = 4.26 · 10^{-3} mM_{Fe} (corresponding to a concentration of 0.024 %w/w) was added to the feed solution before filtration. The protein deposit on the membrane can also be measured by exploring the native MRI contrast, i.e., without a contrasting agent. However, a better contrast between feed and deposit is achieved because of the high transverse relativity of MIONs (Schork et al., 2019). Lower signal intensities are induced because of the dominantly transverse paramagnetic relaxation enhancement of the nanoparticles. The contrast agent used in the experiments, commercially available as ‘nanomag-D-spio’, was purchased from micromod Partikeltechnologie GmbH, Germany. The MIONs with a mean diameter of 100 nm are composed of iron oxide clusters embedded in a matrix of dextran and are coated with casein proteins to be chemically compatible with the feed. In previous studies (Arndt et al., 2016b; Arndt et al., 2016a; Arndt et al., 2017; Schork et al., 2018; Schuhmann et al., 2018; Schork et al., 2019; Schuhmann et al., 2019), it was shown that the contrast agent is embedded in the deposit layer and does not diffuse back into the feed solution separately from the deposit nor significantly permeates the membrane. To confirm and investigate the behavior of these MIONs, the deposit layer was taken out of the hollow fiber membrane after filtration with MIONs and put into a glass tube filled with skim milk, also including the contrast agent. For direct comparison, a second glass tube with a reference skim milk was placed around the inner tube (Figure 3.1).

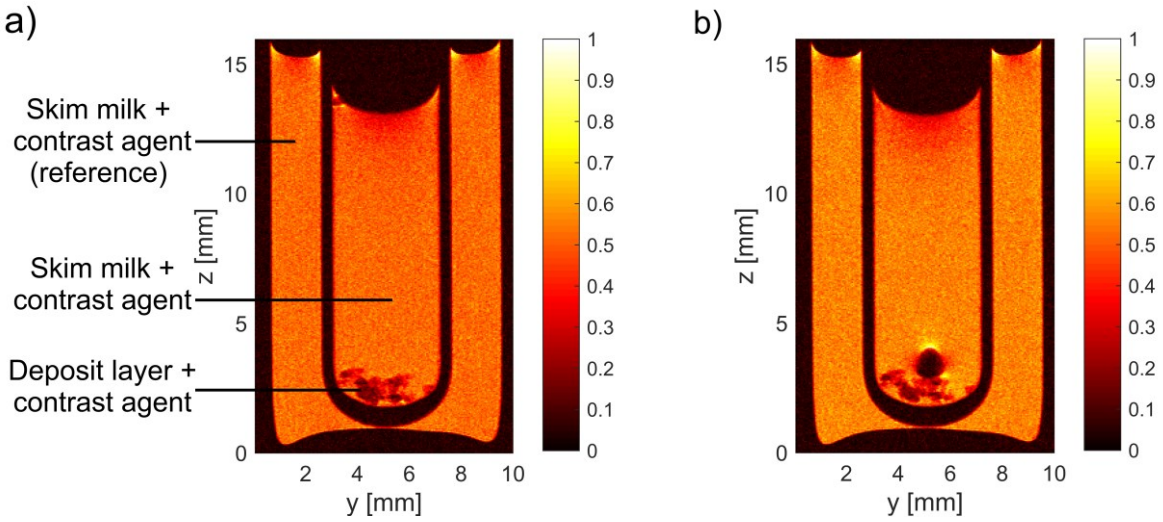

Figure 3.1. MIONs are embedded into the deposit layer during filtration. (a) After filtration, the deposit was taken out of the hollow fiber and placed into a double glass tube filled with feed. (b) The nanoparticles are still embedded in the deposit after t = 53 h and do not diffuse back into the surrounding feed. Only a gas bubble formed on the deposit layer. If the contrast agent had diffused back into the souring skim milk, a difference in the signal intensity to the reference solution would have been measured.

3.2.4 In situ MRI

The *in situ* MRI measurements were performed by implementing the filtration module containing the membrane in a Bruker Avance HD III SWB 200 MHz spectrometer (Bruker Biospin GmbH Rheinstetten, Germany) (Arndt et al., 2017; Schork et al., 2018; Schuhmann et al., 2018) (Figure 3.2).

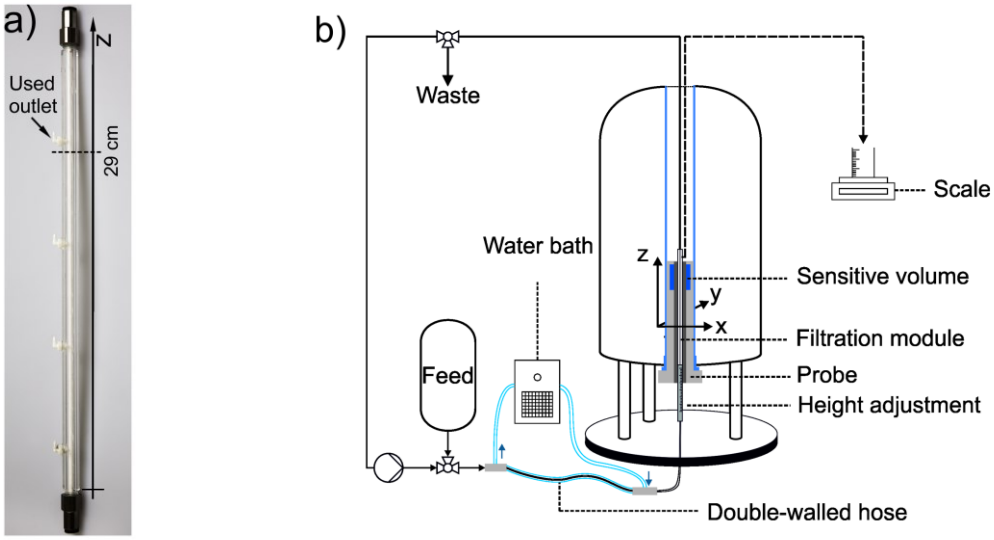

Figure 3.2. (a) The ceramic hollow fiber membrane was placed into an MRI-compatible filtration module for *in situ* MRI. The permeate outlet at z = 32 cm was used and an axial slice at z = 29 cm was measured directly underneath the permeate outlet. (b) Scheme of the setup for the *in situ* filtration. The hollow fiber module is connected to a filtration rig. A double-

walled hose with a counter-current flow system is integrated before the membrane module to enable measurements at different skim milk temperatures. Additionally, the temperature of the gradient system inside the magnet bore, directly around the MRI probe is adjusted accordingly.

The filtration module was attached to the adjustment rod with an inscribed length scale that can be carefully set to the measurement point along the z-axis of the hollow fiber, in this case at z = 29 cm, just below the permeate outlet (Schuhmann et al., 2018). The filtration module was connected to a filtration rig and placed into a 20 mm birdcage of the MICWB40 series.

Skim milk filtrations monitored by MRI were performed in dead-end filtration mode at three different feed pressures p = 0.25, 0.75, and 1.25 bar. Because no permeate back pressure was applied to the filtration system the transmembrane pressure is equivalent to the feed pressure in the dead-end filtration mode. To investigate the temperature-dependent deposit formation, the filtration was also performed at three different temperatures (ϑ = 15, 22, and 45 °C). The highest temperature of 45 °C was chosen with a small safety window because the gradient cooling system has an overheating protection at 50 °C. To ensure a fully tempered skim milk, the feed solution was thermostated while stirred either with a heating plate or precooled in a refrigerator. To prevent a heat loss during filtration, the skim milk was kept at the desired temperature by a double-walled hose system. The skim milk was fed into the inner hose (2.5 mm diameter) while distilled water streams in counter-current flow through the outer hose (10 mm diameter) that was tempered to the desired temperature by a Thermo Scientific DC30 thermostat. During filtration, the temperature of the magnetic field gradient system, in which the imaging birdcage is installed, was additionally set to the desired temperature to ensure a minimal temperature gradient. Additionally, all inlet tubes were thermally insulated to keep the temperature loss of the milk as low as possible. After the experiments, the temperature of the milk in the module was measured with a PT100 thermometer. A deviation of about 2 °C from the set temperature was measured. It should be noted that it is only possible to measure the milk temperature after the module has been removed from the *in situ* MRI setup for which the pressure needs to be slowly released and the imaging probe containing the filtration module carefully removed from the magnet system. Afterward, the insulation needs to be taken off before a temperature sensor can be inserted into the module, which takes a few minutes leading to an increase in the temperature deviation.

During the first 20 to 30 min of the dead-end filtration, the measured flux rapidly declined until nearly a steady-state was reached. A “Rapid Acquisition with Relaxation Enhancement” (RARE) MRI pulse sequence was chosen. The measurements were acquired with a time resolution of approximately 5 min. MR measurements are known

to be susceptible to flow. The repetition time (T_R) needs to be set sufficiently long and the RARE factor (RF) needs to be low to prevent inacceptable large flow artefacts (Table 3.2). The measurement time of 5 min 8 s for MRI data is set sufficiently short to measure the deposit formation during filtration while still allowing an almost artefact-free quantification of the acquired data.

Table 3.2. Main RARE parameters for *in situ* MR measurements of dead-end filtration of skim milk.

RARE Parameter	Value
T_R	4 s
τ_E	5.5 ms
pixel size Δx = Δy	32.5 µm
RF	2
No. of averages	1
Slice thickness along z	3 mm
Time for the measurement	5 min 8 s
Encoding order	Centric
Partial Fourier Factor (Phase)	1.3

3.2.5 MR Image Data Processing

The deposit layer is radially uniformly distributed on the membranes' inner surface, which is evidenced by the MR images. However, the ceramic hollow fibers are not always perfectly round owing to the manufacturing process. Therefore, before filtration, a reference MR image was acquired in which the membrane was filled with water. This allows an accurate definition of the geometry for the segmentation of the membrane lumen from the hollow fiber membrane via an intensity threshold. An equivalent channel diameter (Equation (3.1)) was defined by the segmented lumen area (A_{Feed}):

$$d_{equiv.} = \left(4 \cdot \frac{A_{Feed}}{\pi}\right)^{\frac{1}{2}} \tag{3.1}$$

To process the MR images quantitatively, a self-written MATLAB script was used to determine the intensity in the lumen and determine the mean height of the deposit layer (Schuhmann et al., 2018; Schork et al., 2019). A mask is defined with the exact shape of the membrane lumen, which enables the processing of not perfectly round or even arbitrarily shaped lumen geometries.

In the MR images acquired during filtration, the deposit can be distinguished from the feed area via a user-defined intensity threshold. The equivalent diameter of the segmented inner lumen mask, which represents the feed area, is calculated according to Equation (1). The determined reference and deposit equivalent diameters are used to finally calculate the average deposit thickness (h_d) (Equation (3.2)):

$$h_d = \frac{\left(d_{equiv.}(reference) - d_{equiv.}(deposit)\right)}{2} \tag{3.2}$$

The quantification of h_d is similar to the method used in (Arndt et al., 2017). A second intensity threshold is applied instead of a second discrete ellipse. Instead of the ellipse diameters, the equivalent diameters (Equation (3.1) and Equation (3.2)) are utilized to quantify the deposit height.

3.2.6 Analysis of the Protein Composition of the Deposit Layer

To correlate MRI and RP-HPLC results, the same pieces of the deposit layer in the hollow fiber membrane measured by MRI (deposit height) were analyzed by RP-HPLC (protein composition and amount). To assess the protein composition, the hollow fiber was cut into accurately defined pieces with a length of Δz = 1 cm at each MRI z measurement position. Then, the cut hollow fiber was placed in 2 mL of a guanidine buffer based on Bonizzi (Bonizzi et al., 2009) (Tris(hydroxymethyl)aminomethane (TRIS, 0.165 mol L^{-1}), urea (8.000 mol L^{-1}), sodium-citrate (0.044 mol L^{-1}), and β-mercaptoethanol (0.3% v/w)). The buffer removed and dissolved the deposited proteins from the hollow fiber membrane. Next, the samples with the dissolved deposit layer were filtrated (0.45 µm) into vials. Casein fractions of α_{S1}, α_{S2}, β, and κ-casein, as well as the whey protein fractions of α-lactalbumin and β-lactoglobulin A and B, were quantitatively analyzed by RP-HPLC using the method described by Dumpler et al. in (Dumpler et al., 2017). In brief, the method works as follows: the separation of the milk proteins was carried out with an Agilent Zorbax 300SB-C18 150 × 4.6 mm resin with a pre-column (Agilent Technologies, Böblingen, Germany) and the gradient elution (Eluent A, 10% acetonitrile (1 mL L^{-1} trifluoroacetic acid)). Eluent B, 90% acetonitrile (0.7 mL L^{-1} trifluoroacetic) was carried out at ϑ = 40 °C and v = 1.2 mL min^{-1}. The injection volume of the samples with the dissolved deposit layer was 100 µL. UV–VIS absorption was measured at a wavelength of 226 nm.

3.3 Results and Discussion

3.3.1 MRI Measurements of Deposit Layer

MR images of the retained skim milk components were measured during dead-end filtration. Filtrations with three different feed pressures and at three different temperatures were carried out while multiple MR images were acquired as a function of filtration time. During all experiments, the deposit on the inner surface of the hollow fiber increased as the filtration time progressed (Figure 3.4). The short time required for the

measurement of an MR image (Table 3.2) allows an adequate time resolution to observe the deposit formation. A progressing accumulation leads to an increase in filtration resistance, which causes a rapid decline in the permeate flux, i.e., water and whey protein permeation.

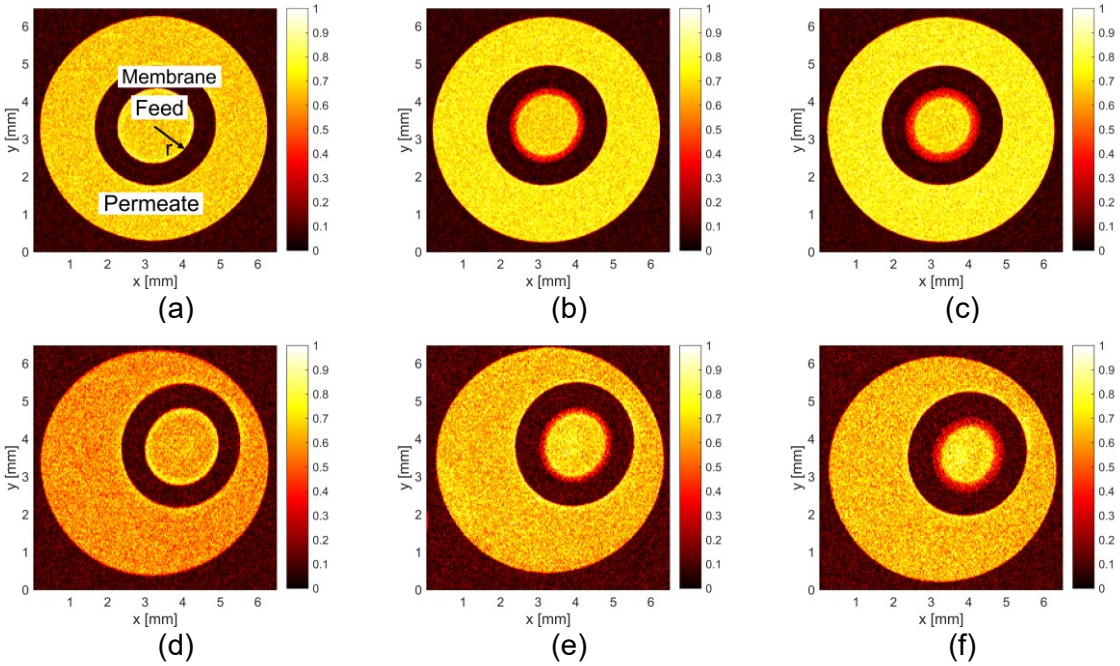

Figure 3.3. Axial MR images were measured every 5 min at z = 29 cm during dead-end filtration at p = 1.25 bar and different temperatures ϑ = 15 °C (a)–(c) and ϑ = 45 °C (d)–(f). The normalized MR intensity I/I_{max} is indicated in the false-color bar. (a), (d): A reference image of the unused hollow fiber was acquired before each filtration. (b): Build-up of the protein deposit at t = 79 min of filtration (red ring at the inner surface of the membranes lumen) and t = 151 min (c) for the lowest temperature ϑ = 15 °C. Progressing accumulation of the deposit was observed on the selective layer of the hollow fiber membrane at t = 67 min (e) and 168 min (f) during the dead-end filtration at ϑ = 45 °C.

At higher temperatures, the NMR signal-to-noise ratio is lower due to the Curie law (compare Figure 3.3 (a)–(c) and (d)–(f)) (Callaghan, 2007). Despite the lower signal-to-noise ratio, a quantification of the intensities was still possible. A lower normalized intensity I/I_{max} at the inner surface of the membranes (Figure 3.3) indicates a higher concentration of retained MIONs and proteins because both, the proteins and contrast agent induce a lower MR signal intensity. Therefore, normalized signal intensities I/I_{max} decrease as a function of radius r at a given filtration time, which indicates the deposit formation when measured as a function of filtration time. While increasing pressure, the steep decrease in I/I_{max} appears at smaller radii at a given filtration time, i.e., the deposit height is slightly larger.

3.3.2 Compositional Analysis of the Deposit Layer

To analyze the protein composition of the deposit layer after filtration, the hollow fiber was cut into a small membrane segment with a length of Δz = 1 cm at the z measurement position of the MRI. Figure 3.4 shows an RP-HPLC chromatogram of the dissolved deposit and the retentate skim milk of caseins and whey proteins at z = 29 cm.

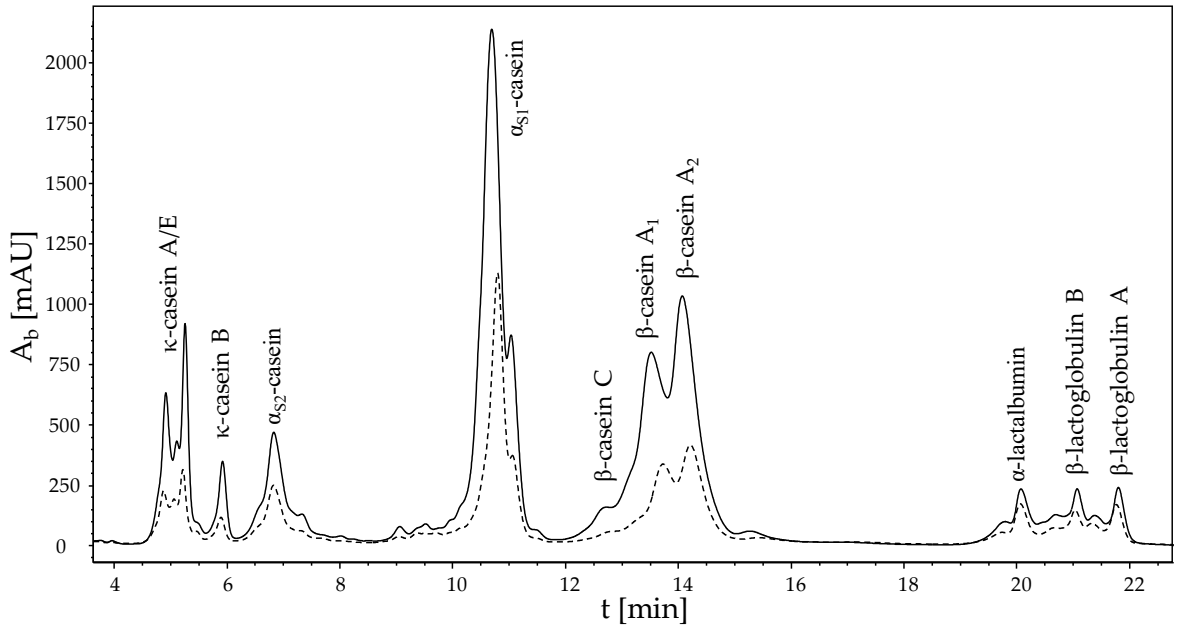

Figure 3.4. RP-HPLC chromatogram of the deposit (solid line) and the retentate skim milk (dashed line) of caseins and whey proteins in a guanidine buffer at z = 29 cm after approximately 3 h of dead-end filtration at p = 1.25 bar and ϑ = 22 °C. An enrichment of the different caseins in the filtration deposit is evident.

All genetic variants of casein and individual whey proteins were detected and analyzed. The chromatogram shows that primarily casein deposited on the membrane surface and formed the deposit layer. As expected, the milk proteins are highly concentrated on the surface. By calculating the amount of proteins deposited on the membrane surface, we identified $c_{protein}$ = 120.1 g m^{-2} of casein and $c_{protein}$ = 11.0 g m^{-2} of whey proteins on the hollow fiber membrane at the end of the dead-end filtration (≈3 h). In other words, there is about 11 times more casein than whey protein on the surface. This can be attributed to the fact that the diameter of the caseins (50 – 400 nm) is larger than the pore size of the membrane with 0.1 µm and are therefore preferentially retained. Although whey proteins are significantly smaller than caseins with a mean diameter of 8 nm, they do not permeate the membrane to 100%. They are also concentrated in the deposit. This can be explained by the additional retention effect of the deposited caseins. This retention effect has also an impact on the filtration performance.

3.3.3 Influence of Pressure on Flux

In dead-end filtration mode, the integral quantities mass and permeability (P) (Figure 3.5), as well as the deposit height h_d on the membrane surface (Figure 3.6 and Figure 3.7), were measured. h_d increased as a function of time at all measured pressures and temperatures (p, T). The deposit height increased rapidly at the start of filtration and flattened slightly over time. As the deposit layer grew, the filtration resistance increased with filtration time, resulting in a lower permeate flux. The convective flow is more hindered, and the deposit layer, therefore, increased progressively slower. Specifically, the change in h_d was at its maximum at the beginning of the filtration because the highest amount of the deposit was transported towards the membrane surface. In the first few minutes of filtration, the integrally measured flux rapidly declined from the pure water flux J_0 to a quasi-stationary flux, which was significantly reduced compared to the initial flux.

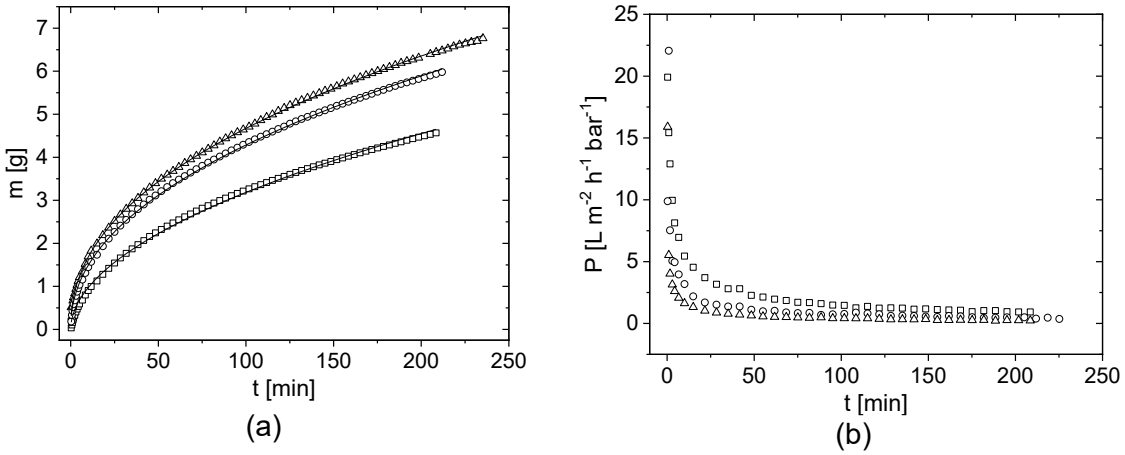

Figure 3.5. (a) Permeate mass m as a function of filtration time t for the three different feed pressures p = 0.25 bar (squares), p = 0.75 bar (circles), and p = 1.25 bar (triangles) at ϑ = 22 °C. Each membrane has a slightly different pure water permeability, which is insignificant on the present scale and therefore neglected here. The integrally measured permeate mass m(t) was described empirically by $m(t) \propto t^{b,integral}$ (lines) (Schork et al., 2019). (b) The integral permeability P = J/p depends on the filtration pressure.

The integral permeability of the module was calculated as P = J/p, where J is the flux and p is the applied pressure. As expected (Figure 3.5b), P decreases with filtration time, starting with the pure water permeability at t = 0 min. In addition, the steepness of P(t) depends on the filtration pressure. The permeability of the filtration with the highest pressure at p = 1.25 bar decreases faster than that at a lower pressure (Figure 3.5b).

3.3.4 Effect of Pressure and Temperature on Deposit Layer Height

Experimental results are compared at the three different pressures for a given temperature (Figure 3.6) and then vice versa (Figure 3.7) to allow an easier interpretation of the influence of p and ϑ. The deposit thickness h_d according to Equation (*3.1*) and (*3.2*) was determined as a function of filtration time for each filtration pressure and temperature combination (p, ϑ) (Figure 3.6 and Figure 3.7). In dead-end mode, the thickness increases with time for all (p, ϑ) in the hollow fiber because more retained proteins accumulate on the membrane surface. At the beginning of filtration, for the first 35 min, the deposit layer height is similar for all three filtration pressures. A small pressure dependence can only be observed at ϑ = 45 °C. The deposit layer height, therefore, seems to be almost pressure-independent for the first 35 min (Figure 3.6c).

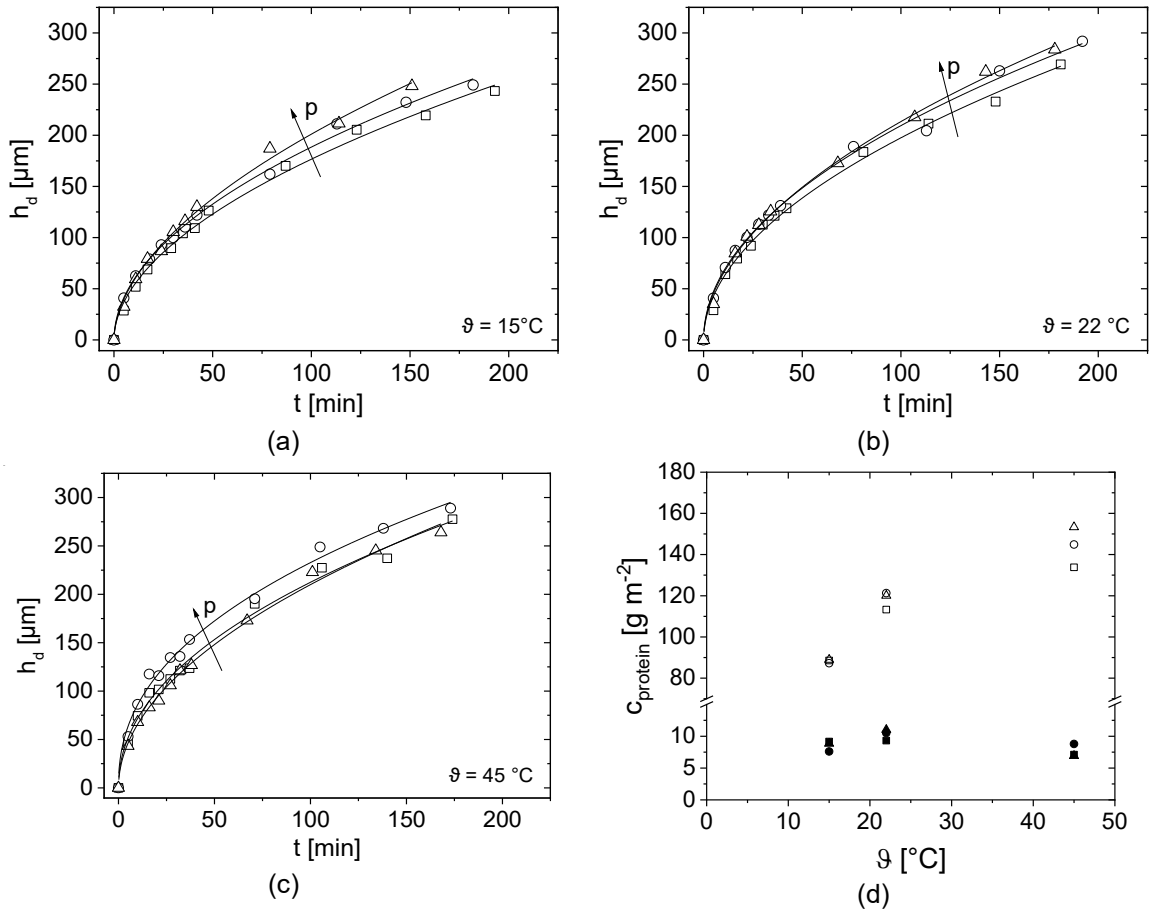

Figure 3.6. Deposit height h_d at z = 29 cm as a function of filtration time t for (a) ϑ = 15 °C (b) ϑ = 22 °C and (c) ϑ = 45 °C. A small difference in deposit height was observed especially at large filtration times for p = 0.25 bar (squares), p = 0.75 bar (circles), and p = 1.25 bar (triangles). The deposit height was empirically modeled by $h_d(t) \propto t^{b,local}$ (lines). (d) Protein concentration $c_{protein}$ on the membrane surface as a function of filtration temperature ϑ for p = 0.25 bar (squares), p = 0.75 bar (circles), and p = 1.25 bar (triangles). Open symbols represent caseins and closed whey proteins.

After t = 35 min, the pressure influence on the deposit layer height is more pronounced for all measured temperatures: At ϑ = 15 °C and ϑ = 22 °C, thicker depositions were measured almost continuously with increasing pressure. However, the differences are small, and the filtration pressure at the two lower temperatures seems to have only a minor effect on accumulation.

The filtration at p = 0.75 bar and ϑ = 45 °C consistently yielded the highest deposit thickness for the whole filtration. The deposit height at the highest filtration pressure p = 1.25 bar at ϑ = 45 °C is very similar compared to the lowest filtration pressure p = 0.25 bar (Figure 3.6c). One possible explanation is that, at p = 1.25 bar and ϑ = 45 °C, the protein deposition is highly compressible and thus the same deposit thickness was measured as for p = 0.25 bar.

Looking at the protein concentration in Figure 3.6d measured on the membrane surface as a function of temperature, it can be clearly seen that the higher the temperature, the higher the casein concentration. At ϑ = 15 °C an average casein concentration of $c_{protein}$ = 88.3 g m^{-2} was measured for all three pressures. The protein concentration at ϑ = 15 °C was independent of pressure. With increasing temperature up to ϑ =45 °C, the casein concentration raises at a pressure of p = 0.25 bar to $c_{protein}$ = 133.8 g m^{-2}. At a pressure of p = 0.75 bar the concentration increases to $c_{protein}$ = 144.9 g m^{-2} and at a pressure of p = 1.25 bar to $c_{protein}$ = 153.3 g m^{-2}. Overall, the pressure-dependence can only be clearly observed at ϑ = 45 °C as (Figure 3.6 (c) and (d)).

To show the effect of temperature, h_d and $c_{Protein}$ were plotted for each of the three pressure levels (Figure 3.7). At lower pressures, the deposit layer height is more temperature-dependent than at p = 1.25 bar.

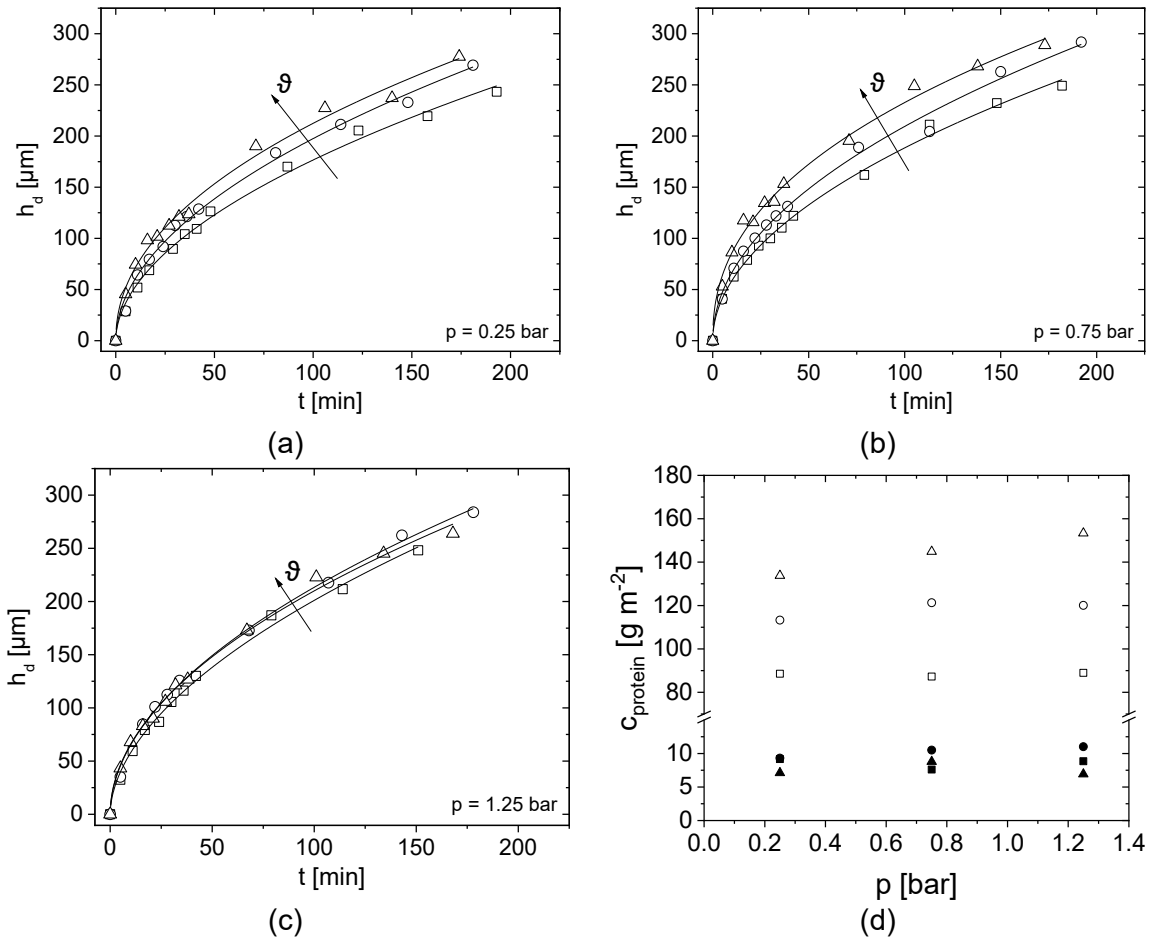

Figure 3.7. h_d at z = 29 cm as a function of filtration time t at (a) p = 0.25 bar (b) p = 0.75 bar and (c) p = 1.25 bar. The temperature was set to ϑ = 15 °C (squares), ϑ = 22 °C (circles) and ϑ = 45 °C (triangles). (d) Protein concentration cprotein for caseins and whey proteins on membrane surface as a function of the pressure p for the three temperatures for p = 0.25 bar (squares), p = 0.75 bar (circles), and p = 1.25 bar (triangles). Open symbols are casein and closed are whey proteins.

Similar deposit layer thicknesses were observed for the investigated pressures, indicated by the constant scale in the figures. One possible explanation is that the deposit layer is highly compressed at p = 1.25 bar, which results in a more compact layer with a similar height.

At pressures of p = 0.25 bar and p = 0.75 bar, the deposit layer formation shows a significant temperature dependence, especially for t > 35 min (Figure 3.7a,b). At the lowest pressure, the deposit height is most pronounced at ϑ = 45 °C and least pronounced at ϑ = 15 °C. At temperatures ϑ > 40 °C, milk tends to undergo structural changes (Dumpler, 2017), which leads to stronger bonds between the milk proteins and the formation of agglomerates, which intrinsically influences compressibility. In the case of aggregation, the deposit layer would grow faster when compared to smaller molecules (Steinhauer et al., 2015a).

The measurements at p = 1.25 bar show almost a temperature independence for t < 75 min (Figure 3.7c). A small difference in deposit height can only be measured for t > 100 min. Concluding, the influence of temperature seems to be less at higher pressures. The pressure probably is so high that structural changes of the milk proteins dominate the process leading to almost no influence of temperature on the overall deposit layer height.

In contrast, the temperature dependence can be seen when the protein concentration is plotted as a function of pressure (Figure 3.7d). At ϑ = 15 °C the casein concentration constantly remains at $c_{protein}$ = 88.3 g m^{-2}. Similarly, at ϑ = 22 °C the casein concentration increases linearly with increasing pressure. Overall, increasing protein concentrations with increasing temperature could be measured at all three pressures. The temperature dependence can be explained by the viscosity change of skim milk (Kersten, 2001). As temperature rises, viscosity decreases, resulting in a higher flux and thus stronger particle deposition forces (Piry, 2011). Consequently, more deposits should be formed. The casein to whey protein ratio is approximately 11:1 at ϑ = 15 °C and ϑ = 22 °C, whereas at ϑ = 45 °C, the ratio increases to 19:1 on average (Figure 3.7d). Consequently, caseins are more abundant in the deposit layer than whey proteins.

By comparing the permeate mass m in Figure 3.5a with h_d in Figure 3.6 and Figure 3.7, a relation for both is observed: during the initial phase, mass increases as flux decreases. Consequently, the deposit height increases simultaneously. When a certain flux is reached, the curves flatten. It is assumed that, at the beginning of filtration, the proteins attach only loosely to each other and a strong increase in the deposit height is observed. Afterward, the flux decreases, and the deposit height only slightly increases because casein micelles pack more densely. The accumulated integral permeate mass was modeled by $m(t) = a_{integral} * t^{b,integral}$ (Schork et al., 2019) which results in pressure and temperature-dependent proportionalities and exponents (Table 3.3). According to Reihanian et al. (Reihanian et al., 1983), an almost exact square root dependence ($b_{integral}$ = 0.5) is expected for a cake filtration The deviation of $b_{integral}$ of 0.5 suggests that not mechanisms of pure cake filtration, but other factors such as pore blocking play a role for filtration performance.

In a first approach, the locally measured deposit height at z = 29 cm was modeled with the same empirical relation, $h_d(t) = a_{local} * t^{b,local}$ to allow a direct comparison between integral mass and local deposit measurements.

Table 3.3. Fit parameters a and b of modeling the permeate mass and deposit height by $m(t)$, $h_d(t) = a * t^b$.

p, bar	ϑ, °C	$a_{integral}$, -	$b_{integral}$, -	a_{local}, -	b_{local}, -
0.25	15	0.32	0.48	15.9	0.52
	22	0.30	0.52	18.8	0.51
	45	0.28	0.56	24.3	0.47
0.75	15	1.29	0.37	18.3	0.51
	22	0.60	0.44	21.2	0.50
	45	0.80	0.44	31.8	0.43
1.25	15	0.089	0.67	16.6	0.54
	22	0.46	0.52	19.8	0.52
	45	0.50	0.52	20.6	0.51

The fit parameter a_{local} increases with temperature (Table 3.3). The fit parameter b_{local} decreases with pressure, apart from the experiments at $\vartheta = 22$ °C. In comparison to the clear correlation between deposit layer formation and temperature, h_d does not always increase with pressure as compression and compaction play a significant role. The fit parameter b_{local} describes the time-dependence of deposit height measured by MRI. There is only a small difference for the different pressures, which indicates a similar deposit growth during dead-end filtration. Within the experimental accuracy, b_{local} ($z = 29$ cm) ≈ 0.5 for all measured pressures. However, the nature and composition of the deposit are assumed to be homogeneous in this approach. In addition, a small trend towards larger $b_{integral}$ is observed in $m(t)$ as a function of pressure. In the present MR image quantification, the deposit is considered as a homogeneous structure. It is not radially differentiated, which is a first attempt. The deposit was shown by MRI to consist of reversible and irreversible parts, and the composition is pressure-dependent (Schork et al., 2019). Additional measurements and quantification tools are necessary to better characterize and quantify the accumulated proteins and their individual geometry and composition with the aim to comprehensively describe and model the deposits as a function of time and spatial coordinates.

3.3.5 Effects on Signal Intensity of the Last Voxel Right before the Selective Membrane Layer

Looking into the details of the images, the following becomes evident: Directly at the inner surface of the membranes, a lower signal intensity at higher feed pressures shows the pressure dependence of the deposit and its structure. At the highest measured feed pressure of $p = 1.25$ bar, the signal intensity is the lowest not only at the membrane surface but also over the entire deposit layer. The MR signal intensity in

each time step I_t is corrected by the reference image before the filtration (t = 0 min, $I_{t=0}$) due to a susceptibility difference at the membrane wall and then normalized by the feed signal intensity in the middle of the membrane's lumen I_{ref} resulting in $(I_t-I_{t=0})/I_{ref}$ (Figure 3.8): Directly at the membrane surface, the signal intensity is shifted towards lower values for higher filtration pressures. This indicates that the deposition becomes more compact. The deposit thickness is almost the same for all pressures during the initial phase of filtration and starts to differ with increasing t (Figure 3.8). Additionally, a temperature dependence is evident: the compactness increases with temperature indicating a better deformability of the proteins at higher temperatures.

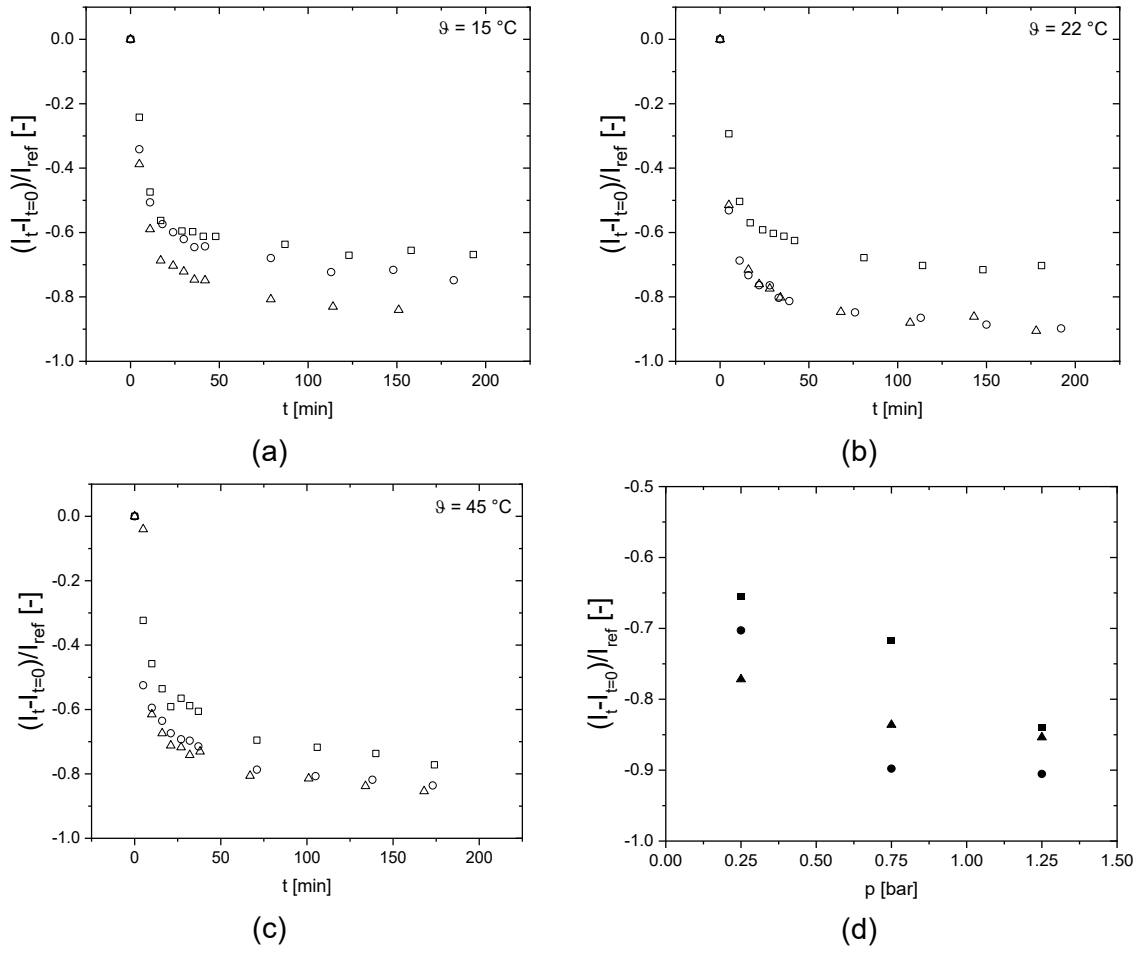

Figure 3.8. Reduced signal intensity of the voxel directly at the inner surface of the membrane as a function of filtration time t for (a) ϑ = 15 °C, (b) ϑ = 22 °C, and (c) ϑ = 45 °C by the concept described in (Schork et al., 2019) and measured for p = 0.25 bar (squares), p = 0.75 bar (circles), and p = 1.25 bar (triangles). (d) Comparing the reduced signal intensity at the selective layer of the membrane for t = t_{max} indicates that with increasing pressure and temperature the deposit found in MRI to be more compact. The temperature was set to ϑ = 15 °C (filled squares), ϑ = 22 °C (filled circles), and ϑ = 45 °C (filled triangles).

These findings are in accordance with other observations: A higher convective flux and compression of the deposit may exist at larger pressures, which may change the nature of the deposit and its reversibility (Ng et al., 2017; Schork et al., 2019). When

the reduced signal intensity at the last measured voxel right at the membrane's selective layer at $t = t_{max}$, a pressure and temperature dependence can be observed. Yet, by measuring on the microscale with MRI, multiple effects need to be considered regarding the experimental uncertainty that can result in the shift of the reduced signal intensities. The signal intensity of the last voxel is affected by an uncertainty because multiple effects need to be considered. The possibility of a partial volume effect and other effects such as susceptibility differences are predominant and the other voxels toward the inside of the membrane lumen are left out of consideration. Additionally, a change or transition of the deposit layer to a gel layer in this pressure and temperature region might occur that contributes to a non-monotonic behavior of the reduced signal intensity. Yet, a dependence of the signal intensity, i.e., deposit layer, on pressure and temperature can be observed.

3.3.6 Impact of Milk Protein Concentration on the Height of the Deposit Layer

To gain a better understanding of how temperature and pressure affect the deposit's chemical and structural composition as well as height, the total protein concentration measured by RP-HPLC was plotted as a function of h_d by MRI (Figure 3.9).

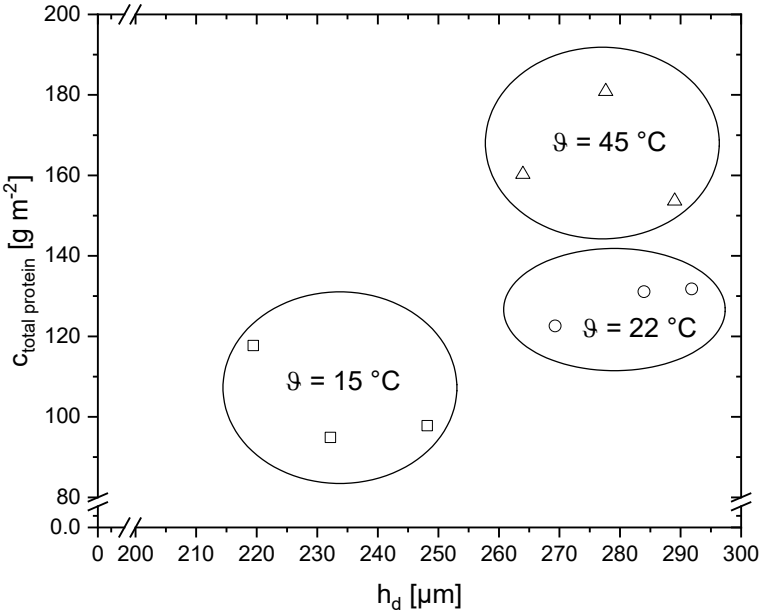

Figure 3.9. Total protein concentration c_{total} protein measured by RP-HPLC as a function of h_d measured by MRI for the three temperatures ϑ = 15 °C (squares), ϑ = 22 °C (circles) and ϑ = 45 °C (triangles).

The plot of total protein concentration versus deposit height shows that higher deposit layers are generally associated with higher protein concentrations. When the temperature was increased from ϑ = 15 °C to ϑ = 22 °C, both the deposit height and the milk protein concentration increase. In comparison to that, the deposit height at

ϑ = 45 °C does not increase further, while the protein concentration increased from approximately 130 to around 170 g m^{-2}. The deposit layer at ϑ = 45 °C is concluded to be more compact or dense than at ϑ = 15 °C and ϑ = 22 °C.

3.4 Conclusions

A method based on magnetic resonance imaging (MRI) to characterize deposit layer formation during milk protein fractionation was presented. Furthermore, a correlation between the time-dependent deposit and integral filtration parameters was found for dead-end skim milk filtration. Skim milk filtration was monitored as a function of pressure and temperature, which results in a deeper understanding of the (local) filtration and fouling mechanisms measured *in situ*, supporting the pursuit of an optimized milk protein fractionation. The protein concentration and the height of the deposit correlate. Moreover, pressure affects filtration behavior on a microscopic length scale. MRI methods will be developed further to allow *in situ* measurements in crossflow filtration mode and to assess whether the reduced height of deposits can also be related to variations in processing conditions such as crossflow velocity and transmembrane pressure as a function of axial position along the membrane.

Author Contributions: R.S., N.S., E.A., and G.G. conceived and designed the experiments under the supervision of H.N. and U.K., R.S. and N.S. performed the experiments and processed the data together with E.A. during her work on the bachelor thesis while all authors were involved in the interpretation and discussion of the data. All authors contributed to writing the manuscript. All authors have read and agreed to the published version of the manuscript.

Funding: This IGF Project of the FEI was supported via AiF within the program for promoting the Industrial Collective Research (IGF) of the German Ministry of Economic Affairs and Energy (BMWi), based on a resolution of the German Parliament. Project AiF 10 EWN. DFG provided financial support for the MRI instrumentation and for Pro2NMR.

Acknowledgments: The authors would like to thank U. Metzger from ‘Milk and Whey Ingredients’, Sachsenmilch Leppersdorf GmbH, Germany for providing the skim milk powder. The authors gratefully thank Heidi Wohlschläger and Claudia Hengst for their assistance concerning the RP-HPLC analysis of the milk samples. Christian Ederer, Franz Fraunhofer, and Erich Schneider are acknowledged for their technical support. The authors thank the German Research Foundation (DFG) for financial support within the instrumental facility Pro2NMR and the instrumentation.

Conflicts of Interest: The authors declare no conflict of interest.

4 Impact of hollow fiber membrane length on the milk protein fractionation [2]

Roland Schopf*, Florian Schmidt, and Ulrich Kulozik

Chair of Food and Bioprocess Engineering, TUM School of Life Sciences, Technical University of Munich, Weihenstephaner Berg 1, 85354 Freising, Germany

*Corresponding author

Summary and contribution of the doctoral candidate

During MF of skim milk spatial effects along the membrane length will occur having a high impact on the filtration performance as well as on deposit layer structure and formation. Length-dependent effects on the filtration in HFM have not been investigated, yet. Although the expectation of spatial effects in HFM are the same as in CTM and SWM, they cannot be transferred directly due to the different pressure and flow conditions in hollow fibers.

Since the permeate side of HFM could not be sectioned because of the bundle of fibers as easy as it was done in CTM and SWM, a new method has to be investigated to measure and access the length-depended effects in HFM. However, HFM modules provide the advantage to be produced more flexibly in terms of module length than SWM and CTM. To investigate the variation of Δp_L on the flux, the whey protein transmission, and on the deposit layer formation on the flow paths, HFM modules with different lengths were produced.

The spatial distribution of flux and whey protein transmission along the flow path as a function of the Δp_{TM} and feed volume flow rate was investigated with HFM modules with different lengths to identify the optimal process conditions in terms of Δp_{TM}, Δp_L, crossflow velocity, flux, whey protein transmission, and module length. We developed membrane modules to analyze and control the length effects during milk protein fractionation in HFM.

The sectioning of HFM modules was carried out by a series connection of four modules with each 30 cm long to show a 1.2 m HFM module length. We identify the rear

[2] Original publication: Schopf et al. (2021a): Schopf, Roland; Schmidt, Florian; Kulozik, Ulrich. 2021. Impact of hollow fiber membrane length on the milk protein fractionation. Journal of Membrane Science 620, 118834. DOI: 10.1016/j.memsci.2020.118834. Adapted original manuscript. Adaptions of the manuscript refer to enumeration type, citation style, spelling, notation of units, format, and merging all lists of references into one at the end of the dissertation. Permission for the reuse of the article is granted by Elsevier Limited.

part of the module, the last two sections, as the one with the best performance in terms of highest whey protein mass flow to low Δp_{TM}. The longer the fibers the higher the Δp_L causing high Δp_{TM} with increased deposition; the shorter the fibers the higher the feed flow reducing deposit layer formation but membrane area will be also reduced. Therefore, we could identify a Δp_{TM} at 0.5 bar and a membrane length of 0.6 m as the best in terms of highest whey protein transmission.

The doctoral candidate specified the experimental concept for this study and designed the HFM prototypes, and critically reviewed the literature. The experimental design for the validation was developed by the doctoral candidate. Furthermore, the doctoral candidate carried out experimental work, data analysis, interpretation, calculation, and plotting. The doctoral candidate wrote and revised the manuscript. The last author initiated the study and all co-authors prepared the project outline. All co-authors contributed to the execution of experiments, the discussion of results, writing and revision of the manuscript.

Abstract

Hollow fiber membranes, HFM, have not been established in milk protein fractionation by microfiltration. HFM of different lengths (0.3 to 1.2 m) were produced to vary the pressure drop along the module and thus to study the length-dependent spatial distribution of flux and whey protein transmission along the flow path as a function of transmembrane pressure, Δp_{TM}, and feed volume flow rate. The objective was to identify the maximally possible module length for various combinations of Δp_{TM} and flow velocity leading to a pressure close to zero at the module outlet, thus avoiding negative Δp_{TM} and reverse permeate flow at the module end. A mean Δp_{TM} of 0.5 bar was identified as optimal for all module lengths to avoid deposit formation above the membrane-controlled limit, reaching a flux of 61.5 L m^{-2} h^{-1}. An optimal HFM length of 0.6 m was identified for milk protein fractionation to obtain the highest flux and whey protein transmission. The shorter the module system, the higher is the possible volume flow rate to prevent excessive deposit formation and thus to achieve the best possible fractionation result.

Keywords: spatial effect; length dependency; microfiltration; deposit layer formation; skim milk

Graphical abstract:

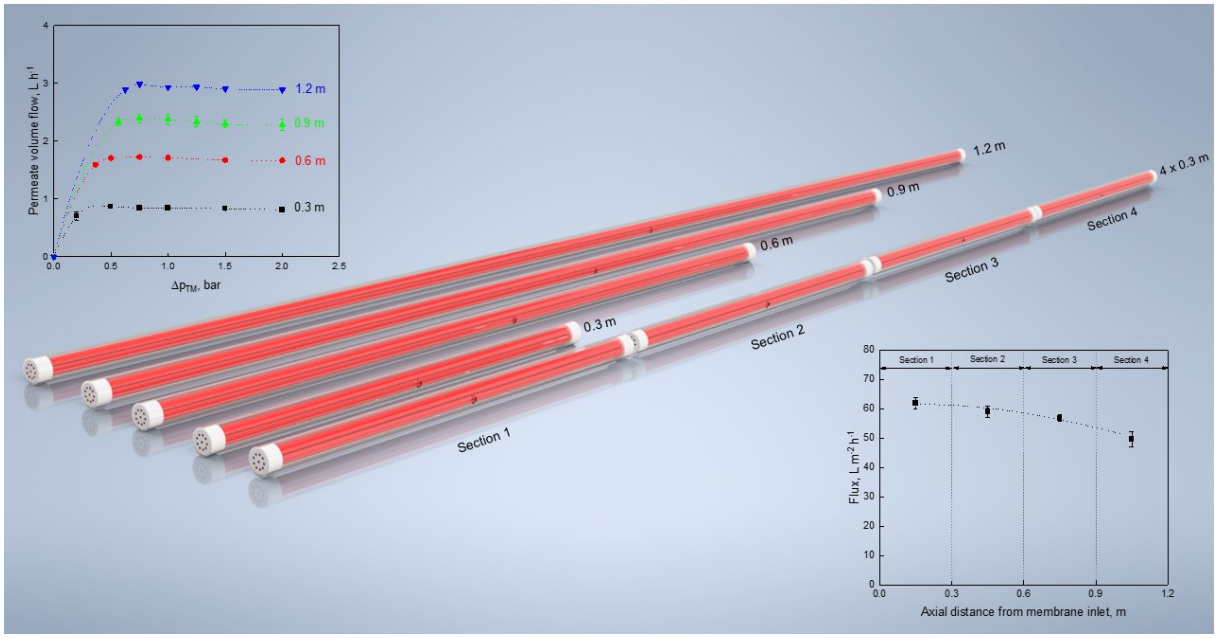

4.1 Introduction

The application of hollow fiber membranes, HFM, for filtration in fields such as water and wastewater treatment in `direct flow mode' with filtration from `outside-in´ as described by Xu et al. (2017) or beverage production in crossflow mode with filtration from `inside-out´ is widespread, since this membrane type provides a high membrane packing density (i.e., a high area of active membrane surface per module volume) and economic and hydrodynamic efficiency. However, in dairy membrane operations the use of HFM for the microfiltration of skim milk has rarely been considered thus far (Schopf et al., 2020; Weinberger and Kulozik, 2020). Milk protein fractionation using microfiltration membranes to separate casein and whey proteins is a key unit operation in the dairy industry (Kulozik and Kersten, 2002; Mohammad et al., 2012; Kumar et al., 2013; Suwal et al., 2015; Ng et al., 2017; Warncke and Kulozik, 2020). As most other module systems, HFM are operated in crossflow mode to control deposit layer formation (Kontopidis et al., 2004; Hilal et al., 2005). Due to friction at the membrane surface, the pressure drops linearly along the flow path (length L), causing a Δp_L. With a given constant pressure at the permeate side of the membrane, this results in a variation in transmembrane pressure, Δp_{TM}, as a function of module length. As a result, parts of longer membranes may be subjected to negative Δp_{TM}, such that not the entire membrane length will be used for filtration and even an unwanted permanent negative flux may occur beyond a certain point.

The problem is that often neither membrane manufacturers nor operators of HFM systems are sufficiently aware of this situation and may choose a non-optimal combination of HFM length and volume flow. In contrast to other module systems, especially

spiral would membranes, SWM, HFM could however be more flexibly produced at different lengths to adopt the modules to special local conditions and filtration tasks thus avoiding negative Δp_{TM} at the outlet of the module, while being able to choose a high volume flow rate to optimize filtration performance. Thus, the open question is, what the optimal length of an HFM is, e.g., for milk protein fractionation at specific processing conditions yielding the maximal separation efficiency between the milk protein fractions mass flow of whey proteins.

Some literature already exists that analyzes the effect of HFM length on the overall filtration characteristics. Xu et al. (2017) suggested hollow fiber lengths of between 1.2 m and 1.8 m would ensure a favorable trade-off between the module productivity and the overall filtration uniformity in water and wastewater treatment when, however, operated in 'direct flow mode'. The optimum module length for the applications operated in the crossflow mode, on the other side, strongly depends on the crossflow velocity (Ali et al., 2016) due to the pressure drop along the membrane and influences productivity more than the module packing density (Cheng et al., 2008). Furthermore, a short HFM provides a higher flux (Doshi et al., 1977; Soltanieh and Gill, 1983; Serra et al., 1998; Kim et al., 2012; Wang et al., 2014; Li et al., 2015). For water filtration, Doshi et al. (1977) demonstrated that if the module length was half of the usual length, the module gave 31% more output under the same experimental conditions. Furthermore, a shorter module with a length of about 40% that of the standard length, studied by Soltanieh and Gill (1983), produced at least 39%.

Extending the hollow fiber length, the pressure profile along the membrane is significantly altered (Sato et al., 2003). Longer HMF typically have more length-dependent, i.e., non-uniform flux distributions and are thus less controllable to prevent severe membrane fouling at the membrane front parts and negative Δp_{TM} at the outlet of the module (Li et al., 2015). Specifically, for particle fouling the initial permeate flux is lower for longer HFM caused by a higher increase in Δp_L for longer fibers than for shorter fibers under the same volume flow (Kim and DiGiano, 2006). The high flux at the membrane inlet for longer fibers that leads to an initially strong particle deposition in this region (Piry et al., 2008). Hence, the deposit-related filtration resistance increases, and the effective Δp_{TM} is reduced (Kim and DiGiano, 2006). This should particularly be considered when HFM are applied for milk filtration, where more intensive deposit layer formation occurs than in water filtration due to the complex composition of milk containing higher amounts of protein as material prone to induce fouling. The formation of the deposit layer is mostly affected by higher Δp_{TM} (Gésan et al., 1994; Samuelsson et al., 1997; Steinhauer et al., 2015a) and lower crossflow velocity (Grandison et al., 2000; Schiffer et al., 2020). In milk filtration, the deposit layer consists mostly of casein micelles compressed by high Δp_{TM} (Bouchoux et al., 2010) forming a gel-like structure

reducing the flux and whey protein transmission (Le Berre and Daufin, 1996; Samuelsson et al., 1997; Carić et al., 2000; Bouchoux et al., 2009b; Schopf et al., 2020).

The length-dependent deposit layer formation will occur in all membrane systems as demonstrated for the milk protein fractionation by ceramic tubular membranes by Piry et al. (Piry et al., 2008; Piry et al., 2012) and by SWM by Hartinger et al. (Hartinger et al., 2019b; Hartinger et al., 2019c). In order to assess the length dependency in HFM, a system allowing the length effects to be determined had to be constructed.

A test plant was developed, where four HFM modules with an active length of 30 cm each could be assembled into a series. Secondly, the HFM modules with different lengths were constructed to measure the pressure drop along the fiber and to investigate the influence of the HFM length on Δp_L, Δp_{TM}, flux, transmission, and whey protein mass flow per module.

The objective was to identify the optimal combination between HFM length and crossflow velocity thus gaining insights valuable also for membrane manufacturers and dairies potentially considering applying HFM for milk protein fractionation. Based on these insights, the possibility of manufacturing HFM with custom-designed lengths for individual applications could be realized, which could be longer or shorter than current standard HFM systems. Thus, the knowledge obtained could be more flexibly used than at SWM and ceramic membrane system manufacture.

4.2 Experimental

4.2.1 Materials

Pasteurized skimmed milk was provided by the local dairy (Molkerei Weihenstephan, Freising, Germany). The milk was pasteurized at 74 °C for 28 s and then stored up to five days at 4 °C before being used. All experiments were performed at 55 °C and at native pH 6.7. Alternatively, low filtration temperatures could be applied, but this leads to a reduction in flux, which requires to install a larger active membrane area to compensate for this effect. It is also known that temperatures around 10 °C reduce purity and yield of the obtained milk protein fractions as explained in more detail in (Bouchoux et al., 2014; Dumpler et al., 2017; Hartinger et al., 2019a; Heidebrecht and Kulozik, 2019), which should be avoided in this study. Viscosities η were measured with an Anton Paar MCR 302 rheometer (Anton Paar, Graz, Austria) using the double-gap geometry. Densities φ were measured with an Anton Paar DMA 1001 density meter (Anton Paar, Graz, Austria).

Table 4.1. Viscosity η and density φ of pasteurized skimmed milk, microfiltration permeate and deionized water at 55 °C.

Properties	Measured Value
η_{Water}	504.2×10^{-6} kg m^{-1} s^{-1}
η_{Milk}	922.1×10^{-6} kg m^{-1} s^{-1}
$\eta_{Permeate}$	730.8×10^{-6} kg m^{-1} s^{-1}
φ_{Water}	985.7 kg m^{-3}
φ_{Milk}	1022.5 kg m^{-3}
$\varphi_{Permeate}$	1009.4 kg m^{-3}

4.2.2 Design and manufacturing of HFM modules

The HFM microfiltration membranes were provided by Pentair-X-Flow (Enschede, The Netherlands). The membranes were made of polyethersulfone (PES) which had a maximum pore size of 0.2 µm (according to the manufacturer's specification), an inner diameter of 1.5 mm, and an outer diameter of 2.25 mm. The HFM were operated in the inside-out filtration mode. Two different types of HFM modules were prepared for the experiments: membranes with a length of 0.32 m to be connected in the series of 1, 2, 3, or 4 units, and membranes with different lengths between 0.32 and 1.22 m, as shown in Table 4.2. In each module, 10 fibers were integrated in a polyvinyl chloride tube, with a length of the potting area of 1 cm at the inlet and at the outlet that did not contribute to the active membrane length and surface. The given active membrane surface is the inner area of the fibers. The inner diameter of the module housing was 13.5 mm, and the outer diameter was 16 mm.

Table 4.2. Characteristics of prototype membranes.

Module	Membrane Length, m	Active Membrane Surface, m^2
Membranes for series connection	4 × 0.32	$4 \times 1.41 \cdot 10^{-2}$
Membranes with different lengths	0.32	$1.41 \cdot 10^{-2}$
	0.62	$2.83 \cdot 10^{-2}$
	0.92	$4.24 \cdot 10^{-2}$
	1.22	$5.65 \cdot 10^{-2}$

4.2.3 Conditioning and cleaning procedure

After each filtration experiment, the HFM and the filtration plant were cleaned with a caustic (0.8% v/v Ultrasil 69, Ecolab Deutschland GmbH, Germany) and an enzymatic agent (0.3% v/v Ultrasil 67, Ecolab Deutschland GmbH, Germany) at 55 °C for 40 min, and finally, acidic cleaning (0.4% v/v Ultrasil 75, Ecolab Deutschland GmbH, Germany) at 55 °C for 30 min was performed. By measuring the pure water flux before each filtration experiment it was verified that the two-step cleaning process was suc-

cessful. Before starting the filtration experiments, membrane conditioning was performed using caustic Ultrasil 69 (0.4% v/v, Ecolab Deutschland GmbH, Germany) at 55 °C for 20 min, followed by water rinsing for 10 min.

4.2.4 Filtration rig

The experiments were performed in a pilot plant from SIMA-tec GmbH (Schwalmtal, Germany), which, however, had to be fundamentally adapted to the needs of this study as described and depicted in chapter 4.3.1). The pilot plant was equipped with a frequency-regulated centrifugal pump (model CRNE 1, Grundfoss, Erkath, Germany). The volume flow for the feed and the permeate was supplied via volume flow meters (model Promag 50, Endress + Hausser, Weil am Rhein, Germany). The temperature was controlled by a double-walled feed tank and circulating temperature-controlled water. The pressure at the inlet and the outlet as well as on the permeate side were measured by digital pressure transmitters (model Eco-1, Wika, Klingenberg, Germany).

4.2.5 Experimental design

All experiments were performed in duplicate using two independent batches of feed. The milk and the MF unit were preheated to 55°C prior to filtration. Pure water flux was measured at Δp_L = 0.50 bar and a mean Δp_{TM} of 0.25, 0.75, 1.25, 1.75, and 2.25 bar noting the required feed volume flow. The pure water permeability was calculated from the slope of the pure water flux graph as a function of Δp_{TM}.

At the start of the skim milk filtration, the remaining water was flushed out with milk with the permeate valve closed. Then, the permeate valve was opened to reach the target mean Δp_{TM}. The mixed-phase with water of the permeate was drained before the first sample was taken for analysis. Thereafter, both retentate and permeate were recirculated into the feed tank. Three different milk filtration protocols were adopted:

- Pressure drop experiments were performed for the membranes of different lengths (0.3, 0.6, 0.9, and 1.2 m) and four feed crossflow velocities of 2.8, 3.9, 5.8, and 6.6 m s^{-1} corresponding to feed volume flows of 1.8, 2.5, 3.7, and 4.2 $m^3 h^{-1}$. The pressure was first measured with a closed permeate valve and again after a steady state was reached at 45 min with the permeate valve opened. The aim was to investigate the influence of the hollow fiber membrane length on Δp_L.
- Mean Δp_{TM} variations were done by a stepwise increase for the membranes of different lengths (0.3, 0.6, 0.9, and 1.2 m) and at a feed volume flow of 2.8 m s^{-1}. The experimental procedure is described in detail elsewhere (Hartinger et al., 2019a). In brief, after adjusting the lowest reachable mean Δp_{TM} with a pressure close to zero

at the membrane end, the mean Δp_{TM} was held constant for 45 min and then increased in 0.2 bar steps. A fixed time interval of 30 min at each pressure level was obeyed to make sure that steady-state filtration condition at each pressure level was reached before moving on to the next level. Prior to each mean Δp_{TM} increase and at the end of the experiment, the flux was measured. The objective here was to investigate the influence of Δp_{TM} on flux, transmission, and whey protein mass flow for different HFM lengths.

- Experiments with constant mean Δp_{TM} were performed for the module elements connected in series (4 × 0.3 m) at a feed volume flow of 2.8 m s^{-1}. After adjusting the lowest reachable mean Δp_{TM} of 0.83 bar, mean Δp_{TM} was held constant for 45 min. With this approach, we investigate the influence of the HFM length on flux, transmission, and whey protein mass flow per module.

Permeate samples were taken for further analysis at the end of each pressure step and the retentate was sampled from the feed tank at the beginning and at the end of the experiment, respectively.

4.2.6 Determination of milk proteins

Casein fractions α_{S1}, α_{S2} and β, and κ-casein, as well as the whey protein fractions α-lactalbumin and β-lactoglobulin A and B, were quantitatively analyzed by the reversed-phase high-performance liquid chromatography (RP-HPLC) using the method described in Dumpler et al. (2017).

4.2.7 Assessment of filtration performance

The mean transmembrane pressure, Δp_{TM}, was calculated from the pressure at the membrane inlet, p_{in}, at the membrane outlet, p_{out}, and at the permeate side, p_{per}, as follows:

$$\Delta p_{TM} = \frac{p_{in} + p_{out}}{2} - p_{per} \tag{4.1}$$

The pressure drop, Δp_L, along the membrane can be calculated as the difference between the pressures at the membrane inlet, p_{in}, and at membrane outlet, p_{out}, as follows:

$$\Delta p_L = p_{in} - p_{out} = \frac{\tau_W \cdot d_i}{4 \cdot L} \tag{4.2}$$

where τ_W is the wall shear stress, d_i is the inner diameter of the fiber, and L is the fiber length, respectively. The pressure drop in tubes, Δp_L, can be estimated as:

$$\Delta p_L = \frac{1}{2} \cdot \lambda \cdot \frac{L}{d_i} \cdot \varphi \cdot v_m^2 \tag{4.3}$$

where λ is the friction factor, φ the density, and v_m the mean crossflow velocity, respectively. The mean crossflow velocity, v_m, was calculated as:

$$v_m = \frac{\dot{V}_{feed}}{A_{cross}} \tag{4.4}$$

where $\dot{V}_{feed}$ is the feed volume flow, and A_{cross} is the free cross-section of the hollow fibers for ten fibers calculated as $1.77 \cdot 10^{-5}$ m^2. The state of flow was characterized by the Reynolds number, Re:

$$Re = \frac{\varphi \cdot v_m \cdot d_h}{\eta} \tag{4.5}$$

where d_h is the hydraulic diameter, and η is the permeate dynamic viscosity, respectively.

The permeate flux, J, the protein transmission, and the mass flow of whey proteins were used to determine the fractionation rate and efficiency. The total filtration resistance, R_F, membrane resistance, R_M, and deposit layer resistance, R_D, were determined according to Darcy's law:

$$J = \frac{\dot{V}_{per}}{A_M} = \frac{\Delta p_{TM}}{\eta \cdot R_F} = \frac{\Delta p_{TM}}{\eta \cdot (R_M + R_D)} \tag{4.6}$$

where J is the permeate flux, $\dot{V}_{per}$ the permeate volume flow, A_M the active membrane surface, and Δp_{TM} the transmembrane pressure, respectively. The transmission of the proteins through the membrane, Tr_i, is calculated as the ratio of their concentration in the permeate, $c_{i,per}$, and the concentration in the retentate, $c_{i,ret}$, for each protein component i as:

$$Tr_i = \frac{c_{i,per}}{c_{i,ret}} \cdot 100\% \tag{4.7}$$

Based on the flux, J, and protein concentration in the permeate, $c_{i,per}$, the whey protein mass flow, $\dot{m}_i$, was calculated as the most decisive criteria for milk protein fractionation:

$$\dot{m}_i = J \cdot c_{i,per} \tag{4.8}$$

4.3 Results and discussion

4.3.1 Development and validation of a concept for a measurement of the length dependency of microfiltration in HFM

A new concept for the assessment of the length dependency of HFM microfiltration

was developed at first, applying the principle idea of previous works (Bouchoux et al., 2009b; Piry et al., 2012; Hartinger et al., 2019b; Hartinger et al., 2019c). Thus, HFM test modules with 0.3 m each were constructed and connected in series of 1 – 4 units, to vary the total HFM length between 0.3 to 1.2 m. The distance between the individual modules was reduced to a practically achievable minimum.

For comparison, HFM prototype modules with different lengths of 0.3, 0.6, 0.9, and 1.2 m were produced to measure the pressure drop along the fibers without the connecting elements required in the HFM-in-series concept to validate that both systems were comparable in terms of Δp_L. With these systems, the influence of the HFM length on Δp_L and Δp_{TM} as well as on the flux, transmission, and whey protein mass flow per module was investigated.

With these technical amendments, the pilot plant schematically depicted in Figure 4.1 was made available. The modules in series concept (a) allowed to measure the transmission in each section separately. Pressure gauges were installed behind each HFM module to monitor the pressure between each section and to compare the Δp_L with the modules (b – e).

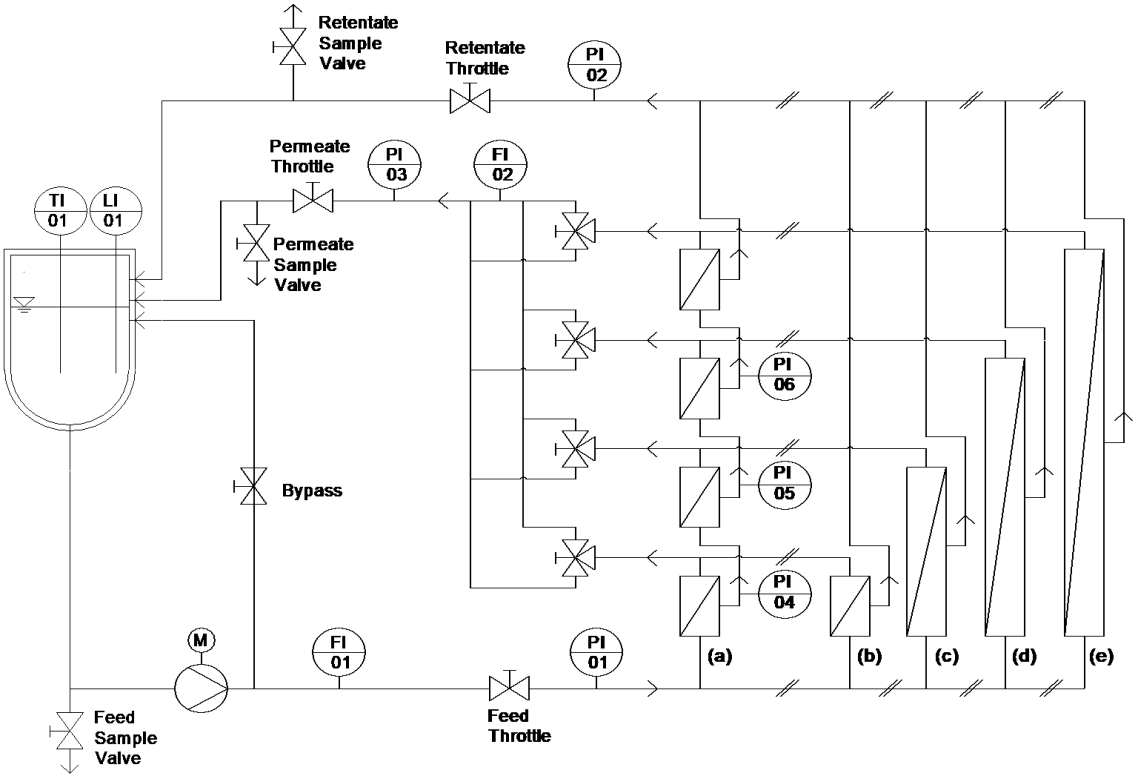

Figure 4.1. Simplified piping and instrumentation diagram of the pilot plant for different HFM modules: (a) series connection (4 x 0.3 m), (b) 0.3 m, (c) 0.6 m, (d) 0.9 m, and (e) 1.2 m fiber length.

As shown in Figure 4.2, the pure water permeability of both systems is in accordance. Thus, it could be concluded that the sectioned module system was applicable to

measure the filtration performance in terms of flux, whey protein transmission, and whey protein mass flow in a length-dependent manner.

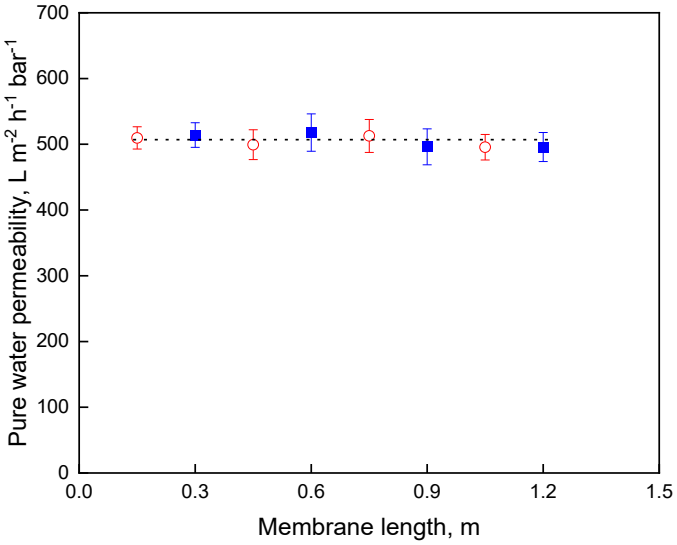

Figure 4.2. Pure water permeability as a function of the membrane length at ϑ = 55 °C and Δp_L = 0.50 bar for membranes of different lengths (■ squares) and sectioned membranes in series connection (○ circle).

The pure water flux depends linearly on the transmembrane pressure, according to Darcy`s law (Equation (4.6)). The slope of the pure water flux yields the pure water permeability and its mean value for all membranes is 505.8 ± 8.4 L m^{-2} h^{-1} bar^{-1}. As can be seen in Figure 4.2, the membranes of different lengths do not differ in their performance, as the flux is approximately the same.

To investigate the influence of the HFM length on the flow characteristics, the feed volume flow and the wall shear stress were determined by the pressure drop for the membranes of different lengths. Note that the feed flow rate had to be reduced and the wall shear stress thus to be varied to obtain a pressure at the module end close to zero, while maintaining a constant pressure drop of 0.50 bar. Figure 4.3 shows the relationship of membrane length, flow rate, and pressure drop Δp_L.

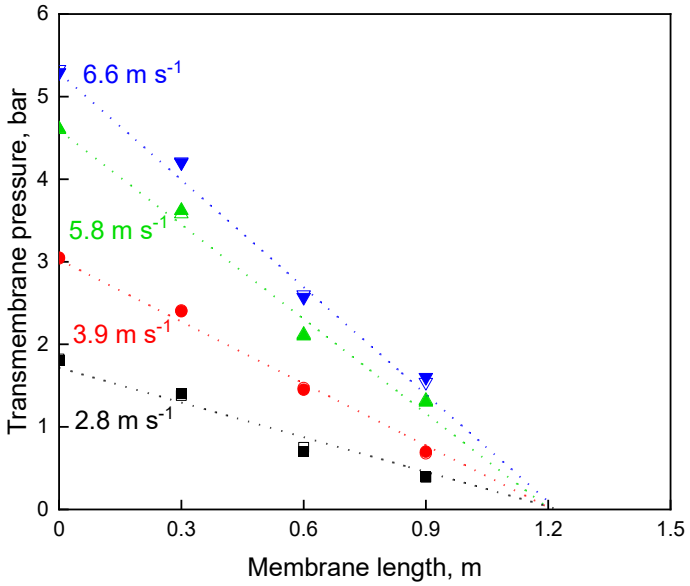

Figure 4.3. Transmembrane pressure as a function of HFM length for skim milk. The empty symbols are for the experiments with closed permeate throttle and the full symbols stand for the experiments with open permeate throttle and deposit layer formation.

As can be seen in Figure 4.3, the pressure is a linear function of length and a function of the crossflow velocity, according to Equation (4.3). All experiments were conducted with either permeate valve open or closed to prevent or induce deposit formation. Results do not differ, however, and it can thus be concluded that the deposit formation taking place with the permeate valve open does not have a sufficient height to significantly reduce the cross-section of the fibers, which otherwise would have led to higher levels of Δp_L. Figure 4.3 provides a clear view and selection criteria for choosing the possible combination of membrane length and crossflow velocity while avoiding negative Δp_{TM}.

The slopes of the linear graphs can be used to determine the friction coefficient and from this, the wall shear stress can be calculated as a function of the crossflow velocity and membrane length, according to Equation (4.3). Figure 4.4 shows the effect of membrane length on the allowed feed flow rate and the resulting wall shear stress, based on the condition that the pressure at the membrane outlet does not get negative.

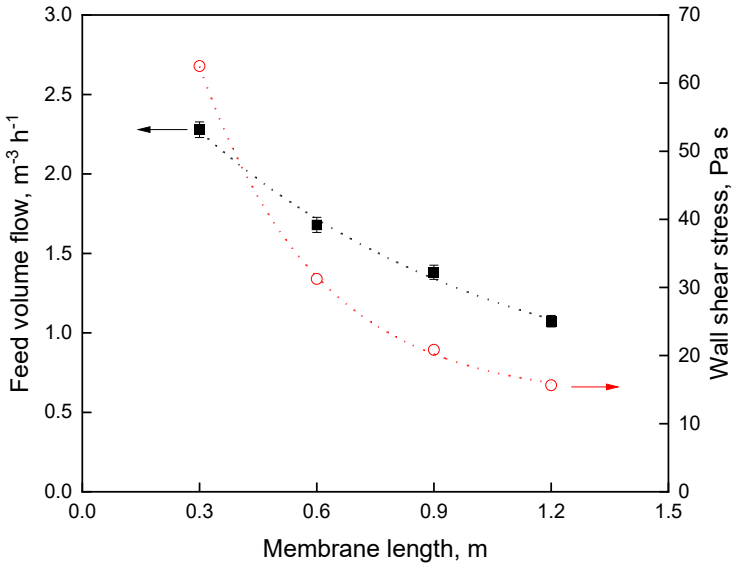

Figure 4.4. Feed volume flow (■ squares) of pure water and wall shear stress (○ circles) as a function of the membrane length at ϑ = 55 °C and Δp_L = 0.50 bar.

The conclusion from these data is that shorter membranes can be operated at a higher feed volume flow and thus a higher wall shear stress for a better control of deposit formation, especially for membrane filtrations with a feed rich in deposit forming material such as milk.

The friction factor and Reynolds number were calculated as functions of the cross-flow velocity in the HFM with a length of 0.3 m (Figure 4.5). It is established knowledge that un-concentrated skim milk of native pH, behaves like a Newtonian fluid (Bienvenue et al., 2003; Karlsson et al., 2005).

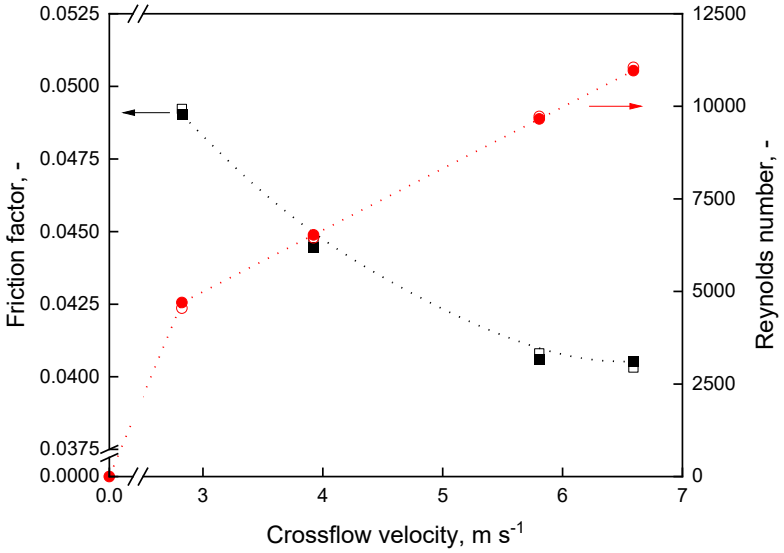

Figure 4.5. Friction factor (■ squares) and Reynolds number (● circles) as a function of crossflow velocity for pasteurized skimmed milk with closed permeate outlet in HFM with a length of 0.3 m. The empty symbols are for the experiments with closed permeate throttle

and the full symbols stand for the experiments with open permeate throttle and deposit layer formation.

As shown in Figure 4.5, the friction factor decreases with increasing crossflow velocity. The Reynolds number increases linearly with increasing crossflow velocity. The friction factor and Reynolds number are used to determine the hydraulic roughness between the fluid and the HFM. A hydraulic roughness maximum of 0.015 mm and a minimum of 0.008 mm were determined with the help of the Moody diagram (Moody, 1944) for experiments with closed as well as with open permeate valve. These values correspond to the range of absolute roughness for new polymer pipes of 0.015–0.007 mm (Wagner, 2001) and could be expected for HFM made of PES. As can be seen from the comparison of open and filled symbols in Figure 4.5, the formation of deposit layer does neither lead to a change of the friction factor nor to changes of Re. Even at the lowest crossflow velocity of 2.8 m s^{-1}, Re = 4.770 is well above the approximate critical value Re = 2300. In other words, flow conditions in HFM even in the longest module are turbulent.

Based on these insights, it is possible to design and operate membrane plants in terms of length and crossflow velocity based on Δp_L. The next chapter presents the data obtained for the impact of membrane length on flux and transmission of whey proteins.

4.3.2 Impact of membrane length on flux and transmission

According to Darcy's law (Equation (4.6)), the flux depends mainly on the transmembrane pressure, Δp_{TM}. This, in turn, is influenced by the pressure drop, Δp_L, along the membrane length, as discussed above. To prevent negative pressure at the module end, it is important to establish which lowest possible Δp_{TM} can be applied to the membrane module system, which is decisive to operate module systems at membrane-controlled conditions below the critical limit resulting in excessive deposit formation. As a new insight for milk protein fractionation by microfiltration using HFM this is shown in Figure 4.6. The minimum adjustable transmembrane pressure is that $\Delta p_{TM,min}$, where no negative pressure occurs at any point along the whole membrane length, and the entire membrane length can then be actively operated for filtration with no negative flux at the module end.

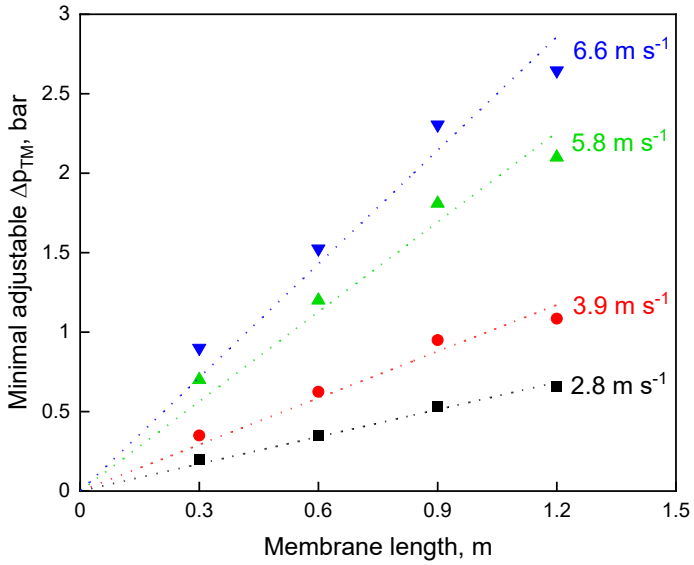

Figure 4.6. Minimum adjustable transmembrane pressure Δp_{TM} as a function of membrane length.

Figure 4.6 shows an increase in the minimally adjustable Δp_{TM} with increasing membrane length. It is clear that with higher crossflow velocities the minimum adjustable Δp_{TM} increases. The longer a module is, the larger is the membrane section, which cannot be operated under membrane-controlled conditions. Shorter membranes can be used with high crossflow velocities and lower Δp_{TM} for the fractionation of milk proteins, thus enabling a better deposit control and a high specific flux.

To ensure that the lowest adjustable Δp_{TM} is reached for all hollow fiber modules, the following experiments were performed at a skimmed milk feed volume flow of 2.8 m s^{-1}. To show the influence of the membrane length on the permeate volume flow, pasteurized skimmed milk was micro-filtered at different Δp_{TM} and the corresponding flux was measured (Figure 4.7).

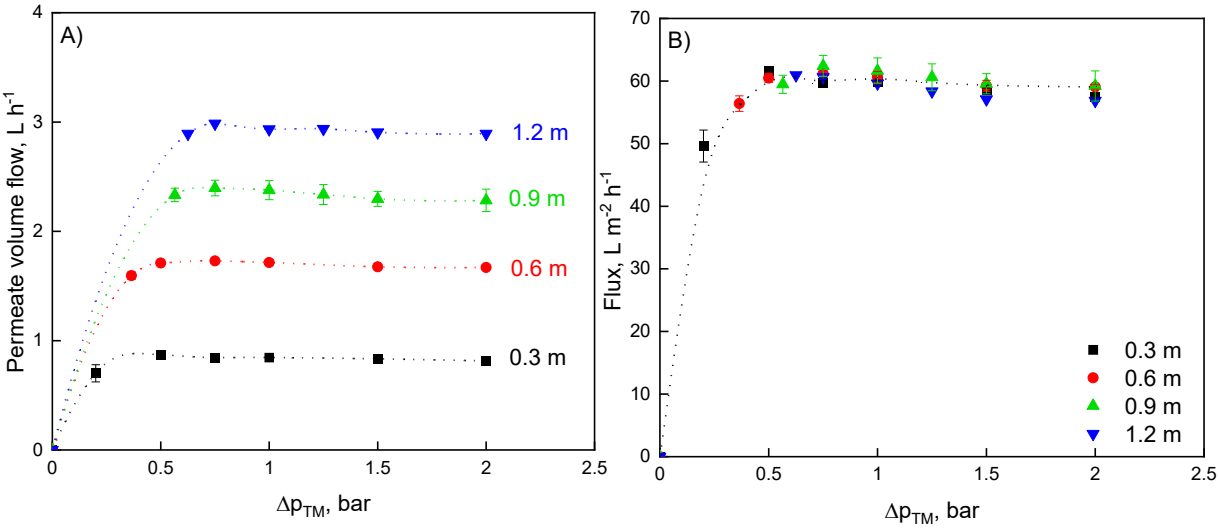

Figure 4.7. Permeate volume flow as a function of membrane length (A). Flux as a function of Δp_{TM} with different lengths (B). Experiments were conducted at a crossflow velocity of 2.8 m s^{-1}.

In Figure 4.7 A, the permeate volume flow was plotted against Δp_{TM} for the different HFM module lengths. With increasing pressure, the permeate volume flow increases until a limiting value depending on the membrane length, and thus the membrane surface area per module is reached. Moreover, Figure 4.7 A shows an increase in the permeate volume flow the longer the HFM length. Obviously, this is due to the increase in membrane surface when using longer fibers (Kim and DiGiano, 2006; Cheng et al., 2008).

To verify this, the specific flux was plotted against Δp_{TM}. Figure 4.7 B shows the typical curve for flux as a function of the Δp_{TM} reported in the literature for other types of membranes (Samuelsson et al., 1997; Hartinger et al., 2019a; Schiffer et al., 2020). With increasing Δp_{TM}, the flux increases until a limiting value is reached. For all HFM modules, the pressure reaching critical flux is 0.5 bar and the limiting flux is 61.5 L m^{-2} h^{-1}, respectively. Longer HFM can on average not be operated under membrane-controlled conditions. Their backpressure for the same feed volume flow determines the minimal adjustable Δp_{TM}. With higher Δp_{TM}, there is more intense fouling on the membrane during milk filtration (Piry et al., 2008).

Δp_{TM} above this limit also forces deposit forming particles into the membrane pores, thus resulting in pore blockage and pore narrowing. Since these pores can no longer be used for filtration, a local reduction of Δp_{TM} along the height of the deposit layer occurs and the flux is thus reduced (Bouchoux et al., 2014). In accordance with the literature (Bouchoux et al., 2010), it seems that the deposit layer structure consisting of compressible casein micelles is changed above the critical Δp_{TM}, thus obtaining a

flux, which is limited by membrane fouling. This leads to an increase in the total membrane resistance and a change in the permeability of the membrane. As a consequence, the transmission of whey proteins is reduced at higher Δp_{TM} levels (Figure 4.8).

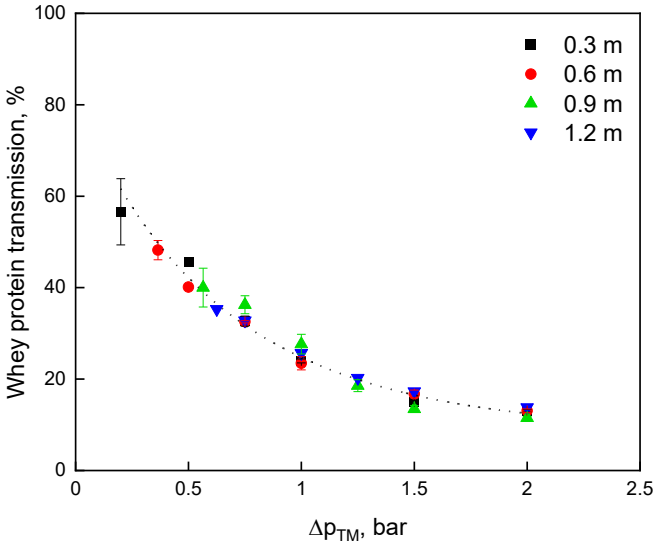

Figure 4.8. Transmission of whey proteins as a function of Δp_{TM} with different membrane lengths. Experiments were conducted at a crossflow velocity of 2.8 m s^{-1}.

Due to the particle size of whey proteins, e.g., β-lactoglobulin of 4.2 nm (Heidebrecht and Kulozik, 2019), the transmission should be unhindered and theoretically reach 100% for membranes with a pore size of 0.1 µm. However, since the deposit layer forms a secondary filtration resistance with a retention effect, and the transmission is thus significantly lower (Kühnl et al., 2010). Therefore, the transmission depends on the more or less compressed structure of the deposit layer, and this, in turn, depends on Δp_{TM}. Therefore, the transmission decreases with increasing Δp_{TM}. At the minimum adjustable Δp_{TM} value, the highest transmission is reached, which means that for the shortest membrane module of 0.3 m the highest transmission of 57% was achieved, whereas the transmission of the longest module was 35% at best. This can be explained by the formation of this deposit layers with differently compressed inner structures (Bouchoux et al., 2009b). At higher pressures, more compact deposited layers are formed, which exhibit a higher filtration resistance, depending on the spatial position along the membrane. Therefore, whey proteins are retained by the deposit layer on their way towards the membrane.

4.3.3 Filtration performance of the sectioned HFM

To assess this in more detail, the sectioned HFM units with a total length of up to 1.2 m were used and the length dependency was analyzed at a crossflow velocity of 2.8 m s^{-1} feed volume flow and a mean Δp_{TM} of 0.83 bar, respectively. Figure 4.9

shows the flux and the filtration resistances as functions of the axial position for the four individual sections with 0.3 m active membrane length each.

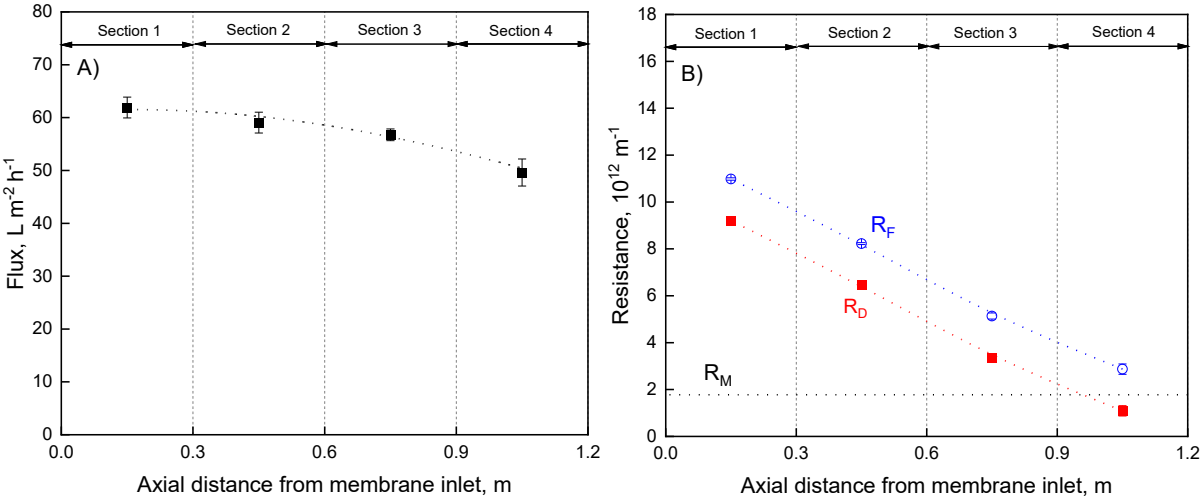

Figure 4.9. Flux (A) and resistance (B) of skimmed milk microfiltration as a function of the axial distance from membrane inlet for sectioned HFM in series connection. R_M is membrane resistance, R_F (○ circles) is total filtration resistance, and R_D (■ squares) is deposit layer resistance.

Figure 4.9 (A) shows that the flux through the first three sections is nearly the same at 61.5 L m^{-2} h^{-1} on average and reaches the limiting flux. These flux values correspond to the flux of the membranes of different lengths in Figure 4.7 (B) for a single membrane of 0.3 m, indicating that a comparison of both membrane systems is permissible. The flux values can be explained by the fact that the filtration is deposit controlled in the first three membrane sections because the flux is independent of the axial distance from the membrane inlet and thus from Δp_{TM}. Only module unit 4 of the HFM is Δp_{TM}-dependent and below the Δp_{TM} of critical flux correlation with the results of Figure 4.7. The friction effects and the pressure drop over the membrane length causing a reduction in Δp_{TM} explain the decline in flux (Piry et al., 2012).

The total filtration resistance, R_F, and the deposit layer resistance, R_D, shown in Figure 4.9B decrease almost linearly between the membrane inlet ($R_F = 11.0 \cdot 10^{12}$ m^{-1}) and the outlet ($R_F = 2.9 \cdot 10^{12}$ m^{-1}). The membrane resistance is constant over the entire membrane length, $R_M = 1.8 \cdot 10^{12}$ m^{-1}. In section 4 the membrane resistance is higher than that of the deposit layer, indicating that the filtration at the outlet of the module of the HFM is membrane-controlled. Due to the lower Δp_{TM}, with increasing axial distance from the membrane inlet, the transport of deposit to the membrane surface decreases, and the deposited proteins will be less compact (Hartinger et al., 2019c). This influences the transmission of whey proteins for the sectioned HFM, too (Figure 4.10).

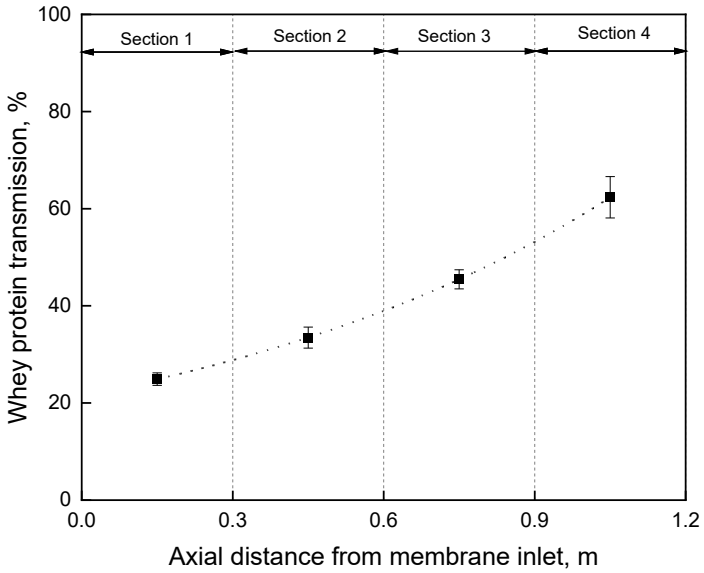

Figure 4.10. Transmission of whey proteins as a function of the axial distance from membrane inlet for sectioned HFM in series connection.

Due to the inhomogeneous deposit layer resistance, the transmission of whey proteins increases with membrane length. At the front end of the membrane 25% and at the rear end 62%. The mechanical compression of the deposited layer can also affect the structure of the casein micelles, which may become more compact due to the intense compaction and dewatering (Bouchoux et al., 2010).

Comparing the transmission for a 0.3 m HFM at a mean Δp_{TM} of 0.2 bar in Figure 4.8 to the transmission in section 4 also with mean Δp_{TM} of 0.2 bar in Figure 4.10, it can be seen that the transmission is the same. This shows both systems were operated at a flux below the fouling limited level of 61.5 L m^{-2} h^{-1}. Furthermore, the change in the flow and transmission corresponds to the position in the module due to the length dependency of Δp_{TM} in HFM. However, both trends are contrary to each other along the HFM length. At high Δp_{TM} at the front part of the membrane (section 1), the flux and thus the deposit layer resistance (Figure 4.9) are high, but the whey protein transmission (Figure 4.10) is low compared to the rear part of the HFM (section 4) at low Δp_{TM}. To address the question asked in the introduction about the optimal HFM length, an optimization problem must be solved. It can be solved using the whey protein mass flow as the evaluation criterion of filtration efficiency. Figure 4.11 shows the whey protein mass flow as a function of Δp_{TM} considering the HFM length. The direction of feed flow in the diagram is from the high pressure to the low pressure, corresponding to the five sections of the membrane from the right to the left had side of the diagram.

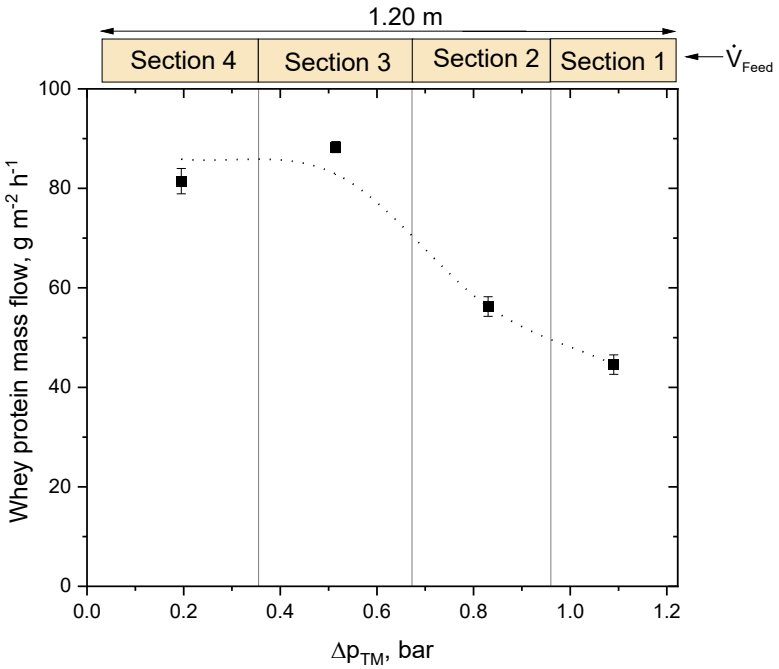

Figure 4.11. Optimal membrane length: whey protein mass flow per module as a function of Δp_{TM} for sectioned HFM in series connection.

Considering the length-dependence of Δp_{TM} in HFM, Figure 4.11 shows the efficiency of the milk protein fractionation used for optimizing the HFM length. Our results agree with the results obtained for ceramic tubular membranes by Piry et al. (Piry et al., 2008; Piry et al., 2012) and SWM by Hartinger et al. (Hartinger et al., 2019b; Hartinger et al., 2019c). Sections 3 and 4 of the HFM have the highest mass flow of approx. 85 g m^{-2} h^{-1}. The best performance of the HFM can be observed in two sections with low Δp_{TM}.

4.4 Conclusions

The objective of this study was to investigate the impact of the HFM length on milk protein fractionation. From the studies on other feed solutions, it was known that due to the pressure drop along the membrane the optimum module length strongly depends on the feed volume flow. Therefore, custom-made HFM modules with different lengths (0.3, 0.6, 0.9, and 1.2 m) were produced in-house and analyzed pure water feed volume flow and wall shear stress as a function of fiber length. We developed membrane modules to analyze and control the length effects during milk protein fractionation in HFM. As expected, the results showed the same trend of length-dependent effects for the microfiltration, but HFM can be more easily realized in the production of modules of different lengths compared to SWM or more ceramic tubular membranes. Compared to the HFM with different lengths, it was shown that the sectioning does not affect filtration performance at all. Only the combination of high flux values and high

transmission at low Δp_{TM}, as well as low fouling resistance and non-compact deposit layer, can guarantee a high mass flow and thus an optimal efficient milk protein fractionation in HFM. The best performance of the HFM can be observed in two sections at low Δp_{TM}. Thus, our study found the optimal length of the HFM for milk protein fractionation to be 0.6 m to ensure low transmembrane pressure. Longer fibers cause a high pressure drop and therefore cannot be operated at low Δp_{TM}, if the entire membrane module is to filter in the optimal range. Depending on the rheological profile of products than milk and on the respective nature of material prone to membrane fouling, the insights gained in this study could also serve for guidance in membrane or module design and selecting processing conditions in other areas, where membranes are operated in crossflow mode.

Funding: This project of the Forschungskreis der Ernährungsindustrie (FEI), Germany was supported via Allianz Industrie Forschung (AiF), Germany within the program for promoting the Industrial Collective Research (IGF) of the German Ministry of Economic Affairs and Energy (BMWi), Germany, based on a resolution of the German Parliament. Project: AiF 10 EWN.

Authors' contributions: R. Schopf and F. Schmidt conceived and designed the experiments, performed the experiments, and processed the data. R. Schopf, F. Schmidt, and U. Kulozik interpreted and discussed the data. All authors contributed to the writing of the manuscript.

Declaration of competing interest: The authors declare that they have no known competing financial interests or personal relationships that could have appeared to influence the work reported in this paper.

Acknowledgments: The authors gratefully thank Heidi Wohlschläger, Claudia Hengst, and Hermine Rossgoderer for their assistance with the RP-HPLC analysis of the milk samples. Siegfried Tuchborn of SIMA-tec GmbH and Christian Ederer, Franz Fraunhofer and Erich Schneider are acknowledged for their technical support. We thank Malou Warncke and Simon Schiffer for their benefits during discussion. We thank Günther Unterbuchberger for his assistance in conducting the experiments.

5 Comparative Assessment of Tubular Ceramic, Spiral Wound, and Hollow Fiber Membrane Microfiltration Module Systems for Milk Protein Fractionation [3]

Roland Schopf*, Florian Schmidt, Johanna Linner, and Ulrich Kulozik

Chair of Food and Bioprocess Engineering, TUM School of Life Sciences, Technical University of Munich, Weihenstephaner Berg 1, 85354 Freising, Germany

*Corresponding author

Summary and contribution of the doctoral candidate

CTM, SWM, and HFM can be used as membrane systems to separate milk proteins during MF. The membrane module selection depends on the performance of the membranes as well as an on the economic cost in acquisition, manufacturing, and maintenance, on the module dimension, and on the operating costs in terms of the selection of process parameters.

Based on the insides in fouling the same effects on deposit layer formation can be expected on HFM as well as on CTM and SWM. However, HFM provides the advantages of a better deposit layer control due to free cross-sections and less Δp_L like CTM and high packing density at low manufacturing costs as SWM. Therefore, the hypothesis is that the variation of local pressure and flow conditions has a higher impact on whey protein mass flow per module of HFM, resulting in a higher fractionation efficiency when compared to CTM and SWM.

The comparative assessment of HFM, CTM, and SWM module systems was performed with industrially sized standard modules with the same dimensions and module footprints in terms of module diameter and length. The Δp_{TM} was varied at a constant feed volume flow rate of 20 $m^3\ h^{-1}$ and secondly at a constant Δp_L of 1.3 bar m^{-1}. Flux, whey protein transmission, and whey protein mass flow were analyzed and correlated to the packing density of the modules. Moreover, the casein-to-whey protein ratio was calculated to obtain an evaluation criterion for the fractionation efficiency.

---

[3] Original publication: Schopf et al. (2021b): Schopf, Roland; Schmidt, Florian; Linner, Johanna; Kulozik, Ulrich. 2021b. Comparative Assessment of Tubular Ceramic, Spiral Wound, and Hollow Fiber Membrane Microfiltration Module Systems for Milk Protein Fractionation. Foods (Basel, Switzerland) 10 (4). DOI: 10.3390/foods10040692. Adapted original manuscript. Adaptions of the manuscript refer to enumeration type, citation style, spelling, notation of units, format, and merging all lists of references into one at the end of the dissertation. No special permission is required to reuse all or part of article published by MDPI.

The results showed that with increasing membrane area a more effective fractionation per module could be obtained. The lower the Δp_L, the higher the crossflow velocity and the better the deposit layer formation could be controlled. The lower the Δp_{TM}, the less intense and the more porous was the deposit layer. HFM modules provide high crossflow velocity and low Δp_L. Therefore, the formation of the deposit layer can be better controlled leading to higher performance in terms of flux compared to SWM. Moreover, HFM provides a higher packing density leading to higher whey protein mass flow per module compared to CTM. Thus, HFM modules seem to be an attractive alternative in the dairy industry for the task of milk protein fractionation which should be verified at the industrial level.

The doctoral candidate specified the experimental concept for this study and did a critically reviewing of the literature. The experimental design for the validation was developed by the doctoral candidate. Furthermore, the doctoral candidate carried out experimental work, data analysis, interpretation, calculation, and plotting. The doctoral candidate wrote and revised the manuscript. The last author initiated the study and all co-authors prepared the project outline. All co-authors contributed to the execution of experiments, the discussion of results, writing and revision of the manuscript.

Abstract

The fractionation efficiency of hollow fiber membranes (HFM) for milk protein fractionation was compared to ceramic tubular membranes (CTM) and spiral wound membranes (SWM). HFM combine the features of high membrane packing density of SWM and the more defined flow conditions and better control of membrane fouling in the open flow channel cross-sections of CTM. The aim was to comparatively analyze the effect of variations in local pressure and flow conditions using single industrially sized standard modules with similar dimensions and module footprints (module diameter and length). The comparative assessment with varied transmembrane pressure was applied first for a constant feed volume flow rate of 20 $m^3\ h^{-1}$ and secondly with the same axial pressure drop along the modules of 1.3 bar m^{-1}, similar to commonly applied crossflow velocity and wall shear stress conditions at industrial level. Flux, transmission factor of proteins (whey proteins and serum caseins), specific protein mass flow per area membrane and per volume of module installed were determined as evaluation criteria. Casein-to-whey protein ratios were calculated as a measure for the protein fractionation effect. Results obtained show that HFM, which so far are under-represented as standard module types in industrial dairy applications, appear to be a competitive alternative to SWM and CTM for milk protein fractionation.

Keywords: separation efficiency; casein; whey protein; deposit layer formation; fouling; transmembrane pressure; limiting flux; transmission; mass flow

Graphical abstract:

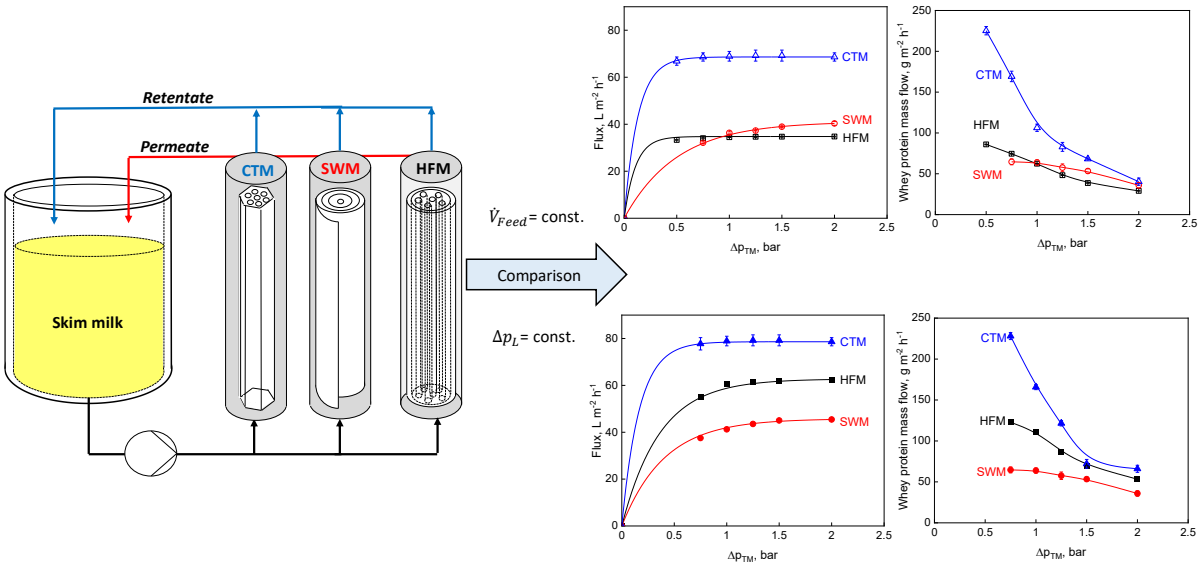

5.1 Introduction

Fractionation of skim milk into micellar casein and whey proteins by means of microfiltration (MF) is an established unit operation in the dairy industry. Usually, ceramic tubular membranes (CTM) (Le Berre and Daufin, 1996; Samuelsson et al., 1997; Samuelsson, 1997; Gésan-Guiziou et al., 2000; Vadi and Rizvi, 2001; Hernández and Harte, 2009; Adams and Barbano, 2016; Schiffer and Kulozik, 2020) or spiral wound membranes (SWM) (Zulewska et al., 2009; Beckman and Barbano, 2013; Zulewska and Barbano, 2013; Hartinger et al., 2019a) are used for this purpose. Whereas SWM provide a high packing density, i.e., high membrane area per module (Hartinger et al., 2019a), CTM are more resistant, more durable, and usually are reported to have better separation characteristics (Samuelsson et al., 1997; Hernández and Harte, 2009). However, CTM are expensive (Baker, 2008) and SWM more difficult to clean (Graf von der Schulenburg et al., 2008). Polymeric hollow fiber membranes (HFM) generally combine the advantages of both types of modules, including a large membrane area per module, free flow cross-sections, low cost, and high separation efficiency (Baker, 2008). Until recently, HFM were rarely used in the dairy sector, although they have been the standard technique in other fields of food processing, like drinking water production, wastewater treatment, and wine and beer filtration (Li et al., 2017).

Deposit formation of retained matter is an issue in all membrane systems, as reported for HFM (Li et al., 2017; Schork et al., 2018; Schopf et al., 2020; Weinberger and Kulozik, 2020; Schopf et al., 2021a), CTM (Samuelsson et al., 1997; Gésan-Guiziou et al., 2000; Schiffer and Kulozik, 2020), and SWM (Beckman and Barbano,

2013; Hartinger et al., 2019a), however at different levels due to the different flow channel configurations. Deposit formation strongly impairs flux and the desired high whey protein mass flow, which is a key aspect in milk protein fractionation (Gésan-Guiziou et al., 2000). Increased transmembrane pressure, Δp_{TM}, leads to a greater transport towards the membrane and results in compaction of the layer of retained casein micelles deposited on the membrane surface, despite crossflow conditions (Bacchin et al., 2002; Bouchoux et al., 2009a; Bouchoux et al., 2010; Qu et al., 2012; Loginov et al., 2020; Doudiès et al., 2021), thereby reducing the porosity of the deposited layer. This creates additional steric resistance to the mass transport of whey proteins and, thus, results in a reduction of whey protein transmission (Hartinger et al., 2019a). Bouchoux et al. (2009a) showed that casein micelles up to concentrations of 125 g L^{-1} do not significantly interact with one another. However, due to the dewatering of the micelles and a gel formation at higher concentrations of about 200 g L^{-1} the casein deposit layer becomes more compact. Qu et al. (2012) reported a critical osmotic pressure of 0.35 bar to be sufficient for irreversible gel formation on the membrane surface. In CTM, the volume flow and the resulting wall shear stress can generally be increased without limitation to reduce deposit layer formation by higher wall shear stress (Samuelsson et al., 1997). However, in SWM the increase in feed volume flow is limited due to structural module instability, occurring above critical backpressure levels (Graf von der Schulenburg et al., 2008; Kavianipour et al., 2017) resulting in module damage, e.g., by the so-called telescoping effect (Karabelas et al., 2018). For milk protein fractionation, flux and whey protein transmission are the most important factors. Next to that, the casein-to-whey protein ratio as the main fractionation effect is an additional decisive evaluation aspect when assessing module types in this context. Deposit-induced reduction of whey protein transmission is the more decisive criteria in the case of milk protein fractionation than flux reduction, as flux reduction can be compensated by increasing the installed membrane area. Given the module characteristics of HFM, the question was whether the less intense deposit formation in open tubular membrane systems like in CTM can beneficially be combined with the advantage of HFM, namely high membrane area packing density, which is also a key feature of SWM.

In previous studies we have reported on MF-based milk protein fractionation by HFM (Schork et al., 2018; Schopf et al., 2020; Weinberger and Kulozik, 2020; Schopf et al., 2021a), however with another perspective on fundamental aspects of deposit formation, therefore using small lab scale modules. We also demonstrated that the length dependency in HFM is equal to that of CTM and that the length-dependent pressure drop is responsible for inhomogeneous fouling along the HFM (Schopf et al., 2021a). Data for milk protein fractionation using industrially sized HFM modules are still lacking. Various works reported on milk protein fractionation using different module systems or

only comparing SWM with CTM, excluding HFM. Adams and Barbano (Adams et al., 2015a) compared the filtration performance of ceramic membranes with different channel diameters, but the same outer module diameter. They showed that ceramic membranes with 6 mm channel diameters could achieve a higher limiting retentate protein concentration than membranes with a channel diameter of 4 mm at the same pressure drop and the same flux due to an increase in crossflow velocity. Moreover, there are some concepts to counteract the length-dependent effects and to get a more homogenous flux and deposit layer formation. In the so-called uniform transmembrane pressure (UTP) mode, Δp_{TM} is kept constant by recirculating the permeate to a permeate side pressure drop (Hurt et al., 2010; Hurt et al., 2015a). The disadvantage of this concept is the higher energy demand and additional investment costs. Another option is to integrate an additional resistance to permeation from inlet to module outlet, either by variation of the thickness of the selective layer or to integrate a gradient in membrane resistance in the support layer (Adams and Barbano, 2013).

To our knowledge, only one study has compared the filtration performance of skim milk MF with different filtration modules (Zulewska et al., 2009). Zulewska et al. (2009) revealed significant differences in the flux of SWM (16 kg h^{-1} m^{-2}) and ceramic gradient membrane (72 kg h^{-1} m^{-2}) at a filtration temperature of 50°C, but HFM were not investigated. The authors found a higher β-lactoglobulin passage through the CTM compared to SWM, attributing this to the material properties of the ceramic membrane (Zulewska et al., 2009). The effects of different Δp_{TM} on the formation of the deposit layer were not included in their assessment. Overall, it can be stated that conditions were such that results from the various studies were not obtained from comparable experimental set-ups, i.e., using different processing conditions, differently sized module types, and different evaluation criteria.

Since the module systems at the industrial level are operated under different volume throughput conditions to achieve the respective desired maximally possible fluid velocities and wall shear stresses for each system, a question for this study was, how to compare HFM, CTM, and SWM in this regard. Options were to operate the systems either at constant pressure drop or at constant feed volume flow. The comparative assessment was therefore performed applying both concepts to realize a relevant comparison of the membranes at common and approximately optimal crossflow velocity and wall shear stress conditions or at the same feed input. The volume flow and the pressure drop chosen were those determined as the maximum for SWM, given the risk of module destruction by membrane telescoping at higher back-pressures.

A key aspect and aim were to compare all three membrane systems at their whey protein mass flow optimum in order to produce results closer to industrial reality using similarly sized commercial modules with similar geometric dimensions, i.e., module

footprints, and to use the module performance as assessment criteria. This enables a comparison of flux, transmission, and whey protein mass flow in relation to the individual module unit rather than per square meter installed membrane area. A comparably systematic approach has not been reported so far to our knowledge.

The expectation was that HFM should perform well compared to CTM in terms of specific flux in L m^{-2} h^{-1} and superior to SWM in terms of flux and mass flow per module volume. This should lead to a higher impact on flux and transmission of HFM resulting in a higher fractionation efficiency compared to CTM and SWM.

5.2 Materials and Methods

5.2.1 Milk

Pasteurized skim milk (74 °C for 28 s) was sourced from a local dairy (Molkerei Weihenstephan, Freising, Germany) and stored (4 °C) for up to five days. The milk pH was 6.6 for all experiments. Table 3.1 shows the viscosity, η, and density, φ, of deionized water, skim milk, and the microfiltration permeate measured according to Schopf et al. (2021a).

Table 5.1. Properties of water, milk and permeate at a temperature of 55 °C.

Properties	55 °C
η_{Water}, 10^{-6} kg m^{-1} s^{-1}	504.2 ± 8.7
η_{Milk}, 10^{-6} kg m^{-1} s^{-1}	922.1 ± 11.3
$\eta_{Permeate}$, 10^{-6} kg m^{-1} s^{-1}	730.8 ± 5.9
φ_{Water}, kg m^{-3}	985.7 ± 1.6
φ_{Milk}, kg m^{-3}	1022.5 ± 4.7
$\varphi_{Permeate}$, kg m^{-3}	1009.4 ± 2.1

5.2.2 Membrane modules

The nominal pore size of the membranes was 0.1 µm according to manufacturer specifications. HFM (polyethersulfone, inner fiber diameter 1.5 mm, outer fiber diameter 2.25 mm, filtration from inside-out) were supplied by Pentair-X-Flow (Enschede, The Netherlands) for an industrial module (R100MF, 1932 fibers) and a self-made module with ten fibers to gain higher crossflow velocities. SWM (V01, module configuration 6338, polyvinylidene fluoride, equipped with a 46 mil diamond spacer) were supplied by Synder Filtration (Vacaville, CA, USA) with two cartwheel-shaped anti-telescoping devices. CTM (7P19-40, 7 elements each with 19 channels, selective layer material α-Al_2O_3, a diameter of each channel 4.0 mm) were supplied by Pall Corporation (Port Washington, NY, USA). The three industrial module types in their dimensions with approximately roughly the same module diameters and membrane lengths were

chosen in order to perform a meaningful comparative assessment of the modules (Table 5.2).

Table 5.2. Module dimensions of hollow fiber membrane (HFM), spiral wound membrane (SWM), and ceramic tubular membrane (CTM).

Type, -	Module length, m	Module diameter, m	Membrane surface, m^2	Module volume, L	Packing density, $m^2\ m^{-3}$
HFM	1.02	0.16	9.3	20.7	449
SWM	0.97	0.17	16.4	22.6	723
CTM	1.02	0.13	1.7	14.4	119

5.2.3 Conditioning and cleaning procedure

At the beginning of the filtration, a conditioning procedure was carried out. At 55 °C polymer HFM and polymer SWM were conditioned for 20 min with 0.4% v/v Ultrasil 69 (Ecolab Deutschland GmbH, Monheim/Rhein, Germany). Ceramic CTM were conditioned for 20 min with a caustic agent (0.5% UF466, Halag Chemie AG, Aadorf, Switzerland) at 65 °C. Then membranes and filtration plant were rinsed (10 min) with deionized water. At the end of the filtration, 0.8% v/v Ultrasil 69 and 0.3% v/v Ultrasil 67 were used for 40 min cleaning procedure (55 °C) for the polymer HFM or polymer SWM. Then, 0.4% v/v Ultrasil 75 was used at 55 °C for 30 min. For ceramic CTM 1% UF466 at 65 °C for 40 min followed by acidic cleaning (0.5% nitric acid (60%), Halag Chemie AG, Aadorf, Switzerland) at 65 °C for 20 min. To ensure that the membranes were clean before filtration, the pure water flux was measured.

5.2.4 Filtration plant

The pilot plant (SIMA-tec GmbH, Schwalmtal, Germany) was had with a multistage centrifugal pump (CRNE, Grundfos GmbH, Erkrath, Germany). The feed volume flow, as well as the permeate volume flow, was measured with electromagnetic flowmeters (FEH311, Endress + Hausser GmbH+Co. KG, Weil am Rhein, Germany). Digital pressure transmitters (A-10, WIKA Alexander Wiegand SE & Co. KG, Klingenberg, Germany) detected the pressure before and after the membrane and in the permeate. The temperature was measured by a digital resistance thermometer (TR30, WIKA Alexander Wiegand SE & Co. KG, Klingenberg, Germany). The filtration was recorded using ServiceLab 12 (ServiceLab, Neu-Ulm, Germany).

5.2.5 Filtration conditions

The microfiltration unit was tempered with pure water at 55 °C prior to filtration to avoid initial temperature changes affecting the filtration process. At a feed volume flow of 15 $m^3\ h^{-1}$ at a temperature of 55 °C and Δp_{TM}, of 0.1, 0.2, 0.3, 0.4, and 0.5 bar the

water flux was recorded. Separately, the skim milk was tempered at 55 °C before being transferred to the feed tank. Due to the lower viscosity of the retentate and the permeate leading to higher flux compared to cold temperatures the filtration temperature of 55 °C was chosen. Moreover, this temperature is above the optimum for microbial growth in milk (Schiffer and Kulozik, 2020) and below the denaturation temperature of the milk proteins (Dumpler et al., 2017). Starting the filtration, the remaining water was drained with skim milk while the permeate valve was closed. The mixed-phase was drained. Afterward, the retentate was recirculated into the reservoir. Two filtration protocols were performed which were applied independently of each other. First, the fractionation was carried out with the industrial membrane modules at a constant feed volume flow of 20 $m^3\ h^{-1}$ for a better comparison of the membranes at the same feed input. Second, the fractionation was carried out at a constant pressure drop of 1.3 bar m^{-1} for a better comparison of the membranes at common crossflow velocity and wall shear stress conditions. The reason for choosing this feed volume flow and pressure drop can be found in the limitation of SWM by structural damages at higher pressure drop, as discussed in the results section in detail. To ensure high pressure drop and crossflow velocity in the hollow fiber, a self-made module with ten fibers was used for this purpose. Mean Δp_{TM} variations for both approaches were done by a stepwise increase and Δp_{TM} was adjusted to 0.5 bar by opening permeate valve. The permeate mixed-phase was drained and the permeate was recirculated into the feed tank. Δp_{TM} was held constant for 45 min to achieve steady-state filtration conditions throughout. Subsequently, Δp_{TM} was increased gradually (every 30 min) to 0.75, 1.00, 1.25, 1.50, and 2.00 bar to obtain filtration data under the steady-state condition for each step.

5.2.6 Analysis of caseins and whey proteins

Permeate and retentate were quantitatively analyzed in the amount and composition of their milk proteins via reversed-phase high-performance liquid chromatography (RP-HPLC) according to Dumpler et al. (2017).

5.2.7 Calculations

The transmembrane pressure, Δp_{TM}, was determined according to Equation (5.1):

$$\Delta p_{TM} = \frac{p_{in} + p_{out}}{2} - p_{per} \tag{5.1}$$

The pressure drop, Δp_L, was calculated as the pressure at the inlet, p_{in}, minus the pressure at the membrane outlet, p_{out}. (Equation (5.2)).

$$\Delta p_L = p_{in} - p_{out} = \frac{\tau_W \cdot d_i}{4 \cdot L} \tag{5.2}$$

where τ_W is the shear stress, d_i is the tube diameter, and L is the length of the tubular membrane. For comparison of the wall shear stress τ_W the wall shear rate, γ_T, was also calculated according to Newton's law of viscosity, η, (Equation (5.3)) assuming the fluid to be Newtonian at the membrane surface (Gésan-Guiziou et al., 1999):

$$\gamma_T = \frac{\tau_W}{\eta} \tag{5.3}$$

For tubular flows the pressure drop, Δp_L, is a function of the mean crossflow velocity, v_m, (Equation (5.4)):

$$\Delta p_L = \frac{1}{2} \cdot \lambda \cdot \frac{L}{d_i} \cdot \varphi \cdot v_m^2 \tag{5.4}$$

with the friction factor, λ, and the density, φ. Therefore, the mean cross velocity, v_m, is the ratio of the feed volume flow, $\dot{V}_{feed}$, and the area of the cross-section, A_{cros}, (Equation (5.5)):

$$v_m = \frac{\dot{V}_{feed}}{A_{cros}} \tag{5.5}$$

The installed membrane area per module, i.e., the so-called packing density Θ, was calculated as a ratio of the area of the membrane A_M and the module volume V_{Mod} (Equation (5.6)):

$$\Theta = \frac{A_M}{V_{Mod}} \tag{5.6}$$

The flux J was calculated according to Darcy's law (Equation (5.7)). The sum of the membrane resistance, R_M, plus the deposit layer resistance, R_D, was the filtration resistance, R_F.

$$J = \frac{\dot{V}_{per}}{A_M} = \frac{\Delta p_{TM}}{\eta \cdot R_F} = \frac{\Delta p_{TM}}{\eta \cdot (R_M + R_D)} \tag{5.7}$$

The protein transmission, Tr_i, was determined as (Equation (5.8)):

$$Tr_i = 100\% \cdot \frac{c_{i,per}}{c_{i,ret}} \tag{5.8}$$

where $c_{i,per}$ was the permeate concentration and $c_{i,ret}$ the retentate concentration. The mass flow, $\dot{m}_i$, was determined as (Equation (5.9)):

$$\dot{m}_i = J \cdot c_{i,per} \tag{5.9}$$

5.2.8 Statistics

Origin 2020b (Origin Lab Corporation, Northampton, United States) was used to plot the graphs. Statistical analysis was done with RStudio 1.3.1093 (RStudio, Boston, United States). The P-value given from a one-way analysis of variance was calculated to indicate the significance level. The data points in the graphs represent the average and the error bars represent the range of the standard deviation of two filtrations.

5.3 Results and Discussion

5.3.1 Influence of the module configuration on the flux

The permeate flux was used as the first criterion to investigate the influence of the transmembrane pressure, Δp_{TM}, variation on the deposit layer formation and thus on the efficiency of milk protein fractionation. High flux values can be achieved by high pressure drops due to increased deposit removal. SWM had high frictional effects, due to the module design with spacer geometry on the retentate side (Kavianipour et al., 2017). In contrast, CTM and HFM have free flow channel cross-sections (Schopf et al., 2021a). For this reason, the pressure drop, Δp_L, in CTM and HTM is lower than in SWM. The maximum permissible Δp_L of 1.3 bar m^{-1} (Hartinger et al., 2020c) to prevent structural damage in the SWM was reached at a mean crossflow velocity, v, of 0.6 m s^{-1} and a feed volume flow rate, $\dot{V}$, of 20 m^3 h^{-1}. This feed volume flow rate was firstly also applied for HFM and CTM as one of the options of parameter choice. The measured flux values are depicted in Figure 5.1.

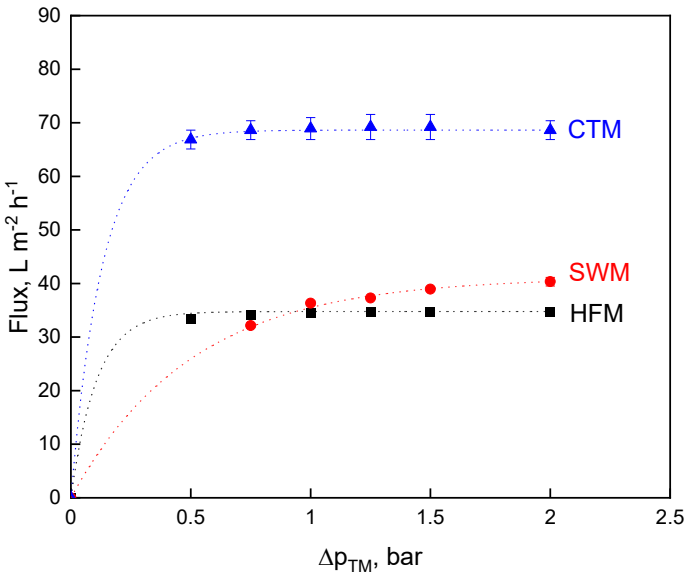

Figure 5.1. Flux as a function of the transmembrane pressure, Δp_{TM}, for spiral wound membrane (SWM; ●), ceramic tubular membrane (CTM; ▲), and hollow fiber membrane (HFM; ■) at a feed volume flow of $\dot{V}$ = 20 m^3 h^{-1}.

The typical relationship for flux over the Δp_{TM} for HFM (Schopf et al., 2021a), SWM (Hartinger et al., 2019a), and CTM (Schiffer and Kulozik, 2020) is shown in Figure 5.1. Increasing Δp_{TM} leads to a flux increase before the curve starts to level off (critical flux level), then approaching an upper level referred to as limiting flux (Field et al., 1995). At higher Δp_{TM} levels, intense membrane fouling occurs. The amount of protein deposited on the membrane surface increases and the deposited layer gets gradually more compressed (Loginov et al., 2020). In particular, casein micelles forming the deposited layer will be compressed into a gel-like structure that reduces flux and permeability (Bouchoux et al., 2010; Qu et al., 2012). Depending on the membrane module, the critical flux was reached at different Δp_{TM} levels. At a Δp_{TM} of 2.0 bar, the highest flux value could be achieved with CTM (67 L m^{-2} h^{-1}) followed by SWM (41 L m^{-2} h^{-1}) and HFM (35 L m^{-2} h^{-1}). The flux values of SWM and HFM did not significantly ($P \leq 0.1$) differ from each other at all Δp_{TM} levels. Polymeric membranes have a higher hydrophobicity compared to ceramic membranes (Baruah et al., 2006), thus the flux of CTM is significantly ($P \leq 0.001$) higher than that of HFM and SWM.

The comparison via constant feed volume flow is not the perfect choice of conditions, because the modules are operated differently at the same volume flow in terms of pressure drop, wall shear stress, τ_w, and crossflow velocity. Except for SWM, the modules were thus operated at volume flow rates and resulting wall shear stresses and crossflow velocity levels lower than under industrial conditions, but still in a range of practical relevance (Table 5.3).

Table 5.3. Mean crossflow velocity v, the resulting pressure drop, Δp_L, the wall shear stress, τ_w, and the wall shear rate, γ_T, for spiral wound membrane (SWM), ceramic tubular membrane (CTM), and hollow fiber membrane (HFM) at a feed volume flow of $\dot{V}$ = 20 m^3 h^{-1}.

Type, -	Mean crossflow velocity v, m s^{-1}	Pressure drop Δp_L, bar m^{-1}	Wall shear stress τ_w, Pa	Wall shear rate γ_T, 10^3 s^{-1}
HFM	1.6 ± 0.01	0.6 ± 0.01	23 ± 2.1	25 ± 2.1
SWM	0.6 ± 0.01	1.3 ± 0.03	-	-
CTM	3.3 ± 0.01	0.8 ± 0.04	76 ± 8.4	82 ± 10.2

In the case of SWM, the velocity (v = 0.6 m s^{-1}) is in the upper range (maximum permissible pressure drop of 1.3 bar m^{-1}) of commonly applied crossflow velocities (Hartinger et al., 2019a). Hartinger et al. (2020c) described that flux and whey protein mass flow in SWM increase with increasing crossflow velocity until a maximum at mean crossflow velocities of 0.6 – 0.78 m s^{-1} is reached. Typical crossflow velocities for HFM are 0.5 – 5.8 m s^{-1} (Weinberger and Kulozik, 2020; Schopf et al., 2021a). For CTM, 3.3 m s^{-1} (τ_w = 76 Pa) is also a common crossflow velocity for milk MF, but rather low: Samuelson et. al. [1] mentioned 1.5 m s^{-1} to a maximum of 8 m s^{-1}as the typical range of crossflow velocities in ceramics membranes. Moreover, Schiffer et al. (2020) re-

ported the optimum for limiting flux at wall shear stresses of 131 Pa. The authors observed that higher wall shear stresses lead to flux reduction. Thus, too high velocities could not only reduce flux but reduce the minimal adjustable transmembrane pressure of a module where no backpressure occurs (Schopf et al., 2021a). Furthermore, focusing on the wall shear rate, calculated from Equation (5.3), the values of 82 000 s^{-1} for CTM and 25 000 s^{-1} for HFM seems to be rather high, but as it is reported from Gésan-Guiziou et al. (1999) for CTM in a common range. They calculated wall shear rates up to 168 000 s^{-1}. However, they also described that the wall shear stress is a more suitable value to describe the tubular flow properties on deposit layer formation compared to the wall shear rate. Therefore, the wall shear stress and the corresponding pressure drop are used for the description of the influence of the module configuration on the flux.

Comparing the membranes with a constant volume flow, HFM and CTM are supposedly disadvantaged due to the crossflow velocity below industrial standard. Therefore, HFM (τ_w = 48 Pa, v = 3,2 m s^{-1}) and CTM (τ_w = 127 Pa, v = 4.7 m s^{-1}) were also operated at the same pressure drop of 1.3 bar m^{-1}, like the SWM, at common industrial conditions and approximately at their optimums, as discussed above (Table 5.4).

Table 5.4. Mean crossflow velocity, v, the resulting pressure drop, Δp_L, the wall shear stress, τ_w, and the wall shear rate, γ_T, for spiral wound membrane (SWM), ceramic tubular membrane (CTM), and hollow fiber membrane (HFM) at a pressure drop of Δp_L = 1.3 bar m^{-1}.

Type, -	**Mean crossflow velocity v, m s^{-1}**	**Pressure drop Δp_L, bar m^{-1}**	**Wall shear stress τ_w, Pa**	**Wall shear rate γ_T, 10^3 s^{-1}**
HFM	3.2 ± 0.01	1.3 ± 0.01	48 ± 2.1	52 ± 2.9
SWM	0.6 ± 0.01	1.3 ± 0.03	-	-
CTM	4.7 ± 0.01	1.3 ± 0.04	127 ± 8.4	138 ± 9.5

The flux values for all three membrane types as a function of the Δp_{TM} were given in Figure 5.2 at a constant pressure drop of 1.3 bar m^{-1}.

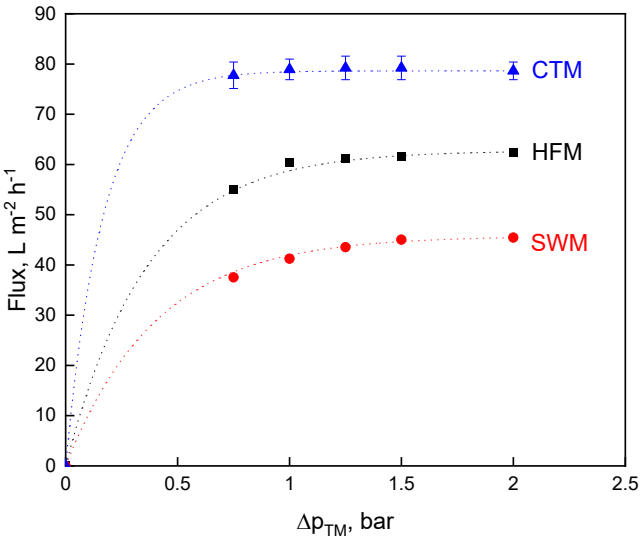

Figure 5.2. Flux as a function of the transmembrane pressure, Δp_{TM}, for spiral wound membrane (SWM; ●), ceramic tubular membrane (CTM; ▲), and hollow fiber membrane (HFM; ■) at a pressure drop of Δp_L = 1.3 bar m^{-1}.

Figure 5.2 demonstrates that higher flux values could be reached with higher wall shear stress for CTM and HFM compared to the results shown in Figure 5.1. High crossflow velocities lead to an increase in the eroding forces removing or at least mitigating the effect of deposit layer formation. Operating at approximately their crossflow velocity optima there are differences in the performance of the membranes operated at the same volume feed flow rate. Comparing the three membranes in terms of flux, CTM indicate the highest limiting flux at 79 L m^{-2} h^{-1} followed by HFM (62 L m^{-2} h^{-1}) and SWM (45 L m^{-2} h^{-1}). The flux of CTM, HFM, and SWM differed significantly ($P \leq 0.001$) from each other. The flux values of CTM and SWM are slightly higher than reported by Zulewska et al. (2009) due to the higher pressure drop. Ceramic membranes are more hydrophilic compared to polymeric membranes resulting in lower protein adsorption to the membrane (Baruah et al., 2006). This effect might well play a role, but we postulate that the flow properties in SWM with irregular flow velocity profiles before and behind the spacer net filaments were mainly responsible for the faster and locally more intense deposit layer formation producing a higher deposit layer resistance compared to the tube flow in HFM.

5.3.2 Influence of the module configuration on milk protein transmission

To assess the influence of Δp_{TM} variation on the transmission of milk proteins the permeate protein composition and protein amount at different Δp_{TM} was analyzed (Figure 5.3). The deposited layer of mainly casein micelles has an additional retention effect (Le Berre and Daufin, 1996; Schopf et al., 2020). Thus, the transmission of proteins (whey proteins, monomeric caseins in the serum, possibly small micelles, depending on the pore size distribution of the membranes) is affected (Weinberger and

Kulozik, 2020), with Δp_{TM} as a variable forming a more compact deposited layer as Δp_{TM} was raised (Bouchoux et al., 2010; Qu et al., 2012). Therefore, the transmission of caseins and whey proteins decreased with increasing transmembrane pressure (Figure 5.3). At the lowest transmembrane pressure, the transmission of both protein fractions, casein, and whey protein was highest for all module types. Moreover, in this context, the undesired casein transmission also decreased by increasing Δp_{TM}. The whey protein transmission at a wall shear stress of 76 Pa and 127 Pa in the CTM does not differ significantly ($P \leq 0.1$). The same applies to HFM. Thus, the transmission is strongly dependent on the Δp_{TM} and not on the wall shear stress. Although a high wall shear stress is expected to result in a more effective deposit removal, the deposited casein micelles form a more compact, gel-like structure at high Δp_{TM} (Qu et al., 2012), so that significantly higher values of whey protein transmission do not occur. As a consequence, the different protein transmissions can be attributed to the different module designs, and in addition to the membrane material.

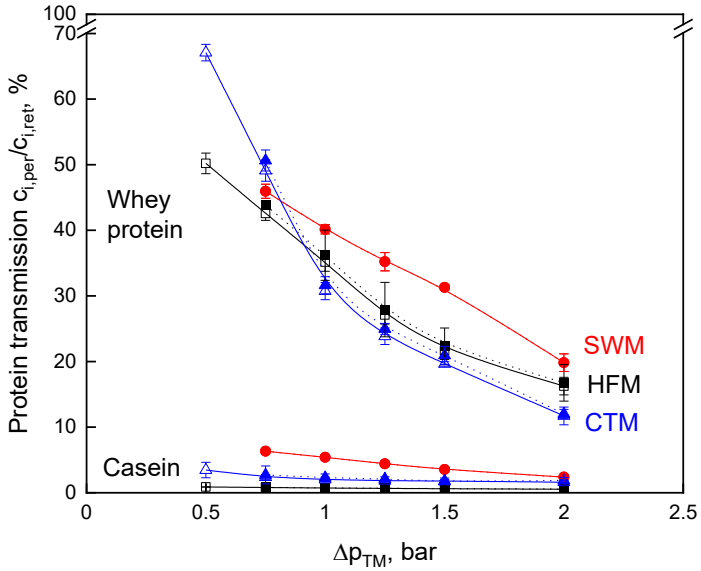

Figure 5.3. Protein transmission as a function of transmembrane pressure, Δp_{TM}, for skim milk microfiltration for spiral wound membrane (SWM; ●), ceramic tubular membrane (CTM; △ τ_w = 76 Pa; ▲ τ_w = 127 Pa) and hollow fiber membrane (HFM; □ τ_w = 23 Pa; ■ τ_w = 48 Pa).

From Figure 5.3, it becomes evident that the HFM achieves the lowest casein transmission level. At Δp_{TM} above 1.0 bar, SWM had the highest whey protein transmission, but at the same time, the casein concentration in the permeate was also high compared with that of CTM and HFM. The casein transmission of 7% at Δp_{TM} of 0.75 bar is in accordance with data reported in the literature (Zulewska et al., 2009; Hartinger et al., 2019a). The casein retention in SWM is dependent on the deposit layer formation. As reported by Zulewska et al (2009), SWM permeate contained a significantly higher amount of casein. At higher Δp_{TM} values, which are more common in the dairy industry,

the casein transmission is reduced. The difference in casein transmission between the different membranes may be due to the different pore size distributions of the membranes, although the nominal pore size was specified as 0.1 µm for all three membranes. Furthermore, the higher casein transmission can be explained by the fact that the SWM was operated at the maximum of the recommended axial flow velocity (Farhat et al., 2016), and therefore, deposit formation was at its lowest possible level. Also, SWM are affected by an inhomogeneous deposit layer formation on the membrane surface caused by extreme differences in shear stress depending on the position within the spacer network (Kavianipour et al., 2017). Therefore, the protein transmission can be expected to be higher in areas of high shear, which leads to a higher overall transmission, compared to CTM and HFM. Both casein and whey protein transmission are affected by the inhomogeneous deposit layer formation. However, this has a stronger effect on casein transmission since caseins are present as micelles and are preferably retained by the deposited layer. Compared to SWM, deposit layer formation in CTM and HFM are more homogeneous (Schopf et al., 2021a).

5.3.3 Impact of the filtration module on the fractionation efficiency

Higher crossflow velocities going along with higher pressure drops along the module for CTM and HFM lead to higher flux values (Figure 5.2), but also to an increase of the minimally adjustable Δp_{TM}, whereby whey protein transmission is reduced (Figure 5.3). Hence, the open question is whether the comparison of the membranes with constant feed volume flow or with constant pressure drop yield a higher mass flow. The dependence of flux and protein transmission on the Δp_{TM} results in a Δp_{TM} optimum for the milk protein fractionation. Equivalent to the mass flow of the aqueous phase, i.e., flux, the whey protein mass flow was calculated according to Equation (5.9) and plotted against the Δp_{TM} (Figure 5.4). This provides an additional and more suitable perspective on the speed of protein fractionation than flux and protein transmission alone.

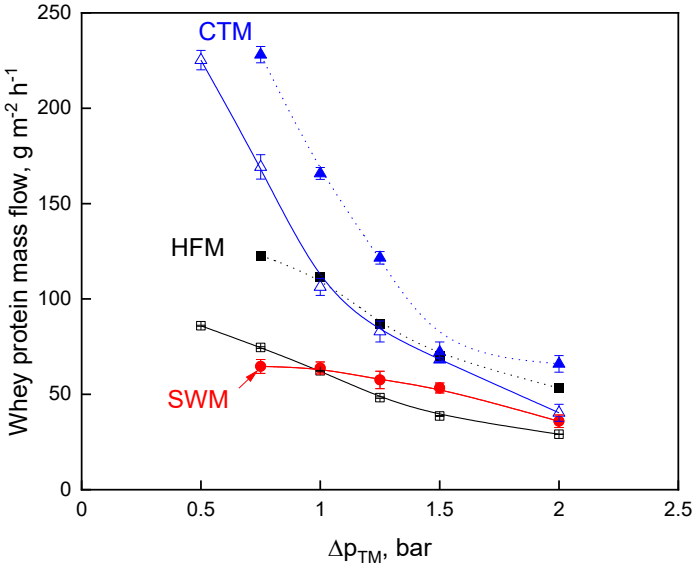

Figure 5.4. Mass flow of whey proteins as a function of transmembrane pressure, Δp_{TM}, for skim milk microfiltration for spiral wound membrane (SWM; ●), ceramic tubular membrane (CTM; △ τ_w = 76 Pa; ▲ τ_w = 127 Pa) and hollow fiber membrane (HFM; □ τ_w = 23 Pa; ■ τ_w = 48 Pa).

At the higher wall shear stress of 127 Pa and 48 Pa for CTM and HFM higher whey protein mass flows were obtained, respectively. Due to higher crossflow velocities, higher flux values are achieved, producing a stronger effect on whey protein mass flow than reaching lower Δp_{TM} (0.5 bar compared to 0.75 bar) and thus increased whey protein transmission. The comparison at constant feed volume flow in relation to a comparison at constant pressure drop shows higher mass flow at a constant pressure drop dependent on the Δp_{TM}. The maximum of the mass flow was at a Δp_{TM} of 0.75 bar and a pressure drop of 1.3 bar m^{-1} for CTM, HFM, and SWM, respectively (Figure 5.4). Operating at this point, CTM provides the highest whey protein mass flow of 229 g m^{-2} h^{-1} flowed by HFM (123 g m^{-2} h^{-1}) and SWM (64 g m^{-2} h^{-1}). In other words, CTM provides 1.9 times and 3.6 times more whey protein mass flow compared to HFM and SWM, respectively. This results from the combination of the high whey protein transmission and the high flux of the CTM at a Δp_{TM} of 0.75 bar compared to HFM and SWM.

To characterize the efficiency of the milk protein fractionation, the casein-to-whey protein ratio in the permeate was calculated at the whey protein mass flow maximum. The casein-to-whey protein ratio for the SWM was 0.77. This is in accordance with the literature, where the casein-to-whey protein ratio in SWM MF permeate was reported as 1.0 after a MF filtration time of 30 min (Hartinger and Kulozik, 2020). The casein-to-whey protein ratio of the HFM was 0.13 and the milk protein fractionation was, therefore, most efficient compared to that of the SWM and CTM with a casein-to-whey protein ratio of 0.35, which is also in the range of the previously reported data (Adams and

Barbano, 2013). We assume that the difference in fractionation efficiency between SWM and HFM/CTM results from the fact that the flow properties in SWM were responsible for faster and in some terms more intense membrane fouling and the fouling by casein changed the separation characteristics.

5.3.4 Impact of the packing density of the module on the filtration efficiency

As shown in Figure 5.2 and Figure 5.4, the flux and the protein mass flow are specific values per square meter membrane installed. However, the protein mass flow output per module, which results from the overall membrane area installed per module volume or module volumetric footprint, appears to be a more suitable measure when comparing module types, given the greatly differing packing densities. An advantage of HFM modules is the ability to pack a very large membrane area into a single module, depending on fiber diameter (Baker, 2008). Therefore, modules with approximately the same dimensions, i.e., module diameter, were compared for flux, transmission, and whey protein mass flow in relation to the different module type volumes, as characterized in Table 5.2. From these data, the whey protein mass flow per module and per volume was calculated and shown in Table 5.5 at its Δp_{TM} optimum for constant feed volume flow and constant pressure drop.

Table 5.5. Filtration performance of hollow fiber membranes (HFM), ceramic tubular membranes (CTM), and spiral wound membranes (SWM) for skim milk microfiltration at their Δp_{TM} optima.

Module, -	**HFM**	**CTM**	**SWM**	**HFM**	**CTM**	**SWM**
	$\dot{V}$ = 20 m³ h⁻¹			Δp_L = 1.3 bar m⁻¹		
Δp_{TM} optimum, bar	0.5	0.5	0.75	0.75	0.75	0.75
Flux, L m⁻² h⁻¹	33	67	32	55	78	32
Whey protein transmission, %	50	67	46	44	51	46
Whey protein mass flow, g m⁻² h⁻¹	86	225	64	123	229	64
Whey protein mass flow per module, g h⁻¹	800	384	1 050	1 144	389	1 050
Whey protein mass flow per volume, g m⁻³ h⁻¹	38 614	26 775	46 272	55 227	27 251	46 272

When HFM and CTM are operated at the same feed volume flow they perform better in terms of transmission as well as mass flow at their Δp_{TM} optima compared to SWM, although they are compared at low crossflow velocities (Table 5.5). This shows a possibility to get a high output of whey protein mass flow at low volume flow and low transmembrane pressure and thus low energy input. Even at the same feed volume flow rate HFM and CTM are competitive compared to SWM. This is also shown by the comparison operating at the same pressure drop: In terms of specific flux, transmis-

sion, and specific mass flow of whey proteins CTM provides the best filtration performance. But, CTM have the lowest module volume-specific membrane packing density with 119 $m^2\ m^{-3}$ compared to HFM with 449 $m^2\ m^{-3}$ and SWM with 723 $m^2\ m^{-3}$ (Table 5.2). Therefore, the whey protein mass flow per module and per volume in a CTM module is notably lower compared to SWM and HFM modules. Viewed from the perspective of the SWM module, a high packing density provides a high whey protein mass flow per module and per volume although the SWM module seems to provide low filtration performance in terms of the lowest membrane area-specific flux and lowest specific whey protein mass flow compared to HFM and CTM. The flux of CTM was 2.4 times higher and the whey protein mass flow 3.6 times higher than in SWM, but the SWM module provided a 2.7 times higher whey protein mass flow per module than the CTM module. With the whey protein mass flow per module as the main criterion for the performance comparison of membrane modules, it is obvious that the HFM module provided the best filtration performance compared to SWM and CTM. Although HFM performed at the level of CTM in terms of specific flux, but superior to SWM, the HFM module provided the best whey protein mass flow per module. Taking all aspects into consideration, HFM provided a higher specific filtration area compared to that of CTM. It can be said that free flow cross-sections of the channels lead to better control of the deposit layer than the spacer-filled flow channels in SWM. Thus, a more efficient milk protein separation with high whey protein mass flow could be achieved.

5.4 Conclusions

When selecting a suitable membrane module for milk protein fractionation, the overall economics of the membrane system should be considered. Here, not only the different acquisition, manufacturing, and maintenance costs play a decisive role, but also the effect of the selection of process parameters on the operating costs as well as the module dimension (membrane diameter and length). Ceramic membranes have higher manufacturing costs but are more durable and resistant than polymer membranes. However, SWM provides acceptable flux values even at lower feed flow rates compared to CTM and HFM. When membrane modules are operated at high crossflow velocity a better control of membrane fouling could be achieved in contrast to operating at the same feed volume flow, however, at the cost of higher energy expenditures to produce higher volume flow rates. This in turn also increases the effect of backpressure, not necessarily decline the module performance. The results of all membrane systems indicated that the bottleneck of a comparative assessment for an effective milk protein fractionation is the packing density and thus the footprint of a membrane module. An increase in the cross-section of the modules would lead to an increase in volume flow and an extension of the module length to more intensive length-dependent

effects of the MF. Both effects increase the operating costs during fractionation. The results reported here for SWM, CTM, and HFM, however, confirm that lower transmembrane pressures and high crossflow velocities seem to be appropriate for performing milk protein fractionation with these module types. Based on the data reported in this study, HFM, which are less often applied in the dairy industry for milk protein fractionation, appear to be a suitable alternative to the more established SWM or CTM, which would be interesting to see verified at the industrial level. Depending on actual and future HFM developments regarding maximization of membrane packing density, the advantage of HFM could become even higher compared to the results presented here.

Author Contributions: Conceptualization, R.S.; Data curation, R.S., F.S., and J.L.; Formal analysis, R.S.; Funding acquisition, U.K.; Investigation, R.S., F.S., J.L., and U.K.; Methodology, R.S., F.S., and J.L.; Project administration, R.S., and U.K.; Resources, U.K.; Software, R.S., F.S. and J.L.; Supervision, U.K.; Validation, R.S.; Visualization, R.S.; Writing—original draft, R.S.; Writing—review & editing, R.S., F.S., J.L. and U.K. All authors have read and agreed to the published version of the manuscript.

Funding: This IGF Project of the FEI was supported via AiF within the program for promoting the Industrial Collective Research, IGF, of the German Ministry of Economic Affairs and Energy, BMWi, based on a resolution of the German Parliament. Project: AiF 10 EWN.

Acknowledgments: The authors gratefully thank Heidi Wohlschläger, Claudia Hengst, and Hermine Rossgoderer for their assistance with the RP-HPLC analysis of the milk samples, Malou Warncke, Simon Schiffer, and Hans-Jürgen Heidebrecht for discussing results.

Conflicts of Interest: The authors declare no conflict of interest. The authors declare that they have no known competing financial interests or personal relationships that could have appeared to influence the work reported in this paper. The funders had no role in the design of the study; in the collection, analyses, or interpretation of data; in the writing of the manuscript, or in the decision to publish the results.

6 Impact of feed concentration on milk protein fractionation by hollow fiber microfiltration membranes in diafiltration mode [4]

Roland Schopf* and Ulrich Kulozik

Chair of Food and Bioprocess Engineering, TUM School of Life Sciences, Technical University of Munich, Weihenstephaner Berg 1, 85354 Freising, Germany

*Corresponding author

Summary and contribution of the doctoral candidate

The results of Chapter 5 showed that HFM could provide higher protein mass flow per module compared to SWM and CTM due to higher feed volume flow owing free cross-sections and due to the more effective deposit control and higher packing density. Based on these findings, optimal process conditions were determined for industrial level for the pre-concentration and the DF process.

The aim was to investigate the efficiency of fractionation according to the feed pre-concentration before starting the DF process. Δp_L and Δp_{TM} were varied to investigate the effect of an increased feed protein concentration on the deposit layer formation and structure in HFM. We compared two kinds of filtration protocols for feed pre-concentration in terms of flux, transmission, whey protein mass flow, and the time which is required to obtain one DF step: a concentration with a constant Δp_L compared to a concentration with constant feed volume flow. The optimal process conditions are determined at a Δp_{TM} of 0.5 bar, a Δp_L of 1.0 bar m^{-1}, and a CF of 2.5.

When using UF permeate as DF medium for transferring the whey proteins into the permeate, we could show that at CF 3, already 80% of the whey protein could be depleted after 2.5 DF steps. The amount of DF medium, as well as the filtration time, could be reduced when performing a DF process with the use of HFM compared to SWM and CTM. Due to the effective control of deposit layer formation, HFM can be operated at concentration levels 47% and 25% higher than those for SWM and CTM systems, respectively.

---

[4] Original publication: Schopf and Kulozik (2021): Schopf, Roland and Kulozik, Ulrich. 2021. Impact of feed concentration on milk protein fractionation by hollow fiber microfiltration membranes in diafiltration mode. Separation and Purification Technology, 119278, DOI: 10.1016/j.seppur.2021.119278; Adapted original manuscript. Adaptions of the manuscript refer to enumeration type, citation style, spelling, notation of units, format, and merging all lists of references into one at the end of the dissertation. Permission for the reuse of the article is granted by Elsevier Limited.

The doctoral candidate specified the experimental concept for this study and did a critically reviewing of the literature. The experimental design for the validation was developed by the doctoral candidate. Furthermore, the doctoral candidate carried out experimental work, data analysis, interpretation, calculation, and plotting. The doctoral candidate wrote and revised the manuscript. All co-authors contributed to the execution of experiments, the discussion of results, writing and revision of the manuscript.

Abstract

Microfiltration (0.1 µm) in the diafiltration mode is performed using hollow fiber membranes (HFM) to separate the casein micelles and whey proteins in skim milk at 10 °C. This method of using HFM has not been widely applied in dairy technology. HFM differ from more established module systems such as ceramic tubular membranes (CTM) and spiral-wound membranes (SWM) in their geometry, flow conditions, and propensity to deposit formation. The objective of this study is to investigate the efficiency of fractionation according to the pre-concentration before starting diafiltration when using ultrafiltration permeate as diafiltration medium for transferring the whey proteins into the permeate. The concentration having constant pressure drop is compared with that having constant feed volume flow. The optimal process conditions are determined based on the following criteria: flux, whey protein transmission, whey protein mass flow, and time required for one volume turnover, i.e., diafiltration step. The process is found to be optimum at a transmembrane pressure of 0.5 bar, a constant pressure drop of 1.0 bar m^{-1}, and a concentration factor (CF) of 2.5. At a CF of 3, 80% whey protein depletion was achieved after 2.5 diafiltration steps. Therefore, HFM are confirmed as effective alternatives to SWM and CTM and are optimized in terms of preconcentration of the casein fraction before starting diafiltration.

Keywords: deposit layer formation; membrane fouling; whey protein depletion; separation; purification

Graphical abstract:

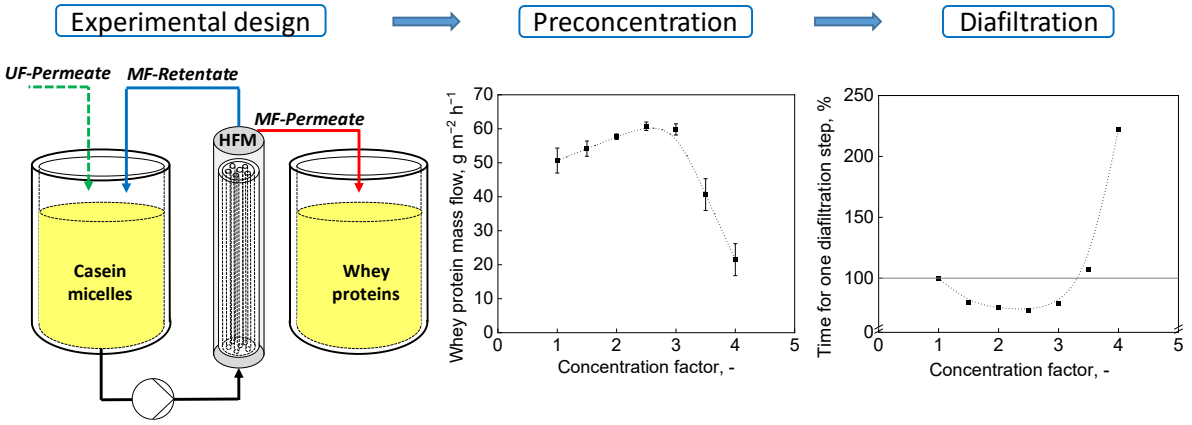

6.1 Introduction

Milk protein fractionation into its two major constituents, casein micelles and whey proteins, by microfiltration in the diafiltration mode is an established unit operation in the dairy industry (Carter et al., 2021). For this purpose, two types of membranes are commonly used: ceramic tubular membranes (CTM) (Adams and Barbano, 2013; Hurt et al., 2015a; Reitmaier et al., 2017; Heidebrecht and Kulozik, 2019; Reitmaier et al., 2020) and spiral-wound membranes (SWM) (Hartinger and Kulozik, 2020). Both membrane types have advantages and limitations. For example, the large membrane area of SWM per module, known as the packing density, compensates for the loss in flux owing to high viscosity if the system is operated in dairies at low temperatures of about 10 °C (Zulewska et al., 2009; Mercier-Bouchard et al., 2017) to keep microbiological growth under control (Govindasamy-Lucey et al., 2007; Schiffer and Kulozik, 2020). This is particularly important during long membrane operation cycle times with recirculation of the retentate into the feed tank, such as that occurring in diafiltration processes. Deposit control is an issue in SWM applications because the spacer nets, which separate the layers of membranes wound around the central permeate collection tube, are known to favor deposit formation behind the spacer-net filaments. This creates high retentate backpressure, thus limiting the axial flow velocity. Moreover, the permeate entering the permeate flow channel at the outer module parts must overcome a considerable backpressure on the permeate side while flowing toward the SWM central permeate collection tube. On the contrary, CTM are more resistant to thermal or chemical stress factors and are more effective for deposit control. However, these membranes have low packing density (Schopf et al., 2021b).

As an alternative, Schopf et al. (Schopf et al., 2020; Schopf et al., 2021b; Schopf et al., 2021a) determined that hollow fiber membranes (HFM) can be used for milk protein fractionation. These membranes combine the advantages of high packing density and effective deposit control in open flow channels exhibited by CTM and SWM and have

shown superior performance in whey protein mass flow and enable sharp separation of whey proteins from the casein micelle fractions (Schopf et al., 2021b). These HFM studies were conducted at 55 °C, i.e., in the high-temperature range, where the viscosity of milk is low. No data exist regarding milk protein fractionation using HFM for microfiltration in the diafiltration mode at low temperatures, and no studies have been conducted on the impact of the protein pre-concentration level. Thus, the effects of the feed protein concentration at low temperatures on the deposit layer structure and the filtration performance as a function of the transmembrane pressure are unknown. Further, the effect of the feed protein concentration prior to starting the diafiltration on the fractionation of milk proteins is poorly understood regarding the amount of ultrafiltration permeate needed as the diafiltration medium and the filtration time required to remove most of the whey proteins from milk when using HFM. It is expected that compared to CTM and SWM, the open flow channels in HFM, their high packing density, and the resulting high mass flow of whey protein will provide effective control of the deposition layer by enabling a diafiltration process with a higher pre-concentration factor (CF) with no added filtration effort exerted for completing one diafiltration step. This means that at a lower starting milk volume with a higher starting protein concentration, the diafiltration is expected to require a lower volume of diafiltration medium and, thus, less filtration time to complete each of the required diafiltration steps.

The composition of the diafiltration medium also plays an important role. Previous research has determined that ultrafiltration permeate as a diafiltration medium does not change the ionic milieu during diafiltration (Renhe et al., 2019) and thus has no impact on the casein micelle structure (Gaucheron, 2005; Dalgleish and Corredig, 2012). Therefore, it is expected that the deposit layer structure does not change during diafiltration. In addition, the concentration of the initial feed volume was carried out in order to increase the yield of both protein fractions (Hurt and Barbano, 2010). As previously mentioned, the volume requirement of the diafiltration medium depends on the feed volume (Hurt and Barbano, 2010). To reduce the amount, the initial feed volume can be reduced (Reitmaier et al., 2020). Renhe and Corredig (2018) reported that compared with ultrafiltration concentrates, microfiltration concentrates showed no difference in the pH, casein micelle particle size, or ionic milieu of the serum phase, although differences were noted in the casein-to-whey protein ratio. However, the effects of the whey proteins partially removed during the microfiltration pre-concentration step on the deposit layer formation and diafiltration in terms of the filtration time and required diafiltration volume have not been investigated.

Moreover, by increasing the feed protein concentration, the deposit layer formation also increases (Zulewska and Barbano, 2013). The accumulation of deposited casein micelles on the membrane surface is known to reduce the flux and the whey protein

transmission (Marshall et al., 1993). Hartinger et al. (2020) reported an optimal CF of 1.7 for obtaining high protein mass flow using SWM owing to the reduction of flux and whey protein transmission resulting from the increase in CF. Higher CF leads to more intense fouling, which is the main issue with SWM but occurs less often in HFM and CTM. One option for counteracting the fouling is to operate at constant feed volume flow in contrast to constant pressure drop. Therefore, the use of HFM appears to be appropriate for obtaining higher CF because the fouling can be better controlled owing to the flow properties and free flow channels of these membranes (Schopf et al., 2021b). Concentrations with constant feed volume flow in HFM should lead to a less intensive deposit layer formation, higher flux values, and even increased transmembrane pressure owing to a higher pressure drop along the membrane. Furthermore, Bouchoux et al. (2010) reported that interactions between casein micelles at a concentration of 200 g L^{-1} lead to hydration loss in the micelles. In addition, Qu et al. (2012) determined that these interactions combined with pressure result in compaction of the deposit layer structure and thus reduced flux and whey protein transmission (Gésan-Guiziou et al., 2000). Moreover, the increase in protein concentration also leads to a flux decrease owing to the increased feed viscosity at higher CF (Le Berre and Daufin, 1996).

Despite these insights from prior works, a lack of understanding remains regarding the effects of these variables on the filtration performance of HFM at different CF and low temperatures with respect to flux, whey protein transmission, filtration time, and the amount of diafiltration volume required to reach a certain whey protein removal target. The achievable level of protein fractionation depends on the number of diafiltration steps and the actual whey protein transmission (Beckman et al., 2010), which is highly sensitive to the intensity of the casein micelle deposits. These micelles form a secondary membrane, the retention characteristics of which depend on the structure of the deposited layer. Therefore, we principally expect a reduced time for the diafiltration process with HFM as well, by reducing the initial feed volume in the microfiltration system before starting the diafiltration process. However, this has not been quantitatively analyzed in the literature. Based on the superior performance of HFM reported in our previous work, however, we postulate that although an optimal range of the most effective pre-CF for HFM milk protein fractionation has not been obtained thus far, it could be determined in further research. Then, the results can be compared with those reported for SWM (Hartinger and Kulozik, 2020) and CTM (Reitmaier et al., 2017). Compared to previous works, in the present study, we combine the effects of the module type (HFM), low-temperature milk protein fractionation, and pre-concentration of the casein fraction by microfiltration prior to starting diafiltration. To further assess the

optimal pre-concentration range, we compare a concentration yielding constant pressure drop with that delivering a constant feed volume flow to determine whether an optimal transmembrane pressure exists for these operations as well.

In brief, our approach to this investigation is as follows. We conduct skim milk concentration experiments at 10 °C using 0.1 µm microfiltration HFM with CF of 1–4 at different transmembrane pressures and different pressure drops simply by removing the microfiltration permeate until certain volume reduction levels, i.e., CF, are achieved. Following pre-concentration, we perform diafiltration with ultrafiltration permeate as diafiltration medium and assess the whey protein depletion over time.

6.2 Experimental

6.2.1 Filtration procedure

Pasteurized (74 °C, 28 s) skim milk with a pH of 6.6 obtained from Molkerei Weihenstephan GmbH & Co. KG (Freising, Germany) was used. The viscosity and density of deionized water and skim milk at different feed protein concentrates were measured according to Schopf et al. (2020) (Table 6.1).

Table 6.1. Viscosity, η, and density, φ, of deionized water, microfiltration retentate, and permeate at different CF at 10 °C.

Concentration factor, -	**1**	**2**	**3**	**4**
η_{Water}, 10^{-6} kg m^{-1} s^{-1}	1306 ± 6	-	-	-
η_{Milk}, 10^{-6} kg m^{-1} s^{-1}	2486 ± 9	5727 ± 12	10071 ± 15	27646 ± 18
$\eta_{Permeate}$, 10^{-6} kg m^{-1} s^{-1}	1463 ± 6	1460 ± 5	1466 ± 3	1469 ± 9
φ_{Water}, kg m^{-3}	999 ± 2	-	-	-
φ_{Milk}, kg m^{-3}	1037 ± 4	1044 ± 3	1065 ± 2	1072 ± 2
$\varphi_{Permeate}$, kg m^{-3}	1023 ± 2	1026 ± 1	1028 ± 3	1030 ± 2

The microfiltration experiments were conducted using an industrially sized HFM supplied by Pentair-X-Flow (R100MF, 1932 polyethersulfone fibers, Enschede, The Netherlands) with a nominal pore size of 0.1 µm, length of 1.022 m, inner fiber diameter of 1.5 mm, outer fiber diameter of 2.25 mm, and total active membrane surface area of 9.3 m^2. To obtain ultrafiltration permeate as the diafiltration medium, ultrafiltration was achieved using an SWM (GR73PE, module 6338, polyethersulfone, Alfa Laval Mid Europe GmbH, Glinde, Germany) with a nominal pore size of 10 kDa, a 48 mil diamond spacer, and a total active membrane surface of 16.5 m^2. Therefore, the permeate of the microfiltration is used as ultrafiltration feed.

Prior conditioning of the membranes was performed according to Schopf et al. (2021a). The filtration unit, as described by Hartinger et al. (2020), was tempered with

demineralized water at 10 °C prior to filtration to avoid the effects of the initial temperature changes on the filtration process. The skim milk was separately tempered to 10 °C before being transferred to the feed tank. With the permeate valve closed, the water was pushed out, and the water/milk mixed-phase was drained. Afterward, the retentate was recirculated into the feed tank. Four different experimental routes were applied. The permeate and retentate samples were quantitatively analyzed by applying reversed-phase high-performance liquid chromatography (RP-HPLC) according to Dumpler et al. (2017). After each filtration experiment, the membranes and the filtration plant were cleaned according to Schopf et al. (2021a), and the cleansing was verified by measuring and comparing the water flux obtained before the experiment and after the cleaning procedure.

6.2.1.1 *Route 1: Concentration at a constant pressure drop*

To investigate the influence of protein concentrations on the deposit layer formation, the CF of the skim milk was varied through microfiltration. The axial pressure drop along the module length was set to 1.0 bar m^{-1}; thus, the initial feed volume flow was 23.8 m^3 h^{-1}. This procedure was applied to generate the same deposit removal forces for each concentration level. The transmembrane pressure was set to 0.5 bar. After removal of the mixed phases from the retentate and permeate, the transmembrane pressure was held constant for 30 min to enable the initial deposit formation to reach the steady-state and thus stable filtration conditions. The microfiltration permeate was drained until the target retentate concentration (CF 2, CF 3, or CF 4) was reached. The pressure drop and the wall shear stress remained constant during the concentration process. Therefore, the flow rate needed to be continuously adjusted per the CF level to compensate for the effect of increased viscosity as the protein concentration increased. The final levels were 23.8, 16.4, 8.2, and 3.1 m^3 h^{-1} for CF 1–4, respectively (Table 6.2).

Table 6.2. Feed volume flow, mean crossflow velocity, resulting pressure drop, transmembrane pressure, wall shear stress, and wall shear rate after reaching CF 1–4 according to Route 1.

Concentration factor, -	Feed volume flow, m^3 h^{-1}	Mean crossflow velocity, m s^{-1}	Pressure drop, bar m^{-1}	Transmembrane pressure, bar	Wall shear stress, kg m^{-1} s^{-2}
1	23.8 ± 0.5	2.0 ± 0.01	1.0 ± 0.01	0.5 ± 0.03	37 ± 1.1
2	16.4 ± 0.7	1.3 ± 0.01	1.0 ± 0.01	0.5 ± 0.02	37 ± 0.9
3	8.2 ± 0.6	0.7 ± 0.01	1.0 ± 0.01	0.5 ± 0.05	37 ± 2.7
4	3.1 ± 0.5	0.3 ± 0.01	1.0 ± 0.01	0.5 ± 0.08	37 ± 3.5

The courses of the volume flow rates are depicted in the flow rate adjustment during pre-concentration by microfiltration as a function of the filtration time for CF 1–4 (Figure 6.1).

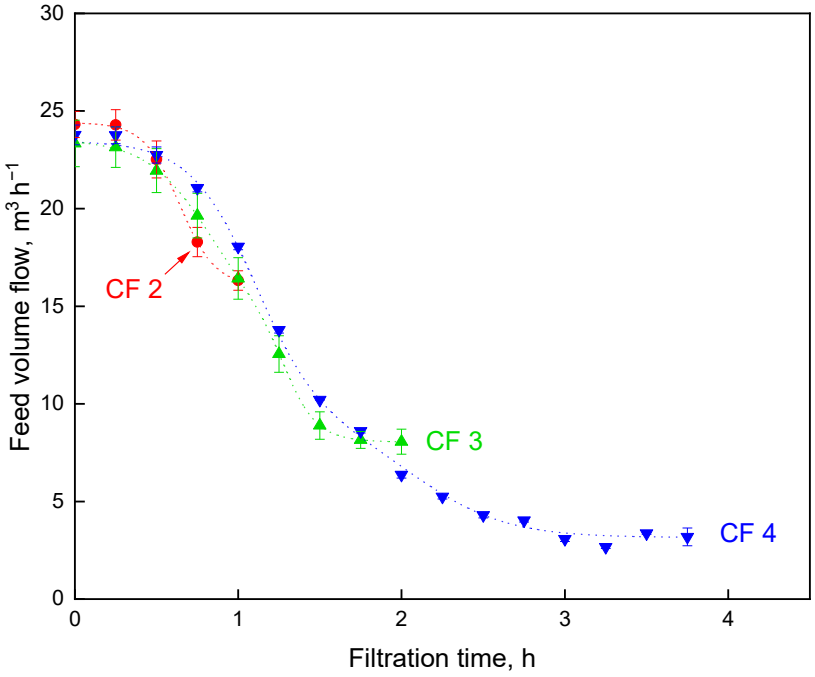

Figure 6.1. Feed volume flow rate adjustment during pre-concentration by microfiltration as a function of filtration time for different CF at a constant pressure drop of 1.0 bar m^{-1} and a transmembrane pressure of 0.5 bar.

6.2.1.2 *Route 2: Concentration at a constant feed volume flow*

In contrast to Route 1, the feed volume flow and, thus, the mean crossflow velocity, was set constant.

The pressure drop was increased with the effect that the deposit layer formation was mitigated by increased removing forces during concentration. At the beginning of the concentration, the feed volume flow was set to 23.8 m^3 h^{-1}; thus, the initial axial pressure drop along the module length was to 1.0 bar m^{-1}, and the transmembrane pressure was 0.5 bar. After 30 min of recirculation, the microfiltration permeate was drained until the target retentate concentration (CF 2, CF 3, or CF 4) was reached. Therefore, the pressure drop was continuously increased from 1.0 bar m^{-1} at CF 1 to 1.2, 1.5, and 2.0 bar m^{-1} at CF 2–4, respectively, owing to the effect of increased viscosity as the protein concentration increased. The minimum adjustable transmembrane pressure, according to Schopf et al. (2021a), was increased by increasing the pressure drop from 0.5 bar at CF 1 to 0.6, 0.75, and 1.0 bar at CF 2–4, respectively (Table 6.3).

Table 6.3. Feed volume flow, mean crossflow velocity, resulting pressure drop, transmembrane pressure, wall shear stress, and wall shear rate after reaching CF 1–4 according to Route 2.

Concentration factor, -	Feed volume flow, $m^3\ h^{-1}$	Mean crossflow velocity, $m\ s^{-1}$	Pressure drop, $bar\ m^{-1}$	Transmembrane pressure, bar	Wall shear stress, $kg\ m^{-1}\ s^{-2}$
1	23.8 ± 0.5	2.0 ± 0.01	1.0 ± 0.01	0.5 ± 0.05	37 ± 1.1
2	23.8 ± 0.5	2.0 ± 0.01	1.2 ± 0.04	0.6 ± 0.08	44 ± 5.3
3	23.8 ± 0.5	2.0 ± 0.01	1.5 ± 0.01	0.8 ± 0.03	55 ± 3.7
4	23.8 ± 0.5	2.0 ± 0.01	2.0 ± 0.06	1.0 ± 0.07	73 ± 5.1

6.2.1.3 *Route 3: Varying transmembrane pressure experiments*

To investigate the effect of increased transmembrane pressure on the deposit layer formation during concentration, pre-concentration was performed according to Route 1. This route was applied to generate the same deposit removal forces for each concentration level, which is not possible for a concentration with constant feed volume flow (Route 2), and to separate the effects of increasing the wall shear stress and the transmembrane pressure. Directly after pre-concentration, the permeate was recirculated in the feed tank. For CF 1, no concentration was performed. After 30 min of recirculation at 0.5 bar, the transmembrane pressure was increased to 1.5 bar in 0.2 bar increments every 30 min to obtain the filtration data under the steady-state condition for each transmembrane pressure step.

6.2.1.4 *Route 4: Filtration in diafiltration mode*

To investigate the impact of pre-concentration on the protein separation by diafiltration, pre-concentration according to Route 1 was performed followed by filtration in the diafiltration mode. The concentration of whey proteins in microfiltration retentate after the pre-concentration is shown in Table 6.4. To obtain the same fluid forces creating friction and wall shear stress at the surface of the deposited layer for each concentration level, the transmembrane pressure and the pressure drop were kept constant at 0.5 bar and 1.0 bar m^{-1}, respectively, during diafiltration. We began the diafiltration by replacing the microfiltration permeate with ultrafiltration permeate while maintaining the fill level of the feed tank at the same height. One diafiltration step corresponded to the addition of ultrafiltration permeate in the amount of the initial feed volume of 100 L. Diafiltration was performed for 3 h to limit the experimental effort, which is discussed subsequently in Section 3. This resulted in different levels of absolute whey protein removal per CF. During this diafiltration time, eight diafiltration steps were performed for CF 1, whereas seven, four, and two steps were completed for CF 2–4, respectively (Table 6.4), to achieve different whey protein reduction levels of more than 90% for

CF 1 and CF 2, 80% for CF 3, and 70% for CF 4. To enable comparison of the four CF experiments, the whey protein reduction levels for CF 4 were slightly extrapolated, and all four CF levels were compared regarding the required number of diafiltration steps required to achieve 80% depletion. During the diafiltration stage, the pH remained constant. Thus, changes in the structure of the casein micelles based on changes in the ionic strength during diafiltration were not expected.

Table 6.4. Concentration of whey proteins in microfiltration retentate after the pre-concentration and the number of diafiltration steps after 3 h diafiltration for CF 1–4.

Concentration factor, -	Concentration of whey proteins in microfiltration retentate after pre-concentration, g L^{-1}	Number of diafiltration steps after 3 h diafiltration, -
1	5.6 ± 0.3	8
2	7.9± 0.5	7
3	6.6 ± 1.7	4
4	11.0 ± 3.2	2

6.2.2 Assessment of filtration performance

The flux, J, is calculated by Equation (6.1) as a function of the volume flow of the permeate, $\dot{V}_{per}$, and the active membrane area, $A_{Membrane}$ as:

$$J = \frac{\dot{V}_{per}}{A_{Mem}} = \frac{\Delta p_{TM}}{\eta \cdot R_F} = \frac{\frac{p_{in} + p_{out}}{2} - p_{per}}{\eta \cdot R_F} \quad (6.1)$$

where Δp_{TM} is the transmembrane pressure calculated by the pressure at the membrane inlet, p_{in}, membrane outlet, p_{out}, and permeate side, p_{per}; η is the viscosity of the permeate, and R_F is the total filtration resistance including the resistances of the membrane and the deposited layer. The pressure drop, Δp_L, over the membrane length, L, is determined as the pressures at the membrane inlet, p_{in}, minus that at outlet, p_{out}, with τ_W as the wall shear stress and d_i as the inner diameter of the fiber (Equation (6.2)):

$$\Delta p_L = p_{in} - p_{out} = \frac{\tau_W \cdot d_i}{4 \cdot L} \quad (6.2)$$

Δp_L can also be calculated by Equation (6.3) as a function of the friction factor, λ, density, ρ, and crossflow velocity, v:

$$\Delta p_L = \frac{1}{2} \cdot \lambda \cdot \frac{L}{d_i} \cdot \rho \cdot v^2 \tag{6.3}$$

The mean crossflow velocity, v, is determined as the ratio of the feed volume flow, $\dot{V}_{Feed}$, and the cross-section of the membrane module, A_{sec}, (Equation (6.4)):

$$v = \frac{\dot{V}_{Feed}}{A_{sec}} \tag{6.4}$$

The protein transmission, Tr_i, is determined as the function of the permeate concentration, $c_{i,per}$, and the retentate concentration, $c_{i,ret}$, for each protein component i (Equation (6.5)):

$$Tr_i = \frac{c_{i,per}}{c_{i,ret}} \tag{6.5}$$

The CF is calculated as the ratio of the concentration of casein in the concentrate, $c_{cas,\,conc}$, against that in the native skim milk, $c_{cas,milk}$ (Equation (6.6)):

$$CF = \frac{c_{cas,conc}}{c_{cas,milk}} \tag{6.6}$$

The concentration of the whey proteins decreases during the concentration with microfiltration according to the whey protein transmission into the permeate. Thus, the effects of the CF and the partial whey protein depletion during microfiltration concentration need to be separated. Therefore, the protein mass flow, $\dot{m}$, is calculated as a function of the protein transmission, Tr_i, the target component i in the skim milk (mainly α-lactoglobulin, β-lactalbumin), $c_{i,milk}$, the CF, and the flux at the respective CF, J_{CF}, according to Equation (6.7).

$$\dot{m}_i = J_{CF} \cdot Tr_i \cdot c_{i,milk} \cdot CF \tag{6.7}$$

The absolute level of protein decrease, ($C_{DF,n}/C_{DF,0}$), in the microfiltration retentate during diafiltration is defined as a function of the transmission and the number of diafiltration steps as the ratio of the total volume of the added diafiltration medium, $V_{DF,n}$, against the initial hold-up volume, $V_{DF,0}$, according to Reitmaier et al. (2021) (Equation (6.8)).

$$\frac{C_{DF,n}}{C_{DF,0}} = e^{Tr_i \cdot \frac{V_{DF,n}}{V_{DF,0}}} \tag{6.8}$$

During the diafiltration process, the filtration time, t, required to obtain one diafiltration step at a target concentration level is defined according to Heidebrecht and Kulozik (2019) (Equation (6.9)).

$$t = \frac{V_{DF,0}}{Tr_i \cdot J_{CF}} \cdot ln\left(\frac{C_{DF,n}}{C_{DF,0}}\right) \tag{6.9}$$

6.2.3 Data evaluation and statistics

The graphs were plotted using Origin 2021 (OriginLab Corporation, Northampton, Massachusetts, United States), and the statistical analysis was performed using RStudio 1.3.1093 (RStudio, Boston, Massachusetts, United States). The significance was evaluated according to the P-value using a one-way analysis of variance combined with Tukey's honestly significant difference post-hoc test. The data are the average values of the results of two independent filtration experiments, and the error bars represent the range of the standard deviation.

6.3 Results and Discussions

6.3.1 Impact of casein concentration on the deposit layer formation during microfiltration

To investigate the influence of different protein concentrations on the deposit layer formation in the HFM, the flux was measured for the different CF of the skim milk. The CF was varied in the microfiltration unit by removing the permeate without recirculation into the feed tank and at a constant pressure drop to obtain the same fluid forces creating the friction and wall shear stress at the surface of the deposited layer for each concentration level according to Route 3. Figure 6.2 shows the effects of the transmembrane pressure on the flux with CF 1–4 as parameters.

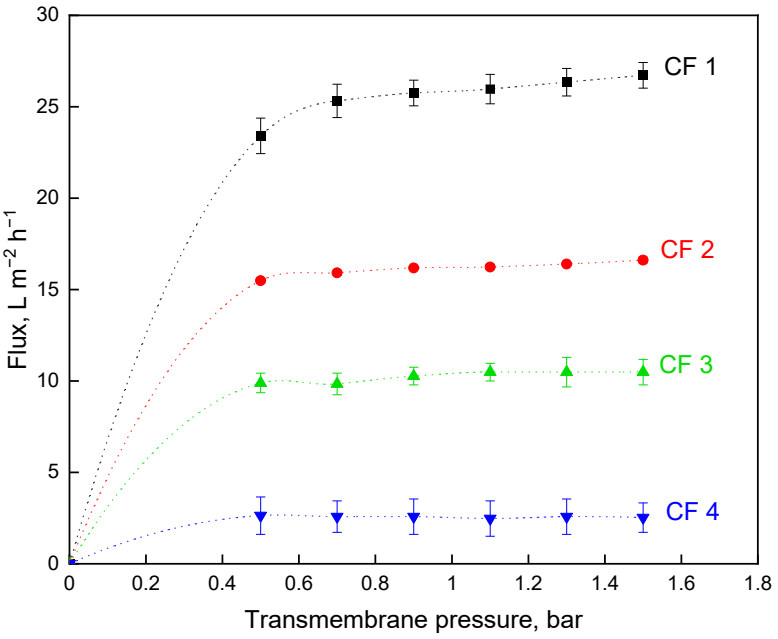

Figure 6.2. Flux as a function of transmembrane pressure for different CF and a constant pressure drop of 1.0 bar m^{-1}.

Figure 6.2 illustrates that the flux decreased with an increase in the CF and reached a stable level, or limiting flux, at about 0.5 bar. Owing to the backpressure of the module, a transmembrane pressure below 0.5 bar could not be established. The limiting flux values clearly differed among the CF ($P < 0.001$). The higher protein concentration leads to enhanced deposit layer formation by the retained casein micelles on the membrane surface (Ng et al., 2017) and increased filtration resistance (Beckman and Barbano, 2013) owing to enhanced protein–protein interactions possibly resulting in the formation of a gel layer (Qu et al., 2012). To illustrate how the transmission into the permeate was influenced by the enhanced deposit layer formed by the increased CF, the whey protein transmission measured separately at CF 1–4 is shown in Figure 6.3 as a function of the transmembrane pressure.

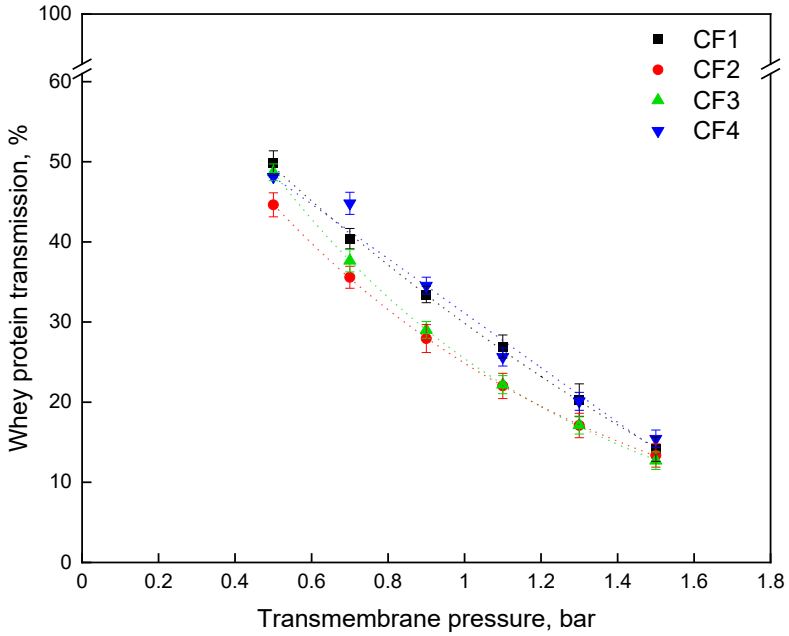

Figure 6.3. Whey protein transmission as a function of transmembrane pressure for different CF and a constant pressure drop of 1.0 bar m^{-1}.

The curves shown in Figure 6.3 are relatively close, which indicates that the CF did not have a significant effect ($P < 0.1$) on the transmission of whey proteins in the HFM. This confirms the findings of Hartinger et al. (2020) for SWM such that high CF will lead to the formation of a thicker deposit layer but no changes in terms of deposit layer porosity and in terms of narrowing of the deposit layer flow channels. The amount of proteins deposited on the fiber membrane surface increased; however, an increase in the transmembrane pressure led to a decrease in the whey protein transmission for all CF (Figure 6.3). This can be explained by a higher compression and compaction of the deposit layer (Bouchoux et al., 2010; Qu et al., 2012) and thus by enhanced resistance to protein transmission and more pronounced retention of whey proteins by the deposited layer of caseins (Bouchoux et al., 2014; Schopf et al., 2020).

To identify the optimal transmembrane pressure for milk protein fractionation for the HFM at different CF, the time required for the permeation of the whey proteins through the membrane needs to be considered. It should be noted that depending on the CF, some of the whey proteins were washed out during the pre-concentration stage. This means that the depletion of whey proteins from the microfiltration concentrates increased with an increase in CF. On the contrary, a lower concentration of whey proteins in the concentrate influenced the mass flow, which is a function of flux and whey protein concentration (Equation (6.7)). Thus, the effects of CF and partial whey protein depletion must be considered separately. Therefore, we calculated the whey protein mass flow according to Equation (6.7) separately for each CF (Figure 6.4).

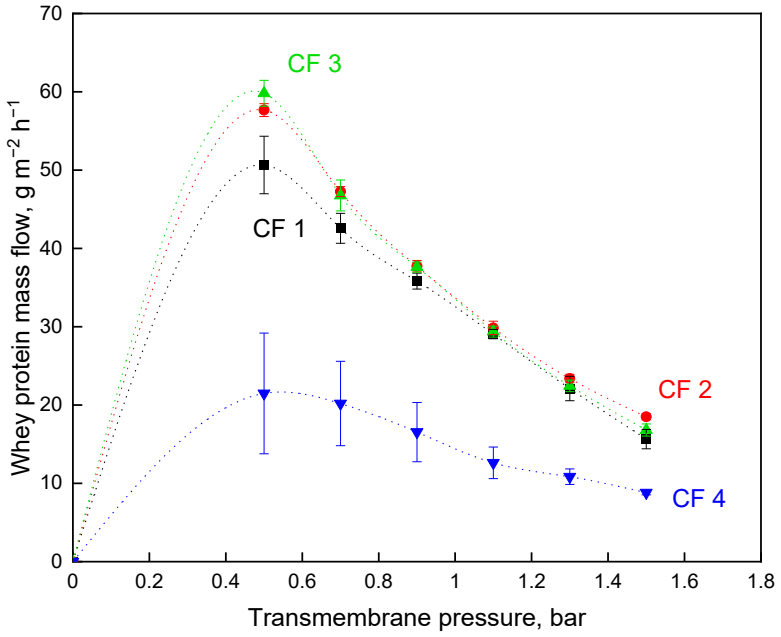

Figure 6.4. Total mass flow of all whey proteins as a function of transmembrane pressure for different CF and a constant pressure drop of 1.0 bar m^{-1}.

Figure 6.4 shows that the highest mass flow of 61 g m^{-2} h^{-1} was reached at a transmembrane pressure of 0.5 bar and CF 3, closely followed by CF 2 with 58 g m^{-2} h^{-1}. The optimal transmembrane pressure for concentration at a constant pressure drop of 1.0 bar m^{-1} reached the minimum adjustable transmembrane pressure at 0.5 bar. Although the mass flow values for CF 1–3 did not differ significantly ($P < 0.1$), the value was remarkably lower at CF 4 ($P < 0.001$). At high feed protein concentration, the flux was low owing to the enhanced deposit formation by the casein micelles; thus, the amount of convectively transported whey protein toward and through the membrane was also low.

6.3.2 Impact of increasing pressure drop during concentration

As previously discussed, the amount of casein micelles and the deposit layer structure are the limiting factors for the filtration performance during concentration. One option to counteract the deposit layer formation is to increase the wall shear stress and thus the deposit layer removal forces. In this method, the pressure drop along the membrane length needs to be increased. During concentration at a constant pressure drop of 1 bar m^{-1}, the feed volume flow is reduced from 23.8 m^3 h^{-1} at CF 1 to 3.1 m^3 h^{-1} at CF 4 (Figure 6.1) owing to the viscosity increase through the increased CF. To determine optimal process conditions, the concentration at a constant pressure drop of 1.0 bar m^{-1} and the optimal transmembrane pressure of 0.5 bar (Route 1) were compared with a concentration at a constant feed volume flow of 23.8 m^3 h^{-1} (Route 2).

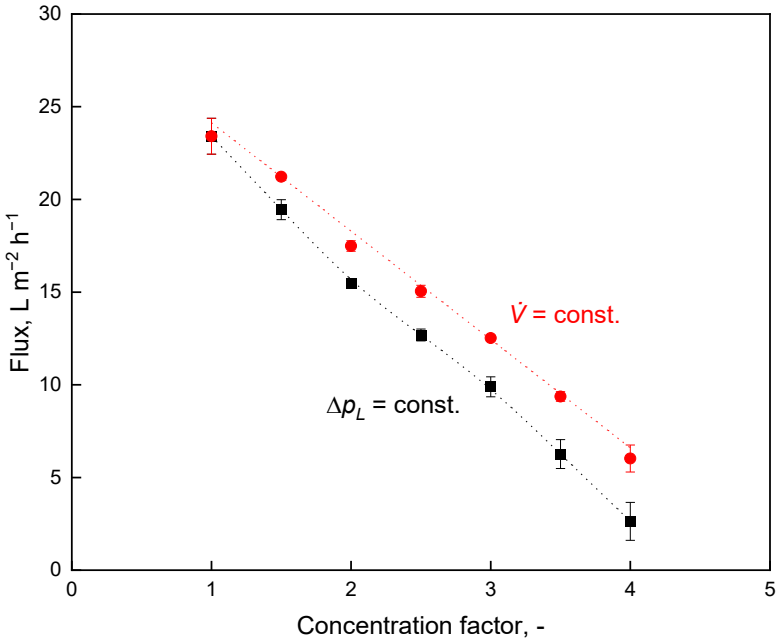

Figure 6.5. Flux as a function of the CF for (■) a constant pressure drop of 1.0 bar m^{-1} and (●) a constant feed volume flow of 23.8 m^3 h^{-1}.

Figure 6.5 shows that the flux decreased with an increase in CF, which increased the total amount of casein micelles deposited on the membrane surface. The flux values at a constant feed volume flow were higher than those at a constant pressure drop owing to the increase in wall shear stress and thus the increase in deposit layer removal forces. Therefore, it can be assumed that at higher CF, the deposit layer is less pronounced for the concentration at a constant feed volume flow compared with that at a constant pressure drop. However, it must be considered that for the concentration at a constant feed volume flow, the pressure drop along the membrane also increases with an increase in CF. Therefore, by avoiding negative transmembrane pressure and reverse permeate flow at the module end, the minimum adjustable transmembrane pressure will also increase, according to Schopf et al. (2021a). As shown in Figure 6.2, the transmembrane pressure increase had no significant effect on the flux because the limiting flux was already reached at a transmembrane pressure of 0.5 bar. However, Figure 6.3 shows that although the whey protein transmission decreased by increasing the transmembrane pressure, it was not significantly changed by increasing the CF. To illustrate the effect of the concentration at a constant feed volume flow on the whey protein transmission, the transmission and the corresponding minimum adjustable transmembrane pressure at different CF are shown in Figure 6.6.

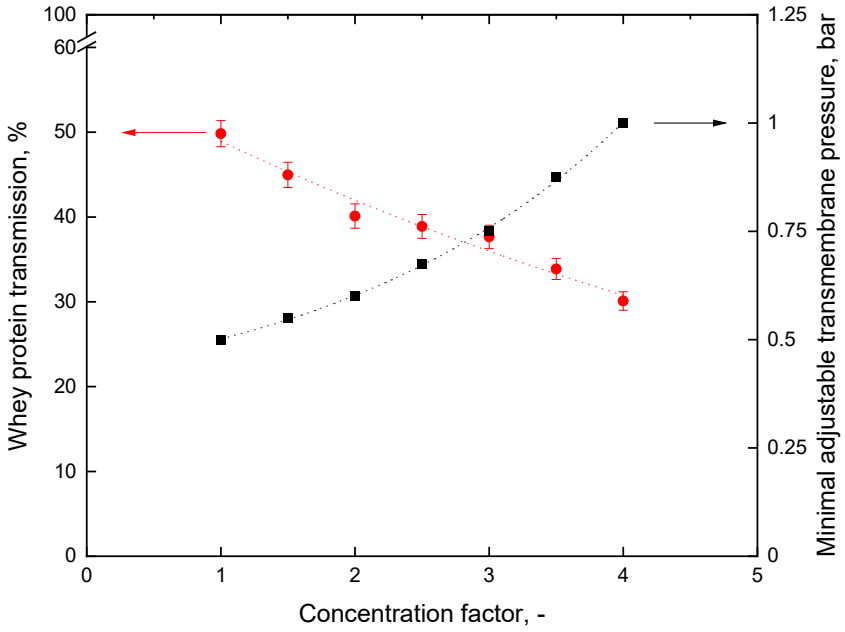

Figure 6.6. Whey protein transmission (●) and the corresponding minimum adjustable transmembrane pressure (■) as a function of the CF at a constant feed volume flow of 23.8 $m^3\ h^{-1}$.

During the concentration at a constant feed volume flow, the minimum adjustable transmembrane pressure and the pressure drop increased with the increase in CF owing to the rise in viscosity. As previously discussed, the higher transmembrane pressure led to a more compact deposit layer with a higher retention effect. Thus, the whey protein transmission decreased by increasing the CF during the concentration at a constant feed volume flow (Figure 6.6). This indicates that the whey protein transmission is influenced mainly by the structure of the deposit layer, which is affected by the transmembrane pressure, and not by the increase in wall shear stress during concentration at constant feed volume flow.

To combine the flux and whey protein transmission, the mass flow at the minimum adjustable transmembrane pressure was calculated according to Equation (6.7) as a function of the CF for both concentration protocols (Figure 6.7).

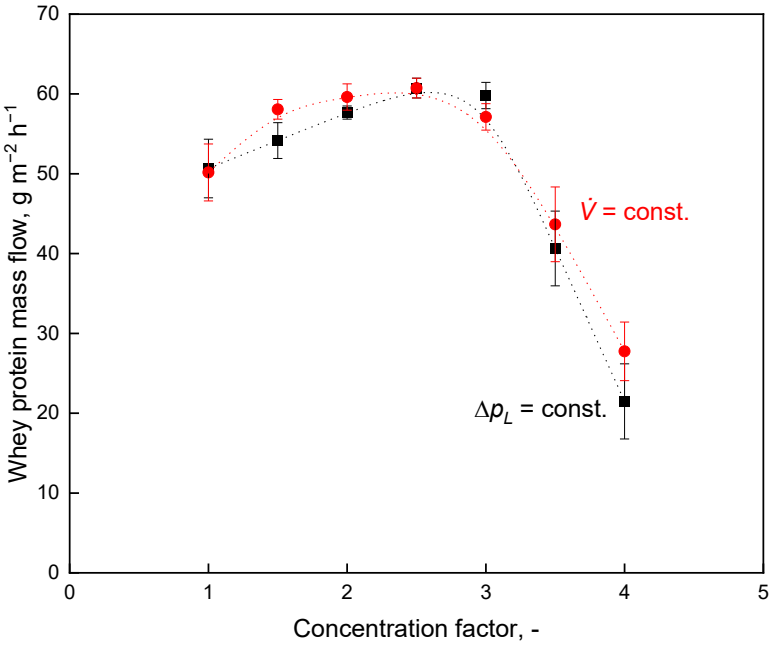

Figure 6.7. Whey protein mass flow at the minimum adjustable transmembrane pressure as a function of the CF for (■) a constant pressure drop of 1.0 bar m^{-1} and (●) a constant feed volume flow of 23.8 m^3 h^{-1}.

The optimal CF value was determined to be 2.5 at a whey protein mass flow of 61 g m^{-2} h^{-1} (Figure 6.7). The whey protein mass flow for the concentrations at constant pressure drop and constant feed volume flow did not significantly differ ($P < 0.1$). The high flux values for both concentration routes (Figure 6.5) were compensated by the degrease in whey protein transmission (Figure 6.6).

6.3.3 Impact of pre-concentration on protein separation by diafiltration with ultrafiltration permeate

To assess the effects of the feed protein CF on the HFM performance, pre-concentration and diafiltration by microfiltration were performed. Because the concentration protocols showed no significant difference in the whey protein mass flow (Figure 6.7) and to obtain the same fluid forces creating the friction and wall shear stress at the surface of the deposited layer for each concentration level, the pre-concentration was conducted at a constant pressure drop of 1.0 bar m^{-1} and the transmembrane pressure optimum value of 0.5 bar. Figure 6.8 shows the decrease in flux during the concentration phase followed by an almost stable flux during the diafiltration process (Route 4).

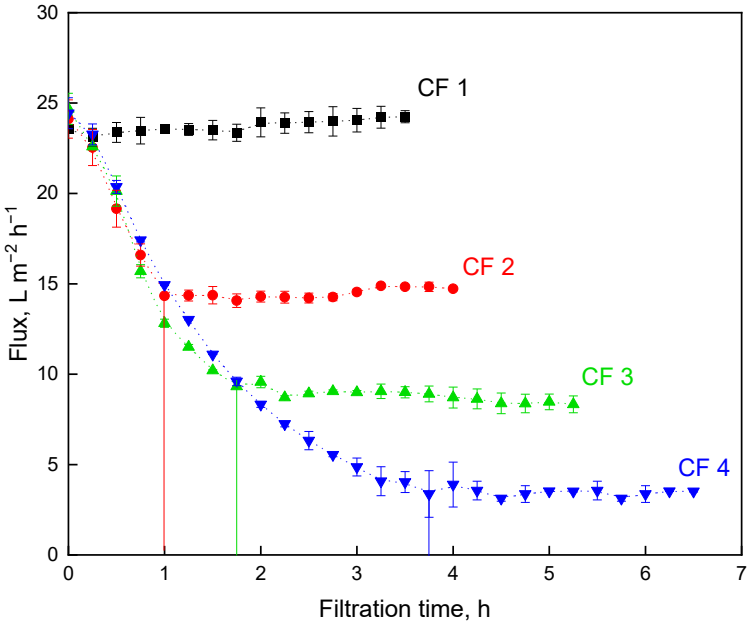

Figure 6.8. Flux as a function of the filtration time for different CF during concentration and filtration in the diafiltration mode. The pressure drop was 1.0 bar m^{-1}, and the transmembrane pressure was 0.5 bar. The vertical lines indicate the start of the filtration in diafiltration mode.

As shown in Figure 6.4, the starting flux level for each of the four experiments was about 24 L m^{-2} h^{-1}. During pre-concentration, the flux steeply dropped during 1 h for CF 2, 1.8 h for CF 3, and about 3.8 h for CF 4. The time required for pre-concentration increased an increase in CF. Once the targeted CF levels were reached, the remaining whey proteins were washed out during diafiltration with ultrafiltration permeate. After 3 h, the diafiltration process was stopped to keep the time effort realistic and to control the microbiological growth (Govindasamy-Lucey et al., 2007; Schiffer and Kulozik, 2020).To provide optimal process parameters, we assumed that 3.8 h for pre-concentration to CF 4 and 3 is not of practical relevance. During the diafiltration phase, the flux levels remained essentially constant, with a slight increase caused by the reduction of whey protein content over time.

It appears that the slight decrease in total feed protein concentration resulting from the partial whey protein depletion had a marginal impact on the flux during diafiltration, which confirms the results of previous research concerning the dominant role of the casein fraction as the main component in determining the effect of the deposit layer (Bouchoux et al., 2010; Qu et al., 2012). The steady-state flux levels during diafiltration (Figure 6.8) were in accordance with the flux levels measured at a transmembrane pressure of 0.5 bar (Figure 6.2). The flux levels, dependent on the CF, remained constant during diafiltration. Therefore, the time required for one diafiltration step remained the same during diafiltration. The diafiltration with ultrafiltration permeate had no impact

on the flux because it obviously did not affect the structure of the deposit layer composed of casein micelles. This is in accordance with the results of Reitmaier et al. (Reitmaier et al., 2020), who reported similar results during diafiltration with ceramic membranes. Therefore, no impact of diafiltration on the whey protein transmission was expected, which was in fact essentially confirmed by the results depicted in Figure 6.9. Only a slight decrease in the whey protein transmission was observed except for CF 4, where the decline in whey protein transmission was somewhat more pronounced.

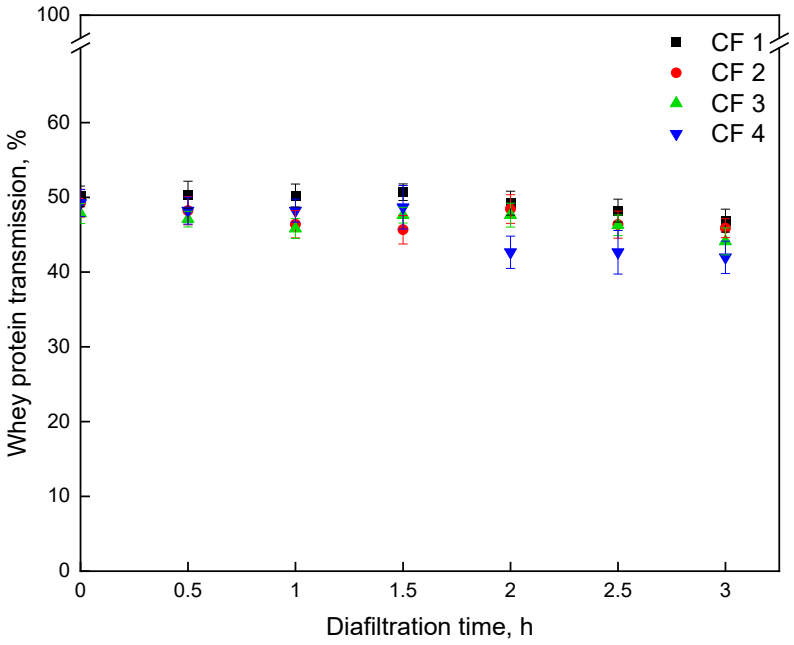

Figure 6.9. Whey protein transmission as a function of the diafiltration time for different CF. The pressure drop was 1.0 bar m^{-1}, and the transmembrane pressure was 0.5 bar.

This is also in accordance with the findings of Heidebrecht et al. (2019) who reported that the whey protein transmission remained constant during diafiltration with ceramic membranes, depending on the transmembrane pressure. The whey protein transmission during diafiltration (Figure 6.9) was in accordance with that for constant concentration and a transmembrane pressure of 0.5 bar (Figure 6.3). During concentration and filtration in diafiltration mode, the whey protein transmission varied little. However, the absolute decrease in whey proteins should therefore continuously decrease. The absolute decrease in whey proteins in the microfiltration retentate during concentration and subsequent diafiltration is shown as a function of the diafiltration steps in Figure 6.10.

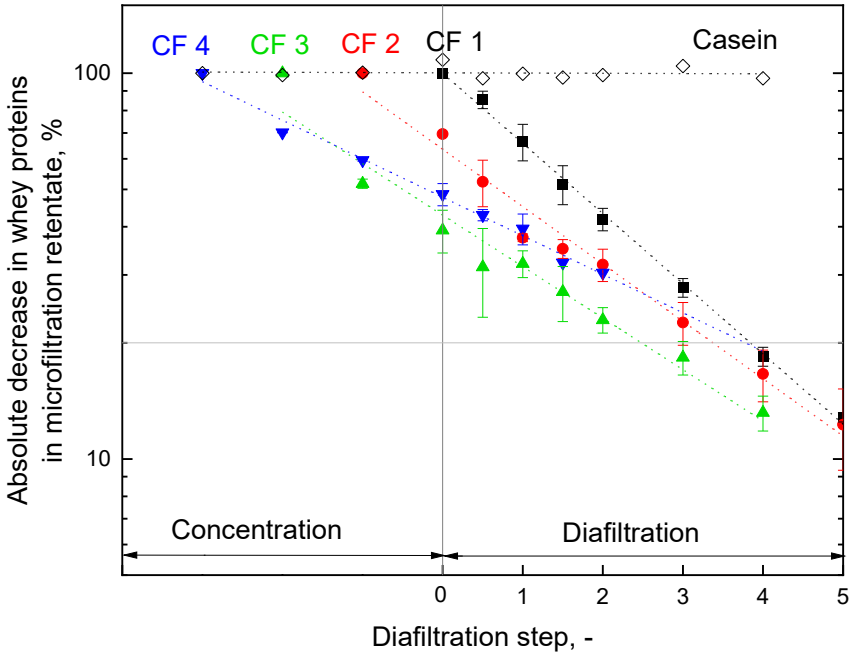

Figure 6.10. Absolute decrease in whey proteins in the microfiltration retentate as a function of the diafiltration steps for CF 1–4. The pressure drop was 1.0 bar m^{-1}, and the transmembrane pressure was 0.5 bar.

The concentration of the casein micelles in the microfiltration retentate remained constant during the diafiltration process, whereas the whey protein concentration in the retentate decreased during diafiltration. During pre-concentration, the whey proteins were already depleted, which resulted in different whey protein concentrations at the beginning of the diafiltration process. The exponential whey protein reduction during diafiltration depended only on the transmission and the number of diafiltration steps according to Equation (6.8). As shown in Figure 6.10, 2.5 diafiltration steps for CF 3, 3.5 for CF 2, and 3.8 for CF 1 and CF 4 (approximately according to Equation (6.8)) were required to achieve 80% whey protein reduction. This means a pre-concentration to CF 3 requires less diafiltration medium than that needed for CF 1, 2, and 4.

6.3.4 Impact of the feed protein concentration on the diafiltration time

As shown in Figure 6.8, the time required for pre-concentration increased with an increase in CF. Moreover, owing to the pre-concentration to 100 L feed volume, different amount of whey proteins was processed during filtration in the diafiltration mode. To determine the optimal CF, the time required to obtain a single diafiltration step was considered. That required for a filtration process operated in the diafiltration mode decreased when either the initial volume or the desired degree of whey protein removal decreased or the transmission or flux increased. Thus, we must consider the volume of the required diafiltration medium as well as the time required to achieve one diafiltration step if a high whey protein removal is targeted. For evaluating the diafiltration

in terms of the specific feed volume, the required membrane area and whey protein transmission, the required filtration time, characterized as the time needed for one diafiltration step, was calculated according to Equation (6.9). Figure 6.11 illustrates the time for one diafiltration step as a function of CF.

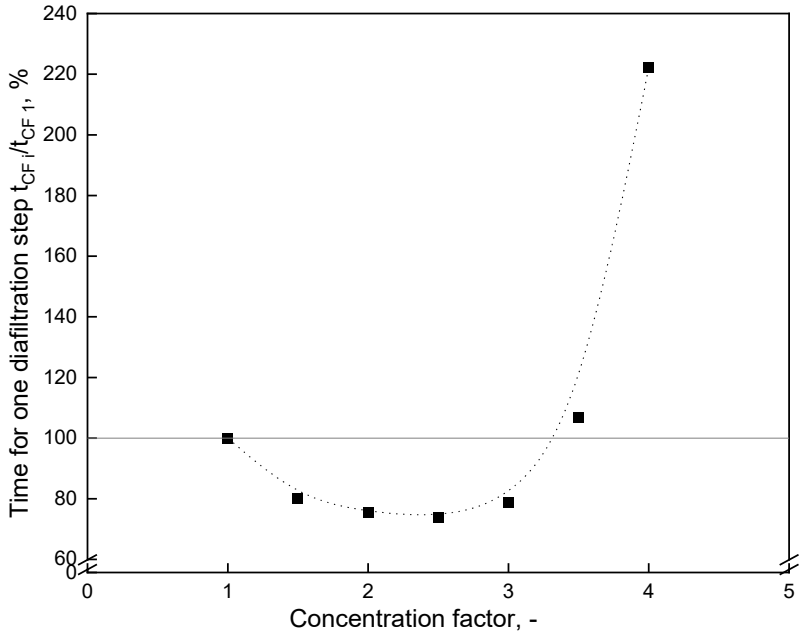

Figure 6.11. Time for one diafiltration step as a function of the CF at a transmembrane pressure of 0.5 bar and a pressure drop of 1.0 bar m^{-1}.

The most efficient milk protein fractionation by diafiltration was determined as the minimum time needed for one diafiltration step at CF 2.5 (Figure 6.11). The time requirement decreased up to 20% at CF 2.5 and then increased sharply. As expected from the whey protein mass flow shown in Figure 6.7, CF 2.5 provided the best filtration conditions at the optimal transmembrane and flow conditions. The pre-concentration of the feed up to CF 2.5 before starting diafiltration led to a faster diafiltration process and a smaller amount of required diafiltration medium owing to the effective control of the deposit layer formation, which enabled high flux values with a high protein load. At low CF, the high flux values were associated with a low whey protein content. By increasing the CF, the volume reduction up to a certain point reduced the filtration time. Above this point, the high feed protein concentration led to low flux values, which reduced the efficiency of the milk protein fractionation by microfiltration in the diafiltration mode.

The optimal pre-CF determined for SWM and CTM were CF 1.7 (Hartinger and Kulozik, 2020) and CF 2 (Reitmaier et al., 2017; Heidebrecht and Kulozik, 2019), respectively. This means that when operating at the optimal CF and the related lower level of

initial feed volume, less diafiltration medium would be required to perform one diafiltration step with HFM. In particular, using the HFM instead of SWM or CTM would result in volume reductions of 19% or 10%, respectively.

6.4 Conclusions

In this study, we evaluated milk protein fractionation by HFM microfiltration in combination with a feed pre-concentration variation in transmembrane pressure and pressure drop. The optimal process conditions according to the whey protein mass flow and the time required for one diafiltration step were determined to be a transmembrane pressure of 0.5 bar, a constant pressure drop of 1.0 bar m^{-1}, and a CF of 2.5. This result is based on the more effective deposit control and higher packing density of HFM compared with that of SWM and CTM, respectively. The open cross-channels of the HFM provided better control of the deposit layer formation. We showed that HFM can be operated at concentration levels 47% and 25% higher than those for SWM and CTM systems, respectively, which enables the necessary amount of diafiltration medium and filtration time to be reduced. The results of this study can be useful in designing milk protein fractionation processes by the deployment of HFM modules operated at the optimal processing conditions, i.e., the lowest possible transmembrane pressure and optimal CF.

Author Contributions: Conceptualization, R.S; Data curation, R.S.; Formal analysis, R.S.; Funding acquisition, U.K.; Investigation, R.S.; Methodology, R.S.; Project administration, R.S. and U.K.; Resources, U.K.; Software, R.S.; Supervision, U.K.; Validation, R.S.; Visualization, R.S.; Writing–original draft, R.S.; Writing–review & editing, U.K. All authors have read and agreed to the published version of the manuscript.

Funding: This IGF Project of the FEI was supported via AiF within the program for promoting the Industrial Collective Research, IGF, of the German Ministry of Economic Affairs and Energy, BMWi, based on a resolution of the German Parliament. Project: AiF 10 EWN.

Acknowledgments: The authors gratefully thank Heidi Wohlschläger, Claudia Hengst, and Hermine Rossgoderer for their assistance with the RP-HPLC analysis of the milk samples, Malou Warncke and Martin Hartinger for their benefits during the discussion, and Andreas Matyssek for his assistance in conducting the experiments.

Conflicts of Interest: The authors declare no conflict of interest. The authors declare that they have no known competing financial interests or personal relationships that could have appeared to influence the work reported in this paper. The funders had no role in the design of the study; in the collection, analyses, or interpretation of data; in the writing of the manuscript, or in the decision to publish the results.

7 Effect of flow channel number in multi-channel tubular ceramic microfiltration membranes on flux and small protein transmission in milk protein fractionation [5]

Roland Schopf*, Felix Desch, Ramona Schmitz, Dilara Arar, and Ulrich Kulozik

Chair of Food and Bioprocess Engineering, Technical University of Munich, TUM School of Life Sciences, Weihenstephaner Berg 1, 85354 Freising, Germany

*Corresponding author

Summary and contribution of the doctoral candidate

CTM could also be manufactured with a smaller channel diameter to converge hollow fibers diameter which will increase the permeate volume flow, as well as the packing density of CTM modules like it does in HFM modules. However, the permeate flow will have different resistance to the outer rim of the element dependent on the channel position. This is expected to affect flux, the advective transport of proteins towards the membrane area, and thus the deposit layer formation. Therefore, the hypothesis was that due to different pressure and flow condition between the inner and outer channels, CTM with higher channel numbers would perform better in terms of flux and whey protein transmission.

We compared CTM with 1-, 7-, 19-, and 37-channels with the same outer diameter to provide the same module footprint as assessment criteria. The flux and the whey protein transmission were analyzed. The results showed that the higher the number of channels, the higher the permeate volume flow and the whey protein transmission. Especially at high Δp_{TM}, significantly higher whey protein transmission could be determined in CTM with a high channel number.

We assume that the higher backpressure on permeate side in the inner channel reduced flux and thus, lead to a less pronounced deposit layer formation. This, in turn, reduces the retention effect of the deposit layer and increases whey protein transmis-

[5] Original publication: Schopf et al. (2022): Schopf, Roland, Desch, Felix, Schmitz, Ramona, Arar, Dilara, Kulozik, Ulrich. 2022. 2022. Effect of flow channel number in multi-channel tubular ceramic microfiltration membranes on flux and small protein transmission in milk protein fractionation. Journal of Membrane Science 644, 120153. DOI: 10.1016/j.memsci.2021.120153. Adapted original manuscript. Adaptions of the manuscript refer to enumeration type, citation style, spelling, notation of units, format, and merging all lists of references into one at the end of the dissertation. Permission for the reuse of the article is granted by Elsevier Limited.

sion. The inner channels contribute more to the total transmission than the outer channel. As a consequence, at high Δp_{TM}, the 37-channel membrane performed superior in terms of specific flux and whey protein transmission compared to membranes with less channel number due to less deposit layer formation in the inner channels.

The doctoral candidate specified the experimental concept for this study and did a critically reviewing of the literature. The experimental design for the validation was developed by the doctoral candidate. Furthermore, the doctoral candidate carried out experimental work, data analysis, interpretation, calculation, and plotting. The doctoral candidate wrote, revised the manuscript, initiated the study, and prepared the project outline. All co-authors contributed to the execution of experiments, the discussion of results, writing and revision of the manuscript.

Abstract

Ceramic multi-channel microfiltration (MF) membrane elements exist in various configurations, partially with high numbers of flow channels to increase the active membrane surface area and flux. The open question was how multi-channel membranes with different channel numbers perform in applications of protein fractionation, where not only flux, but more importantly, also transmission of components counts as decisive criteria. In this study, ceramic membrane elements with 1-, 7-, 19-, and 37-channels with the same outer diameter were compared with the task of milk protein fractionation in their main fractions (casein micelles, about d = 180 nm in diameter, and whey proteins, 4-8 nm in size) using 0.1 µm MF as technical example. Flux and therefore the advective protein transport towards the membrane surface was expected to differ between outer and inner channels owing to the different resistance to flow of the permeate from the inner channels to the outer rim of the ceramic element. In fact, the fouling intensity exerted by the retained biopolymers differed. Permeate flux, as well as whey protein transmission, depend on number and position of the individual channels. The 37-channel membrane element with more inner channels was found superior in terms of permeate volume flow and whey protein transmis-sion. The results can be explained by the less pronounced deposit layer formation on the inner channels due to the higher backpressure for the permeate, which reduces the flux and, thus, the intensity of deposit layer formation of retained casein micelles rendering the membrane surface more open for whey protein transmission.

Keywords: skim milk; deposit layer formation; transmembrane pressure; pressure drop; channel configuration.

Graphical abstract:

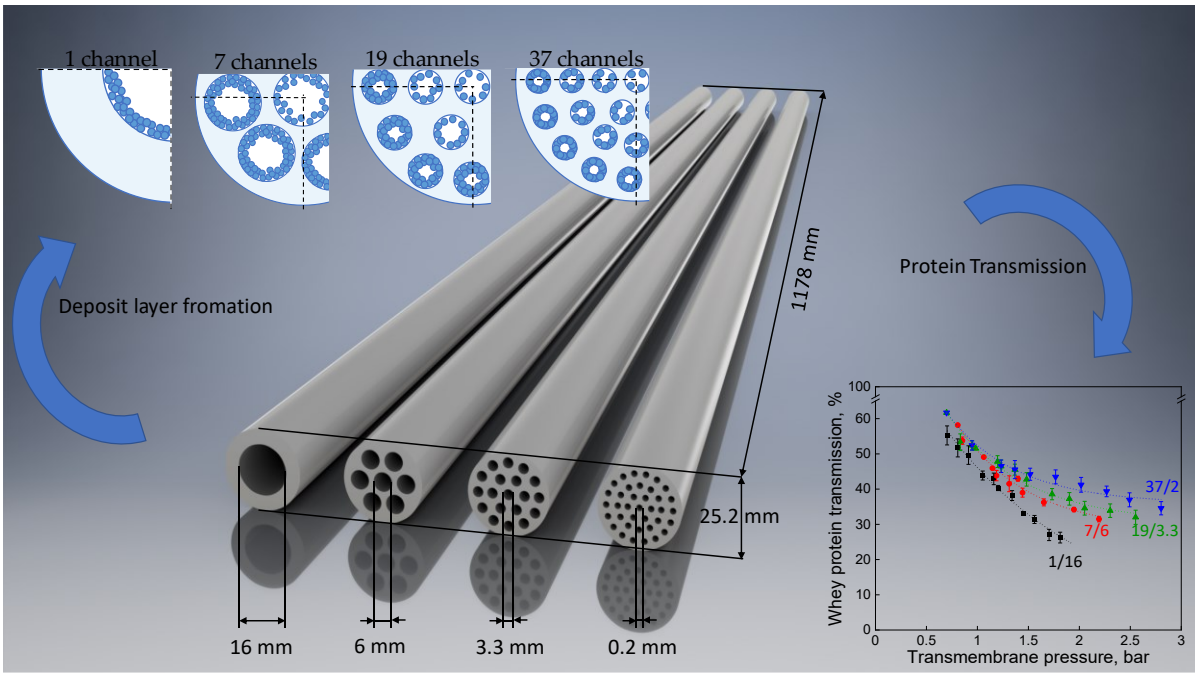

7.1 Introduction

Multi-channel tubular ceramic microfiltration (MF) membrane elements are widely used in the dairy industry for milk protein fractionation obtaining the native protein fractions with minimal thermal or chemical processing stress (Zulewska et al., 2009; Ng et al., 2017). The influence of the processing variables temperature (ϑ) (Schiffer and Kulozik, 2020), transmembrane pressure (Δp_{TM}) (Hurt and Barbano, 2010), feed protein concentration factor (CF) (Hurt et al., 2010), and wall shear stress (τ_W) (Schiffer et al., 2020) and membrane properties (Jørgensen et al., 2016; Schiffer et al., 2021) on the filtration behavior, as well as the length dependence of the filtration (Piry et al., 2012), have already been extensively investigated to optimize milk protein fractionation by MF. Another factor influencing filtration is membrane geometry (Adams et al., 2015a; Hurt et al., 2015b), whereby the number of channels per module can be varied in addition to the use of different channel cross-sectional shapes (Springer et al., 2010). Adams et al. (2015a) compared diamond-shaped channels with round-shaped ones, which were reported to result in a better control of deposit formation and in flux increase. They explained the flux increase with the increase in shear at the membrane surface of round channels (Adams et al., 2015a). However, this is expected to be more pronounced if membranes with fewer channels will be used for this purpose. Astudillo-Castro et al. (2020) reported that the limiting flux increased during skim milk MF when the channels´ inner diameter of multi-channel membranes was low. However, the module volume and the packing density of multi-channel membranes were not considered

as evaluation criteria. Compared to that, a more appropriate basis for comparing modules seems to be using the same module footprint as parameter. An increase in membrane area per module is realized by increasing the number of channels per module while keeping the module´s outer diameter constant (Ghidossi et al., 2006). Adams and Barbano (2016) showed that multi-channel membranes with 6 mm channel inner diameter, compared to 4 mm, could be operated at a lower pressure drop (Δp_L) or higher crossflow velocity, leading to a higher limiting retentate protein concentration. However, the effect of backpressure on the permeate side on flux and protein transmission varies, depending on the number of channels and their position, which was not reported in this work or considered in the discussion of results.

Ghidossi et al. (2010) investigated the pressure gradient of the membrane cross-section by means of computational fluid dynamics simulation and reported an uneven water flux distribution between the individual channels, depending on the distance between the channels and the outer rim of the module. Owing to the longer permeate flow path from the inner channels to the edge of the module element, the contribution of the inner channels to the total flux was lower than that of the outer channels. Thus, the backpressure was higher and, therefore, Δp_{TM} and the flux of the inner channels decreased (Ebrahimi et al., 2018). Deposit formation by suspended biopolymers and the effects on protein fractionation was not investigated in these studies. However, various works showed that high Δp_{TM} levels at first increase the flux and the transport of material towards the membrane, resulting in a more intense deposit layer formation up to the level of complete compaction at Δp_{TM} levels above the critical limit, leading to deposit controlled permeation and high whey protein retention (Bouchoux et al., 2009a; Bouchoux et al., 2010; Qu et al., 2012; Loginov et al., 2020; Doudiès et al., 2021; Schopf and Kulozik, 2021). This should also apply to the radial distribution of Δp_{TM} between outer and inner flow channels in multi-channel elements. To minimize deposit formation, the uniform Δp_{TM} (UTP) concept (Hurt et al., 2010; Hurt et al., 2015a) could be applied, which, however, applies a pressure gradient on the permeate side in longitudinal module direction, but does not affect the radial pressure gradient within the module elements. Concerning skim milk microfiltration, the main fouling mechanism reducing flux and whey protein transmission is deposit layer formation (Kühnl et al., 2010), whereby mainly casein micelles will deposit on the membrane surfaces (Schopf et al., 2020). Nevertheless, pore blocking, pore constriction, solute adsorption, and concentration polarization, will also occur and influence filtration performance (Bacchin et al., 2002; Iritani, 2013). The effect is an increase of the total filtration resistance with an additional retention effect decreasing filtration performance in terms of flux and whey protein transmission (Steinhauer et al., 2011).

It can be expected that the inhomogeneous Δp_{TM} and flux distribution, depending on the channel position in the radial direction, will have an impact on the deposition of retained material and thus on the filtration performance. Frederic et al. (Frederic et al., 2018) investigated the influence of deposit layer formation on the flux distribution among the individual channels of a multi-channel tubular membrane when concentrating suspended coarse particles in water, where deposit formation affects flux, which is another matter compared to fractionation of differently sized particles like small and large proteins. Another report on concentrating sodium alginate in an aqueous model solution with a 7-channel polymer membrane showed that fouling was more intense on the membrane surface of the outer channels than in the central channel (Schuhmann et al., 2019).

In all of these studies on water filtration removing or concentrating suspended solids, flux and achievable concentration level were the decisive evaluation criteria. If, however, multi-channel modules are used in the filtration of more complex fluids (e.g., milk) for the considerably more difficult task of separating the whey proteins contained therein as permeation target components from the main protein fraction of casein, the evaluation criteria have to be chosen accordingly. It can be expected that the advective protein transport of material to the membrane surface will also have different effects owing to the different transmission rates and whey protein mass flow of the inner and outer channels since the fouling phenomenon by the retained biopolymers also differs. Thus, the homogeneity of the permeate flux should depend on the number of flow channels in multi-channel tubular elements. Whether these effects also occur at higher channel number modules providing higher flux per module due to the increased membrane surface is an open point. Inhomogeneity of channel conditions in terms of static pressure and distribution of volume flow probably increases, but the number of outer channels is also increased. However, the open question of which number of channels performs best in terms of specific flux and whey protein transmission compared to the multi-channel membrane with similar dimensions and module footprints (module diameter and length) cannot be simply answered based on the state of current knowledge.

The objective of this study, therefore, was to assess the impact of the module configuration in terms of channel number on flux and transmission of membrane-permeable substances in milk. Two opposing effects could be at work. On the one hand, the selective membrane surface is increased with the number of individual flow channels. On the other hand, the permeate flow path through the ceramic support structure differs between the inner and the outer channels, and therefore, no linear increase in permeation performance with the number of channels can be expected. The hypothesis was that a high channel number should lead to a better filtration performance in terms of protein fractionation, with the inner channels contributing less to the overall

flux, but more to whey protein transmission because of a lower impact of deposit formation in these inner channels. The active membrane area changes depending on the number of channels, but the influence of the position of the individual flow channels within the tube bundle of a ceramic membrane on small protein transmission and mass flow remains to be assessed.

In this study, milk protein fractionation was investigated using ceramic multi-channel modules with 1, 7, 19, and 37 channels, varying Δp_{TM} and CF to gain insights on protein transmission in different situations of deposit formation intensity. The approach was to vary the number of channels and thus the inner diameter of the multi-channel membranes, while the outer module diameter remained similar, and thus, the module volume (spatial footprint) remained unchanged to provide a practically relevant basis for comparison. The impact of the number of channels on the longitudinal Δp_L, the cross-flow velocity, the τ_w, and the feed volume flow was investigated.

7.2 Experimental

7.2.1 Skim milk and membranes

Skim milk pasteurized at 74 °C for 28 s obtained from Molkerei Weihenstephan GmbH & Co. KG (Freising, Germany) was stored at 4 °C up to 4 days (pH 6.6) until use. Prior to the experiments, the skim milk was separately tempered to 55 °C. Ultrafiltration (UF) was performed to vary the total protein concentration using a spiral wound membrane (GR73PE, module 6338, polyethersulfone, Alfa Laval Mid Europe GmbH, Glinde, Germany) with a nominal pore size of 10 kDa, a 48 milli-inch diamond spacer, and a total active membrane surface of 16.5 m^2. The UF permeate was drained until the target retentate protein concentration (CF 2 and CF 3) was reached. The concentrated retentate was then used for the MF experiments. The viscosity and density during MF of the retentate and the permeate at CF 1–3 and deionized water were measured according to Schopf et al. (2021b) (data shown in Table 7.1).

Table 7.1. Viscosity η and density φ of MF retentate and MF permeate at different CF and deionized water at 55 °C.

CF	1	2	3	H_2O
$\eta_{Retentate}$, 10^{-6} kg m^{-1} s^{-1}	922 ± 11	1,498 ± 12	2,074 ± 15	504 ± 9
$\eta_{Permeate}$, 10^{-6} kg m^{-1} s^{-1}	731 ± 6	735 ± 5	741 ± 3	504 ± 9
$\varphi_{Retentate}$, kg m^{-3}	1,023 ± 5	1,038 ± 3	1,047 ± 2	986 ± 2
$\varphi_{Permeate}$, kg m^{-3}	1,009 ± 2	1,011 ± 1	1,013 ± 3	986 ± 2

Four MF ceramic tubular multi-channel membranes with an α-Al_2O_3 supporting structure, a selective layer made of ZrO_2, and a nominal pore size of 0.1 µm from Atech Innovations GmbH (Gladbeck, Germany) were used. All multi-channel membranes had

a total membrane length of 1.178 m and an outer diameter of 0.0252 m, respectively, the volume of all modules was $6.0 \cdot 10^{-4}$ m^3 (Figure 7.1).

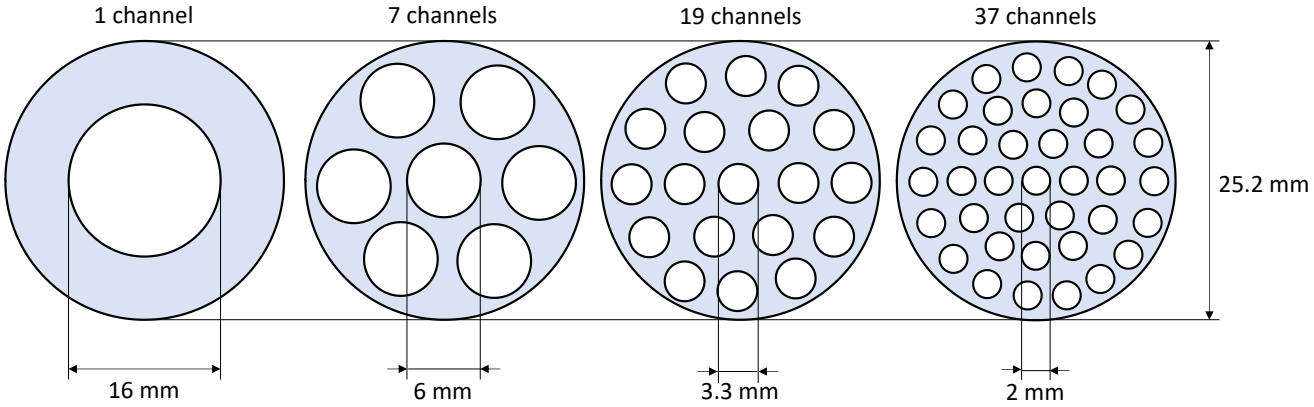

Figure 7.1. Schematic illustration of the multi-channel membranes with the same outer diameter and a different number of channels.

The multi-channel membranes differ in terms of the number of channels, the channel hydraulic diameter, and their active membrane area as shown in Table 7.2.

Table 7.2. Characteristics of microfiltration membranes.

Type	Number of channels	Channel hydraulic diameter, mm	Active membrane area, cm^2
1/16	1	16.0	59.2
7/6	7	6.0	155.4
19/3.3	19	3.3	232.0
37/2	37	2.0	273.9

7.2.2 Experimental setup

All experiments were performed as independent duplicates. The data represent the average values, and the error bars are the range of the standard deviation. All experiments were performed at 55 °C with the modules integrated into a custom-made pilot plant from SIMA-tec GmbH (Schwalmtal, Germany) described in detail by Schiffer et al. (2021) (Figure 7.2).

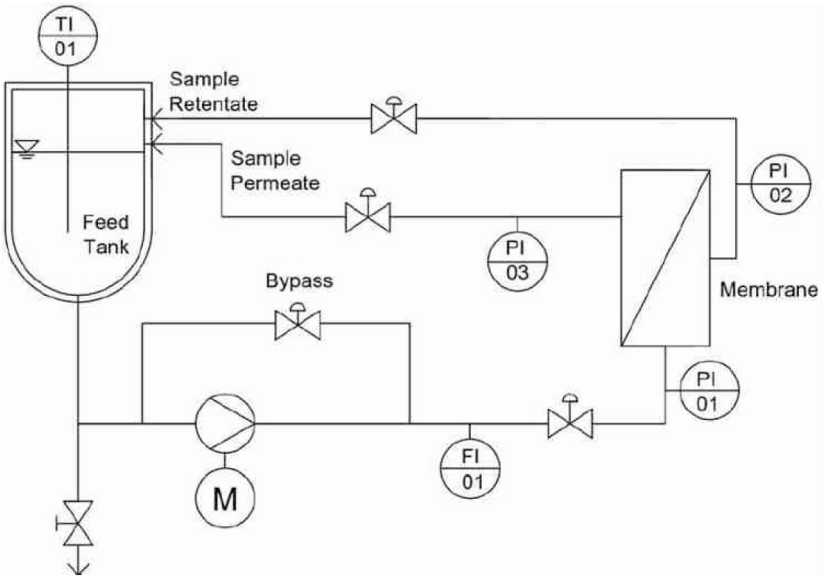

Figure 7.2. Flow chart of the filtration plant (Schiffer et al. (2021)).

Cleaning of the membranes and the filtration unit was performed according to Schiffer et al. (2020). In brief, after each experiment, the filtration plant was flushed with 60 L softened water tempered at 65 °C and then cleaned with caustic 1% UF466 (Halag Chemie AG, Aadorf, Swiss) for 40 min at 65 °C. Then the plant was flushed again with 60 L softened water at 65 °C, followed by an acidic cleaning step with 0.5% nitric acid (60%) (Halag Chemie AG, Aadorf, Swiss) for 20 min at 65 °C. Afterward, the filtration plant was flushed with 60 L softened water at 65 °C. Before starting the filtration experiments, membrane conditioning was performed using caustic 1% UF466 (Halag Chemie AG, Aadorf, Swiss) for 20 min at 65 °C followed by flushing the plant with 60 L softened water where the plant was tempered at 55 °C. Then the pure water flux was measured to verify that the cleaning process was successful.

The amount and composition of the milk proteins in permeate and retentate samples were determined via reversed-phase high-performance liquid chromatography according to Dumpler et al. (2017). Three different MF protocols were adopted:

To investigate the flow behavior of the four membrane modules with their number of channels and inner channel diameter (1/16, 7/6, 19/3.3, and 37/2), the Δp_L for pure water and skim milk with CF 1–3 were analyzed. Δp_L was measured with a closed permeate valve up to a mean crossflow velocity of 13 m s^{-1} calculated by Equation (7.5). Then, the friction factor (λ) and the Reynolds number (Re) were calculated according to Equations (7.2) and (7.3), respectively.

To study the influence of the number of channels on the fouling behavior, and of the membrane area per module with the same module footprint, and inner channel diameter on the filtration performance, experiments at Δp_{TM} = 1.5 bar = const. were performed for the 1-, 7-, 19-, and 37-channel tubular membranes at CF 1–3 at

τ_w = 100 Pa. The Δp_{TM} of 1.5 bar was chosen because the effective flux per module was independent of Δp_{TM} at that level. As a consequence, the limiting flux in different channels depending on the channel position within the multi-channel module was reached. Therefore, the same filtration behavior can be assumed according to Schiffer et al. (2020).

To assess the influence of the Δp_{TM} on flux, whey protein transmission, and fouling as a function of the channel number, experiments with varying Δp_{TM} levels at CF 3 and τ_w = 100 Pa (calculated by Equation (7.2)) were performed with a stepwise Δp_{TM} increase from 0.7 to 2.8 bar as described by Hartinger et al. (2019c) and Schiffer et al. (2020). In brief, Δp_{TM} was adjusted at the lowest reachable pressure to prevent reverse flux from the permeate side at the module end (Schopf et al., 2021a), held constant for 45 min to achieve steady-state filtration conditions, and then increased stepwise with a fixed time interval of 30 min per step according to Table 7.3. In summary, nine pressure steps were performed.

Table 7.3. Transmembrane pressure Δp_{TM} steps and the corresponding pressure drop along the membrane Δp_L for the 1-, 7-, 19-, and 37-channel tubular membranes at CF 3, τ_w = 100 Pa, and ϑ = 55 °C.

Type	**Δp_{TM}, bar**									**Δp_L, bar m^{-1}**
1/16	0.7	0.8	0.9	1.0	1.2	1.3	1.5	1.7	1.9	0.3
7/6	0.8	0.9	1.0	1.2	1.3	1.5	1.7	1.9	2.2	0.8
19/3.3	0.8	0.9	1.0	1.2	1.5	1.7	2.0	2.3	2.5	1.5
37/2	0.9	1.2	1.4	1.5	1.8	2.0	2.2	2.5	2.8	1.8

At the end of each pressure step, quasi-stationary filtration conditions in terms of constant flux and constant whey protein transmission were reached indicating that there were no more changes in deposit layer formation, which is in accordance to the literature (Opong and Zydney, 1991; Hartinger et al., 2019a; Schiffer et al., 2020). We verified this by measuring the flux every 5 to 10 min (Figure 7.3). τ_w = 100 Pa was chosen to keep the deposit layer-reducing forces constant as suggested by Gésan-Guiziou et al. (1999) for the comparison of different membrane modules to assess flux and whey protein transmission in skim milk MF instead of the Re or the mean crossflow velocity as parameters.

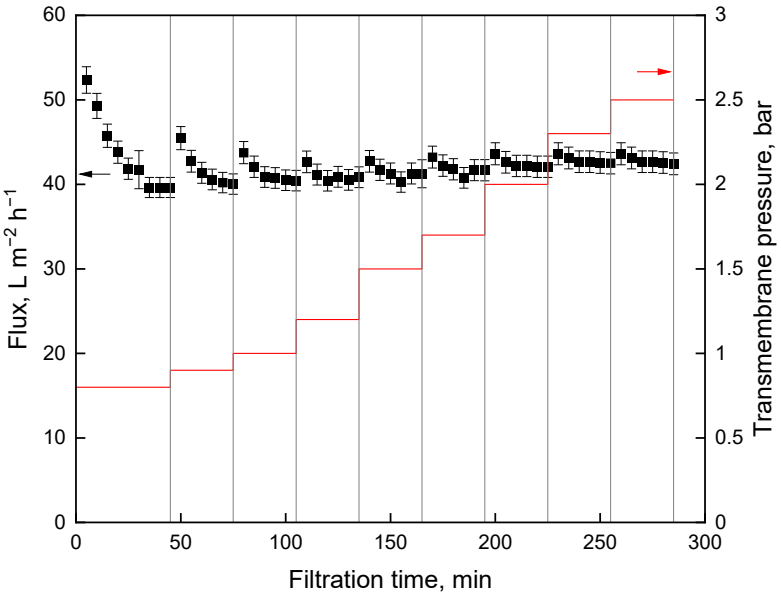

Figure 7.3. Flux as a function of the filtration time for the stepwise Δp_{TM} increase for the 19-channel MF membrane at τ_w = 100 Pa, at skim milk CF 3, and ϑ = 55 °C.

7.2.3 Characteristics of crossflow filtration

Owing to the friction between the flowing fluid and the membrane, Δp_L on the retentate side decreased from the module inlet (p_1) to the module outlet (p_2). This can be calculated with the pipe friction coefficient (λ), the membrane length (L), the pipe inside diameter (d_i), the density of the fluid (φ), and the average crossflow velocity (v_m) following Equation (7.1):

$$\Delta p_L = p_1 - p_2 = \lambda \cdot \frac{L}{2 \cdot d_i} \cdot \varphi \cdot v_m^2 \tag{7.1}$$

τ_w was calculated according to Equation (7.2):

$$\tau_W = \frac{\lambda \cdot \varphi \cdot v_m^2}{8} = \frac{\Delta p_L \cdot d_i}{4 \cdot L} \tag{7.2}$$

λ is a dimensionless parameter to calculate the pressure loss caused by pipe friction, considering the properties of the fluid and the pipe condition. For hydraulically smooth pipes, λ is only a function of Re, a dimensionless ratio that indicates the relationship between the inertial and viscous forces or the degree of flow turbulence.

To calculate Re, the hydraulic diameter of the pipe (d_h) and the dynamic viscosity of the fluid (η) are used (Equation (7.3)):

$$Re = \frac{\varphi \cdot v_m \cdot d_h}{\eta} \tag{7.3}$$

The relationship between Re and λ can be calculated by combining Equation (7.2) and Equation (7.3) (Equation (7.4)).

$$\lambda = \frac{8 \cdot \tau_W \cdot d_h}{\eta \cdot Re} \tag{7.4}$$

The mean crossflow velocity (v_m) represents the volume flow ($\dot{V}_{feed}$) related to the cross-sectional area (A_{cros}) with the channel inner diameter (d_i) and the number of channels (n) of the multi-channel element (Equation (7.5)):

$$v_m = \frac{\dot{V}_{feed}}{A_{cros}} = \frac{\dot{V}_{feed}}{\pi \cdot \left(\frac{d_i}{2}\right)^2 \cdot n} \tag{7.5}$$

The retentate-side pressures (p_1 and p_2) and the backpressure on the permeate-side (p_3) result in the averaged Δp_{TM}, which represents the driving pressure gradient of filtration and can be calculated according to Equation (7.6).

$$\Delta p_{TM} = \frac{p_1 + p_2}{2} - p_3 \tag{7.6}$$

One criterion for assessing performance is the permeate volume flow (J) (flux) related to the membrane surface (A_M), determined according to Darcy's law (Equation (7.7)) with the total filtration resistance (R_F):

$$J = \frac{\dot{V}_{feed}}{A_M} = \frac{\Delta p_{TM}}{\eta \cdot R_F}. \tag{7.7}$$

The total filtration resistance (R_F) is defined as the membrane resistance (R_M) and the additional resistance caused by the deposited fouling (R_D), which is the sum of all fouling effects, i.e., deposit layer formation, adsorption, pore/ intermediate blocking, and the concentration polarization (Equation (7.8)):

$$R_F = R_M + R_D \tag{7.8}$$

Protein transmission (Tr), which quantifies the passage of a component (i) through the membrane to the permeate side, is also used to further assess the filtration performance. The concentration ratio of the substance in the permeate ($c_{i,per}$) and in the retentate ($c_{i,ret}$) was calculated according to Equation (7.9):

$$Tr_i = \frac{c_{i,per}}{c_{i,ret}} \tag{7.9}$$

7.3 Results and discussion

7.3.1 Investigation of the pressure drop in ceramic multi-channel membranes

To compare the filtration performance as a function of the number of channels at different protein concentrations, the flow behavior of the different membrane geometries for pure water and skim milk with CF 1, 2, and 3 were analyzed. Figure 7.4 shows the influence of CF, i.e., of the protein concentration, on the axial pressure drop along the membrane and on the corresponding wall shear stress as a function of the feed volume flow and the mean crossflow velocity for the 19-channel membrane as an example.

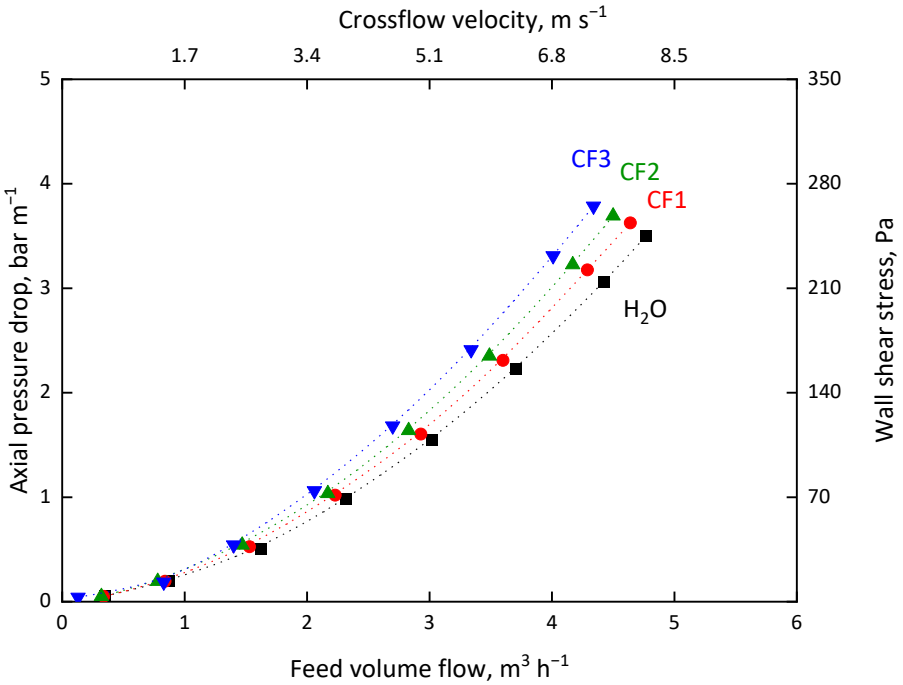

Figure 7.4. Axial pressure drop and wall shear stress as a function of the feed volume flow and the crossflow velocity for the 19-channel membrane for water and skim milk at CF 1–3.

Figure 7.4 shows that the axial pressure drop with increasing feed volume flow along the membrane length increases for all four filtration media due to the increased frictional losses between the fluid and the membrane. As the CF of the skim milk increases, the pressure drop increases further due to the higher viscosity at a higher CF. Skim milk is a Newtonian fluid (Warncke and Kulozik, 2020), whereas concentrated skim milk exhibits a structurally viscous flow behavior that is more pronounced with increasing CF (van Vliet et al., 2004). The increase in shear forces along the membrane surface is a function of feed velocity and viscosity. However, in which way the different number of channels affects the flow behavior in multi-channel tubular membranes is an open question. The area of the cross-section and the inner diameter of the channels change by varying the number of channels at a constant outer module diameter, which will influence the flow behavior. Therefore, the axial pressure drop along the membrane was measured as a function of the crossflow velocity for water and skim milk at CF 3 for membranes with 1, 7, 19, and 37 channels (Figure 7.5).

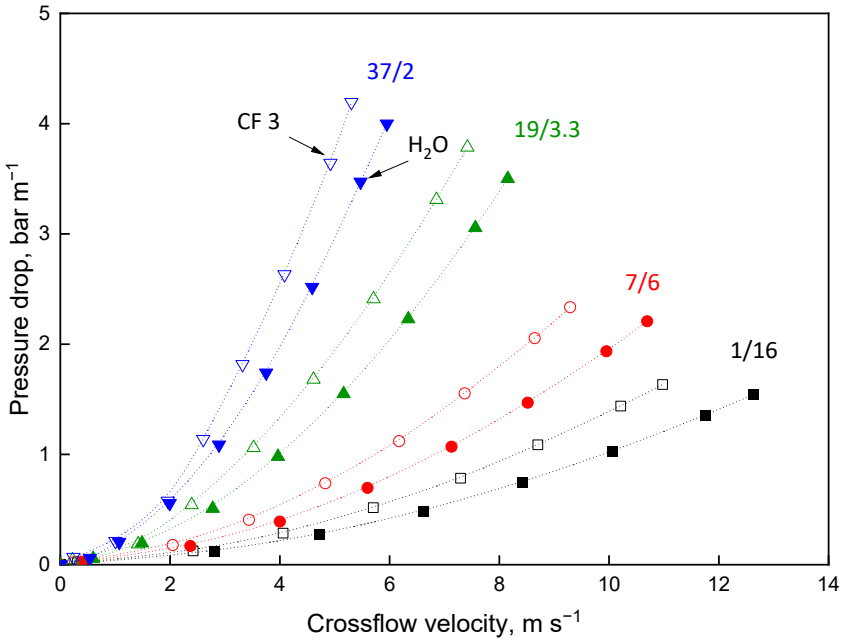

Figure 7.5. Pressure drop as a function of the crossflow velocity for multi-channel membranes (number of channels/inner diameter of the channels) for water and skim milk at CF 3.

Obviously, the pressure drop increases for all four geometries with increasing crossflow velocity. However, the increase in pressure drop is greater for the higher the channel numbers (Figure 7.5). This observation is due to the decrease of the flow channel cross-section for the modules with the larger channel numbers, which increases the frictional loss at constant crossflow velocity. The filtration experiments were carried out at a wall shear stress of 100 Pa to compare the filtration performance of the different membrane geometries despite their different hydrodynamic flow behavior. This keeps the deposit layer-reducing forces constant.

7.3.2 *Influence of the number of channels on the flux*

The main limitation of membrane processes like skim milk MF is that the substance to be retained tends to be deposited on the membrane surface (so-called fouling) initiated by concentration polarization, which then can block the membrane pores and form a deposit layer producing an additional filtration resistance, reducing flux and transmission. To investigate the influence of the channel number on the fouling in multi-channel ceramic MF membranes, the effective flux was measured. The effective flux is an average of all fluxes of the individual module channels. Figure 7.6 shows the effective flux as a function of Δp_{TM} for skim milk CF3.

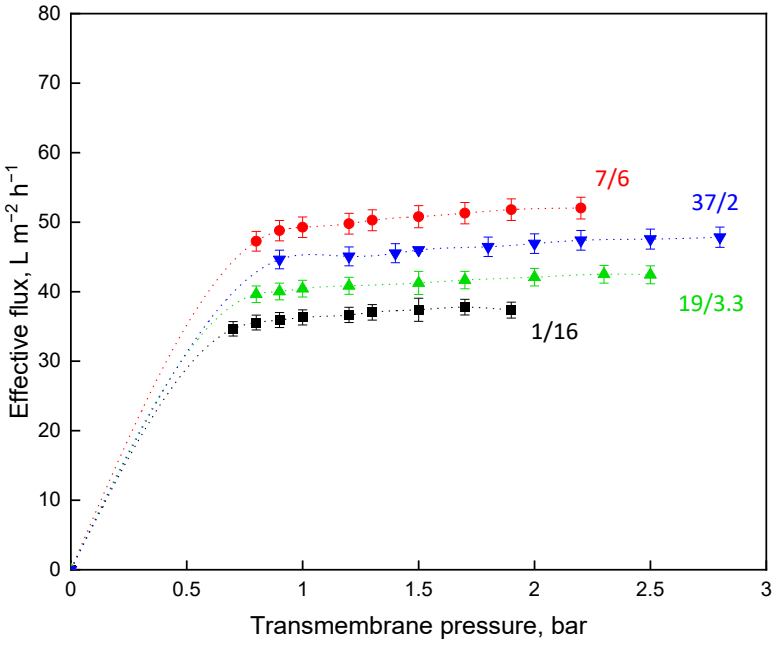

Figure 7.6. Effective flux as a function of Δp_{TM} for multi-channel MF membranes (number of channels/ inner diameter of the channels) for skim milk CF3 at τ_w = 100 Pa and ϑ = 55 °C.

Figure 7.6 illustrates that the effective flux reached a stable level, at the lowest reachable Δp_{TM}, which has to be applied to prevent reverse flux at the rear part of the module. The results show that an increase in Δp_{TM} does not lead to an increase in the effective flux per module, although different Δp_{TM} levels occur depending on the channel position. We assume that the inner channels do not work under limiting conditions, while for the entire module limiting conditions were determined. However, at higher levels of Δp_{TM}, an increase of flux would result in higher backpressure (depending on channel position) and the flux per module can therefore not be increased by higher Δp_{TM}. This will be explained in conjunction with the whey protein transmission further below.

Comparing the effective flux of the multi-channel membranes it is obvious that the 7-channel membrane provides the highest effective flux, followed by the 37-, 19-, and

1-channel membrane. However, the effective flux for all multi-channel modules should be the same if all filtration conditions, i.e., τ_w and deposit layer formation, were the same and the modules would only differ in terms of the channel number and channel position. Obviously, however, the 7-channel membrane is superior regarding flux compared to the other modules with other ratios of number of outer versus inner channels. To verify the effect of the channel number on flux fouling potential, the effective flux as a function of the channel number for skim milk at CF 1–3 is shown in Figure 7.7.

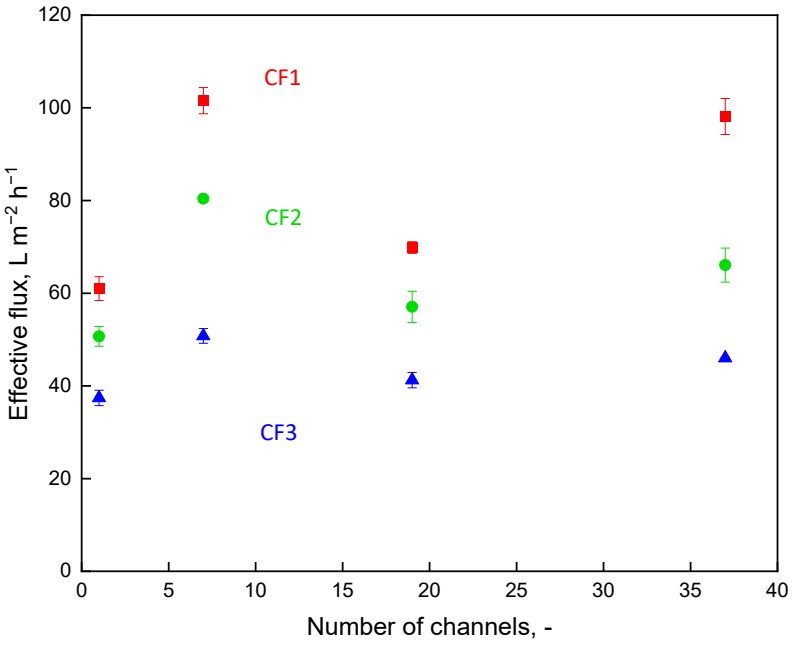

Figure 7.7. Effective flux as a function of the channel number of multi-channel MF membranes for skim milk CF 1–3 at τ_w = 100 Pa, Δp_{TM} = 1.5 bar, and ϑ = 55 °C.

As expected, the flux decreases with increasing CF for all four membrane geometries. This is attributed to a higher viscosity at higher CF levels and a more pronounced deposition of proteins on membrane surface compared to lower CF (Hurt et al., 2015c). Both higher viscosity and more intense fouling reduce flux according to Darcy's law (Equation (7.7)).

Comparing the flux values for each CF, however, the highest flux values are obtained for the 7-channel membrane for all CF, and the lowest flux values are for the 1-channel membrane. The flux of the 37-channel membrane is slightly below the values of the 7-channel membrane. An increase in the membrane area should not affect the specific flux per square meter of membrane if filtration conditions were otherwise unchanged. However, as reported by Ghidossi et al. (2010), the inner channels contribute less to the total flux than do the outer channels as a result of the backpressure on the permeate side depending on the longer permeate flow path, i.e., the distance of the channels and the outer rim of the module.

Ghidossi et al. (2010) were able to calculate this pressure gradient occurring in the supporting layer of multi-channel MF membranes. They attributed the pressure gradient to the creation of backpressure caused by the permeate volume flow in the supporting layer (Ghidossi et al., 2010). This will influence Δp_{TM}, the transport of particles towards to the membrane surface, the deposition of particles on the membrane surface, and, thus, the formation of fouling. As a consequence, the fouling will differ in amount and concentration of the proteins, due to the inhomogeneous flux distribution between channels and differ in the deposit layer structure, due to the different Δp_{TM} distribution depending on the channel position.

To determine the effect of increasing channel number on fouling, the permeate volume flow per membrane module was analyzed as a function of the absolute membrane area of each module (Figure 7.8).

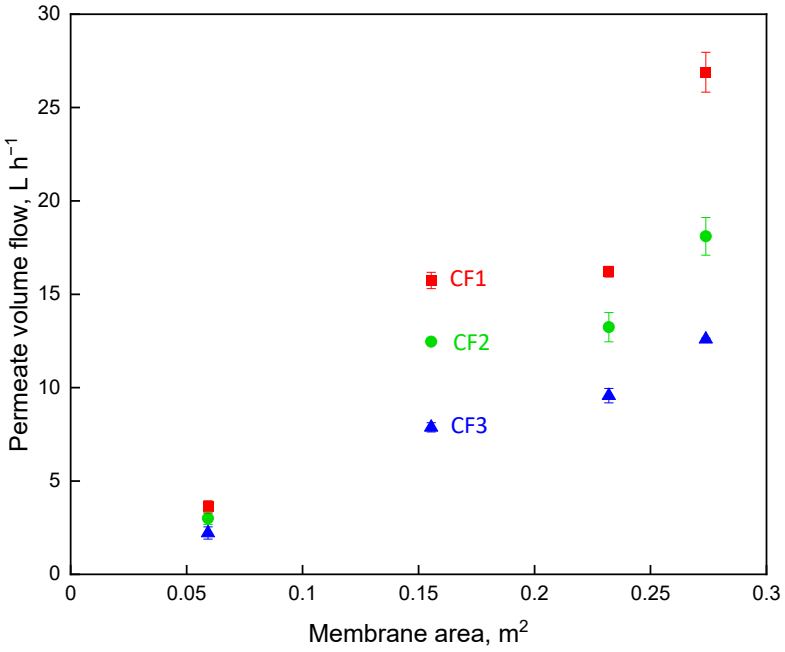

Figure 7.8. Permeate volume flow per module as a function of the membrane area for multi-channel MF membranes for skim milk CF 1–3 at τ_w = 100 Pa, Δp_{TM} = 1.5 bar, and ϑ = 55 °C.

Figure 7.8 shows the increase in absolute permeate volume flow per module for CF 1 and CF 2, between the 7- and 19-channel membrane elements, within the range of the standard deviation of 0.5 L h^{-1} (CF 1) and 0.8 L h^{-1} (CF 2). In other words, the increase in membrane area per module is compensated by the decrease in flux. For CF 3, the absolute permeate volume flow increases with increasing active membrane area from 16 L h^{-1} for the 7-channel membrane to 27 L h^{-1} for the 37-channel membrane. Since the flux differences were not very pronounced, the increase in membrane area leads to an increase in permeate volume flow (compare Figure 7.7). For the 37-

channel membrane, the highest permeate volume flow was observed for each CF, although the 37-channel membrane has a module volume similar to those of the 1-, 7-, and 19-channel membranes. Furthermore, the membrane area of the outer channels is larger for the 19-channel membrane with 147 cm^2 than for the 7- and 37-channel membranes with 133 cm^2 each. The permeate flow of the inner channels is hindered from being discharged owing to the longer flow path towards the outside of the module. The effective average of the fouling resistance was calculated according to eqs. (7.7) and (7.8) (Figure 7.9). The fouling resistance is the sum of all fouling effects, as mentioned above.

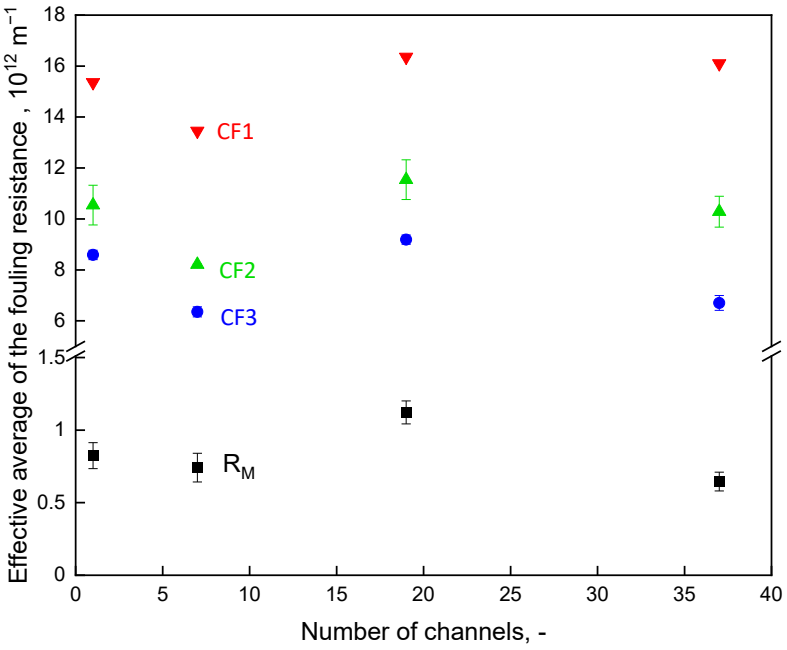

Figure 7.9. Membrane resistance R_M and the effective average of the fouling resistance for skim milk CF 1–3 as a function of the channel number of multi-channel MF membranes at τ_w = 100 Pa, at a Δp_{TM} = 1.5 bar, and ϑ = 55 °C.

The highest average membrane resistance was observed for the 19-channel membrane, whereas those of the 1-, 7-, and 37-channel membranes were lower, but at an insignificant level of difference ($P < 0.1$) between these three modules. It can be stated that all membrane elements were produced by the same procedure and materials and that, therefore, manufacturing-related variabilities are considered negligible.

The effective averages of the fouling resistances within each CF level significantly differ ($P < 0.001$). We assume that the differences in the effective average of the fouling resistance can rather be attributed to differently intense fouling formation depending on the channel number. The inner channels are affected by the sum of fouling effects and backpressure from the permeate side, whereas the outer channels are mainly or almost exclusively affected by intense fouling. For all four membrane geometries, the effective average of the fouling resistance increases with increasing CF

(Figure 7.9). The difference between CF 2 and CF 3 is significantly ($P < 0.001$) larger than that between CF 1 and CF 2. For the 7-channel membrane, the effective average of the fouling resistance increases by 30% from CF 1 to CF 2 and by 64% from CF 2 to CF 3. This can be attributed to more intense fouling, to concentration polarization, and to structural changes during the formation of a deposited layer above a certain protein concentration. Concentration polarization increases (as long as the limiting flux is not reached) and the deposit becomes more densely packed and tighter due to more protein-protein interaction. Bouchoux et al. (2009a) showed that with increasing casein concentration the micelles interact more and the casein deposit layer becomes more compact owing to the dewatering of the micelles by compression. A gel layer will be formed stabilized by hydrophobic and electrostatic interactions of the casein micelles (Qu et al., 2012). Beckman and Barbano (2013) reported that flux was decreasing by increasing CF with spiral wound membranes, which they explained by more intense fouling.

The effective average of the fouling resistance was highest for the 19-channel membrane and lowest for the 7-channel membrane. The ones for the 1-channel and the 37-channel membrane lay between. If the filtration conditions were the same for all modules, the fouling resistance would depend on the respective Δp_{TM} in each channel depending on the number and position of the channels within the module. We assume that the increased effective average of the fouling resistance for the 19-channel membrane is caused by the larger number of outer channels, which are affected by a higher intensity of fouling. Owing to the radial pressure gradient in the membrane module, the Δp_{TM} is greater in the outer channels than in the inner channels. As a consequence, the 7-channel membrane provides superior conditions in terms of the ratio of inner-to-outer channels, which, however, is difficult to define (Ghidossi et al., 2010), because there is a gradient in position from outer to the inner channels, followed by the 37-, 1-, and 19-channel membranes.

7.3.3 Influence of the number of channels on the whey protein transmission

Both flux and transmission have to be considered as they can be influenced separately according to Hartinger et al. (2019c). It can be assumed that the inhomogeneous Δp_{TM} distribution within the channels leads to a different transmission. To investigate the influence of the number of channels on the deposit layer formation and its effect on protein transmission, the whey protein transmission was analyzed for varying levels of Δp_{TM} for the four membrane modules at CF 3 (Figure 7.10). CF 3 was chosen to obtain the most intensive deposit layer and clearly distinctive differences.

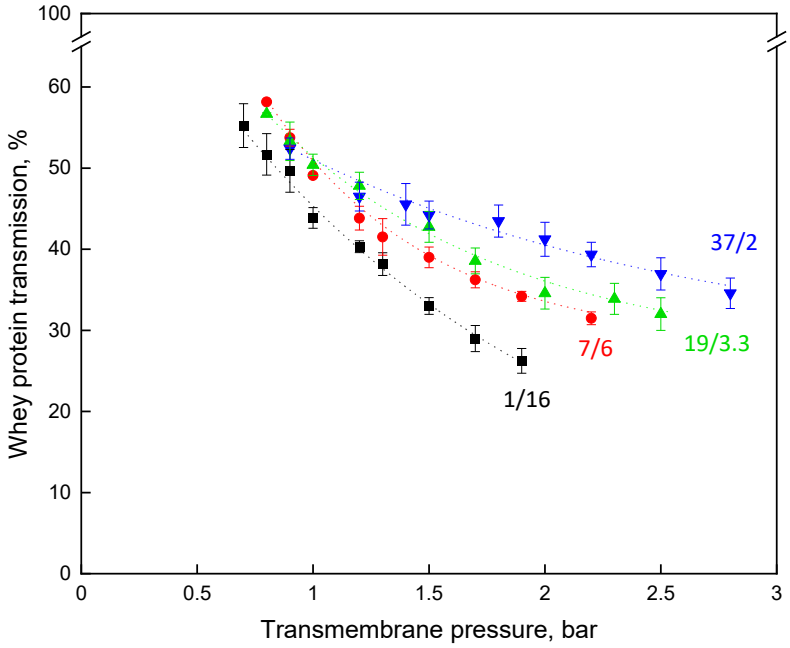

Figure 7.10. Whey protein transmission as a function of Δp_{TM} for multi-channel MF membranes (number of channels/ inner diameter of the channels) at skim milk CF 3, τ_w =100 Pa, and ϑ = 55 °C.

It can be seen that increasing the Δp_{TM} leads to a decrease of the whey protein transmission owing to a more intense membrane fouling and a change of deposit layer formation at high Δp_{TM} depending on the channel number. At low Δp_{TM}, however, the channel number does not influence the protein transmission. However, at Δp_{TM} > 1.5 bar, the whey protein transmission declines less at higher Δp_{TM} the higher the channel number. This indicates that Δp_{TM} in the inner channels was lower than that of the outer channels. Therefore, the deposit layer will be less compact in the inner channels, and this leads to a high whey protein transmission. Therefore, multi-channel membranes with a high number of inner channels have transmission values higher than those of membranes with only a single inner channel related to the same module volume.

7.4 Conclusions

Figure 7.11 provides a schematic impression of the radial profile of multi-channel membranes with the inhomogeneous distribution of deposit layer formation, depending on the number and position of channels, is provided as a schematic illustration of the conclusions drawn from the results presented above.

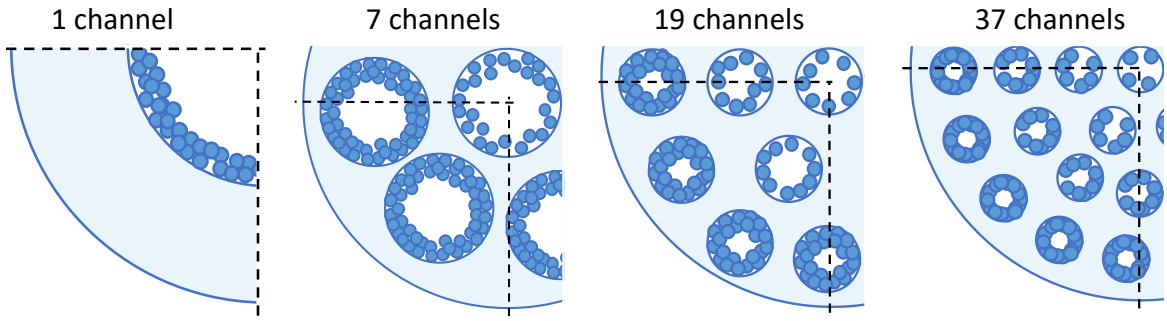

Figure 7.11. Schematic illustration of the axial profile of multi-channel membranes and the inhomogeneous deposit layer formation dependent on the number of channels and their position in multi-channel membranes.

As the scheme illustrates, those channels with low backpressure at first yield a high flux, which rapidly results in intense membrane fouling. This, in turn, reduces the transmission of whey proteins, while the inner channels, e.g., of the 37-channel membrane studied here, are less affected by deposit formation, therefore contributing more to the overall transmission of whey proteins.

These results happen to be in good accordance with a report by Piry et al. (2012), where a ceramic membrane with a three-times higher membrane resistance R_M (deliberately fabricated as an experimental prototype with a thicker selective layer) was superior in terms of whey protein transmission to conventional ceramic membranes with lower R_M. The explanation was that this caused a lower initial flux and, thus, a lower transport of deposit forming material towards the membrane surface. As a result, a lower fouling intensity and a lower R_D with less retention of whey proteins were observed. The same line of thinking applies here, but for multichannel membranes, where the R_M is naturally varied simply by a longer flow path for the permeate generating a higher membrane resistance for the inner channels instead of a thicker selective layer.

The results reported here allow for a fact-based selection of the number of channels of a multi-channel membrane with the same module volume to improve the total efficiency of industrial filtration systems with optimized milk protein fractionation efficiency. If one would consider applying mono-tubular ceramic membranes instead of multichannel elements, these would have to be operated in parallel to obtain the same installed membrane area and the same flux. In terms of sustainability, the same overall volume throughput and energy consumption would be required. The filtration result for the purpose of protein fractionation, however, would not be the same, because the mono-tubular membranes would be highly affected by deposit formation and a high level of undesired retention of whey proteins (or other small target components. Using ceramic membranes with a high number of inner channels could reduce the total number of required multi-channel membranes to reach the required membrane surface with an

increased whey protein transmission. Regarding practical consideration of industrial membrane plant configuration, taking into account the effect of radial Δp_{TM} distribution evaluated in this study, in combination with the axial gradient of Δp_{TM} as studied in (Piry et al., 2012; Hartinger et al., 2019c; Schopf et al., 2021a) would, in our opinion, help to design the optimal plant layout and module selection.

Author Contributions: Conceptualization, R.S.; Data curation, R.S., F.D., Ra.S., and D.A.; Formal analysis, R.S.; Funding acquisition, U.K.; Investigation, R.S.; Methodology, R.S., F.D., Ra.S., and D.A.; Project administration, R.S., and U.K.; Resources, U.K.; Software, R.S., F.D., Ra.S., and D.A.; Supervision, U.K.; Validation, R.S.; Visualization, R.S.; Writing – original draft, R.S.; Writing – review & editing, F.D., Ra.S., D.A., and U.K. All authors have read and agreed to the published version of the manuscript.

Funding: This IGF Project of the FEI was supported via AiF within the program for promoting the Industrial Collective Research, IGF, of the German Ministry of Economic Affairs and Energy, BMWi, based on a resolution of the German Parliament. Project: AiF 10 EWN.

Acknowledgments: The authors gratefully thank Heidi Wohlschläger, Claudia Hengst, and Hermine Rossgoderer for their assistance with the RP-HPLC analysis of the milk samples and Malou Warncke and Simon Schiffer for discussing results.

Conflicts of Interest: The authors declare no conflict of interest. The authors declare that they have no known competing financial interests or personal relationships that could have appeared to influence the work reported in this paper. The funders had no role in the design of the study; collection, analyses, or interpretation of data; writing of the manuscript; or in the decision to publish the results.

8 Overall discussion and main findings

Fouling is the main issue in all membrane systems but in MF it is not only responsible for the flux decline, moreover, intense fouling will also decrease protein transmission and thus the protein mass flow over the membrane. For best filtration performance it is essential to control deposit layer formation. This can be done by assessing the best filtration conditions in terms of Δp_{TM}, Δp_L, feed volume flow, crossflow velocity, feed protein concentration, and filtration temperature. But also the right selecting of a suitable membrane module depending on their build-up has a high impact on the control of fouling.

Intense and diverse research on protein fouling on membrane surfaces has been conducted during the last decades. However, research is lacking regarding the formation of the deposit layer under varying process conditions as well as the characterization of the structure of the length-dependent deposit layer in correlation to the composition and amount of the deposited proteins. Based on this, the basic insights for potential implementation of HFM for milk protein fractionation in the dairy industry and its optimization for an efficient fractionation process to find the best filtration conditions were presented in the current study. The following chapters aim to discuss the main findings of the presented publications and put them in a meaningful context.

8.1 Effective control of deposit layer formation in HFM

Fouling occurs in all membrane systems, therefore, the effective control of deposit layer formation was investigated in MF HFM as an example membrane system. To control deposit layer formation effectively, first, the deposit layer structure was investigated, and secondly, the milk protein fractionation was optimized.

8.1.1 Investigation on deposit layer structure in HFM

To optimize milk protein fractionation, the deposit layer formation has to be controlled and therefore, its structure has to be investigated. As shown in Chapter 1.3, the structure of the deposited proteins is affected by different conditions. Initially, the deposit layer structure in dead-end filtration was investigated to establish a standard operating procedure to visualize the formation and the chemical structure of the deposit without the effect of the length-dependency of the filtration.

MR images in Figure 3.3 showed that the deposit on the inner surface of the hollow fiber increased as the filtration time progressed. The fouling is mainly caused by caseins that deposit on the membrane surface and thus can be detected by the NMR tomography. Furthermore, the chemical characterization of the deposit layer (Figure

3.4) confirms that mainly caseins are responsible for the deposit layer formation concentrated on the membrane surface. Eleven times higher casein concentration than whey protein concentration could be measured on the membrane surface. Schopf et al. (2020) explained this by the retention effect due to the different particle sizes of both fractions (Figure 1.6). The accumulation processed during filtration (Figure 3.5) and leads to an increase in the filtration resistance causing a flux decline and a reduction of the whey protein permeation. However, not only the mechanisms of deposit formation on the membrane surface will influence the filtration performance, but other factors such as pore blocking also play a role (Table 3.3).

In the initial phase of the filtration, the change in the deposit height is at its maximum because the adventive transport of proteins towards the membrane decrease with filtration time. This is in accordance with Piry et al. (2012) who reported a less intensive and less compact deposit layer formation when filtrating with membranes with increased membrane resistance due to the reduced drag forces towards to the membrane. After the initial phase when already some proteins are deposited on the membrane surface, the pressure influence on the deposit layer height is more pronounced (Figure 3.6 and Figure 3.7). The deposit layer thicknesses were approximately similar for the investigated pressures, but higher protein concentration on membrane surface could be analyzed by an increased pressure (Figure 3.7 d). This can be attributed to a more compact layer with a similar height, the compression of the deposit layer at high pressures, and the change in the internal structure to a gel layer (Qu et al. 2012; 2015). Directly at the membrane surface, the signal intensity gained by MRI is shifted towards lower values for higher filtration pressures (Figure 3.8). This also indicates that the deposition becomes more compact.

The investigation could not directly be transferred to the crossflow filtration since the deposit layer height is significantly reduced by the deposit removal forces so that it was not possible to image deposit layer height via NMR. However, the composition of the deposit layer on the membrane surface during crossflow filtration and its pressure-dependency could be analyzed. For this purpose, Figure 8.1 shows the deposited amount of whey proteins, caseins and the resulting total protein amount related to 1 m^2 of membrane surface plotted against Δp_{TM}.

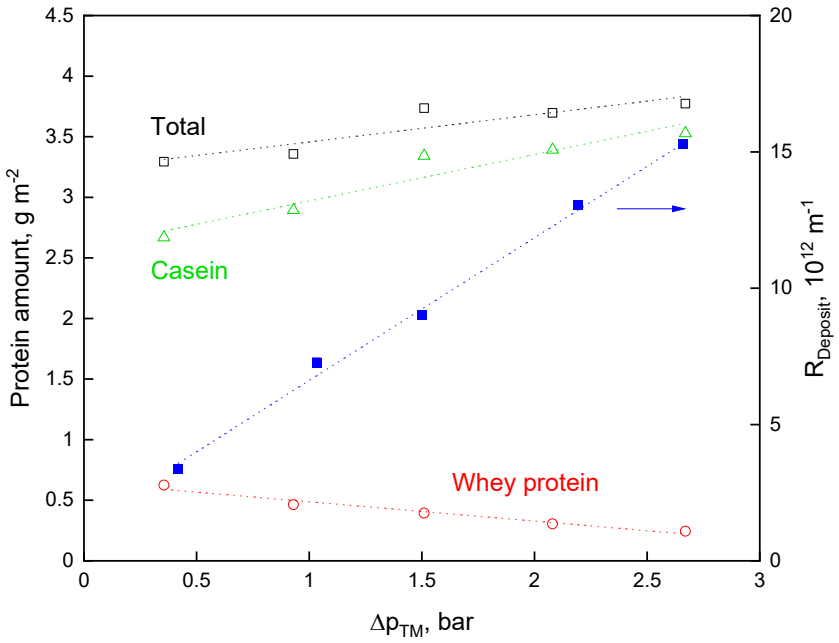

Figure 8.1: Total protein (□), casein (△), and whey protein (○) amount per 1 m^2 as a function of the transmembrane pressure in correlation to the deposit layer resistance (■) at a pressure drop of 1.9 bar m^{-1} and a filtration temperature of 10 °C.

Increasing Δp_{TM} leads to an increase in the total protein amount on the membrane surface and an increase in deposit layer resistance. Taking a closer look into the composition of the deposited proteins it is obvious that the amount of casein deposit on membrane surface increases. In contrast, the amount of whey proteins decreased upon increasing pressure. It is clear that first, the formation of the deposit layer is predominantly due to caseins, and second, that the caseins cause the increase in deposit layer resistance.

Steinhauer (2016) showed that when whey proteins are incorporated into casein deposit layers, the casein micelles become more compact due to the binding of whey proteins by thiol-disulfide reactions at the micelle surface. At the same time, these casein whey protein clusters form a more porous structure and thus exhibit lower deposit layer resistance compared to pure casein deposit layers. Furthermore, it can be seen in Figure 8.1 that at a Δp_{TM} of 1.5 bar, there is only a slight increase in the protein amount. However, an increase in the deposit layer resistance was observed at the same time. This indicates that an increase in Δp_{TM} leads to a compaction of the deposit layer as it could be shown during dead-end filtration (Figure 3.7). The composition and structure of the deposit layer indicate a strong dependence on the Δp_{TM}. However, Δp_{TM} strongly depends on the length of the membrane (Hartinger, 2021).

8.1.2 Optimization of the filtration conditions for milk protein fractionation with HFM

The optimization of the milk protein fractionation was performed with the following filtration parameters: Length-dependency of the hollow fibers, Δp_{TM}, Δp_L, feed volume flow, crossflow velocity, and CF. Schopf et al. (2021b; 2021a; 2021) showed that a high mass flow and thus an optimal efficient milk protein fractionation in HFM can be reached by combining high flux and high transmission at low Δp_{TM} (e.g., Figure 4.11). At low Δp_{TM}, the fouling resistance is low and this leads to a less intensive deposit layer (Piry, 2011). This is also shown in Figure 6.4, at all CF levels, low Δp_{TM} enables high whey protein mass flow. The higher protein concentration leads to enhanced deposit layer formation by the retained casein micelles on the membrane surface (Ng et al., 2017) and increased filtration resistance (Beckman and Barbano, 2013).

However, Schopf and Kulozik (2021) reported that an increasing CF has no significant influence on whey protein transmission (Figure 6.3). Thus, the porosity of the deposit layer was considered to not significantly decrease at higher CF. The lower flux values at high CF (Figure 6.2) are caused by a strong increase of deposit layer height due to an increase in the amount of deposited protein. Bouchoux et al. (2010) described that the deposit layer consists out of compressible casein micelles changed above the critical Δp_{TM} its structure. This leads to an increase in the deposit layer resistance, a decrease in the permeability of the deposit layer, and thus, in a decrease in whey protein mass flow. These effects occur in all membrane systems (Schopf et al., 2021b). However, especially for CTM, the control of Δp_{TM} has a high impact on the deposit layer formation and structure influencing whey protein transmission due to the different back pressure on the permeate side of the flow channels dependent on their position in the CTM module (Schopf et al., 2022).

However, Δp_{TM} strongly depends on the membrane length (Figure 4.3). Therefore, in Chapter 4.3.1, a new method was investigated to measure and to access the length-depended effects in HFM. The approaches from CTM and SWM, which divide the modules on the permeate side to collect the permeate of each section selectively, could not be easily adapted to HFM modules. Cutting the HFM module, like it was done for CTM (Piry, 2011), would result in loose ends of the fibers. Gluing the sections on permeate side, like it was done in SWM (Hartinger, 2021), cannot be realized because of the low accessibility of the fiber bundle on the permeate side. However, HFM modules provide the advantage to be produced more flexibly in terms of module length than SWM and CTM. Therefore, Schopf et al. (2021a) constructed and connected HFM with 0.3 m each were in series of 1 – 4 units and modules with different lengths of 0.3, 0.6, 0.9, and 1.2 m (Figure 4.1). They could show that the optimal fiber length was at 0.6 m to ensure low Δp_{TM} because longer fibers cause a high Δp_L (Figure 4.3) and therefore

cannot be operated at low Δp_{TM}, if the entire membrane module is to filter in the optimal range (Figure 4.6). The length-dependent Δp_L is responsible for inhomogeneous fouling along the HFM (Schopf et al., 2021a).

Furthermore, Schopf et al. (2021a) showed that the higher the crossflow velocities, the higher was the minimally adjustable Δp_{TM}. Thus, it is not possible to operate longer HFM under membrane-controlled conditions, which will lead to a higher deposit layer resistance and its negative effect on the whey protein mass flow, as discussed above. In reverse, shorter fibers provide the option to be used by higher crossflow velocities, higher feed volume flow, low Δp_L, and low Δp_{TM} at the same time (Figure 4.3). Thus, the deposit layer formation can be better controlled and high flux and high transmission can be achieved.

This plays a main role during the concentration of skim milk MF. There are two suitable options for the concentration process: to run the process with constant Δp_L or with constant feed volume flow. With increasing CF, the viscosity increase, and thus the Δp_L, will increase or the feed volume flow will decrease. HFM provides the option to be run by high Δp_L in contrast to SWM due to fewer friction effects and free cross-sections (Schopf et al., 2021b). When concentrating at constant feed volume flow, the deposit layer is less pronounced at higher CF compared to a concentration with constant Δp_L due to higher deposit removal forces (Figure 6.5). But the minimally adjustable Δp_{TM} will also increase as the Δp_L increases. As a consequence, higher Δp_{TM} leads to a more compact deposit layer with a higher retention effect. Thus, transmission decrease (Figure 6.6) and whey protein mass flow do not significantly differ when comparing both concentration processes (Figure 6.7).

Comparing the findings of the influence of Δp_{TM} and Δp_L leads to the conclusion that the whey protein transmission is influenced mainly by the structure and the compaction of the deposit layer, which is affected by the Δp_{TM}, and not by the feed protein concentration, i.e., the CF, and the amount of deposited proteins (Schopf and Kulozik, 2021). Higher crossflow velocities and higher Δp_L levels will not lead to an increase in whey protein transmission in HFM (Figure 5.3). This confirms the findings of Hartinger et al. (2020c; 2020) for SWM that high CF or less cross flow velocity leads to a thicker deposit layer but no changes in terms of deposit layer porosity and in terms of narrowing of the deposit layer flow channels.

8.2 Comparison of industrial membrane modules concerning their fractionation task

Based on the insights in fouling discussed above, the same effects on deposit layer formation are reported on HFM as they occur on CTM and SWM. However, HFM provides the advantages of first a better deposit layer control due to free cross-sections and less Δp_L like CTM and second a high packing density as SWM.

8.2.1 Comparison of open flow paths of tubular membranes with spacer-filled flow path of SWM regarding deposit layer formation

In contrast to SWM, HFM, like CTM, possess free cross-sections, which allows HFM to be operated at high crossflow velocities and low Δp_L. Schopf et al. (2021b; 2021) reported that the variation of local pressure and flow conditions has a higher impact on whey protein mass flow per module of HFM, resulting in a higher fractionation efficiency when compared to CTM and SWM. Table 5.5 shows that HFM has a higher mass flow compared to SWM, although they are compared at low crossflow velocities. Schopf et al. (2021b) demonstrated that this is an option to achieve a high output of whey protein mass flow at low volume flow and low Δp_{TM} and thus low energy input.

Higher crossflow velocity leads to an effective erosion of the deposit layer due to higher deposit removal forces resulting in a higher flux, higher mass flow, but, as described above, transmission is independent of the crossflow velocity. Especially during pre-concentration and along the entire DF process, effective control of the deposit layer due to free cross flow sections can reduce the overall filtration effort in terms of filtration time, the amount of DF medium, and the number of required DF steps. Schopf and Kulozik (2021) reported that the optimal pre-CF in HFM is 2.5 compared to SWM and CTM with CF 1.7 (Hartinger and Kulozik, 2020) and CF 2 (Reitmaier et al., 2017; Heidebrecht and Kulozik, 2019), respectively. They showed that HFM can be operated at concentration levels 47% and 25% higher than those for SWM and CTM systems, respectively, which would result in DF volume reductions of 19% or 10%, respectively.

Taking these findings into consideration it can be concluded that open flow cross-sections of the fibers lead to better control of the deposit layer than the spacer-filled flow channels in SWM. Consequently, the question that arose from that was, how HFM perform if they also were equipped with flow breakers inducing turbulence such as spacers in SWM, but are superior in terms of specific flux and open cross-sections. As discussed in Chapter 1.4.3 options to influence the feed flow behavior in HFM are a helically shaped, rod-like structure at the membrane surface (Broussous et al., 2000), or a helically shaped baffle (Horie et al., 2018).

Wiese et al. (2019) reported that they polymerized a helix at the inner surface of a HFM as a flow breaker to increase turbulence inside the fibers. Schork et al. (2021) could visualize deposit layer formation of a helical ridge of HFM during crossflow filtration by compressed sensing MRI. However, the increased shear rate on the deposit layer and its abrasive effects along the helical ridge could not be explained. Therefore, flux and deposit layer formation was investigated in polymer UF tubular membranes during skim milk UF (Figure 8.2). UF membranes provide the advantage of a more intensive deposit layer on the membrane compared to MF membranes where the inner pore blocking is expected to be more pronounced.

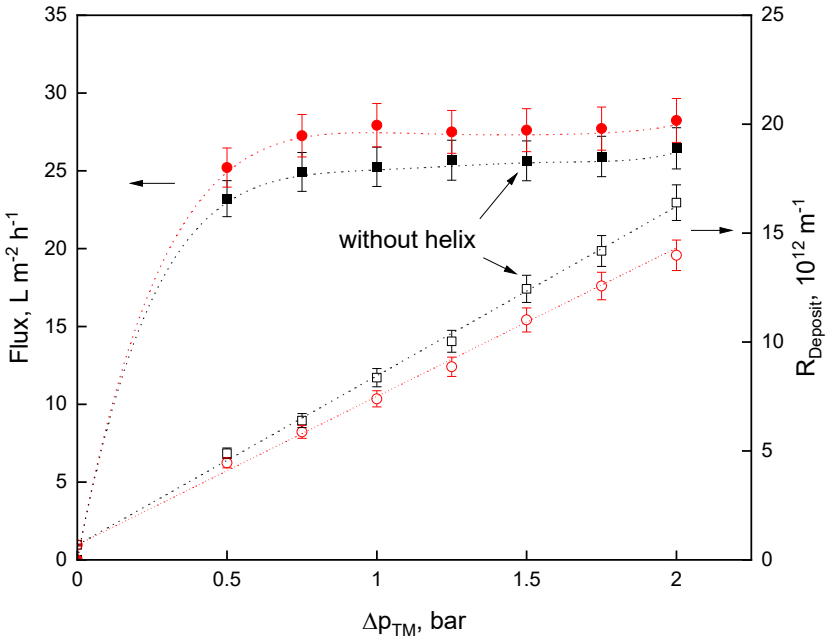

Figure 8.2. Flux (closed symbols) and deposit layer resistance (empty symbols) as a function of the transmembrane pressure for UF membranes without (■) and with (●) a helix polymerized in the inner side of the fibers at a temperature of 10 °C and a mean crossflow velocity of 2.3 m s^{-1}.

As expected, Figure 8.2 shows higher flux values for the helically shaped membranes. Turbulent flows prevail in both membranes since the Reynolds number was higher than 2,300. It can be assumed that the helix serves as a flow breaker on the inside of the fibers and thus counteracts the formation of the deposit layer and reduces fouling. Furthermore, it is interesting to see that with increasing Δp_{TM}, the difference in fouling resistance increases. It can be assumed that at high Δp_{TM}, a more intensive deposit layer is formed. If in this case turbulence is generated by flow breakers, this will have a high mitigating effect on the intensity of the deposit layer formation.

These findings were obtained from studies on UF tubular membranes. It can be assumed that the same effects will also be seen in MF tubular membranes, and that turbulence promoters will also have a decisive influence on whey protein transmission

in MF due to a lower intensity of deposit layer formation and thus higher whey protein transmission. Concluding that milk protein fractionation can be optimized by the use of MF HFM at the optima process parameters and if helix structures are used as flow barkers to increase the effective control of deposit layer formation.

8.2.2 Influence of backpressure in multichannel CTM compared to a bundle of HFM

Compared to CTM, HFM modules have a higher packing density at the same module footprint (Table 5.2) leading to a higher whey protein mass flow per module. But, CTM have also free cross-sections and so, there should be also effective control of deposit layer formation. Moreover, the channel diameter of CTM could also be reduced to reach a higher packing density, which should provide a better filtration performance per module. Therefore, the open question is, how does the increase in channel number, the reduction of channel diameter, and the increase in packing density affect deposit layer formation in CTM, and how does this differ from the deposit layer formation in HFM.

For the first point, Schopf et al. (2022) reported, based on the findings of Ghidossi et al. (2010), that multichannel CTM have different back pressures on the permeate side depending on their individual position of each tubular channel in the CTM module. This has an influence on the deposit layer formation (Figure 7.9) and thus on flux (Figure 7.7) and transmission (Figure 7.10). The specific flux per square meter of the membrane should not be affected by an increase in the membrane area. However, Schopf et al. (2022) reported that the inner channels contribute less to the total flux than the outer channels as a result of the back pressure on the permeate side (Ghidossi et al., 2010), which will influence deposit layer formation dependent on the channel position. Thus, whey protein transmission is also influenced by the channel position and the corresponding local Δp_{TM}. At high Δp_{TM}, the deposit layer will be less compact in the inner channels which lead to an increase in whey protein transmission (Figure 7.10). , Schopf et al. (2022) experimentally confirmed that multi-channel membranes with a high number of inner channels have transmission values higher than those of membranes with only a single inner channel related to the same module volume due to the different transmembrane pressure levels of the channels.

It was, however, not investigated whether these effects would also occur in HFM modules. This must be particularly taken into account since HFM modules are not only comprised of several thousand, densely packed fibers per module, bundled together. To investigate if different backpressures on permeate side would occur in HFM dependent on the fiber number, flux and whey protein transmission was plotted against the Δp_{TM} for HFM with ten compared to 2,000 fibers (Figure 8.3).

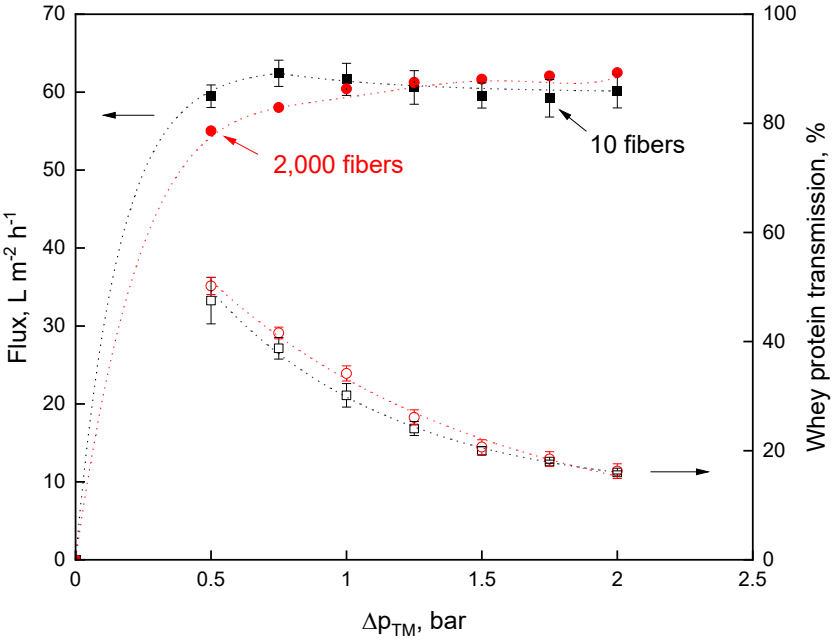

Figure 8.3. Flux (closed symbols) and whey protein transmission (open symbols) as a function of the transmembrane pressure for HFM with ten (■) compared to 2,000 fibers (●) at a temperature of 55 °C and a pressure drop of 1.3 bar m^{-1}.

The flux, as well as the whey protein transmission, of the modules with ten or 2,000 fibers did not significantly differ ($P < 0.1$). Thus, it is assumed that no different backpressures on permeate side would occur in HFM modules so that there is no difference in deposit layer formation depending on the position of the fiber in the HFM module. All fibers are washed around with permeate. Only the different pathways of the permeate flow in the supporting layer in CTM are responsible for the differences in backpressure.

In conclusion, fibers in large HFM modules do not differ in terms of backpressure and Δp_{TM}. Thus, could be directly controlled by the permeate pressure. Therefore, the structure and the formation of the deposit layer could be effectively controlled due to the open cross-sections and due to homogeneous backpressure on the permeate side. Nevertheless, Δp_{TM} will be affected by the length-dependency as discussed above.

8.3 Conclusions for an optimized industrial filtration plant equipped with HFM

As reported low Δp_{TM}, shorter modules, optimal CF, and high crossflow velocities lead to an optimized milk protein fractionation in SWM, CTM, and HFM. An increase in crossflow velocities and also an increase in module length will lead to an increase in Δp_L which increases the minimal adjustable Δp_{TM} increasing fouling and reducing protein mass flow (Schopf et al., 2021a). It can be concluded that an effective Δp_{TM} control will lead to an optimized milk protein fractionation. One option for an optimized industrial filtration plant equipped with HFM would be to use HFM modules with reduced fiber length to guaranty high crossflow velocity at low Δp_L reaching low Δp_{TM} values. Thereby, the whole membrane length could be operated at optimal conditions and the deposit layer formation could be effectively controlled. Another option is to reduce the number of modules per housing to decrease length-depended effects.

However, SWM, CTM, and HFM are used at different crossflow velocities owing to their individual permissible Δp_L (Schopf et al., 2021b). Naturally, a higher crossflow velocity requires a higher feed volume flow and thus a higher energy input by the pumps (Schopf and Kulozik, 2021). This is the main point at a filtration at low temperatures, e.g., 10 °C, where cooling requirements have to be considered when comparing the use of SWM and HFM. The best selection of the used membrane system has to be based on an economical balancing of energy consumption, manufacturing and maintenance costs, and filtration performance.

Based on the data of this thesis on a more effective deposit control, one has to conclude that HFM, which are less often applied in the dairy industry for milk protein fractionation, seem to be a suitable alternative to the more established SWM or CTM. Depending on actual and future HFM developments regarding maximization of membrane packing density, the use of flow breakers inside of the fibers, and a smaller width of the membrane pore size distribution, the advantages of HFM could become even higher.

Another option for an optimized industrial filtration plant would be to use different membrane systems regarding their filtration tasks dependent on the stage where the module is used (Figure 1.20) for protein concentration and protein fractionation in separate stages. However, these concepts have to be investigated and validated under local conditions in industrial filtration plants.

9 Summary & Zusammenfassung

9.1 Summary

In pressure-driven separation and concentration processes for biopolymers filtration, fouling is a key issue reducing the membrane performance in terms of flux, protein transmission, and mass transport through the membrane along the module. The objective of this study was to investigate the phenomenon of fouling by retained proteins during milk protein fractionation under varying process conditions as well as the characterization of the amount, composition, and structure of the length-dependent deposit layer.

Hollow fiber membranes as an alternative membrane system were compared to SWM and CTM. HFM, like CTM, are characterized by open cross-sections and, thus, by a lower length-dependent Δp_L, and a high packing density like SWM. The hypothesis was that the local pressure and flow conditions in HFM result in a higher flux and transmission, resulting in a higher fractionation efficiency when compared to CTM and SWM.

The focus of this work was to investigate the formation and structure of the deposit layer under different process conditions to optimize milk protein fractionation by the effective control of deposit layer formation.

The deposited layer height and density were visualized by an *in situ*, non-invasive, and non-destructive measurement method based on MRI technology. It turned out, however, that the resolution capability of MRI was insufficient to determine deposited layer height and structure under crossflow conditions. Nevertheless, insights on the potential and limitations of this technology could be assessed under dead-end filtration conditions, where the deposited layer was sufficiently thick.

During crossflow filtration, length-dependent effects will occur in all membrane systems having a high impact on the filtration performance as well as on deposit layer structure and formation. However, spatial effects on the skim milk filtration in HFM had not been investigated so far. Compared to CTM and SWM, the pressure and flow conditions in HFM are different. To measure and access the length-dependent effects in HFM, a new module construction was required.

Different lengths of HFM modules were produced to investigate the impact of Δp_L on flux, whey protein transmission, and deposit layer formation along the flow path. Δp_{TM} and feed volume flow rate were varied to identify the optimal process conditions in terms of Δp_{TM}, Δp_L, crossflow velocity, flux, whey protein transmission, and module length. The sectioning of a 1.2 m HFM module length was carried out by four modules in series, each 30 cm long.

The rear part of the module, the last two sections, was identified as the one with the best performance in terms of highest whey protein mass flow to low Δp_{TM}. The longer the fibers the higher Δp_L; the shorter the fibers the higher the feed flow for reducing deposit layer formation. A Δp_{TM} of 0.5 bar and a membrane length of 0.6 m were identified as the best conditions to achieve the highest whey protein transmission.

Based on these insights, a scale-up of the results was performed by applying industrially sized standard modules for a comparative assessment of HFM, CTM, and SWM module systems, all with the same spatial module footprint (i.e., diameter and length). The Δp_{TM} was varied as part of two concepts, i.e., at a constant feed volume flow rate of 20 $m^3\ h^{-1}$ and a constant Δp_L of 1.3 bar m^{-1}. Flux, whey protein transmission, whey protein mass flow, and the casein-to-whey protein ratio in the permeate were analyzed as assessment criteria. HFM turned out to be superior compared to CTM and SWM under pilot plant conditions, which appears as an attractive starting point for validation of these results at an industrial level.

Based on these findings, optimal process conditions were determined for the preconcentration and the DF process. Δp_L and Δp_{TM} were varied to investigate the effect of an increased feed protein concentration on the deposit layer formation. Two filtration protocols were compared with flux, transmission, whey protein mass flow, and the time required for one DF step as criteria: concentration with the same Δp_L for all module types was compared to concentration with the same feed volume flow. The optimal process conditions are determined at a Δp_{TM} of 0.5 bar, a Δp_L of 1.0 bar m^{-1}, and a CF of 2.5. It could be shown that at CF 3, already 80% of the whey protein could be depleted after 2.5 DF steps. Due to the effective control of deposit layer formation, HFM can be operated at concentration levels 47% and 25% higher than those for SWM and CTM systems, respectively.

As part of the study, CTM with 1-, 7-, 19-, and 37-channels with the same outer diameter were investigated in order to assess the impact of channel number on flux and whey protein transmission. A higher number of channels led to higher permeate volume flow and higher whey protein transmission due to the lower deposit formation intensity on the surfaces of the inner channels. Especially at high Δp_{TM}, a significantly higher whey protein transmission could be determined in CTM with a high channel number, which can be explained by higher back pressure on the permeate side of the inner channels, reducing the transport of proteins towards the membrane surface. This resulted in a less pronounced deposit layer formation, which, in turn, reduces the retention effect of the deposit layer and increases whey protein transmission. As a consequence, at high Δp_{TM}, the 37-channel membrane performed superior in terms of specific flux and whey protein transmission compared to membranes with less channel number due to less deposit layer formation in the inner channels.

9.2 Zusammenfassung

Bei druckgetriebenen Trenn- und Konzentrationsprozessen wie die Filtration von Biopolymeren ist Fouling ein zentrales Problem, welche die Membranleistung in Bezug auf Durchfluss, Proteintransmission und Stofftransport über die Membran verringert. Das Phänomen des Foulings ist jedoch noch nicht vollständig verstanden. Ziel der Arbeit war, das Phänomen des Foulings durch zurückgehaltene Proteine bei der Milchproteinfraktionierung hinsichtlich der Deckschichtbildung unter verschiedenen Prozessbedingungen zu untersuchen sowie die Struktur der längenabhängigen Deckschicht in Korrelation zur Zusammensetzung und Menge der abgelagerten Proteine zu charakterisieren.

Zur Feststellung der Trennleistung und zur effektiven Kontrolle der Deckschicht wurden HFM als alternatives Membransystem im Vergleich zu SWM und CTM zur Milchproteintrennung eingesetzt. HFM bieten die Vorteile einer besseren Deckschichtkontrolle durch freie Strömungsquerschnitte bei geringem Δp_L, wie es bei CTM der Fall ist, und eine hohe Packungsdichte wie bei SWM. Daher lautet die Hypothese, dass die Variation der lokalen Druck- und Strömungsbedingungen in HFM einen größeren Einfluss auf den Flux und die Transmission haben als CTM und SWM, was zu einer höheren Fraktionierungseffizienz führen sollte.

Der Schwerpunkt dieser Arbeit lag auf der Untersuchung der Bildung und Untersuchung der Struktur der Deckschicht unter verschiedenen Prozessbedingungen, um die Milchproteinfraktionierung durch die effektive Steuerung der Deckschichtbildung zu optimieren, die dann auf alle Membransysteme angewendet werden kann.

Um die gebildete Deckschichthöhe und -dichte auf HFM in Abhängigkeit von Filtrationsdruck und -temperatur zu visualisieren, wurde eine *in situ*, nicht-invasive und zerstörungsfreie Messmethode auf Basis der MRT angewandt. Wie sich jedoch herausstellte, war die Auflösungsfähigkeit der MRT Technik unzureichend, um die Deckschichthöhe bzw. –struktur unter crossflow-Bedingungen zu bestimmen. Nichtsdestoweniger konnten Erkenntnisse zum Potential und den Limitationen der MRT-Technik unter dead-end Filtrationsbedingungen ermittelt werden.

Bei der Querstromfiltration treten in allen Membransystemen längenabhängige Effekte auf, die einen großen Einfluss auf die Filtrationsleistung sowie auf die Deckschichtstruktur und -bildung haben. Diese Effekte wurden aber bei der Filtration von Magermilch mittels HFM jedoch noch nicht untersucht wurden. Um die längenabhängigen Effekte in HFM bestimmen zu können, wurde analog zu CTM eine Reihenschaltung von 30 cm Modulen entwickelt, deren Gesamtlänge einem industrieüblichen Modul von 1,2 m entspricht.

Es wurden verschieden lange HFM-Module hergestellt, um die Variation von Δp_L auf den Flux, die Molkenproteintransmission und die Deckschichtbildung zu untersuchen. Δp_{TM} und der Feed-Volumenstrom wurden variiert, um die optimalen Prozessbedingungen in Bezug auf Δp_{TM}, Δp_L, und Modullänge zu ermitteln. Die letzten beiden Segmenten wurden als diejenigen mit der besten Leistung in Bezug auf den höchsten Molkenprotein-Massenstrom bei gleichzeitig niedrigstem Δp_{TM} ermittelt. Es konnten ein Δp_{TM} von 0,5 bar und einer Membranlänge von 0,6 m als das Optimum im Hinblick auf die höchste Molkenproteintransmission identifiziert werden.

Für die Bewertung von kommerziellen HFM-, CTM- und SWM-Modulsystemen wurden Standardmodule in Industriegröße verwendet. Die Module haben die gleichen Abmessungen in Bezug auf die Modulgrundgrößen wie Durchmesser und Länge. Der Δp_{TM} wurde zum einen bei einem konstanten Feed-Volumenstrom von 20 $m^3\ h^{-1}$ und zum anderen bei einem konstanten Δp_L von 1,3 bar m^{-1} variiert. Flux, Molkenproteintransmission und Molkenproteinmassenstrom wurden analysiert und mit der Packungsdichte der Module korreliert. Außerdem wurde das Verhältnis von Kasein zu Molkenprotein berechnet, um ein Bewertungskriterium für die Effizienz der Fraktionierung zu erhalten.

Mit zunehmender Membranfläche pro Modul konnte eine effektivere Fraktionierung erzielt werden. Je niedriger der Δp_L, desto höher die mögliche Überströmgeschwindigkeit und desto besser konnte die Deckschichtbildung kontrolliert werden. Je niedriger Δp_{TM}, desto weniger intensiv und poröser war die Ablagerungsschicht. HFM-Module erlauben eine hohe Querströmungsgeschwindigkeit bei gleichzeitig niedrigem Δp_L. Darüber hinaus bietet HFM eine höhere Packungsdichte, was im Vergleich zu CTM zu einem höheren Molkenproteinmassenstrom pro Modul führt.

Auf Grundlage dieser Erkenntnisse wurden für die Vorkonzentration und den DF-Prozess optimale Prozessbedingungen für ein kommerziell erhältliches Industriemodul ermittelt. Δp_L und Δp_{TM} wurden variiert, um die Auswirkungen einer erhöhten Feed-Proteinkonzentration auf die Deckschichtbildung und -struktur aufzuklären. Zwei Arten von Filtrationsprotokollen für die Vorkonzentrierung in Bezug auf Flux, die Transmission, den Molkenproteinmassenstrom und die Zeit, die erforderlich ist, um einen DF-Schritt zu erhalten, wurden verglichen: eine Konzentrierung mit konstantem Δp_L im Vergleich zu einer Konzentrierung mit konstantem Feed-Volumenstrom. Die optimalen Prozessbedingungen wurden bei einem Δp_{TM} von 0,5 bar, einem Δp_L von 1,0 bar m^{-1} und einem CF von 2,5 ermittelt. Bereits beim Vorkonzentrieren auf CF 3 konnten 80 % des Molkenproteins nach 2,5 DF-Schritten abgereichert werden konnten. Aufgrund der effektiveren Kontrolle der Deckschichtbildung können HFM mit Proteinkonzentrationen betrieben werden, die 47 % bzw. 25 % höher sind als bei SWM und CTM.

Als Teil dieser Arbeit wurden CTM mit 1-, 7-, 19- und 37-Kanälen mit demselben Modulaußenvolumen verglichen, um den Einfluss der Kanalanzahl und des Kanaldurchmessers auf Flux und Transmission zu ermitteln. Je höher die Kanalanzahl, desto höher der Flux und die Molkenproteinpermeation, weil die inneren Kanäle wegen des längeren Fließweges einen höheren permeatseitigen Gegendruck erfahren. Insbesondere bei hohem Δp_{TM} konnte eine signifikant höhere Molkenproteintransmission in CTM mit hoher Kanalzahl festgestellt werden. Die inneren Kanäle tragen demnach mehr zur Gesamttransmission bei als die äußeren Kanäle.

10 References

Adams, M.C., Barbano, D.M., 2013. Serum protein removal from skim milk with a 3-stage, 3× ceramic Isoflux membrane process at 50°C. Journal of Dairy Science 96 (4), 2020–2034. 10.3168/jds.2012-6007.

Adams, M.C., Barbano, D.M., 2016. Effect of ceramic membrane channel diameter on limiting retentate protein concentration during skim milk microfiltration. Journal of Dairy Science 99 (1), 167–182. 10.3168/jds.2015-9897.

Adams, M.C., Hurt, E.E., Barbano, D.M., 2015a. Effect of ceramic membrane channel geometry and uniform transmembrane pressure on limiting flux and serum protein removal during skim milk microfiltration. Journal of Dairy Science 98 (11), 7527–7543. 10.3168/jds.2015-9753.

Adams, M.C., Hurt, E.E., Barbano, D.M., 2015b. Effect of soluble calcium and lactose on limiting flux and serum protein removal during skim milk microfiltration. Journal of Dairy Science 98 (11), 7483–7497. 10.3168/jds.2015-9474.

Airey, D., Yao, S., Wu, J., Chen, V., Fane, A., Pope, J., 1998. An investigation of concentration polarization phenomena in membrane filtration of colloidal silica suspensions by NMR micro-imaging. Journal of Membrane Science 145 (2), 145–158. 10.1016/S0376-7388(98)00051-9.

Akhondi, E., Zamani, F., Tng, K., Leslie, G., Krantz, W., Fane, A., Chew, J., 2017. The Performance and Fouling Control of Submerged Hollow Fiber (HF) Systems: A Review. Applied Sciences 7 (8), 765. 10.3390/app7080765.

Ali, A., Quist-Jensen, C.A., Macedonio, F., Drioli, E., 2016. Optimization of module length for continuous direct contact membrane distillation process. Chemical Engineering and Processing: Process Intensification 110, 188–200. 10.1016/j.cep.2016.10.014.

Andrews, A.T., Varley, J.R., 1994. Biochemistry of Milk Products, 1st ed. Elsevier Reference Monographs, s.l.

Armbruster, S., Cheong, O., Lölsberg, J., Popovic, S., Yüce, S., Wessling, M., 2018. Fouling mitigation in tubular membranes by 3D-printed turbulence promoters. Journal of Membrane Science 554, 156–163. 10.1016/j.memsci.2018.02.015.

Arndt, F., Heidebrecht, H.-J., Schork, N., Schuhmann, S., Kulozik, U., Schütz, S., Nirschl, H., Guthausen, G., 2016a. Deposit layer formation during skim milk dead-end filtration with ceramic hollow fiber membranes using magnetic resonance imaging, in: , Proceedings of the XIII International Conference on the Applications of Magnetic Resonance in Food Science. IM Publications, p. 55–55.

Arndt, F., Roth, U., Nirschl, H., Schütz, S., Guthausen, G., 2016b. New insights into sodium alginate fouling of ceramic hollow fiber membranes by NMR imaging. AIChE Journal 62 (7), 2459–2467. 10.1002/aic.15226.

Arndt, F., Schuhmann, S., Guthausen, G., Schütz, S., Nirschl, H., 2017. In situ MRI of alginate fouling and flow in ceramic hollow fiber membranes. Journal of Membrane Science 524, 691–699. 10.1016/j.memsci.2016.11.079.

Astudillo-Castro, C., Cordova, A., Oyanedel-Craver, V., Soto-Maldonado, C., Valencia, P., Henriquez, P., Jimenez-Flores, R., 2020. Prediction of the Limiting Flux and Its Correlation with the Reynolds Number during the Microfiltration of Skim Milk Using an Improved Model. Foods 9 (11). 10.3390/foods9111621.

Astudillo-Castro, C.L., 2015. Limiting Flux and Critical Transmembrane Pressure Determination Using an Exponential Model: The Effect of Concentration Factor, Temperature, and Cross-Flow Velocity during Casein Micelle Concentration by Microfiltration. Ind. Eng. Chem. Res. 54 (1), 414–425. 10.1021/ie5033292.

Bacchin, P., 2004. A possible link between critical and limiting flux for colloidal systems: consideration of critical deposit formation along a membrane. Journal of Membrane Science 228 (2), 237–241. 10.1016/j.memsci.2003.10.012.

Bacchin, P., Aimar, P., Field, R., 2006. Critical and sustainable fluxes: Theory, experiments and applications. Journal of Membrane Science 281 (1-2), 42–69. 10.1016/j.memsci.2006.04.014.

Bacchin, P., Si-Hassen, D., Starov, V., Clifton, M., Aimar, P., 2002. A unifying model for concentration polarization, gel-layer formation and particle deposition in cross-flow membrane filtration of colloidal suspensions. Chemical Engineering Science 57 (1), 77–91. 10.1016/S0009-2509(01)00316-5.

Baker, R.W., 2008. Membrane technology and applications, 2nd ed. Wiley, Chichester, United Kingdom.

Bannwarth, S., Trieu, T., Oberschelp, C., Wessling, M., 2016. On-line monitoring of cake layer structure during fouling on porous membranes by in situ electrical impedance analysis. Journal of Membrane Science 503, 188–198. 10.1016/j.memsci.2016.01.009.

Baruah, G.L., Belfort, G., 2003. A predictive aggregate transport model for microfiltration of combined macromolecular solutions and poly-disperse suspensions: model development. Biotechnology progress 19 (5), 1524–1532. 10.1021/bp030009f.

Baruah, G.L., Nayak, A., Belfort, G., 2006. Scale-up from laboratory microfiltration to a ceramic pilot plant: Design and performance. Journal of Membrane Science 274 (1-2), 56–63. 10.1016/j.memsci.2005.07.046.

Basheer, C., Lee, H.K., 2004. Hollow fiber membrane-protected solid-phase microextraction of triazine herbicides in bovine milk and sewage sludge samples. Journal of chromatography. A 1047 (2), 189–194. 10.1016/j.chroma.2004.06.130.

Baum, B., Holley, W., White, R.A., 1976. Hollow Fibres in Reverse Osmosis, Dialysis, and Ultrafiltration. Membrane Separation Processes, 187–228.

Beckman, S.L., Barbano, D.M., 2013. Effect of microfiltration concentration factor on serum protein removal from skim milk using spiral-wound polymeric membranes. Journal of Dairy Science 96 (10), 6199–6212. 10.3168/jds.2013-6655.

Beckman, S.L., Zulewska, J., Newbold, M., Barbano, D.M., 2010. Production efficiency of micellar casein concentrate using polymeric spiral-wound microfiltration membranes. Journal of Dairy Science 93 (10), 4506–4517. 10.3168/jds.2010-3261.

Belitz, H.-D., Grosch, W., Schieberle, P., 2008. Lehrbuch der Lebensmittelchemie: Mit 634 Tabellen, 6th ed. Springer, Berlin.

Bienvenue, A., Jiménez-Flores, R., Singh, H., 2003. Rheological Properties of Concentrated Skim Milk: Importance of Soluble Minerals in the Changes in Viscosity During Storage. Journal of Dairy Science 86 (12), 3813–3821. 10.3168/jds.S0022-0302(03)73988-5.

Bolton, G.R., Apostolidis, A.J., 2017. Mechanistic modeling of the loss of protein sieving due to internal and external fouling of microfilters. Biotechnology progress 33 (5), 1323–1333. 10.1002/btpr.2514.

Bonizzi, I., Buffoni, J.N., Feligini, M., 2009. Quantification of bovine casein fractions by direct chromatographic analysis of milk. Approaching the application to a real production context. Journal of Chromatography A 1216 (1), 165–168. 10.1016/j.chroma.2008.11.045.

Bottino, A., Capannelli, G., Grosso, A., Monticelli, O., Cavalleri, O., Rolandi, R., Soria, R., 1994. Surface characterization of ceramic membranes by atomic force microscopy. Journal of Membrane Science 95 (3), 289–296. 10.1016/0376-7388(94)00132-4.

Bouchoux, A., Cayemitte, P.-E., Jardin, J., Gésan-Guiziou, G., Cabane, B., 2009a. Casein micelle dispersions under osmotic stress. Biophysical journal 96 (2), 693–706. 10.1016/j.bpj.2008.10.006.

Bouchoux, A., Debbou, B., Gésan-Guiziou, G., Famelart, M.-H., Doublier, J.-L., Cabane, B., 2009b. Rheology and phase behavior of dense casein micelle dispersions. The Journal of chemical physics 131 (16), 165106. 10.1063/1.3245956.

Bouchoux, A., Gésan-Guiziou, G., Pérez, J., Cabane, B., 2010. How to squeeze a sponge: casein micelles under osmotic stress, a SAXS study. Biophysical journal 99 (11), 3754–3762. 10.1016/j.bpj.2010.10.019.

Bouchoux, A., Qu, P., Bacchin, P., Gésan-Guiziou, G., 2014. A general approach for predicting the filtration of soft and permeable colloids: the milk example. Langmuir : the ACS journal of surfaces and colloids 30 (1), 22–34. 10.1021/la402865p.

Broussous, L., Schmitz, P., Boisson, H., Prouzet, E., Larbot, A., 2000. Hydrodynamic aspects of filtration antifouling by helically corrugated membranes. Chemical Engineering Science 55 (21), 5049–5057. 10.1016/S0009-2509(00)00126-3.

Buetehorn, S., Utiu, L., Küppers, M., Blümich, B., Wintgens, T., Wessling, M., Melin, T., 2011. NMR imaging of local cumulative permeate flux and local cake growth in submerged microfiltration processes. Journal of Membrane Science 371 (1-2), 52–64. 10.1016/j.memsci.2011.01.018.

Callaghan, P.T., 2007. Principles of nuclear magnetic resonance microscopy. Clarendon Press, Oxford, UK.

Cano, G., Wyart, Y., Daurelle, J.V., Glucina, K., Bourdiol, D., Moulin, P., 2012. Determination of Pressure and Velocity in a Dead–end Inside–out Membrane Module used in Drinking Water Production. Procedia Engineering 44, 229–232. 10.1016/j.proeng.2012.08.369.

Careri, M.N.R., 2005. Advanteges and disadvantages of Mivroporous Membranes in a Hollow Fiber Bioreactor for Space Aplications. Master thesis, Texas, USA.

Carić, M.Đ., Milanović, S.D., Krstić, D.M., Tekić, M.N., 2000. Fouling of inorganic membranes by adsorption of whey proteins. Journal of Membrane Science 165 (1), 83–88. 10.1016/S0376-7388(99)00221-5.

Carter, B.G., Cheng, N., Kapoor, R., Meletharayil, G.H., Drake, M.A., 2021. Invited review: Microfiltration-derived casein and whey proteins from milk. Journal of Dairy Science 104 (3), 2465–2479. 10.3168/jds.2020-18811.

Chang, S., Fane, A., 2001. The effect of fibre diameter on filtration and flux distribution — relevance to submerged hollow fibre modules. Journal of Membrane Science 184 (2), 221–231. 10.1016/S0376-7388(00)00626-8.

Chen, J.C., Li, Q., Elimelech, M., 2004a. In situ monitoring techniques for concentration polarization and fouling phenomena in membrane filtration. Advances in colloid and interface science 107 (2-3), 83–108. 10.1016/j.cis.2003.10.018.

Chen, V., Li, H., Fane, A.G., 2004b. Non-invasive observation of synthetic membrane processes - a review of methods. Journal of Membrane Science 241 (1), 23–44. 10.1016/j.memsci.2004.04.029.

Cheng, L.-H., Wu, P.-C., Chen, J., 2008. Modeling and optimization of hollow fiber DCMD module for desalination. Journal of Membrane Science 318 (1-2), 154–166. 10.1016/j.memsci.2008.02.065.

Cheryan, M., 1998. Ultrafiltration and microfiltration handbook. Technomic Publishing Company, Inc., Lancaster, Pennsylvania, USA.

Cheryan, M., Kuo, K.P., 1984. Hollow Fibers and Spiral Wound Modules for Ultrafiltration of Whey: Energy Consumption and Performance. Journal of Dairy Science 67 (7), 1406–1413. 10.3168/jds.S0022-0302(84)81455-1.

Cho, B., Fane, A., 2002. Fouling transients in nominally sub-critical flux operation of a membrane bioreactor. Journal of Membrane Science 209 (2), 391–403. 10.1016/S0376-7388(02)00321-6.

Chudacek, M., 1984. The dynamics of polarisation in unstirred and stirred ultrafiltration. Journal of Membrane Science 21 (2), 145–160. 10.1016/S0376-7388(00)81551-3.

Cimini, A., Moresi, M., 2016. Beer Clarification by Novel Ceramic Hollow-Fiber Membranes: Effect of Pore Size on Product Quality. Journal of Food Science 81 (10), E2521-E2528. 10.1111/1750-3841.13436.

Crowley, S.V., Caldeo, V., McCarthy, N.A., Fenelon, M.A., Kelly, A.L., O'Mahony, J.A., 2015. Processing and protein-fractionation characteristics of different polymeric membranes during filtration of skim milk at refrigeration temperatures. International Dairy Journal 48, 23–30. 10.1016/j.idairyj.2015.01.005.

Cui, Z.F., Jiang, Y., Field, R.W., 2010. Fundamentals of Pressure-Driven Membrane Separation Processes, in: Cui, Z.F., Muralidhara, H.S. (Eds.), Membrane technology: A practical guide to membrane technology and applications in food and bioprocessing. Butterworth-Heinemann, Oxford, pp. 1–18.

Çulfaz, P.Z., Buetehorn, S., Utiu, L., Kueppers, M., Bluemich, B., Melin, T., Wessling, M., Lammertink, R.G.H., 2011. Fouling behavior of microstructured hollow fiber membranes in dead-end filtrations: critical flux determination and NMR imaging of particle deposition. Langmuir : the ACS journal of surfaces and colloids 27 (5), 1643–1652. 10.1021/la1037734.

Dalgleish, D.G., 2011. On the structural models of bovine casein micelles—review and possible improvements. Soft Matter 7 (6), 2265–2272. 10.1039/C0SM00806K.

Dalgleish, D.G., Corredig, M., 2012. The structure of the casein micelle of milk and its changes during processing. Annual Review of Food Science and Technology 3, 449–467. 10.1146/annurev-food-022811-101214.

Delaunay, D., Rabiller-Baudry, M., Gozálvez-Zafrilla, J.M., Balannec, B., Frappart, M., Paugam, L., 2008. Mapping of protein fouling by FTIR-ATR as experimental tool to study membrane fouling and fluid velocity profile in various geometries and validation by CFD simulation. Chemical Engineering and Processing: Process Intensification 47 (7), 1106–1117. 10.1016/j.cep.2007.12.008.

Doshi, M.R., Gill, W.N., Kabadi, V.N., 1977. Optimal design of hollow fiber modules. American Institute of Chemical Engineers Journal 23 (5), 765–768. 10.1002/aic.690230520.

Doudiès, F., Loginov, M., Hengl, N., Karrouch, M., Leconte, N., Garnier-Lambrouin, F., Pérez, J., Pignon, F., Gésan-Guiziou, G., 2021. Build-up and relaxation of membrane fouling deposits produced during crossflow ultrafiltration of casein micelle dispersions at 12 °C and 42 °C probed by in situ SAXS. Journal of Membrane Science 618, 118700. 10.1016/j.memsci.2020.118700.

Dumpler, J., 2017. Heat Stability of Concentrated Milk Systems: Kinetics of the Dissociation and Aggregation in High Heated Concentrated Milk Systems, 1st ed. Springer Fachmedien Wiesbaden GmbH, Wiesbaden.

Dumpler, J., Wohlschläger, H., Kulozik, U., 2017. Dissociation and coagulation of caseins and whey proteins in concentrated skim milk heated by direct steam injection. Dairy Science & Technology 96 (6), 807–826. 10.1007/s13594-016-0304-3.

Ebrahimi, M., Kerker, S., Daume, S., Geile, M., Ehlen, F., Unger, I., Schütz, S., Czermak, P., 2015. Innovative ceramic hollow fiber membranes for recycling/reuse of oilfield produced water. Desalination and Water Treatment 55 (13), 3554–3567. 10.1080/19443994.2014.947780.

Ebrahimi, M., Kerker, S., Schmitz, O., Schmidt, A.A., Czermak, P., 2018. Evaluation of the fouling potential of ceramic membrane configurations designed for the treatment of oilfield produced water. Separation Science and Technology 53 (2), 349–363. 10.1080/01496395.2017.1386217.

Farhat, N.M., Staal, M., Bucs, S., van Loosdrecht, M., Vrouwenvelder, J.S., 2016. Spatial heterogeneity of biofouling under different cross-flow velocities in reverse osmosis membrane systems. Journal of Membrane Science 520, 964–971. 10.1016/j.memsci.2016.08.065.

Field, R.W., Pearce, G.K., 2011. Critical, sustainable and threshold fluxes for membrane filtration with water industry applications. Advances in colloid and interface science 164 (1-2), 38–44. 10.1016/j.cis.2010.12.008.

Field, R.W., Wu, D., Howell, J.A., Gupta, B.B., 1995. Critical flux concept for microfiltration fouling. Journal of Membrane Science 100 (3), 259–272. 10.1016/0376-7388(94)00265-Z.

France, T.C., Bot, F., Kelly, A.L., Crowley, S.V., O'Mahony, J.A., 2021a. The influence of temperature on filtration performance and fouling during cold microfiltration of skim milk. Separation and Purification Technology 262, 118256. 10.1016/j.seppur.2020.118256.

France, T.C., Kelly, A.L., Crowley, S.V., O'Mahony, J.A., 2021b. Cold Microfiltration as an Enabler of Sustainable Dairy Protein Ingredient Innovation. Foods (Basel, Switzerland) 10 (9). 10.3390/foods10092091.

Frederic, E., Guigui, C., Jacob, M., Machinal, C., Krifi, A., Line, A., Schmitz, P., 2018. Modelling of fluid flow distribution in multichannel ceramic membrane: Application to the filtration of produced water. Journal of Membrane Science 567, 290–302. 10.1016/j.memsci.2018.09.021.

Fritz, A., 1995. Abscheidegesetz zur Querstromfiltration in turbulent durchströmten Rohrfiltern. VDI Verlag GmbH, Düsseldorf, Germany.

Garoutte, C.A., Amundson, C.H., Hill, C.G., 1982. Ultrafiltration of whole milk with hollow fiber membranes. Journal of Food Process Engineering 5 (4), 191–202. 10.1111/j.1745-4530.1982.tb00273.x.

Gaucheron, F., 2005. The minerals of milk. Reproduction, Nutrition, Development 45 (4), 473–483. 10.1051/rnd:2005030.

Gebhardt, R., Steinhauer, T., Meyer, P., Sterr, J., Perlich, J., Kulozik, U., 2012. Structural changes of deposited casein micelles induced by membrane filtration. Faraday discussions 158, 77-88; discussion 105-24. 10.1039/c2fd20022h.

Geraldes, V., Semiãob, V., Pinho, M.N. de, 2002. Flow management in nanofiltration spiral wound modules with ladder-type spacers. Journal of Membrane Science 203 (1-2), 87–102. 10.1016/S0376-7388(01)00753-0.

Gernedel, C., 1980. Über die Ultrafiltration von Milch und die den Widerstand der Ablagerungsschicht beeinflussenden Faktoren. Ph. Thesis, München, Germany.

Gésan, G., Daufin, G., Merin, U., 1994. Whey crossflow microfiltration using an M14 Carbosep membrane: influence of initial hydraulic resistance. Le Lait 74 (4), 267–279. 10.1051/lait:1994422.

Gésan, G., Daufin, G., Merin, U., Labbé, J.-P., Quémerais, A., 1993. Fouling during constant flux crossflow microfiltration of pretreated whey. Influence of transmembrane pressure gradient. Journal of Membrane Science 80 (1), 131–145. 10.1016/0376-7388(93)85138-M.

Gésan-Guiziou, G., Daufin, G., Boyaval, E., 2000. Critical stability conditions in skimmed milk crossflow microfiltration: Impact on operating modes. Le Lait 80 (1), 129–138. 10.1051/lait:2000114.

Gésan-Guiziou, G., Daufin, G., Boyaval, E., Le Berre, O., 1999. Wall shear stress: effective parameter for the characterisation of the cross-flow transport in turbulent regime during skimmed milk microfiltration. Le Lait 79 (3), 347–354. 10.1051/lait:1999330.

Ghidossi, R., Carretier, E., Veyret, D., Dhaler, D., Moulin, P., 2010. Optimizing the compacity of ceramic membranes. Journal of Membrane Science 360 (1-2), 483–492. 10.1016/j.memsci.2010.05.050.

Ghidossi, R., Veyret, D., Moulin, P., 2006. Computational fluid dynamics applied to membranes: State of the art and opportunities. Chemical Engineering and Processing: Process Intensification 45 (6), 437–454. 10.1016/j.cep.2005.11.002.

Glover, F.A., Brooker, B.E., 1974. The structure of the deposit formed on the membrane during the concentration of milk by reverse osmosis. The Journal of Dairy Research 41 (1), 89–93. 10.1017/S0022029900014953.

Goosen, M.F.A., Sablani, S.S., Al‐Hinai, H., Al‐Obeidani, S., Al‐Belushi, R., Jackson, D., 2005. Fouling of Reverse Osmosis and Ultrafiltration Membranes: A Critical Review. Separation Science and Technology 39 (10), 2261–2297. 10.1081/SS-120039343.

Govindasamy-Lucey, S., Jaeggi, J.J., Johnson, M.E., Wang, T., Lucey, J.A., 2007. Use of cold microfiltration retentates produced with polymeric membranes for standardization of milks for manufacture of pizza cheese. Journal of Dairy Science 90 (10), 4552–4568. 10.3168/jds.2007-0128.

Grace, H.P., 1956. Structure and performance of filter media. II. Performance of filter media in liquid service. AIChE Journal 2 (3), 316–336. 10.1002/aic.690020308.

Graf von der Schulenburg, D., Vrouwenvelder, J., Creber, S., van Loosdrecht, M., Johns, M., 2008. Nuclear magnetic resonance microscopy studies of membrane biofouling. Journal of Membrane Science 323 (1), 37–44. 10.1016/j.memsci.2008.06.012.

Grandison, A.S., Youravong, W., Lewis, M.J., 2000. Hydrodynamic factors affecting flux and fouling during ultrafiltration of skimmed milk. Le Lait 80 (1), 165–174. 10.1051/lait:2000116.

Han, Q., Lay, H.T., Li, W., Chew, J.W., 2021. Effect of initial particle deposition rate on cake formation during dead-end microfiltration. Journal of Membrane Science 618, 118672. 10.1016/j.memsci.2020.118672.

Hartinger, M., 2021. Milk protein fractionation by spiral-wound membranes: Optimization of process and module design. Ph thesis, 1st ed. Verlag Dr. Hut, München, Germany.

Hartinger, M., Heidebrecht, H.-J., Schiffer, S., Dumpler, J., Kulozik, U., 2019a. Milk Protein Fractionation by Means of Spiral-Wound Microfiltration Membranes: Effect

of the Pressure Adjustment Mode and Temperature on Flux and Protein Permeation. Foods 8 (6). 10.3390/foods8060180.

Hartinger, M., Heidebrecht, H.-J., Schiffer, S., Dumpler, J., Kulozik, U., 2019b. Technical Concepts for the Investigation of Spatial Effects in Spiral-Wound Microfiltration Membranes. Membranes 9 (7). 10.3390/membranes9070080.

Hartinger, M., Kulozik, U., 2020. Milk protein fractionation by spiral-wound microfiltration membranes in diafiltration mode - Influence of feed protein concentration and composition on the filtration performance. International Dairy Journal 102, 104606. 10.1016/j.idairyj.2019.104606.

Hartinger, M., Napiwotzki, J., Schmid, E.-M., Hoffmann, D., Kurz, F., Kulozik, U., 2020a. Influence of Spacer Design and Module Geometry on the Filtration Performance during Skim Milk Microfiltration with Flat Sheet and Spiral-Wound Membranes. Membranes 10 (4). 10.3390/membranes10040057.

Hartinger, M., Napiwotzki, J., Schmid, E.-M., Kurz, F., Kulozik, U., 2020b. Semi-quantitative, spatially resolved analysis of protein deposit layers on membrane surfaces. MethodsX 7, 100780. 10.1016/j.mex.2019.100780.

Hartinger, M., Schiffer, S., Heidebrecht, H.-J., Dumpler, J., Kulozik, U., 2019c. Investigation on the spatial filtration performance in spiral-wound membranes – Influence and length-dependent adjustment of the transmembrane pressure. Journal of Membrane Science 591, 117311. 10.1016/j.memsci.2019.117311.

Hartinger, M., Schiffer, S., Heidebrecht, H.-J., Dumpler, J., Kulozik, U., 2020c. Milk protein fractionation by custom-made prototypes of spiral-wound microfiltration membranes operated at extreme crossflow velocities. Journal of Membrane Science 605, 118110. 10.1016/j.memsci.2020.118110.

Heidebrecht, H.-J., Kulozik, U., 2019. Fractionation of casein micelles and minor proteins by microfiltration in diafiltration mode. Study of the transmission and yield of the immunoglobulins IgG, IgA and IgM. International Dairy Journal 93, 1–10. 10.1016/j.idairyj.2019.01.009.

Heidebrecht, H.-J., Toro-Sierra, J., Kulozik, U., 2018. Concentration of Immunoglobulins in Microfiltration Permeates of Skim Milk: Impact of Transmembrane Pressure and Temperature on the IgG Transmission Using Different Ceramic Membrane Types and Pore Sizes. Foods 7 (7). 10.3390/foods7070101.

Hermans, P.H., Bredée, H.L., 1935. Zur Kenntnis der Filtrationsgesetze. Recl. Trav. Chim. Pays-Bas 54 (9), 680–700. 10.1002/recl.19350540902.

Hermans, P.H., Bredée, H.L., Lepper, W., Yohe, G.R., Elford, W.J., Ferry, J.D., 1936. Filtration. Zeitschrift für analytische Chemie 105 (3-4), 118–120. 10.1007/BF01364549.

Hermia, J., 1982. Constant pressure blocking filtration laws-application to power-law non-Newtonian fluids. Chemical Engineering Research and Design 60, 183–187.

Hernández, A., Harte, F.M., 2009. Isolation of caseins from whey proteins by microfiltration modifying the mineral balance in skim milk. Journal of Dairy Science 92 (11), 5357–5362. 10.3168/jds.2009-2335.

Hilal, N., Ogunbiyi, O.O., Miles, N.J., Nigmatullin, R., 2005. Methods Employed for Control of Fouling in MF and UF Membranes: A Comprehensive Review. Separation Science and Technology 40 (10), 1957–2005. 10.1081/SS-200068409.

Holt, C., Carver, J.A., Ecroyd, H., Thorn, D.C., 2013. Invited review: Caseins and the casein micelle: their biological functions, structures, and behavior in foods. Journal of Dairy Science 96 (10), 6127–6146. 10.3168/jds.2013-6831.

Horie, T., Shiota, S., Akagi, T., Ohmura, N., Wang, S., Eze, V., Harvey, A., Hirata, Y., 2018. Intensification of hollow fiber membrane cross-flow filtration by the combination of helical baffle and oscillatory flow. Journal of Membrane Science 554, 134–139. 10.1016/j.memsci.2018.01.058.

Horne, D.S., 2003. Casein micelles as hard spheres: limitations of the model in acidified gel formation. Colloids and Surfaces A: Physicochemical and Engineering Aspects 213 (2-3), 255–263. 10.1016/S0927-7757(02)00518-6.

Horne, D.S., 2020. Casein micelle structure and stability, in: Boland, M., Singh, H. (Eds.), Milk proteins: From expression to food, 3rd ed. Elsevier; Academic Press, Amsterdam, pp. 213–250.

Hurt, E., 2015. Production of micellar casein concentrates using ceramic microfiltration membranes: Optimal process design and system operation. Ph. Thesis, Ithaca, New York, USA.

Hurt, E., Barbano, D.M., 2010. Processing factors that influence casein and serum protein separation by microfiltration. Journal of Dairy Science 93 (10), 4928–4941. 10.3168/jds.2010-3121.

Hurt, E., Zulewska, J., Newbold, M., Barbano, D.M., 2010. Micellar casein concentrate production with a 3X, 3-stage, uniform transmembrane pressure ceramic membrane process at 50°C. Journal of Dairy Science 93 (12), 5588–5600. 10.3168/jds.2010-3169.

Hurt, E.E., Adams, M.C., Barbano, D.M., 2015a. Microfiltration of skim milk and modified skim milk using a 0.1-μm ceramic uniform transmembrane pressure system at temperatures of 50, 55, 60, and 65°C. Journal of Dairy Science 98 (2), 765–780. 10.3168/jds.2014-8775.

Hurt, E.E., Adams, M.C., Barbano, D.M., 2015b. Microfiltration: Effect of channel diameter on limiting flux and serum protein removal. Journal of Dairy Science 98 (6), 3599–3612. 10.3168/jds.2014-9225.

Hurt, E.E., Adams, M.C., Barbano, D.M., 2015c. Microfiltration: Effect of retentate protein concentration on limiting flux and serum protein removal with 4-mm-channel ceramic microfiltration membranes. Journal of Dairy Science 98 (4), 2234–2244. 10.3168/jds.2014-9032.

Iritani, E., 2013. A Review on Modeling of Pore-Blocking Behaviors of Membranes During Pressurized Membrane Filtration. Drying Technology 31 (2), 146–162. 10.1080/07373937.2012.683123.

Iritani, E., Katagiri, N., 2016. Developments of Blocking Filtration Model in Membrane Filtration. KONA 33 (0), 179–202. 10.14356/kona.2016024.

Iritani, E., Katagiri, N., Takenaka, T., Yamashita, Y., 2015. Membrane pore blocking during cake formation in constant pressure and constant flux dead-end microfiltration of very dilute colloids. Chemical Engineering Science 122, 465–473. 10.1016/j.ces.2014.09.052.

Iritani, E., Sumi, H., Murase, T., 1991. Analysis of filtration rate in clarification filtration of power-law non-Newtonian fluids-solids mixtures under constant pressure by stochastic model. J. Chem. Eng. Japan / JCEJ 24 (5), 581–586. 10.1252/jcej.24.581.

Jenness, R., 2012. 2 d protein composition of milk: Milk Proteins V1: Chemistry and Molecular Biology. Elsevier, Amsterdam, The Netherlands.

Jimenez-Lopez, A., Leconte, N., Dehainault, O., Geneste, C., Fromont, L., Gesanguiziou, G., 2008. Role of milk constituents on critical conditions and deposit structure in skimmilk microfiltration (0.1µm). Separation and Purification Technology 61 (1), 33–43. 10.1016/j.seppur.2007.09.023.

Jimenez-Lopez, A., Leconte, N., Garnier-Lambrouin, F., Bouchoux, A., Rousseau, F., Gésan-Guiziou, G., 2011. Ionic strength dependence of skimmed milk microfiltration: Relations between filtration performance, deposit layer characteristics and colloidal properties of casein micelles. Journal of Membrane Science 369 (1-2), 404–413. 10.1016/j.memsci.2010.12.026.

Jørgensen, C.E., Abrahamsen, R.K., Rukke, E.-O., Johansen, A.-G., Schüller, R.B., Skeie, S.B., 2016. Optimization of protein fractionation by skim milk microfiltration: Choice of ceramic membrane pore size and filtration temperature. Journal of Dairy Science 99 (8), 6164–6179. 10.3168/jds.2016-11090.

Karabelas, A.J., Koutsou, C.P., Sioutopoulos, D.C., 2018. Comprehensive performance assessment of spacers in spiral-wound membrane modules accounting for compressibility effects. Journal of Membrane Science 549, 602–615. 10.1016/j.memsci.2017.12.037.

Karlsson, A.O., Ipsen, R., Schrader, K., Ardö, Y., 2005. Relationship Between Physical Properties of Casein Micelles and Rheology of Skim Milk Concentrate. Journal of Dairy Science 88 (11), 3784–3797. 10.3168/jds.S0022-0302(05)73064-2.

Kavianipour, O., Ingram, G.D., Vuthaluru, H.B., 2017. Investigation into the effectiveness of feed spacer configurations for reverse osmosis membrane modules using Computational Fluid Dynamics. Journal of Membrane Science 526, 156–171. 10.1016/j.memsci.2016.12.034.

Kersten, M., 2001. Proteinfraktionierung mittels Membrantrennverfahren. Zugl.: München, Techn. Univ., Diss. VDI Verlag GmbH, Düsseldorf, Germany.

Kessler, H.G., 2002. Food and bio process engineering: Dairy technology; 109 tables, 5th ed. A. Kessler, München, Germany.

Kim, J., DiGiano, F.A., 2006. Particle fouling in submerged microfiltration membranes: effects of hollow-fiber length and aeration rate. Journal of Water Supply: Research and Technology-Aqua 55 (7-8), 535–547. 10.2166/aqua.2006.054.

Kim, Y.-J., Yun, T., Han, J., Lee, S., Park, P.-K., Hwang, B.-K., Park, J.-S., 2012. Design optimization of ultrafiltration membrane module for desalination applications.

Desalination and Water Treatment 43 (1-3), 291–297. 10.1080/19443994.2012.672204.

Kimura, S., Sourirajan, S., 1967. Analysis of data in reverse osmosis with porous cellulose acetate membranes used. AIChE Journal 13 (3), 497–503. 10.1002/aic.690130319.

Kirk, D.E., Montgomery, M.W., Kortekaas, M.G., 1983. Clarification of Pear Juice by Hollow Fiber Ultrafiltration. Journal of Food Science 48 (6), 1663–1667. 10.1111/j.1365-2621.1983.tb05055.x.

Klein, G.-M., Kottke, V., 1996. Untersuchungen zum Deckschichtaufbau bei der Querstrom-Mikrofiltration polydisperser Suspensionen unter definierten Stromungsbedingungen. Chemie Ingenieur Technik 68 (9), 1073.

Kontopidis, G., Holt, C., Sawyer, L., 2004. Invited Review: β-Lactoglobulin: Binding Properties, Structure, and Function. Journal of Dairy Science 87 (4), 785–796. 10.3168/jds.S0022-0302(04)73222-1.

Koutsou, C.P., Karabelas, A.J., Goudoulas, T.B., 2013. Characteristics of permeate-side spacers of spiral wound membrane modules. Desalination 322, 131–136. 10.1016/j.desal.2013.05.015.

Koutsou, C.P., Yiantsios, S.G., Karabelas, A.J., 2009. A numerical and experimental study of mass transfer in spacer-filled channels: Effects of spacer geometrical characteristics and Schmidt number. Journal of Membrane Science 326 (1), 234–251. 10.1016/j.memsci.2008.10.007.

Kuhn, M., Briesen, H., 2021. Optimizing the Axial Resistance Profile of Submerged Hollow Fiber Membranes. Processes 9 (1), 20. 10.3390/pr9010020.

Kühnl, W., 2011. Kolloidale Wechselwirkungen zwischen Proteinen im Zusammenspiel mit fluid-dynamischen Kräften an der Grenzfläche von Filtrationsmembranen: Gezeigt am Beispiel der Fraktionierung von Milchproteinen mittels Mikrofiltration. Zugl.: München, Techn. Univ., Diss., 2010. VDI Verlag GmbH, Düsseldorf, Germany.

Kühnl, W., Piry, A., Kaufmann, V., Grein, T., Ripperger, S., Kulozik, U., 2010. Impact of colloidal interactions on the flux in cross-flow microfiltration of milk at different pH values: A surface energy approach. Journal of Membrane Science 352 (1-2), 107–115. 10.1016/j.memsci.2010.02.006.

Kühnl, W., Piry, A., Kulozik, U., 2008. Einfluss des Membranwiderstands auf die Filtrationsleistung bei der Proteinfraktionierung entlang von Mikrofiltrationsmodulen. Chemie Ingenieur Technik 80 (8), 1199–1205. 10.1002/cite.200800048.

Kulozik, U., Kersten, M., 2002. Membrane Fractionation of Dairy Proteins by Means of Microfiltration. Engineering in Life Sciences 2 (9), 275–278. 10.1002/1618-2863(20020910)2:9<275:AID-ELSC275>3.0.CO;2-6.

Kumar, P., Sharma, N., Ranjan, R., Kumar, S., Bhat, Z.F., Jeong, D.K., 2013. Perspective of membrane technology in dairy industry: a review. Asian-Australasian journal of animal sciences 26 (9), 1347–1358. 10.5713/ajas.2013.13082.

Laksono, S., ElSherbiny, I.M., Huber, S.A., Panglisch, S., 2020. Fouling scenarios in hollow fiber membranes during mini-plant filtration tests and correlation to microalgae-loaded feed characteristics. Chemical Engineering Journal, 127723. 10.1016/j.cej.2020.127723.

Laukemper-Ostendorf, S., Lemke, H.D., Blümler, P., Blümich, B., 1998. NMR imaging of flow in hollow fiber hemodialyzers. Journal of Membrane Science 138 (2), 287–295. 10.1016/S0376-7388(97)00241-X.

Le Berre, O., Daufin, G., 1996. Skimmilk crossflow microfiltration performance versus permeation flux to wall shear stress ratio. Journal of Membrane Science 117 (1-2), 261–270. 10.1016/0376-7388(96)00076-2.

Le Berre, O., Daufin, G., 1998. Microfiltration (0·1 μm) of milk: effect of protein size and charge. The Journal of Dairy Research 65 (3), 443–455. 10.1017/S0022029998003008.

Lehmkuhl, S., Wiese, M., Schubert, L., Held, M., Küppers, M., Wessling, M., Blümich, B., 2018. Continuous hyperpolarization with parahydrogen in a membrane reactor. Journal of magnetic resonance (San Diego, Californien, USA: 1997) 291, 8–13. 10.1016/j.jmr.2018.03.012.

Li, H., Hsu, Y.-C., Zhang, Z., Dharsana, N., Ye, Y., Chen, V., 2016. The influence of milk components on the performance of ultrafiltration/diafiltration of concentrated skim milk. Separation Science and Technology 52 (2), 381–391. 10.1080/01496395.2016.1217243.

Li, X., Li, J., Wang, H., Huang, X., He, B., Yao, Y., Wang, J., Zhang, H., Ngo, H.H., Guo, W., 2015. A filtration model for prediction of local flux distribution and optimization of submerged hollow fiber membrane module. American Institute of Chemical Engineers Journal 61 (12), 4377–4386. 10.1002/aic.14906.

Li, X., Li, J., Wang, J., Zhang, H., Pan, Y., 2012. In situ investigation of fouling behavior in submerged hollow fiber membrane module under sub-critical flux operation via ultrasonic time domain reflectometry. Journal of Membrane Science 411-412, 137–145. 10.1016/j.memsci.2012.04.024.

Li, X., Mo, Y., Li, J., Guo, W., Ngo, H.H., 2017. In-situ monitoring techniques for membrane fouling and local filtration characteristics in hollow fiber membrane processes: A critical review. Journal of Membrane Science 528, 187–200. 10.1016/j.memsci.2017.01.030.

Loginov, M., Doudiès, F., Hengl, N., Pignon, F., Gésan-Guiziou, G., 2020. Influence of membrane resistance on swelling and removal of colloidal filter cake after filtration pressure release. Journal of Membrane Science 595, 117498. 10.1016/j.memsci.2019.117498.

Luelf, T., Bremer, C., Wessling, M., 2016. Rope coiling spinning of curled and meandering hollow-fiber membranes. Journal of Membrane Science 506, 86–94. 10.1016/j.memsci.2016.01.037.

Luelf, T., Tepper, M., Breisig, H., Wessling, M., 2017. Sinusoidal shaped hollow fibers for enhanced mass transfer. Journal of Membrane Science 533, 302–308. 10.1016/j.memsci.2017.03.030.

Luhr, S., 2016. Conceptual Design of Membrane Modules for an Efficient Separation of Carbon Dioxide from Gas Mixtures. Ph. Thesis. Forschungszentrum Jülich GmbH, Zentralbibliothek, Verlag, Jülich, Germany.

Mahon, H.I., 1966. Permeability Separatory Apparatus, Permeability Separatory Membrane Element, Method of Making the Same and Process Utilizing the Same, US Patent US3228876A.

Makabe, R., Akamatsu, K., Tatsumi, R., Koike, O., Nakao, S., 2021. Numerical simulations of lift force and drag force on a particle in cross-flow microfiltration of colloidal suspensions to understand limiting flux. Journal of Membrane Science 621, 118998. 10.1016/j.memsci.2020.118998.

Marshall, A.D., Munro, P.A., Trägårdh, G., 1993. The effect of protein fouling in microfiltration and ultrafiltration on permeate flux, protein retention and selectivity: A literature review. Desalination 91 (1), 65–108. 10.1016/0011-9164(93)80047-Q.

McKelvey, S.A., Clausi, D.T., Koros, W.J., 1997. A guide to establishing hollow fiber macroscopic properties for membrane applications. Journal of Membrane Science 124 (2), 223–232. 10.1016/S0376-7388(96)00249-9.

McLaughlin, J.B., 1993. The lift on a small sphere in wall-bounded linear shear flows. Journal of Fluid Mechanics 246, 249–265. 10.1017/S0022112093000114.

McMahon, D.J., Oommen, B.S., 2008. Supramolecular structure of the casein micelle. Journal of Dairy Science 91 (5), 1709–1721. 10.3168/jds.2007-0819.

Melin, T., Rautenbach, R., 2007. Membranverfahren: Grundlagen der Modul- und Anlagenauslegung, 3rd ed. Springer, Berlin, Germany.

Mercier-Bouchard, D., Benoit, S., Doyen, A., Britten, M., Pouliot, Y., 2017. Process efficiency of casein separation from milk using polymeric spiral-wound microfiltration membranes. Journal of Dairy Science 100 (11), 8838–8848. 10.3168/jds.2017-13015.

Moch, I., 1995. Hollow-Fiber Membranes: Encyclopedia of Chemical Technology p. 312, 4th ed. John Wiley-InterScience Publishing, New York.

Mohammad, A.W., Ng, C.Y., Lim, Y.P., Ng, G.H., 2012. Ultrafiltration in Food Processing Industry: Review on Application, Membrane Fouling, and Fouling Control. Food and Bioprocess Technology 5 (4), 1143–1156. 10.1007/s11947-012-0806-9.

Mondor, M., Moresoli, C., 2000. Experimental verification of the shear-induced hydrodynamic diffusion model of crossflow microfiltration, with consideration of the transmembrane pressure axial variation. Journal of Membrane Science 175 (1), 119–137. 10.1016/S0376-7388(00)00410-5.

Moody, R., 1944. Negro minstrelsy. Quarterly Journal of Speech 30 (3), 321–328. 10.1080/00335634409381008.

Mulder, M., 1996. Basic principles of membrane technology, 2nd ed. Kluwer, Dordrecht.

Ng, K.S., Dunstan, D.E., Martin, G.J., 2018. Influence of processing temperature on flux decline during skim milk ultrafiltration. Separation and Purification Technology 195, 322–331. 10.1016/j.seppur.2017.12.029.

Ng, K.S., Haribabu, M., Harvie, D.J., Dunstan, D.E., Martin, G.J., 2017. Mechanisms of flux decline in skim milk ultrafiltration: A review. Journal of Membrane Science 523, 144–162. 10.1016/j.memsci.2016.09.036.

Opong, W., Zydney, A.L., 1991. Hydraulic permeability of protein layers deposited during ultrafiltration. Journal of Colloid and Interface Science 142 (1), 41–60. 10.1016/0021-9797(91)90032-4.

Panglisch, S., 2003. Formation and prevention of hardly removable particle layers in inside-out capillary membranes operating in dead-end mode. Water Science and Technology: Water Supply 3 (5-6), 117–124. 10.2166/ws.2003.0157.

Panglisch, S., Kouchaki Shalmani, A., Weber, M., Gronwald, O., Berg, P., Heijnen, M., Krug, M., Koti, M., Nahrstedt, A., Abetz, V., Handge, U.A., Grünig, L., Ulbricht, M., Stratmann, I., 2019. Material ‐ Auswahlbox zur Herstellung fortgeschrittener Polymermembranen für die Wasseraufbereitung. Chemie Ingenieur Technik 91 (8), 1162–1167. 10.1002/cite.201900038.

Patel, R.S., Reuter, H., 1985. Deposit formation on a hollow fiber ultrafiltration membrane during concentration of skimmilk. Milchwissenschaft 10 (40), 592–595.

Piry, A., 2011. Untersuchung zur Längenabhängigkeit der Filtrationsleistung bei der Fraktionierung von Milchproteinen mittels Mikrofiltration. Zugl.: München, Techn. Univ., Diss., 2010, 1st ed. Verl. Dr. Hut, München, Germany.

Piry, A., Heino, A., Kühnl, W., Grein, T., Ripperger, S., Kulozik, U., 2012. Effect of membrane length, membrane resistance, and filtration conditions on the fractionation of milk proteins by microfiltration. Journal of Dairy Science 95 (4), 1590–1602. 10.3168/jds.2011-4292.

Piry, A., Kühnl, W., Grein, T., Tolkach, A., Ripperger, S., Kulozik, U., 2008. Length dependency of flux and protein permeation in crossflow microfiltration of skimmed milk. Journal of Membrane Science 325 (2), 887–894. 10.1016/j.memsci.2008.09.025.

Pouliot, Y., Gauthier, S.F., Bard, C., 1993. Fractionation of casein hydrolysates using polysulfone ultrafiltration hollow fiber membranes. Journal of Membrane Science 80 (1), 257–264. 10.1016/0376-7388(93)85150-U.

Qu, P., Bouchoux, A., Gésan-Guiziou, G., 2015. On the cohesive properties of casein micelles in dense systems. Food Hydrocolloids 43, 753–762. 10.1016/j.foodhyd.2014.08.005.

Qu, P., Gésan-Guiziou, G., Bouchoux, A., 2012. Dead-end filtration of sponge-like colloids: The case of casein micelle. Journal of Membrane Science 417-418, 10–19. 10.1016/j.memsci.2012.06.003.

Reihanian, H., Robertson, C.R., Michaels, A.S., 1983. Mechanisms of polarization and fouling of ultrafiltration membranes by proteins. Journal of Membrane Science 16, 237–258. 10.1016/S0376-7388(00)81313-7.

Reitmaier, M., Bachmann, I., Heidebrecht, H.-J., Kulozik, U., 2021. Effect of changes in ionic composition induced by different diafiltration media on deposited layer properties and separation efficiency in milk protein fractionation by microfiltration. International Dairy Journal 120, 105089. 10.1016/j.idairyj.2021.105089.

Reitmaier, M., Barbosa, B., Sigler, S., Heidebrecht, H.-J., Kulozik, U., 2020. Impact of different aqueous phases on casein micelles: Kinetics of physicochemical changes under variation of water hardness and diafiltration conditions. International Dairy Journal 109, 104776. 10.1016/j.idairyj.2020.104776.

Reitmaier, M., Heidebrecht, H.-J., Kulozik, U., 2017. Milk protein fractionation by means of microfiltration: Influence of preconcentration and diafiltration medium – part 1. International Dairy Magazine 8, 16–19.

Renhe, I.R.T., Corredig, M., 2018. Effect of partial whey protein depletion during membrane filtration on thermal stability of milk concentrates. Journal of Dairy Science 101 (10), 8757–8766. 10.3168/jds.2018-14407.

Renhe, I.R.T., Zhao, Z., Corredig, M., 2019. A comparison of the heat stability of fresh milk protein concentrates obtained by microfiltration, ultrafiltration and diafiltration. The Journal of Dairy Research 86 (3), 347–353. 10.1017/S0022029919000426.

Riesmeier, B., Kroner, K.H., Kula, M.-R., 1989. Tangential filtration of microbial suspensions: filtration resistances and model development. Journal of biotechnology 12 (2), 153–171. 10.1016/0168-1656(89)90013-8.

Ripperger, S., Altmann, J., 2002. Crossflow microfiltration – state of the art. Separation and Purification Technology 26 (1), 19–31. 10.1016/S1383-5866(01)00113-7.

Romero, C.A., Davis, R.H., 1990. Transient model of crossflow microfiltration. Chemical Engineering Science 45 (1), 13–25. 10.1016/0009-2509(90)87076-5.

Romero, C.A., Davis, R.H., 1991. Experimental verification of the shear-induced hydrodynamic diffusion model of crossflow microfiltration. Journal of Membrane Science 62 (3), 249–273. 10.1016/0376-7388(91)80042-5.

Samuelsson, G., 1997. Predicting limiting flux of skim milk in crossflow microfiltration. Journal of Membrane Science 129 (2), 277–281. 10.1016/S0376-7388(97)00013-6.

Samuelsson, G., Dejmek, P., Trägårdh, G., Paulsson, M., 1997. Minimizing whey protein retention in cross-flow microfiltration of skim milk. International Dairy Journal 7 (4), 237–242. 10.1016/S0958-6946(97)00009-5.

Sato, Y., Mineshima, M., Ishimori, I., Kaneko, I., Akiba, T., Teraoka, S., 2003. Effect of hollow fiber length on solute removal and quantification of internal filtration rate by Doppler ultrasound. The International journal of artificial organs 26 (2), 129–134. 10.1177/039139880302600206.

Schiffer, S., Hartinger, M., Matyssek, A., Kulozik, U., 2020. On the reversibility of deposit formation in low temperature milk microfiltration with ceramic membranes depending on mode of adjustment of transmembrane pressure and wall shear stress. Separation and Purification Technology 247, 116962. 10.1016/j.seppur.2020.116962.

Schiffer, S., Kulozik, U., 2020. Effect of Temperature-Dependent Bacterial Growth during Milk Protein Fractionation by Means of 0.1 µM Microfiltration on the Length of Possible Production Cycle Times. Membranes 10 (11). 10.3390/membranes10110326.

Schiffer, S., Matyssek, A., Hartinger, M., Bolduan, P., Mund, P., Kulozik, U., 2021. Effects of selective layer properties of ceramic multi-channel microfiltration membranes on the milk protein fractionation. Separation and Purification Technology 259, 118050. 10.1016/j.seppur.2020.118050.

Schiffer, S., Schopf, R., Hartinger, M., Kulozik, U., 2018. Fractionation of complex foods through the use of membrane separation technology using milk as an example: Global Guide 2018-2020. Filtrieren und Separieren, 202–209.

Schmidt, D.G., 1980. Colloidal aspects of casein. Netherlands Milk and Dairy Journal 34 (1), 42–64.

Schopf, R., Desch, F., Schmitz, R., Arar, D., Kulozik, U., 2022. Effect of flow channel number in multi-channel tubular ceramic microfiltration membranes on flux and small protein transmission in milk protein fractionation. Journal of Membrane Science 644, 120153. 10.1016/j.memsci.2021.120153.

Schopf, R., Kulozik, U., 2021. Impact of feed concentration on milk protein fractionation by hollow fiber microfiltration membranes in diafiltration mode. Separation and Purification Technology, 119278. 10.1016/j.seppur.2021.119278.

Schopf, R., Schmidt, F., Kulozik, U., 2021a. Impact of hollow fiber membrane length on the milk protein fractionation. Journal of Membrane Science 620, 118834. 10.1016/j.memsci.2020.118834.

Schopf, R., Schmidt, F., Linner, J., Kulozik, U., 2021b. Comparative Assessment of Tubular Ceramic, Spiral Wound, and Hollow Fiber Membrane Microfiltration Module Systems for Milk Protein Fractionation. Foods 10 (4), 692. 10.3390/foods10040692.

Schopf, R., Schork, N., Amling, E., Nirschl, H., Guthausen, G., Kulozik, U., 2020. Structural Characterisation of Deposit Layer during Milk Protein Microfiltration by Means of In-Situ MRI and Compositional Analysis. Membranes 10 (4), 59. 10.3390/membranes10040059.

Schork, N., Schuhmann, S., Arndt, F., Schütz, S., Guthausen, G., Nirschl, H., 2018. MRI investigations of filtration: Fouling and cleaning processes. Microporous and Mesoporous Materials 269, 60–64. 10.1016/j.micromeso.2017.05.042.

Schork, N., Schuhmann, S., Nirschl, H., Guthausen, G., 2019. In situ measurement of deposit layer formation during skim milk filtration by MRI. Magnetic resonance in chemistry : MRC 57 (9), 738–748. 10.1002/mrc.4826.

Schork, N., Schuhmann, S., Nirschl, H., Guthausen, G., 2021. Compressed sensing MRI to characterize sodium alginate deposits during cross-flow filtration in membranes with a helical ridge. Journal of Membrane Science 626, 119170. 10.1016/j.memsci.2021.119170.

Schuhmann, S., Schork, N., Beller, K., Nirschl, H., Oerther, T., Guthausen, G., 2018. In-situ characterization of deposits in ceramic hollow fiber membranes by compressed sensing RARE-MRI. AIChE Journal 64 (11), 4039–4046. 10.1002/aic.16201.

Schuhmann, S., Simkins, J.W., Schork, N., Codd, S.L., Seymour, J.D., Heijnen, M., Saravia, F., Horn, H., Nirschl, H., Guthausen, G., 2019. Characterization and quantification of structure and flow in multichannel polymer membranes by MRI. Journal of Membrane Science 570-571, 472–480. 10.1016/j.memsci.2018.10.072.

Serra, C., Clifton, M.J., Moulin, P., Rouch, J.-C., Aptel, P., 1998. Dead-end ultrafiltration in hollow fiber modules: Module design and process simulation. Journal of Membrane Science 145 (2), 159–172. 10.1016/S0376-7388(98)00075-1.

Shirato, M., Aragaki, T., Iritani, E., 1979. Blocking filtration laws for filtration of power-law non-Newtonian fluids. J. Chem. Eng. Japan / JCEJ 12 (2), 162–164. 10.1252/jcej.12.162.

Soltanieh, M., Gill, W.N., 1983. A note on the effect of fiber lenght on the productivity of hollow fiber modules. Chemical Engineering Communications 22 (1-2), 109–113. 10.1080/00986448308940049.

Song, L., Elimelech, M., 1995. Theory of concentration polarization in crossflow filtration. Journal of the Chemical Society, Faraday Transactions 91 (19), 3389. 10.1039/FT9959103389.

Springer, F., Ghidossi, R., Carretier, E., Veyret, D., Dhaler, D., Moulin, P., 2010. Study of the Effect of Geometry on Wall Shear Stress and Permeate Flux for Ceramic Membranes: CFD and Experimental Approaches. Engineering Applications of Computational Fluid Mechanics 4 (1), 17–28. 10.1080/19942060.2010.11015296.

Steinhauer, T., 2016. On the micro- and ultrafiltration of dairy fluids. Dissertation, 1st ed., Freising, Germany.

Steinhauer, T., Kühnl, W., Kulozik, U., 2011. Impact of Protein Interactions and Transmembrane Pressure on Physical Properties of Filter Cakes Formed during Filtrations of Skim Milk. Procedia Food Science 1, 886–892. 10.1016/j.profoo.2011.09.134.

Steinhauer, T., Lonfat, J., Hager, I., Gebhardt, R., Kulozik, U., 2015a. Effect of pH, transmembrane pressure and whey proteins on the properties of casein micelle deposit layers. Journal of Membrane Science 493, 452–459. 10.1016/j.memsci.2015.06.007.

Steinhauer, T., Marx, M., Bogendörfer, K., Kulozik, U., 2015b. Membrane fouling during ultra- and microfiltration of whey and whey proteins at different environmental conditions: The role of aggregated whey proteins as fouling initiators. Journal of Membrane Science 489, 20–27. 10.1016/j.memsci.2015.04.002.

Suwal, S., Doyen, A., Bazinet, L., 2015. Characterization of protein, peptide and amino acid fouling on ion-exchange and filtration membranes: Review of current and recently developed methods. Journal of Membrane Science 496, 267–283. 10.1016/j.memsci.2015.08.056.

Taddei, C., Aimar, P., Daufin, G., Sanchez, V., 1988. Factors affecting fouling of an inorganic membrane during sweet whey ultrafiltration. Le Lait 68 (2), 157–176. 10.1051/lait:1988211.

Thompson, S.J., deMan, J.M., 1975. Concentration and Fractionation of Milk by Ultrafiltration. Canadian Institute of Food Science and Technology Journal 8 (2), 113–116. 10.1016/S0315-5463(75)73733-1.

Tiller, F.M., Lu, R., Kwon, J.H., Lee, D.J., 1999. Variable flow rate in compactible filter cakes. Water Research 33 (1), 15–22. 10.1016/S0043-1354(98)00192-4.

Tolkach, A., 2007. Thermisches Denaturierungsverhalten von Molkenproteinfraktionen: Selektive Denaturierung – Fraktionierung mit Membranen – Reaktions-, Auffaltungs- und Aggregationskinetik. Ph Thesis, Freising, Germany.

Tolkach, A., Kulozik, U., 2007. Reaction kinetic pathway of reversible and irreversible thermal denaturation of β-lactoglobulin. Le Lait 87 (4-5), 301–315. 10.1051/lait:2007012.

Töpel, A., 2016. Chemie und Physik der Milch: Naturstoff, Rohstoff, Lebensmittel, 4th ed. Behr's Verlag, Hamburg, Germany.

Vadi, P., Rizvi, S., 2001. Experimental evaluation of a uniform transmembrane pressure crossflow microfiltration unit for the concentration of micellar casein from skim milk. Journal of Membrane Science 189 (1), 69–82. 10.1016/S0376-7388(01)00396-9.

van Hekken, D.L., Holsinger, V.H., 2000. Use of cold microfiltration to produce unique beta-casein enriched milk gels. Le Lait 80 (1), 69–76. 10.1051/lait:2000108.

van Vliet, T., Lakemond, C.M., Visschers, R.W., 2004. Rheology and structure of milk protein gels. Current Opinion in Colloid & Interface Science 9 (5), 298–304. 10.1016/j.cocis.2004.09.002.

Vilker, V.L., Colton, C.K., Smith, K.A., 1981. The osmotic pressure of concentrated protein solutions: Effect of concentration and ph in saline solutions of bovine serum albumin. Journal of Colloid and Interface Science 79 (2), 548–566. 10.1016/0021-9797(81)90106-5.

Wagner, W., 2001. Strömung und Druckverlust: Mit Beispielsammlung, 5th ed. Vogel, Würzburg, Germany.

Walstra, P., Jenness, R., 1984. Dairy chemistry and physics. Wiley, New York.

Wang, J., Cui, Z., Jia, H., Zhang, H., 2014. The effect of fiber length on non-uniform and hysteresis phenomenon in hollow fiber membrane backflushing. Desalination 337, 98–108. 10.1016/j.desal.2013.11.016.

Warncke, M., Kulozik, U., 2020. Impact of temperature and high pressure homogenization on the solubility and rheological behavior of reconstituted dairy powders of

different composition. Powder Technology 376, 285–295. 10.1016/j.powtec.2020.08.039.

Weinberger, M.E., Andlinger, D.J., Kulozik, U., 2021. A novel approach for characterisation of stabilising bonds in milk protein deposit layers on microfiltration membranes. International Dairy Journal 118, 105044. 10.1016/j.idairyj.2021.105044.

Weinberger, M.E., Kulozik, U., 2020. Effect of low-frequency pulsatile crossflow microfiltration on flux and protein transmission in milk protein fractionation. Separation Science and Technology, 1–16. 10.1080/01496395.2020.1749080.

Wiese, M., Nir, O., Wypysek, D., Pokern, L., Wessling, M., 2019. Fouling minimization at membranes having a 3D surface topology with microgels as soft model colloids. Journal of Membrane Science 569, 7–16. 10.1016/j.memsci.2018.09.058.

Xu, Q., Pearce, G.K., Field, R.W., 2017. Pressure driven inside feed (PDI) hollow fibre filtration: Optimizing the geometry and operating parameters. Journal of Membrane Science 537, 323–336. 10.1016/j.memsci.2017.05.010.

Xu, X., Li, J., Li, H., Cai, Y., Cao, Y., He, B., Zhang, Y., 2009a. Non-invasive monitoring of fouling in hollow fiber membrane via UTDR. Journal of Membrane Science 326 (1), 103–110. 10.1016/j.memsci.2008.09.042.

Xu, X., Li, J., Xu, N., Hou, Y., Lin, J., 2009b. Visualization of fouling and diffusion behaviors during hollow fiber microfiltration of oily wastewater by ultrasonic reflectometry and wavelet analysis. Journal of Membrane Science 341 (1-2), 195–202. 10.1016/j.memsci.2009.06.009.

Yamamoto, K., Kobayashi, K., Endo, K., Miyasaka, T., Mochizuki, S., Kohori, F., Sakai, K., 2005. Hollow-fiber blood-dialysis membranes: superoxide generation, permeation, and dismutation measured by chemiluminescence. Journal of artificial organs : the official journal of the Japanese Society for Artificial Organs 8 (4), 257–262. 10.1007/s10047-005-0315-y.

Yao, S., Costello, M., Fane, A.G., Pope, J.M., 1995. Non-invasive observation of flow profiles and polarisation layers in hollow fibre membrane filtration modules using NMR micro-imaging. Journal of Membrane Science 99 (3), 207–216. 10.1016/0376-7388(94)00219-O.

Yeh, H., 2000. Membrane ultrafiltration in a tubular module with a steel rod inserted concentrically for improved performance. Journal of Membrane Science 168 (1-2), 121–133. 10.1016/S0376-7388(99)00315-4.

Yeo, A., Fane, A.G., 2005. Performance of individual fibers in a submerged hollow fiber bundle. Water Science and Technology 51 (6-7), 165–172. 10.2166/wst.2005.0635.

Yoon, S.-H., Kim, H.-S., Yeom, I.-T., 2004. Optimization model of submerged hollow fiber membrane modules. Journal of Membrane Science 234 (1-2), 147–156. 10.1016/j.memsci.2004.01.018.

Zhu, L., Huey Ee, K., Zhao, L., Lee, H.K., 2002. Analysis of phenoxy herbicides in bovine milk by means of liquid–liquid–liquid microextraction with a hollow-fiber membrane. Journal of chromatography. A 963 (1-2), 335–343. 10.1016/S0021-9673(02)00138-3.

Zulewska, J., Barbano, D.M., 2013. Influence of casein on flux and passage of serum proteins during microfiltration using polymeric spiral-wound membranes at 50°C. Journal of Dairy Science 96 (4), 2048–2060. 10.3168/jds.2012-6032.

Zulewska, J., Newbold, M., Barbano, D.M., 2009. Efficiency of serum protein removal from skim milk with ceramic and polymeric membranes at 50 degrees C. Journal of Dairy Science 92 (4), 1361–1377. 10.3168/jds.2008-1757.

Zydney, A.L., Colton, C.K., 1986. A concentration polarization model for the filtrate flux in cross-flow microfiltration of particulate suspensions. Chemical Engineering Communications 47 (1-3), 1–21. 10.1080/00986448608911751.